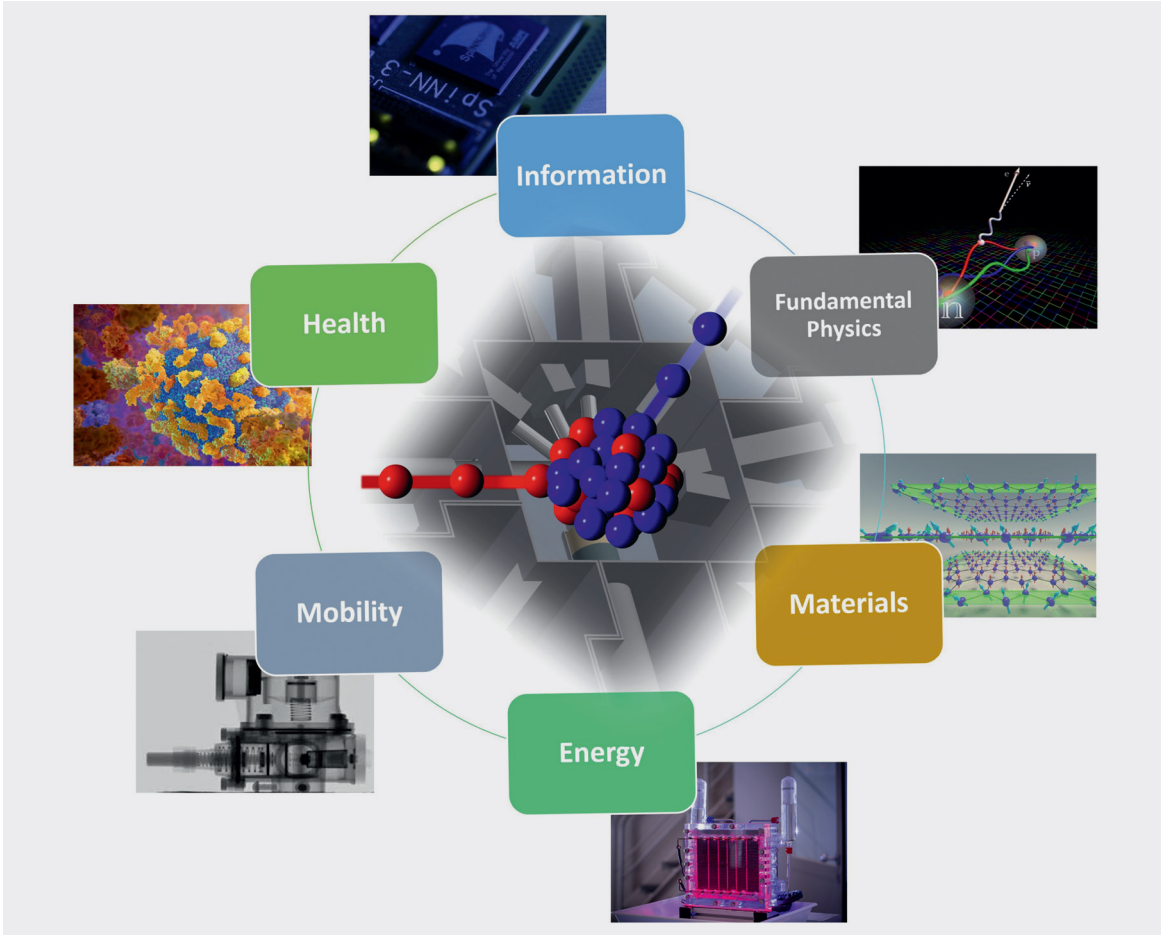

Technical Design Report HBS
Volume 3 – Instrumentation

K. Lieutenant, J. Voigt (Vol. Eds.), T. Brückel, T. Gutberlet (Ser. Eds.)

R. Bewley, J. Fenske, M. Feygenson, C. Franz, H. Frielinghaus, M. Ganeva, A. Glavic, A. Houben, S. Jaksch, N. Kardjilov, G. Kemmerling, H. Kleines, I. Krasnov, Z. Ma, S. Mattauch, E. Mauerhofer, Y. Meinerzhagen, S. Pasini, U. Rücker, K. Schmalzl, N. Schmidt, T.E. Schrader, W. Schweika, M. Strobl, E. Vezhlev, N. Violini, R. Zorn

Allgemeines / General
Band / Volume 9-03
ISBN 978-3-95806-711-0

Mitglied der Helmholtz-Gemeinschaft

JÜLICH
Forschungszentrum

Schriften des Forschungszentrums Jülich
Reihe Allgemeines / General Band / Volume 9-03

Forschungszentrum Jülich GmbH
Jülich Centre for Neutron Science (JCNS)
Quantenmaterialien und kollektive Phänomene (JCNS-2 / PGI-4)

Technical Design Report HBS
Volume 3 – Instrumentation

K. Lieutenant, J. Voigt (Vol. Eds.)
T. Brückel, T. Gutberlet (Ser. Eds.)

R. Bewley, J. Fenske, M. Feygenson, C. Franz, H. Frielinghaus, M. Ganeva, A. Glavic, A. Houben, S. Jaksch, N. Kardjilov, G. Kemmerling, H. Kleines, I. Krasnov, Z. Ma, S. Mattauch, E. Mauerhofer, Y. Meinerzhagen, S. Pasini, U. Rücker, K. Schmalzl, N. Schmidt, T.E. Schrader, W. Schweika, M. Strobl, E. Vezhlev, N. Violini, R. Zorn

Schriften des Forschungszentrums Jülich
Reihe Allgemeines / General Band / Volume 9-03

ISSN 1433-5565 ISBN 978-3-95806-711-0

Bibliografische Information der Deutschen Nationalbibliothek.
Die Deutsche Nationalbibliothek verzeichnet diese Publikation in der
Deutschen Nationalbibliografie; detaillierte Bibliografische Daten
sind im Internet über http://dnb.d-nb.de abrufbar.

Herausgeber und Vertrieb:	Forschungszentrum Jülich GmbH Zentralbibliothek, Verlag 52425 Jülich Tel.: +49 2461 61-5368 Fax: +49 2461 61-6103 zb-publikation@fz-juelich.de www.fz-juelich.de/zb
Umschlaggestaltung:	Grafische Medien, Forschungszentrum Jülich GmbH
Druck:	Grafische Medien, Forschungszentrum Jülich GmbH
Copyright:	Forschungszentrum Jülich 2023

Schriften des Forschungszentrums Jülich
Reihe Allgemeines / General, Band / Volume 9-03

ISSN 1433-5565
ISBN 978-3-95806-711-0

Vollständig frei verfügbar über das Publikationsportal des Forschungszentrums Jülich (JuSER)
unter www.fz-juelich.de/zb/openaccess.

CONTENTS

I. INTRODUCTION

Accelerator-based neutron sources provide a versatile and effective opportunity to improve and spread neutron access in Europe and also a new route for the supply of neutrons to science and industry with leading-edge research infrastructures. The HBS project pushes the performance of such sources to the technological limits by employing state-of-the-art technologies in accelerator development, target and moderator design as well as beam extraction, beam optics and instrumentation. Based on a high current low energy proton accelerator, which produces powerful pulsed beams hitting a metal target (tantalum for HBS) to release a thermal neutron flux comparable to existing medium to high flux reactor sources, a variable suite of neutron instruments and applications can be served.

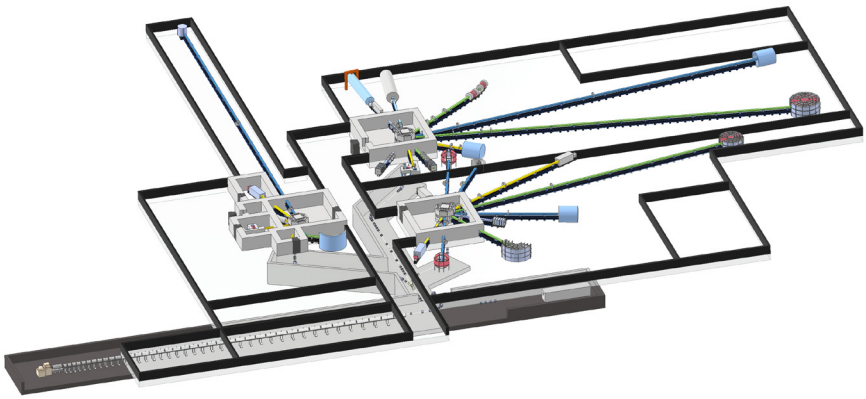

Figure I.1: *General layout of the HBS facility*

Main components of the HBS (Fig. III.1 are

- a dedicated proton accelerator (described in TDR Accelerator) with an optimized energy of 70 MeV and a current of 100 mA that is multiplexed to feed several target stations operated at different frequencies.

- a target – moderator combination (described in TDR Target Stations and Moderators) that offers a pulsed neutron beam at optimal frequency, pulse duration and neutron spectrum to fulfil the needs of the corresponding instruments.

- optimized moderators (described in TDR Target Stations and Moderators) according to the spectral needs of individual instruments.
- a number of instruments at each target station, typically around 6 to 8.

The construction of the buildings, organisation and sustainable operation of the facility are outlined in the TDR Infrastructure and Sustainability. This volume of the TDR series concentrates on the design and description of possible instruments to be operated at the HBS.

II.

DESIGN DRIVERS FOR INSTRUMENTS

The neutron is a unique probe to explore matter and materials. Its features are so attractive that large and expensive facilities have been built around the globe. In particular in Europe, a vivid community of neutron users is established, which is the reason for the scientific success of the worlds strongest neutron source at the ILL, but also of the different medium to high flux national facilities. This user community is now waiting for the next generation high flux facility, the ESS, which has a similar source strength as the ILL today, but boosts the number of usable neutrons at the instruments making use of the pulsed nature of the source. Along a similar line, we present in this TDR our vision for the next generation national neutron source, the High Brilliance Source (HBS) [BE20, GV22]. This source is also pulsed and encodes the energy of the neutron by the time of flight, so one does not need to discard a large number of neutrons by monochromatization. However this pulsed source does not rely on the spallation reaction requiring expensive high energy particle accelerators and heavy and costly shielding, but uses proton beams of less than 100 MeV energy.

The neutron is an analytical probe that can be used to get deep insights into matter and materials. This can be taken literally as the neutron can penetrate matter deeper than most other microscopic probes. It can be used to image large objects, for example running engines or large geological specimen. Studying objects in operando promises a better understanding and, based on that, improvement of the processes inside the studied objects. For the ongoing transformation of our energy system, the high sensitivity of neutrons to elements like hydrogen and lithium is crucial for the improvement of hydrogen storage materials, Li-ion batteries or fuel cells (see II.1). Uniquely, the neutron can also image magnetic areas, e.g in electric drives, which can have an important impact on the evolution of automotive technology.

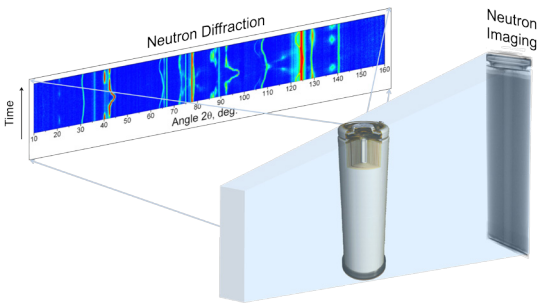

Figure II.1: *Neutron imaging and neutron diffraction pattern of Li-ion battery (Graphic: FRM II / TUM).*

Making use of activation analysis techniques, neutrons provide information about the composition deep in potentially hazardous samples in a non-destructive way. The study of precious and unique pieces of art and archaeology is often only possible with a soft probe such as the neutron to gain

insight about ancient culture and techniques.

With thermal neutrons, researcher can determine the position of atoms in novel compounds to the precision of pm and relate the functional properties to the structural details. Here neutrons come into play, when the contrast conditions of widely available x-rays sources are not sufficient to distinguish elements of similar atomic weight or when light elements such as hydrogen or lithium need to be precisely localised for the understanding of how a technical material works.

But the neutron as a quantum particle probes also the structure and dynamics on microscopic length and time scales. Neutron scattering in the thermal and cold energy range explores correlations in condensed matter from pm to μm and from ps to μs.

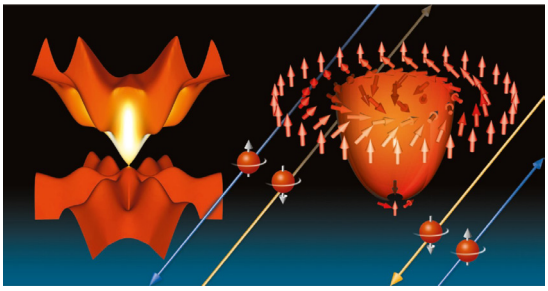

Figure II.2: *Dispersion and spin states in topological materials probed with neutrons.*

The arrangement of atomic spins is crucial for the understanding of both, basic and applied research areas. The quickly emerging field of topological materials or the still unsolved puzzle of high temperature and unconventional superconductivity are only two examples, where neutrons are necessary to solve the spin structures and benchmark new theoretical approaches. The completely understood cross sections, in particular the polarisation resolved ones, give ultimate answers how and in which directions the spins are aligned (see II.2). Only inelastic neutron scattering can be calculated model free from first principles to reveal the temporal evolution of spin systems, which distinguishes it from any other method. The HBS will therefore be equipped with instruments to combine the strength of existing instrumentation from continuous and pulsed sources to provide this unique opportunity to the scientific user community.

In particular for basic research, extreme sample environment conditions lead to the discovery of fascinating phenomena and new states of matter. Also here the neutron properties allow investigations that are not possible with any other probe. The study of the behaviour at lowest temperatures in the mK range is prevented for many microscopic probes, as they interact strongly with the electron cloud of the atoms leading to a substantial heating. The neutron, having only a kinetic energy in the meV range, hardly changes the sample temperature. Therefore, it provides precise information e.g. about quantum phase transitions or frustrated materials, where competing interactions allow ordering only at very low temperatures and subtle variations in the sample temperature change the balance. High pressure or large magnetic fields push many systems into new states, by changing both the atomic and the electronic structure. Neutrons can easily access the samples through bulky cells. However, the reduced sample volumes in these types of sample environment often limit the application of neutron scattering methods. Here the high brightness of the compact HBS moderators allows novel instrument designs that enable the illumination of small volumes with a brightness that exists today only at the high flux sources.

Soft matter conquers an ever widening range of technical applications. Be it light weight carbon materials or organic electronics to name a few, light elements play a important role for the function and the processing of the compounds. These materials are crucial in order to address the challenges of climate change, e.g. to produce lighter and hence more efficient vehicles or to have solar cells with cheaper and cleaner production processes. Here neutrons play a special role due to their sensitivity to light elements and in particular to hydrogen and carbon, oxygen or nitrogen.

Because of all these properties, a strong user community performs research with neutrons. The high sensitivity to light elements, in particular hydrogen, is explored in soft matter research. Structure investigations in polymers, colloids and novel nanostructured materials resolve the relation between the arrangement of atoms and molecules and the functional properties of the material. Using different neutron scattering methods, the hierarchy of structure sizes is elucidated. Protein crystallography determines hydrogen positions within pm precision (see II.3), while SANS shows the arrangement of larger functional groups in a range of hundreds of nm (see II.4).

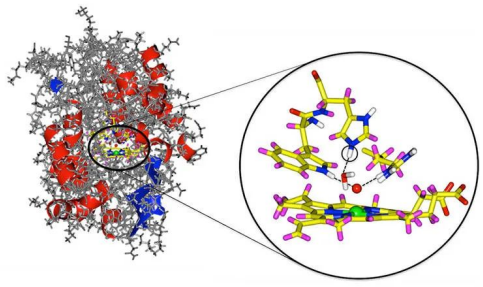

Figure II.3: *Protonation state of the ferryl heme in peroxidase resolved by neutron cryo-crystallography [CGM^{+}14]. (Graphic: A. Ostermann / TUM)*

Technical and biological function is often related to the structure and dynamics of large molecules like DNA, RNA or protein complexes. Small angle neutron scattering is a standard tool to explore soft and biological matter on the length scale from nm to μm. When a macromolecule does its work in a biological or physical process, it is usually related to its motion on a wide range of timescales. They can generally not be explored by a single method but require a large toolbox of techniques. The neutrons explore here the wide region from tens of ps up to slow motions in the μs range. In particular for biological samples it is important, that the neutron beam does not impose radiation damage to the sample.

Today, neutron investigations of biological samples are often limited by the small amount of material available. Here, the HBS with its brilliant beams can illuminate samples with intense beams of mm diameter, thus improving the signal-to-background ratio.

The evolving field of nanoparticles and here in particular magnetic nanoparticles has just begun to gain technical relevance. Neutrons provide the answers about internal structure of these particles and how they can form larger structure leading to emergent phenomena. Often, the nanoparticles are assembled on the surface yielding 2 dimensional structures. But also low dimensional arrangements of small molecules or elements exhibit functionalities that cannot be easily deduced from their bulk behaviour, but are a consequence of the reduced number of neighboring atoms. The reflectivity of neutrons also reveals the information about buried interfaces. And grazing incidence scattering and off-specular scattering are unique methods to explore lateral correlations on technologically important length scales from nm to μm. Typical samples have only a tiny footprint of fractions of a mm in the direction of the illuminating beam. So the compact and pre-collimated high brightness moderators can be

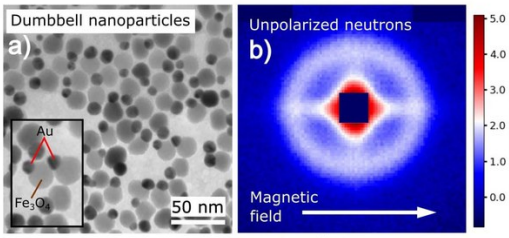

Figure II.4: *2D small angle neutron scattering (SANS) pattern of dumbbell nanoparticles in an applied magnetic field.*

combined with novel neutron optics to limit the illuminated area around the sample more precisely than today to optimize experiments for unprecedented signal-to-noise ratio.

HBS is a novel type of neutron facility which overturns some of the established design criteria, e.g. striving for the highest source strength. Instead, brightness and flexibility are maximized under the constraint of keeping construction and operation cost as low as possible for such a powerful facility. How these goals are achieved is detailed in the other volumes of the TDR and here only briefly reviewed in Chapter III. The chapters V, VI and VII present, how these special properties of the source can be used to enable new science by state-of-the-art instrumentation.

For a large scale user facility, the research is being done by the international community of scientists. Therefore the instrument suite, the need for ancillary equipment and laboratories must be defined by the future users, tailored to the science that can be done on such a source. What is presented in this volume of the TDR is the result of frequent interaction with and feedback from the users, starting with an HBS science case workshop in 2017, followed by several presentations and discussion sessions at conferences, interaction with other facilities and projects through LENS and ELENA [HAB+22], and leading to a series of instrument workshops each one dedicated to a particular instrument class in 2021 and 2022 [GRM+20]. Discussion within the community is continuing, and while the instrument concepts are already rather clearly defined, the need for equipment like sample environment or user laboratories is still evolving together with the scientific applications of neutrons. We envision that in instrumentation and its ancillary equipment users are directly involved e.g. by contributing instrument components or sample environment through the highly successful ErUM funding provided by the German Federal Ministry Of Education. A common process will have to be initiated prior to the construction of the facility to define and prioritize the construction of the instruments with the needs of the communities. Therefore, the reference instrument suite of the HBS facility presented in this TDR provides a "menu" to choose from, not the final layout. The actual realization will depend on concrete interests from all partners and will involve a design-update phase.

III.

TARGET STATION PARAMETERS

III.1 Target Stations

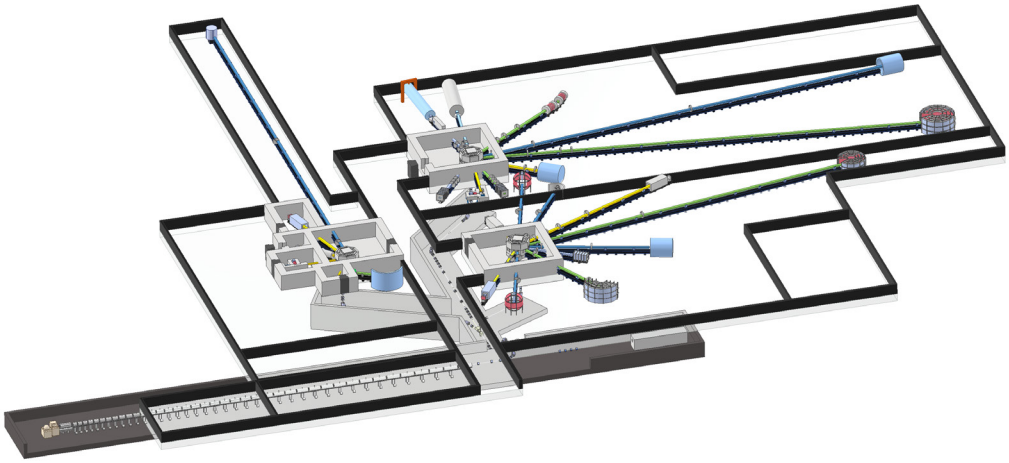

Figure III.1: General layout of the HBS facility

In the reference design, HBS will operate 3 target stations to produce neutrons, which can be operated with different frequencies. Each target-moderator-reflector (TMR) unit is surrounded by a shielding block of about 4 m diameter. Additionally, the target station is surrounded by a wall of 1.4 m thick shielding material, which creates a bunker of about 12 x 12 m^2. Outside the bunker, the radiation level is low enough that people can work there permanently, while the neutron source is in operation. Inside the bunker, this is only possible, when the proton beam is switched off. Therefore, sample positions have to be outside the bunker wall, while components of the beamline (like choppers) can also be inside the bunker. Guides and optical components like slits or mirrors can even be installed inside the target shielding as close as 50 cm from the center. The target stations are positioned outside the center of the bunker to enable different distances between source and wall, and thus different sample and chopper positions (see Fig. III.1.)

Each of these target stations receives the same average proton beam power of 100 kW. We have shown that this beam power can be safely deposited on and handled by a tantalum target. A proton energy of 70 MeV has been chosen to enhance the neutron yield of the target while keeping

the production of fast neutrons low. Thus, HBS minimizes the amount of very heavy shielding and provides a cost efficient accelerator technology. The 100 kW mean target power at 70 MeV proton energy leads to a mean proton current per target station of 1.43 mA.

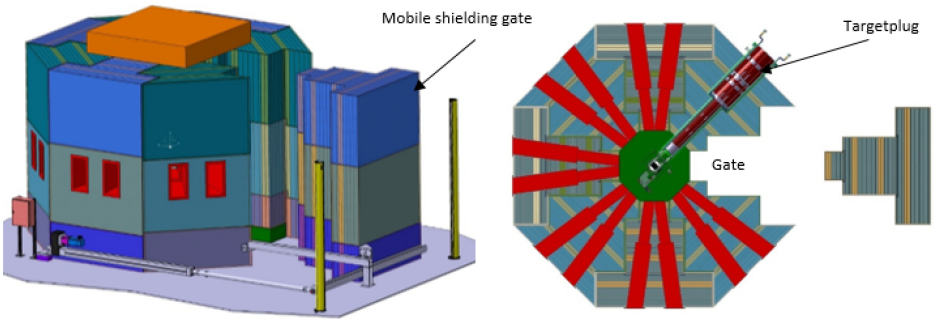

Figure III.2: *Technical drawing of the shielding block in side view (left) and top view (right)*

Following the results of a survey among the developers of the HBS instruments, frequencies of 96 Hz for two target stations and 24 Hz for a third target station and a duty cycle of 1.6% were chosen, yielding a peak current of $\approx$ 90 mA, close to the nominal design limit of the ion source, which will provide up to 100 mA reliably. It should be noted that the accelerator holds the potential to increase the total proton beam power by a factor of 2 and hence the source brightness is limited by the heating power that the target can withstand. So far, we have proven a heat load of 100 kW, but we have not yet reached the point where the target fails.

The two target stations with a repetition rate of 96 Hz (TS-96 and TS-Epi) feature short proton pulses of 167 μs and the one with a repetition rate of 24 Hz (TS-24) a long pulse of 667 μs length. This pulse pattern can be modified dynamically in a similar way as synchrotron radiation sources provide different operation modes. While most instruments will be optimized for a certain combination of pulse length and frequency, one could envision applications receiving a special pulse pattern for some fraction of the operation time. In particular the TS-epi with applications for fast and epithermal neutrons can benefit from this unique feature of the accelerator.

The neutrons produced in the nuclear reaction are slowed down in the water beamstop of the target and in the subsequent water moderator into the thermal energy range (see Fig. III.3). In each target station, there is a common thermal moderator installed, but each instrument can choose its own cold moderator. So far, hydrogen, methane and mesitylene moderators have been developed, built and tested at the JULIC cyclotron.

The target-moderator-reflector (TMR) designs vary between the target stations:

- TS-96 matches the proton pulse length and the neutron lifetime in the thermal moderator. The resulting neutron pulse length of 250 μs (see Fig. III.4) is well suited for applications with modest wavelength resolution requirements for a instrument length between 20 and 40 m without additional pulse shaping. These instrument lengths result in a usable bandwidth of 1 Å$< \Delta\lambda <$ 2 Å, ideally suited for typical diffraction applications. Also direct geometry spectrometers fit to this target station as its repetition rate provides the correct timeframe to record energy transfers of interest.

- TS-24 loads 4 times more protons into an individual pulse. The proton pulse length dominates the FWHM of the time distribution for the moderated neutrons, as shown in the right panel of

Fig. III.4. The target station hosts applications that require low wavelength resolution such as SANS or Spin Echo and applications employing pulse shaping. Among them are in particular powder diffractometers. As a consequence of the pulse shaping, the longest instruments are installed on this target station.

- TS-epi is optimized to provide neutrons with energies above the thermal range. These are in particular used for imaging methods or neutron analytics. In the energy regime of 10 eV and above, the neutron pulse length equals practically the proton pulse length, because the slowing down of the neutrons into the thermal energy range takes about 10 μs in a hydrogen rich materials such as water. We envision that special pulse patterns will be used on this target station for applications using fast or epithermal neutrons, such as PGNAA.

III.2 Moderator Characteristics

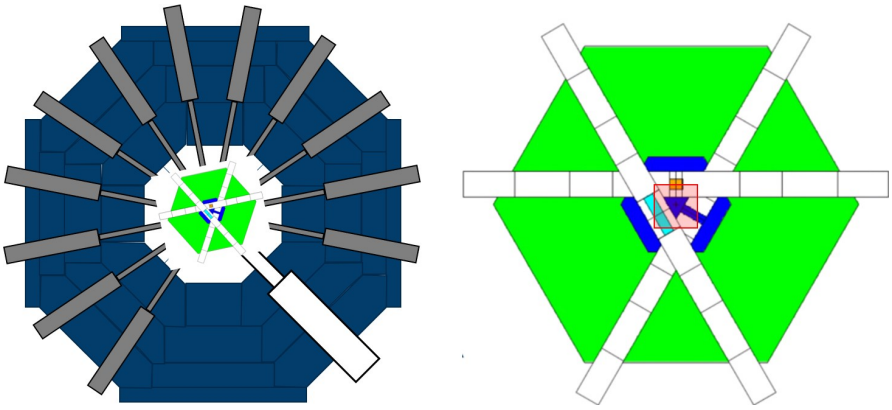

Figure III.3: *Top view of the triangular moderator geometry for 6 beam channels as simulated using MCNP inside the target shielding (left) and enlarged (right). Dark blue areas indicate water volume, cyan the liquid para-hydrogen moderator and the orange volume the solid methane moderator. In red, the target is indicated. The green area is the Pb reflector.*

To obtain moderator characteristics for the instrument simulations presented in this volume of the TDR, simulations of the target-moderator-reflector (TMR) system were performed using the progrem MCNP, vsn. 6 [GJB$^+$12] (see also volume 2 (TMR) of this TDR [BEB$^+$23]). First, a simple, spherical model with the tantalum target (10 x 10 cm^2) feeding only one beam channel was used. Then, a more realistic model of a triangular arrangement of six extraction channels was introduced. The extraction channels were filled with different cylindrical moderators: a liquid parahydrogen moderator of 24 mm diameter, 100 mm length at 20 K (cyan), a solid methane moderator of the same diameter and 40 mm length at 5K (orange) and a water moderator at ambient temperature of 25 mm thickness filling the entire extraction channel of 60 mm diameter (see Fig. III.3).

The events of the MCNP simulation were read and convoluted with the proton pulse to obtain the moderator characteristics like peak shape, wavelength dependent flux etc.: The FWHM neutron pulse length is about 250 µs for the 96 Hz station and 667 µs for the 24 Hz station (see Fig. III.4). The wavelength dependence of the flux could be described by one Maxwellian (thermal moderator) or two Maxwellian functions (cold moderator) and a function describing under-moderated neutrons (as used e.g. for the ESS). The results have been implemented in the instrument simulation programs VITESS [WZSM00] and McStas [LN99].

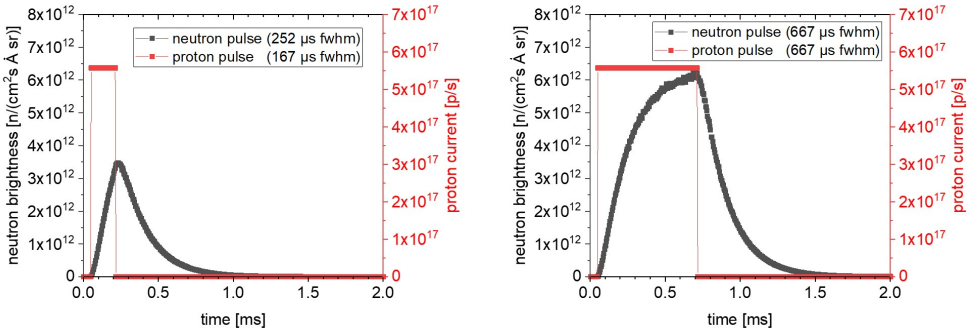

Figure III.4: *Time distribution of neutron pulses (black) of 2 Å wavelength emitted from the cold moderator on a 96 Hz (left) and the 24 Hz target station (right) in a VITESS simulation in comparison with the corresponding proton pulses (red)*

As 12 beam channels have to be supplied with neutrons (see Fig. III.2, a more complicated arrangement was developed in a further approach, which is presented in the Volume Target Stations and Moderators of this technical design report [BEB+23]. Since the TMR development for the different target stations is still ongoing and instrument simulations take time, the results of the MCNP simulations of the triangular geometry, were used for the instrument simulations.

The VITESS program was then used to simulate pulse shapes and brightness of the HBS in comparison with brightness of other sources. Figure III.5 compares the peak brightness emitted from the para hydrogen moderator and from the water moderator to the average/peak brightness of selected continuous and spallation neutron sources. Despite the fact that 1000 times less neutrons are released from the nuclei within the target compared to the other sources, the thermal and cold brightness of the moderators at the HBS reach a similar level. The 1D para-hydrogen moderator profits from the good coupling to the thermal moderator and the large extraction volume for cold neutrons. Therefore cold neutrons leaving the moderator through the top and bottom surfaces of the cylinder

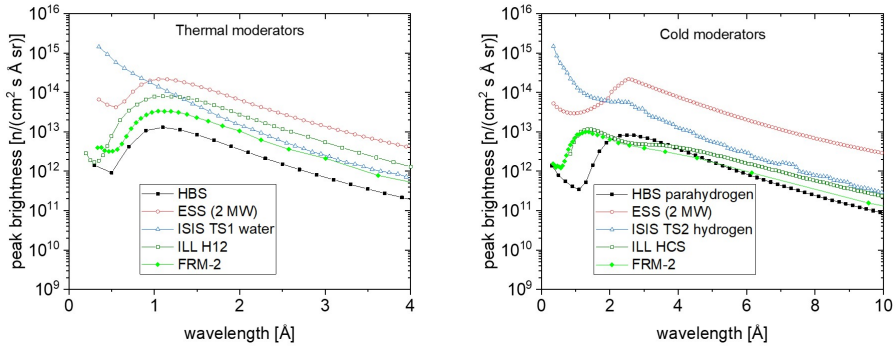

Figure III.5: *Simulated brightness as a function of wavelength of the 24 Hz HBS target station for the thermal (left) and a cold moderator (right) arranged in the triangular moderator geometry (see Fig. III.3) in comparison with simulated brightness values of neutron facilities that exist or are under construction.*

are emitted preferentially into a cone with opening angle of 5° around the surface normal. Both effects together lead to a peak brightness comparable to the average brightness of existing high flux reactor sources. So reactor instruments using time-of-flight would perform comparably at the HBS without further optimization. The following instrumentation sections show, how instruments can be optimized to the special features of this source to provide powerful and versatile spectrometers at the next generation medium power neutron facility.

For the thermal beam channels the situation is less favourable. The moderator-reflector geometries, that have been studied so far, are optimized to feed the cryogenic moderators ideally. The target station for high energy neutrons (Epi) will allow the extraction of thermal and epithermal neutrons from the surfaces with the highest brightness in the respective spectral range. Nevertheless the investigated extraction channels reach a peak brightness only a factor 2.7 below the brightness of the FRM-2 high flux reactor (see Figure III.5 left). The lower thermal peak brightness is compensated by the instruments imaging a virtual source onto the sample with the short distance between moderator and virtual source, which allows the extraction of less collimated beams to increase the intensity at the sample position. Further optimization of the geometry for thermal beamtubes will be done in a design-update process.

IV.

NEUTRON OPTICS AND TRANSPORT

The last decade has seen a tremendous improvement of neutron transport systems triggered by the requirements in particular of the ESS with its very long instruments. Here transport systems that feature a brilliance transfer of 70 % and above are now realized also for instruments that can digest large phase space volumes, e.g. cold spectrometers. The improvement in the supermirror technology today allows coatings which exceed $m = 7$ and also the reflectivity at intermediate coatings, such as $m = 4$, yields values of 0.8, shifting the neutron wavelength, where the brilliance transfer breaks down, to ever shorter limits.

The HBS instrument suite profits extremely from these developments, as the comparably low source strength enables high m-coatings of the supermirrors in close proximity to the moderators, with a minimum distance of 0.4 m. So even for the narrow moderator surfaces of the cylindrical cryogenic moderators with a diameter of 1 - 3 cm, one can extract a neutron beam with a wide collimation $\Delta\phi \leq 5^\circ$ (FWHM) and transport it over long distances.

On the other hand, transport systems have been developed that transport a very well defined phase space volume, which illuminate basically only the sample and not any sample environment to optimize the signal-to-noise ratio rather than the flux at the sample position. At HBS this approach can be pushed to the limits, as the reduced production of fast neutrons compared to both, spallation and reactor sources holds the promise to reach new levels of signal-to-noise ratio with intensities that are similar to some of the best existing instruments.

The Selene concept, applied at the ESS reflectometer ESTIA [GSS16] and established already at the SINQ instrument AMOR [KBFS18], represents such a novel transport system. It employs a virtual source close to the moderator and then transports only the requested beam collimation: The combination of two confocal ellipses corrects the Koma aberration and the (virtual) source is imaged with a very high quality to the sample position, if the source is small and only the middle half of the ellipse is used. The concept is perfectly suited to provide beam spots < 2 mm normal to the elliptic mirror surface. Typical applications include reflectometers with very narrow footprint on the sample or diffractometers for small sample, e.g. protein single crystals or single crystals in pressure cells.

Limiting the transported phase space close to the neutron source reduces also the required beamline shielding. As also the primary (fast) neutron source strength is 50 times weaker as compared to reactor sources, the shielding can be significantly lighter as for existing instrumentation. This feature can be used to have flexible experimental setups, that can be adapted between two facility cycles similar to the use of different end stations at synchrotron radiation facilities. Each instrument will be equipped with two shutters, a neutron beam shutter, that stops all neutrons within the beamline to allow access to the experimental area while the target station is operating and a Gamma-beam shutter as part of the target shielding that absorbs radiation from the activated target and permits access to the bunker area, when the target station does not receive protons.

As for any pulsed neutron source, choppers are critical components for any application requiring high resolution. This is even more true for the HBS, as the comparably long proton pulse provides a wavelength independent pulse length, which is defined by the diffusion and absorption properties of the moderator/reflector assembly and the proton pulse length. As mentioned before, the HBS instruments profit from the short distance between the moderators and the first chopper assembly $L_1 \approx 2$ m. This allows high resolution instruments with a total length $L_{\mathrm{tot}} < 100$ m. Fast counter rotating disc chopper assemblies can realize pulse length down to 20 μs, which is sufficient to cover the resolution requirements of the instruments. Spinning frequencies below 300 Hz are well within the reach of present magnetic bearings and drives, but any improvement on this side results immediately in an improved performance of the instruments. Here, HBS will become a technology driver with an impact for the entire neutron community in Europe and world wide.

Novel indirect geometry spectrometer concepts promise to combine the best of the worlds of three axis spectroscopy (TAS) and time-of-flight spectroscopy. Using the time-of-flight to decode the initial neutron energy, they can digest a large fraction of the moderator spectrum and hence achieve extremely high sample fluxes. The crystal analyzers combined with position sensitive detectors have been optimized recently for small samples and increased acceptance without deteriorating the energy resolution making use of prismatic focusing. These concepts require only a small bright neutron source and modest time-of-flight resolution, as the required resolution is easily realized even for intermediate length instruments, and are perfectly suited for the HBS.

HBS will also profit from and drive the development of large focusing monochromators, which are nowadays mainly used at reactor neutron sources. Due to the lower radiological constraints, monochromators can be installed at rather short distance from the moderators having an undisturbed view on a large solid angle. In particular for higher neutron energies, which cannot be chopped easily with the requested time resolution and absorption of the chopper, they offer a valid option following the development towards the PANTHER [FRMM22] hybrid time-of-flight spectrometer recently commissioned at the ILL.

Most of the instruments at HBS will be equipped with polarization analysis. Typically this is considered a very flux hungry application, but it should be noted that it makes the result of an experiment more significant. As an example, if we consider a typical QENS spectrum from a sample with a spin-incoherent scatterer: The spin-flip channel contains only the incoherent signal of interest, while the non-spin-flip channel counts additionally the coherent scattering, both from the sample but also from any sample environment that cannot be discriminated by other means. So the signal in the spin-flip channel will be reduced by $2/3\times$ efficiency of the PA, but the noise will be reduced by the flipping ratio. So one can expect a potential to improve the signal-to-noise ratio by at least one order of magnitude.

Polarized neutrons are particularly foreseen at all large scale structure instruments (SANS, Reflectometry), 2 diffractometers, 2 spectrometers, an imaging station and the test beamline. Moreover, different instruments will be equipped with different types of neutron spin-filters: supermirrors, wide-angle supermirror analyzers, He3 spin-filters for polarization and analysis. This ambitious plan requires a dedicated neutron polarization program that will cover all necessary activities in designing, preparation, commissioning and maintenance of the variety of neutron polarization devices. This program builds on the expertise of JCNS as available at the JCNS instruments operated at MLZ.

To fulfil special demands on a sample environment for user experiments, HBS plans to have state-of-the-art equipment and to provide expertise in a wide area of applications: magnetic fields, low and high temperatures, high pressure, vacuum, electronics, automated control and beyond (furnaces, levitation devices, stop flow, humidity cells etc.) for particular experimental needs. Efforts in supporting the users with reliable and stable operating sample environment will guarantee successful realization of a beamtime. Additionally, the HBS facility will provide special sample preparation, sample handling and sample pre-characterization laboratories for the users. The supplementary laboratories

will be equipped with basic tools (e.g. gloveboxes, centrifuges, rheometers, baths, refrigerators) as well as with neutron scattering specific requirements (e.g. a deuteration facility). The HBS will here rely strongly on the expertise and support by the JCNS sample environment and deuteration groups.

V.

INSTRUMENTATION FOR STRUCTURE DETERMINATION

Diffraction is one of the key techniques to study matter. It allows the determination of the atomic structure of crystalline materials, but also of the local structure in amorphous materials and liquids. Due to the ease of access on a laboratory scale, X-ray diffraction is usually the first method used to approach the determination of the structure of new materials. However, for many complex topical materials, X-rays alone do not provide the answer. Neutron diffraction gives complementary and unrivalled information. Firstly, it allows determining the positions of light atoms, especially hydrogen, in the vicinity of heavier ones and distinguishing atoms of similar atomic number. Secondly, it enables determining magnetic structures because of their interaction with the magnetic moments of the neutrons. Accordingly, the main applications of neutron diffraction are magnetic materials and superconductors, where the magnetic interaction is crucial, as well as biomolecules and energy materials, where the hydrogen atoms or light atoms as Li or Na play essential roles.

The diffractometers at the HBS naturally use the time-of-flight method. To resolve the details of the units cells to a precision of pm requires neutrons in the wavelength range from 1 Å to 5 Å with a collimation of approx. 1°. Therefore the cold para hydrogen moderators and the thermal moderators are ideally suited to feed the instruments with a bright spectrum. Compact instruments at the high repetition rate target station can use a sufficiently wide bandwidth and the neutron pulse length of the moderators provide the required time resolution for single crystal and diffuse scattering spectrometers. In particular the measurement of small samples profit from the bright small area moderators. To distinguish lattice spacings to a high precision pulse shaping and wavelength frame multiplication are employed.

For the HBS instrument reference suite, 6 diffractometers are suggested : a Disordered Materials Diffractometer (DMD) for Pair-Distribution-Function (PDF) measurements on liquids, amorphous and nano-materials, a single crystal diffractometer (MMD) for small single crystal samples (especially macro-molecules), a Polarized Diffuse Neutron Spectrometer (PDNS) for TOF-Laue measurements of magnetic samples, an instrument for Diffuse Elastic Neutron Scattering (DENS) for magnetic materials using a pseudo-statistical chopper, a Thermal Powder Diffractometer (TPD) for high resolution or high intensity powder diffraction, and an Engineering Diffractometer for texture, strain and stress analysis (of engineering materials) (Table VIII.1).

Wavelength band and resolution

The wavelength band is determined by the period T_{src} of the source and the total instrument length L. The maximal bandwidth $\Delta\lambda$ that can be evaluated at the detector has a time-of-flight range ΔT

equal to the source period T_{src}

$$\Delta\lambda = \frac{h}{m_n} T_{\mathrm{src}}/L = 3956 \text{ m Å/s } T_{\mathrm{src}}/L \tag{V.1}$$

The d-spacing resolution $\delta d/d$ has (apart from a path length variation δL that is usually negligible) two contributions: an uncertainty $\delta\theta$ in scattering angle and a wavelength spread $\delta\lambda$. The uncertainty in scattering angle is caused by variations in the flight direction of the incoming neutrons $\delta\theta_{\mathrm{in}}$ and the angular variation resulting from sample and detector cell size $\delta\theta_{\mathrm{out}}$. The wavelength spread is given by the uncertainty in time-of-flight T caused by the neutron pulse length τ_{pulse}:

$$\frac{\delta\lambda}{\lambda} = \frac{\tau_{\mathrm{pulse}}}{T} = \frac{\tau_{\mathrm{pulse}} \frac{h}{m_n}}{L\lambda} \tag{V.2}$$

The total resolution is then given by

$$\frac{\delta d}{d} = \sqrt{(\frac{\delta\lambda}{\lambda})^2 + (\frac{\delta L}{L})^2 + (\cot\theta \frac{\delta\theta}{\theta})^2} \tag{V.3}$$

Pulse shaping and Wavelength frame multiplication (WFM)

If the wavelength resolution is not sufficient, it can be improved by cutting out a part of the pulse using choppers, which let neutrons pass only for a short time. This serves as the new, virtual source. As this so-called pulse shaping chopper, can only be positioned in a distance L_{chop} from the source, neutrons will have a different flight time from real to virtual source depending on their wavelength. Slow neutrons can only pass, it they are emitted in the beginning of the pulse, fast neutrons will come from the end of the pulse. As a consequence, the chopper will not only shorten the pulse length, but also limit the wavelength band of neutrons that can pass. The bandwidth can be calculated using equation V.1 for the distance chopper distance L_{chop}, which is 2 m at the HBS giving a bandwidth 1.32 Å for the 24 Hz target station (τ_{pulse} = 0.67 ms) and 0.495 Å for the 96 Hz target station (τ_{pulse} = 0.25 ms).

The further away from the virtual source, the larger the time difference between shortest and longest wavelengths in the pulse. Ideally, a total instrument length L_{tot} should be chosen in a way that this time difference is just as large as the source period. A calculation yields that the bandwidth is determined by the ratio α of the pulse length to the period of the source cycle, the so-called duty cycle

$$\alpha = \frac{\tau_{\mathrm{pulse}}}{T_{\mathrm{src}}} \tag{V.4}$$

The 'natural' instrument length is then given by

$$L_{\mathrm{tot}} = L_{\mathrm{chop}} + \frac{L_{\mathrm{chop}}}{\alpha} \tag{V.5}$$

A broader bandwidth can be obtained by the so-called 'wavelength frame multiplication' (WFM), where N pulses are generated by N succeeding openings of the pulse chopper, separated in time by roughly the pulse length. Then the length, where the time difference is as large as the source period, is given by

$$L_{\mathrm{tot}} = L_{\mathrm{chop}} + \frac{L_{\mathrm{chop}}}{N\alpha} \tag{V.6}$$

For HBS, L_{chop} = 2 m and α = 1.6% giving $L_{\mathrm{tot}} = (2 + 125/N)$ m.

V.1 Disordered Materials Diffraction (DMD)

Mikhail Feygenson, Zhanwen Ma, Klaus Lieutenant

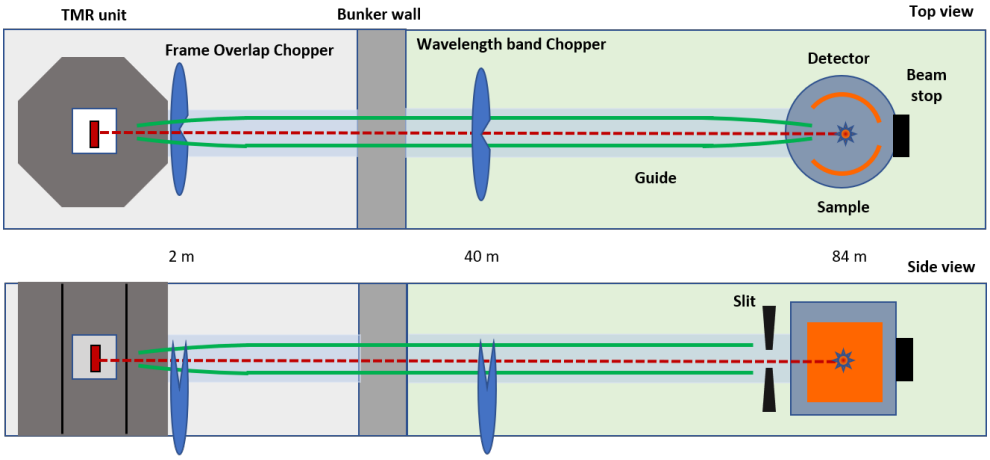

Figure V.1: *Layout of DMD instrument, showing top and side views.*

The Disordered Materials Diffractometer (DMD) will be used for pair-distribution function (PDF) measurements of crystalline, liquids, amorphous and nanomaterials. It uses short wavelengths of about 0.1 to 0.6 Å to reach high Q values of more than 100 $Å^{-1}$. Therefore, it will be placed at the 3rd target station that will offer a LiF moderator with increased flux in the epithermal range (cf. Table VIII.1). For sufficient resolution, a length of 85 m is planned. Calculations and virtual experiments show the competitiveness to existing and planned instruments.

V.1.1 Introduction

PDF measurements are used for studies of the local crystal structure of materials. In the crystalline materials, the information about local crystal structure is buried underneath strong Bragg peaks in the form of a weak diffuse scattering. This scattering intensity is not modelled by the conventional Rietveld refinement method and usually treated as a background. When the PDF method is used the entire scattering pattern is Fourier transformed and both weak diffuse and strong Bragg scattering intensities are simultaneously modelled in the real space. Thus, it is often dubbed as a total scattering method.

The PDF studies of the local crystal structure are particularly helpful for nanocrystalline materials. They are prone to short-range distortions and dislocations of their crystal structure due to a large number of atoms on the surface. Those atoms with a reduced coordination number often drive structural and magnetic properties of nanoparticles. Large surface of nanoparticles can be decorated with a variety of surfactants for hyperthermia treatments and targeted drug-delivery. In battery materials, nanoscaled anode and cathode materials offer much higher capacities and recharging rates as compared to their bulk counterparts. Yet, just like in powder diffraction, understanding of the local crystal structure is the key for enabling real-life applications of nanoscaled materials. PDF studies are also applicable for gases and liquids. For example, the isotope substitution PDF experiments are needed for understanding the hydrogen bonding mechanisms, solid-liquid interface in the energy storage materials, phase transitions in the bulk-metallic glasses at elevated temperatures and

pressure-induced structural changes in glasses.

The number of PDF studies of materials using in-situ or in-operando conditions is steadily increasing. In these studies, the local crystal structure is constantly monitored as a function of external pressure, electric and magnetic fields and so on. Enough space around the sample position will enable users to bring their own highly customised and bulky sample environment for in-situ PDF studies. The majority of such experiments are being carried out at synchrotron x-ray beamlines, which allow a relatively easy access to the sample position. The design of DMD is taking full advantage of the reduced shielding requirements at HBS by allowing an easy access to the sample position with a variety of sample environment.

The DMD instrument uses the entire neutron pulse, without a need for a complicated chopper array besides the frame overlap and wavelength band chopper. Q-resolution is moderate and only limited information about the average crystal structure could be obtained from the Rietveld refinements. The advantage of the DMD instrument is an access to Q-values up to 100 $Å^{-1}$, which is used at large-scale neutron spallation sources of today. Here neutrons have an advantage over X-rays in providing information up to very high momentum transfers. This is due to the fact that nuclear scattering does not suffer from the form factor decay of X-rays. Another advantage of DMD is a constant d-resolution over a wide range of scattering angles. The position sensitivity of detectors will provide an additional capability for the TOF Laue single-crystal diffraction. In the future, we envision using polarised neutrons to discriminate a weak magnetic scattering for magnetic PDF studies.

V.1.2 Layout

The layout of the instrument is shown in Fig. V.1. The design is rather straight forward with the direct line-of-sign to the moderator. Only two choppers are used to avoid the frame overlap and to set the wavelength band. Detailed neutron beam extraction and transport are reported in [MLV+21]. VITESS [ZLNF14] studies have demonstrated that beam transport on the sample position strongly depends on the guide shape. The optimum performance for DMD is achieved with $\frac{1}{4}$ ballistic guide with both converging and diverging parts being elliptical with m=5 coating. It also offers additional cost reductions as compared to a truly elliptical guide.

Instrument parameters	
Target station	TS-epi, 96 Hz
Moderator	Water
Moderator-to-sample distance	84 m
Sample-to-detector distance	1 m
Detector range	$10^\circ < 2\theta < 140^\circ$
Wavelength band	0.48 Å, standard: 0.10 Å $< \lambda < 0.58$ Å
Wavelength resolution	$0.015 < \delta\lambda/\lambda < 0.039$
Q-range	1.9 $Å^{-1} < Q <$ 118 $Å^{-1}$
d-spacing resolution	$0.015 < \delta d/d < 0.125$
Expected flux	about 10^7 n cm^{-2} s^{-1} for 1.1° FWHM divergence

Table V.1: *Instrument parameters for the diffractometer for disordered materials*

The instrument is optimised for a sample size of 1 x 1 cm^2. Samples with smaller dimensions will be

possible to measure, after additional alignment in the beam. DMD will be equipped with volume detectors based on ^{10}B absorbing cathode layers in a multi-wire gas detection chamber. This detection technology is relatively new and currently being built for the DREAM [SVL^{+}16], MAGiC and HEIMDAL [HLH^{+}16] instruments at European Spallation Source [AAJ^{+}20]. The detector consists of several cathode layers covered with 1 μm ^{10}B, which are inclined in order to effectively increase absorption. The concept is known as the "Jalousie" type detector. The detector coverage will be similar to a classic neutron powder diffractometers, such as D20 at ILL. Detectors will cover $10^\circ < 2\theta < 140^\circ$. The height of the detector would be about 200 cm at most.

V.1.3 Performance

A flux estimation is difficult, because the target-moderator-reflector (TMR) unit of the target station for epithermal neutrons (TS-epi) is still under development. We expect a flux of at least 10^7 n cm^{-2} s^{-1} for 1.1° divergence. This flux is comparable with a flagship neutron diffractometer D20 at ILL. The combination of such high-flux, 2D position-sensitive detectors and easy access to the sample position will enable fast in-operando PDF measurements.

There are two parameters that are important for experimental PDF Q_{max} and Q_{damp}. Q_{max} is the value used in the Fourier transformation of the measured powder diffraction data to obtain PDF. It is inversely proportional to the PDF resolution in the real-space: $\Delta r = \pi/Q_{max}$. The DMD instrument allows to reach up to Q_{max}= 100 Å^{-1}. However, in the real experiment Q_{max} is chosen as a sensibly compromise between counting time and level of noise at given Q_{max}. Having Q_{max}= 31.1 Å^{-1}, results in 0.1 Å resolution in the real-space, which is more then enough for the majority of the samples.

Q_{damp} is the parameter describing the dampening of the experimental PDF at higher values of r. For high Q-resolution neutron diffraction instruments Q_{damp} is around 0.006 - 0.028, allowing to resolve PDF signal above 500 Å. This is a cross-over range between local and averaged crystal structures and it is helpful for studies of local disorder in the bulk materials. For synchrotron x-ray PDF instruments Q_{damp} is usually lower and equal to 0.028 - 0.058 and experimental PDF is vanishing at about r = 60 Å. The preliminary simulations of the DMD instrument with VITESS showed that Q_{damp} = 0.05. It is higher than for other neutron PDF instruments at neutron spallation source, but it is very well suited for detailed studies of the local crystal structure of glasses, liquids and nanocrystalline materials.

V.1.4 Sample environment

We aim for a very open access to the sample position in order to make it possible to use a variety of customised sample environment. Besides the standard sample environment available at other facilities (Orange-type cryostat and ILL-type vacuum furnace), we envision a design of the instrument that will allow accommodating the following equipment:

- Linear sample changer with cryostream (90 – 500 K) will allow measurements of very small samples in quartz capillaries. It will offer an intermediate temperature range which overlaps with ILL furnace and Orange cryostat. It has a very simple and cost-effective design.
- Diamond anvil cells (DAC) of up to 90 GPa. The pressure cells have to be custom designed for a specific instrument. If small enough, they can be placed inside the cryostat.
- Paris-Edinburgh cells (25 GPa). They can handle larger samples, as compared to DACs
- Electrochemical cell for in-situ battery studies. They have to be specifically designed for the instrument.

- Gas-Handling System will allow in-situ studies of chemical reactions, absorption and oxidation processes.
- Aerodynamic levitator (300 – 3273 K) can offer container-less measurements at elevated temperatures.

V.1.5 Requirements

DMD is a high-throughput instrument capable of supporting operations of a variety of sample environments. In order to reduce the turnaround between experiments, the floor space around the experimental cave has to be reserved for preparation of the next experiment. Examples include precooling of the sample in cryostat, charging electrochemical cell or installing the sample in a pressure cell. Thus, utilities outside of the experimental cave have to include cooling water, helium gas and liquid helium recovery system. We will also require additional gas recovery system for detectors.

Reliable and robust software will be required to support the autoreduction of the experimental data. It will have to be user friendly and it will have to address the needs of the powder, PDF and high-pressure communities. This development has to be a collaborative effort with other large-scale facilities, like European Spallation Source. Common software for data reduction and visualisation can reduce significantly a learning curve for a user.

V.2 Thermal Powder Diffraction (TPD)

Klaus Lieutenant, Andreas Houben, Yannick Meinerzhagen

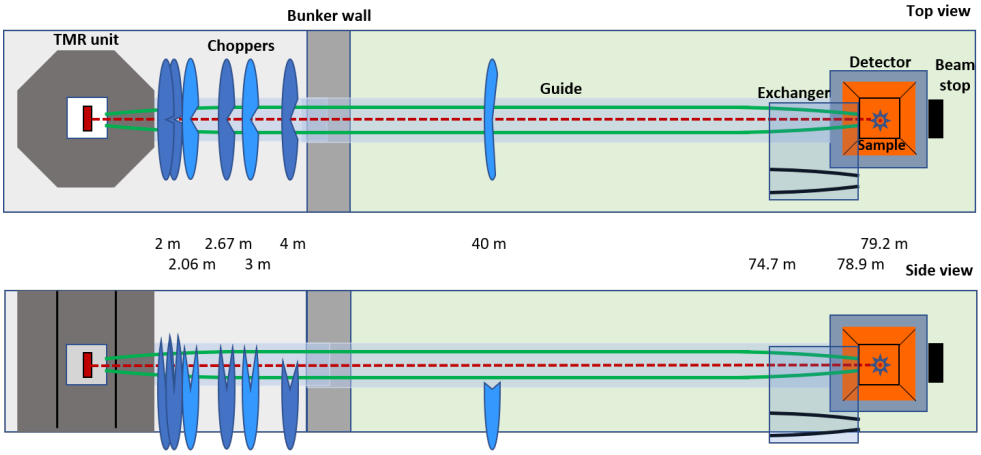

Figure V.2: *Layout of the Thermal Powder Diffractometer (TPD). High speed choppers are shown in dark blue (cf. Table V.3 and Fig. V.3)., The black guide section indicates the absorbing nose for the high resolution set-up.*

V.2.1 Motivation for the Thermal Powder Diffractometer

This instrument is supposed to be the standard instrument for powder diffraction, a method that is widely used at all neutron facilities in a large variety of scientific fields, because structure determination is the first thing to do, before the results of other techniques can be understood. Applications comprise energy materials (e.g. batteries, hydrogen storage materials), magnetic materials (e.g. superconductors), nano-particles and various other kinds of novel materials.

To be able to measure sufficiently small d-spacings (of inorganic samples), a minimal wavelength of 0.6 Å is foreseen and a bandwidth of 1.5 to 2.5 Å is desirable for a TOF diffractometer, since a large maximal wavelength enables measuring large unit cells and gives high resolution.

The length of an HBS instrument should not exceed 80 m to limit the costs for the instrument halls. This sets a limit to the achievable resolution, if the whole pulse is used: with an estimated neutron pulse length τ_{pulse} of 250 µs at the 96 Hz station, the wavelength resolution of the minimum wavelength of 0.6 Å is 2.06% according to equation V.2; (for the 667 µs long pulse of the 24 Hz station it is 5.50%). In many cases, this will not be sufficient to resolve the diffraction peaks. Therefore, pulse shaping choppers will be included to allow reducing the pulse length in a wide range. The goal is to achieve a resolution of $\delta d/d = 10^{-3}$ for 1.5 Å wavelength. On the other hand, there is more and more interest in time-resolved measurements, where a special part of the diffraction pattern is chosen to study a transition. This does usually not require high resolution, but high intensity so that the whole pulse will be used. As state of the art beam transport systems achieve a brilliance transfer of up to 80% even over distances of 80 m, this gives a high flux at the sample for these measurements. A large detector coverage will be realized on this instrument to achieve short measuring times, improve data evaluation and enable single crystal measurements in the thermal range on this instrument.

V.2.2 Instrument Layout

V.2.2.1 Target station, moderators, overall design

Pulse shaping creates a virtual source in a distance from the moderator, which is fed by the pulse at the moderator. As the s-t-diagram shown in Fig. V.3 illustrates, the wavelength range of neutrons passing through the opening of the pulse shaping choppers is limited by the pulse length and the distance from moderator to pulse shaping choppers. The highest bandwidth is achieved by a long pulse and a short distance. As installing a chopper in the TMR shielding is not practical, the shortest distance is about 2 m. Together with the duty cycle, this determines the ideal detector distance, where the whole period of the source frequency is filled by neutrons of different wavelengths (cf. Fig. V.3). Applying equation V.5 to calculate this length yields 127 m for the chosen duty cycle of 1.6%, which exceeds the maximum length of 80 m. Reducing the length to 80 m means that the usable wavelength band is smaller than the possible one. The solution is to use a second wavelength frame by installing choppers with 2 apertures, the first for the short wavelengths (1st sub-frame) and the second for the long wavelength (2nd sub-frame). According to equation V.6, the whole period can now be filled at a distance of 64.5 m giving a bandwidth of 2.56 Å. As this is more than needed and achieving a good resolution is still the main goal, it is preferable to choose the maximum instrument length of 80 m, which gives 2.06 Å bandwidth. It has the additional advantage that only the central part of the pulse will be used, where the intensity is high. As the 24 Hz target yields a higher brightness than the 96 Hz target stations (see Fig. III.4), this target station is chosen.

To get the whole diffraction pattern with one setting, a large detector coverage will be needed. As a TOF instrument does not have a distinguished direction perpendicular to the beam direction, a cylindrical detector geometry as used for POWTEX@MLZ [HSBD12] or DREAM@ESS [SVL+16] is the natural choice.

As the HBS source does not produce particles of more than 70 MeV energy and guide cross-sections are much smaller than on existing neutron sources, the radiation background at sample and detector will be much lower. Therefore, getting out of direct line of sight seems not to be necessary for a long instrument like this. However, the guide will be designed in a way that this can be included if it should turn out to be necessary (see section 2.2.2).

Instrument parameters	
Target station	TS-24
Moderator	Water
Moderator-to-sample distance	79.2 m
Sample-to-detector distance	0.8 m
Wavelength band	2.06 Å, typical 0.62 Å $< \lambda <$ 2.68 Å
Resolution	variable by pulse shaping
Elliptic-ballistic guide	1/4 elliptic, m=6 — 1/2 straight, m=2 — 1/4 elliptic, m=4 to m=6
Detector range and coverage	$10^\circ < 2\theta < 170^\circ$ 5.71 - 10.15 sr coverage
d-spacing range	0.22 Å$< d <$ 7.1 Å

Table V.2: Instrument parameters of the Thermal Powder Diffractometer

V.2.2.2 Beam extraction and transport

The chosen wavelength range of 0.6 to 2.7 Å requires thermal neutrons, but above about 1.75 Å the cold source delivers a higher brightness than the thermal source (see Fig. III.5). Therefore, a

bi-spectral beam extraction system was tested with the guide pointing to the thermal ring around the cold moderator (see Fig. III.3), and the neutrons from the cold source being reflected by a supermirror stack into the guide. As the simulation showed that the overall performance is worse, the thermal moderator was used.

The HBS moderators are small compared to those at existing sources. This can be compensated by a small distance between moderator and guide, which enables to have a large phase space in the guide system. Therefore the beginning of the guide was set to the minimum possible value of 40 cm. Preliminary simulations showed high brilliance transfer for HiCANS sources over long distances both for elliptical guides and ballistic-elliptical guides consisting of a diverging elliptical section (ending at its maximal cross section), a section of constant cross-section and a converging elliptical section (starting from its maximal cross section). This solution avoids kinks in the cross-section profile along the guide, which cause gaps in the divergence distribution. An analysis of different guide installed at HBS showed that a ballistic-elliptic guide using a forth of the length for the elliptical parts gives the same performance as a completely elliptical shape [MLV+21]. This solution was chosen, because it offers the possibility to get out of direct line of sight if needed. The guide widens from 1.52x1.52 cm² (at 0.4 m) to 6x6 cm² (at 19.8 m) using a coating of m=6, is constant up to 59.4 m (m=2) and narrows down to 1.04x1.04 cm² 30 cm from the sample (m=4,5,6). One or two of the converging sections can be made exchangeable by absorbing sections.

A straight beamline gives the best beam profile in terms of symmetric spatial and divergence profile (see Fig. V.5). But this also means that it does not avoid direct line of sight from moderator to sample and detector. At the moment, we assume that this will not cause problems for this instrument, because of the long distance between source and sample giving a small solid angle for high energetic particles, the small guide cross-section that reduces the gaps in the shielding to several square cm and the relatively low maximum particle energy of 70 MeV in the whole system. However, if it will be necessary to get out of direct line of sight, a kink will be included in the 40 m long straight part using one of the several ideas suggested earlier, e.g. in [ZNL14].

V.2.2.3 Chopper system

The goal is to achieve a resolution of 10^{-3} in $\Delta d/d$ for 1.5 Å in backscattering direction (agreement of the HBS diffraction group, 9 - 10 May 2022, Garching). Given a total instrument length of 80 m, a detector resolution of 0.47 deg and 170 deg maximal detector angle, this can be reached by pulses of 26 µs for the first, 52 µs for the second sub-frame and an incoming FWHM divergence matching the detector resolution, which results in a resolution of about 0.6% for 90 deg.

Apart from this high-resolution option and the set-up using the whole pulse, an option for medium resolution measurements using pulses of 100 µs and 200 µs is simulated, which gives a resolution of 0.33% for 170 deg and 0.69% for 90 deg for a wavelength of 1.5 Å. For both, medium and high-resolution options, the pulses of the second sub-frame are twice as long as those of the first sub-frame, because the average wavelength of the second sub-frame is about twice as large as that of the first one - 2.2 Å compared to 1.1 Å - resulting in a similar resolution in the whole wavelength band.

The pulse shaping choppers create two pulses per period, one for each sub-frame. One pair of chopper windows is built in for the high resolution pulses (26 and 52 µs) and a second pair for the mediums resolution measurements (100 and 200 µs). Their rotational frequencies can only be multiples of the source frequency (24 Hz = 1440 rpm), because they need to have the same phase (relative to source and wavelength band chopper) for each pulse. To reach pulse lengths of 26 and 52 µs resp., fast rotating choppers are needed. Large windows at higher speed are more efficient than small window on slower choppers, as their half shadow time is smaller. On the other hand, close to the technical limit of 20'000 rpm choppers tend to break. Therefore, 10 x 1440 rpm = 14400

rpm seems to be a good compromise. To prevent further pulses to get into the system, a 3rd chopper running with the frequency of the source is added that opens only during the first and second pulse. All chopper parameters are listed in Table V.3

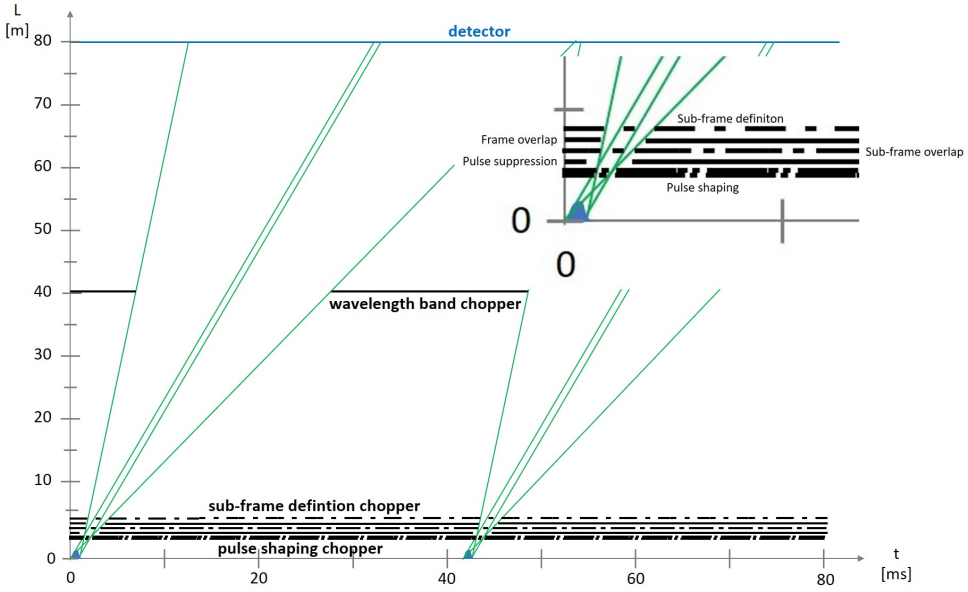

Figure V.3: *Space-time diagram of the Thermal Powder Diffractometer of the HBS. The inset is a zoom into the range below 10 m and 15 ms*

A wavelength band chopper will be positioned half way between virtual source and detector and have an aperture of somewhat less than 180°. It will run with the frequency of the source (24 Hz) and define the wavelength band. The standard setting will be 0.6 - 2.7 Å, but depending on the application the band can be shifted to shorter or longer wavelengths by simply varying the phase relative to the source. Choosing 160 deg reduces the frame to about 41 ms, thus separating the frames of succeeding pulses generated every 41.7 ms.

Two types of frame overlap choppers are needed for the chopper system. One is needed to suppress overlap of the frames, i.e. to prevent long wavelength neutrons of the previous pulses to pass through the chopper system (FO choppers). The other type is used to prevent neutrons from switching the sub-frame, i.e. passing through the first chopper window and arriving in the second sub-frame and vice versa (SFO choppers). The former ones run with the frequency of the source and can be placed at any position. As a distance of 1.5 times the distance of the pulse shaping choppers has turned out to be a good solution, they are placed 3 m from the source. The positioning of the sub-frame overlap choppers has to consider that frequency is a function of the position and must be a multiple of the the source frequency (cf. Fig. V.3). Following a procedure described earlier [LM06], positions and apertures for the sub-frame definition and sub-frame overlap chopper were calculated. Starting with calculated widths of the chopper windows, they were reduced until a separation of the sub-frames in time was obtained (cf. Fig. V.9). A detailed analysis may show that one of the frame overlap choppers is not needed, if ideal positions are found for the other choppers.

Chopper parameters						
function	no	position [m]	speed [rpm]	window	position [deg]	width [deg]
pulse shaping	1a	2.000	14400	1	0.0	4.71
				2	-45.0	6.95
				3	-120.0	11.10
				4	-165.0	19.74
pulse shaping	1b	2.012	-14400	1	0.0	4.71
				2	45.0	6.95
				3	-120.0	11.10
				4	-75.0	19.74
pulse suppress	2	2.060	1440		0.0	17.40
sub-frame overlap	3	2.667	14400	1	0.0	22.00
				2	-60.0	26.30
frame overlap	4	3.000	1440		0.0	22.20
sub-frame definition	5	4.000	14400	1	0.0	37.00
				2	-90.0	37.00
				3	180.0	28.00
				4	90.0	28.00
wavelength band	6	40.000	1440		0.0	160.00

Table V.3: *Parameters of the chopper system for the Thermal Powder Diffractometer of the HBS*

V.2.2.4 Sample and detector

Diffractometers on continuous sources using a monochromator have a limited solid angle where the resolution is good - on one side of the sample not too far from the equatorial plane, which limits the detector solid angle to a small fraction of 4π. In contrast, the resolution of a time-of-flight diffractometer does not depend on the azimuth angle ϕ. This allows using a large detector area yielding the whole diffraction pattern in one setting and high count rates and allows using the instrument for single crystal diffraction, where the whole TOF-Laue diagram can also be obtained in one setting. One example for such a detector is the detector [MHH^{+}14] built for the POWTEX diffractometer [HSBD12], which is currently installed at the FRM-II reactor in Garching. It uses a 2θ range from 10 to 170 deg and 270 deg in ϕ resulting in a solid angle of 10.15 sr. The geometry is a cylinder with its axis coinciding with the incoming beam direction, which reflects the independence of the resolution from the ϕ angle. The detector has a diameter and a length of 1.6 m. In forward and backward direction, there are additional detectors (see Fig. V.4). Accordingly, the sample will be chosen in the same geometry; for the simulations, 7 mm diameter and 10 mm lengths were assumed.. Binning is in constant values of θ (0.469 deg) and ϕ (1.125 deg). Detection is realized by 1.5 µm of B_4C in jalousie geometry with 10 deg inclination. As this detector is well suited for the Thermal Powder Diffractometer at the HBS, its parameters are used for the simulation of this instrument. Data will be stored in event mode.

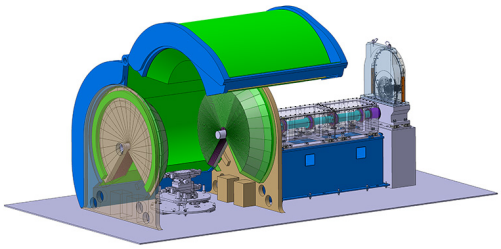

Figure V.4: Technical drawing of the POWTEX detector, which would be ideal for the Thermal Powder Diffractometer of the HBS (taken from MLZ homepage https://mlz-garching.de/powtex).

V.2.3 Performance

The performance numbers of this diffractometer, obtained from Monte Carlo simulations using the VITESS package [ZLNF14] are listed in the Table V.4.

Instrument performance				
Option		High resolution	Medium resolution	High intensity
	unit			
Pulse length	µs	30 and 54	100 and 200	667
Divergence (hor.=vert.)	deg	0.46	0.85	1.72
Flux at sample	n/(cm^{2}s)	5.5×10^5	5.1×10^6	1.6×10^8
Resolution $\delta d/d$ for 1.5 Å		0.11% - 7.1%	0.34% - 10.1%	2.2% - 17.6%

Table V.4: Performance parameters of the 3 set-ups simulated in Monte Carlo simulation for the Thermal Powder Diffractometer of the HBS

Both the spatial and the divergence distribution of the beam profile at the sample are very symmetric for all 3 set-ups simulated. The beam spot at the sample is about 1 cm² in all cases; it is rectangular for the hi-resolution set-up and close to circular in the high intensity set-up (see Fig. V.5).

The brilliance transfer of the guide system was determined in a separate simulation, in which the whole guide was used. In contrast to the simulations of the high resolution optiions, the divergence is not restricted, but the fraction of the brightness within a certain range is compared that at the source to judge the quality of the guide.

Figure V.6 shows the brilliance transfer as a function of wavelength for two different divergences, +/-0.5 deg and +/- 1.0 deg. For the lowest divergence, the brilliance transfer reaches nearly 95% indicating the quality of the beam transport system. With increasing divergence and decreasing wavelength, the brilliance transfer drops because of the reduced reflectivity of the coating. It is restricted to the bandwidth of 0.62 - 2.68 Å by the chopper system.

A virtual experiment of $Na_2Ca_3Al_2F_{14}$ (NAC), based on experimental data, has been carried out to reveal the performance of the HBS powder diffractometer. Figure V.7 shows the detector count rate as a function of d-spacing for the high resolution option. For large d-spacing, the second sub-frame

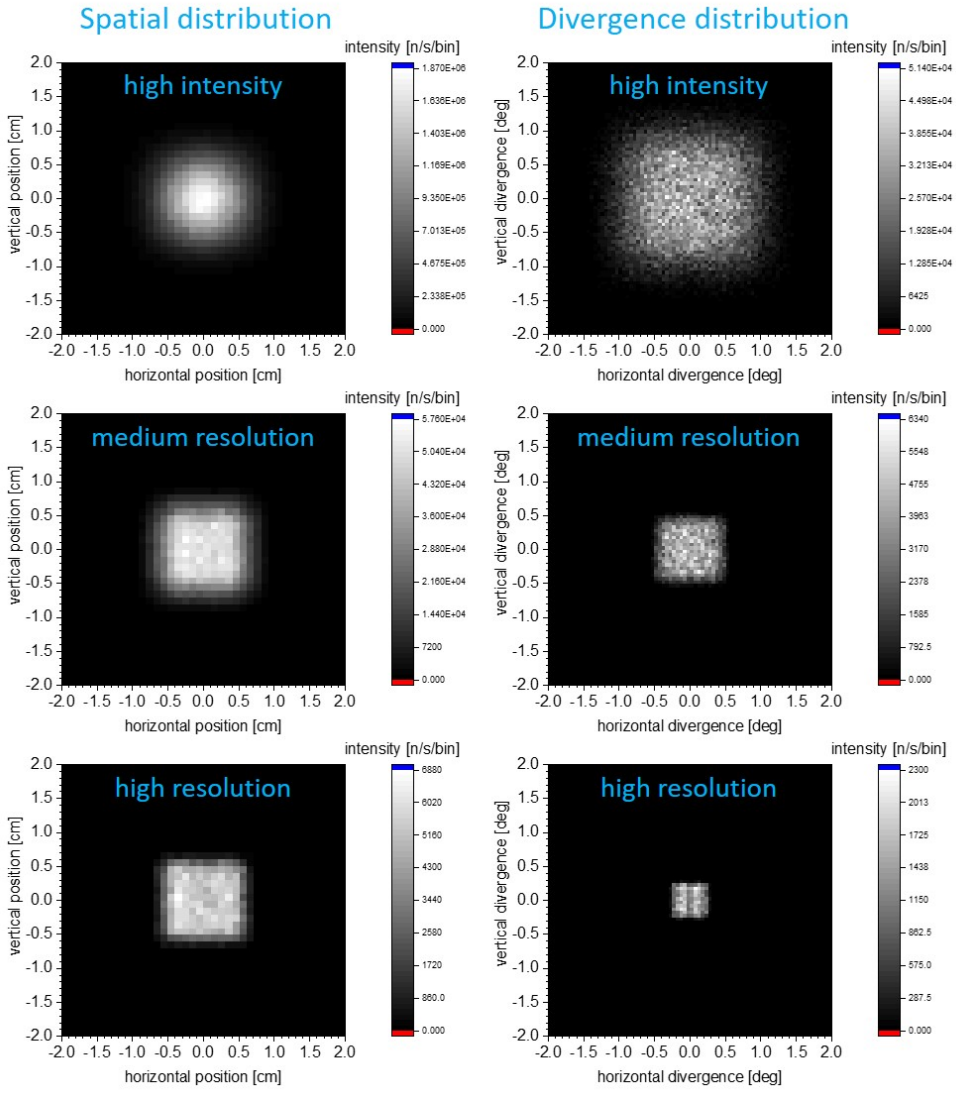

Figure V.5: *Spatial (left) and divergence distribution (right) for the 3 set-ups of the diffractometer: high intensity (top), medium resolution (center) and high resolution (bottom).*

(1.65 - 2.68 Å) yields higher resolution and intensity, while the first sub-frame (0.62 - 1.65 Å) extends the d-spacing range to smaller values.

NAC was chosen to enable a comparison with other powder diffractometers. It is used as standard in many facilities and was already used to estimate the performance of the ESS instrument DREAM [SVL^{+}16]. A comparison of HBS with other powder diffractometers shows that it is competitive to POWGEN at SNS and WISH at ISIS. 420 n/s in the most intensive peak compare to 620 n/s (POWGEN) and 330 n/s (WISH) at comparable resolution and with preferable peak shape. Only DREAM at ESS

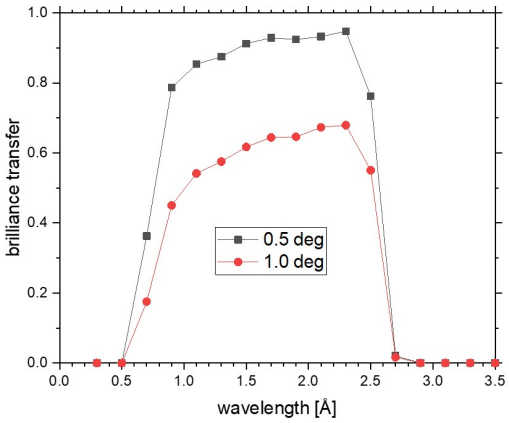

Figure V.6: *Brilliance transfer from source to sample for the hi-intensity set-up of the Thermal Powder Diffractometer for different divergences*

will have a much better performance (see Fig. V.8).

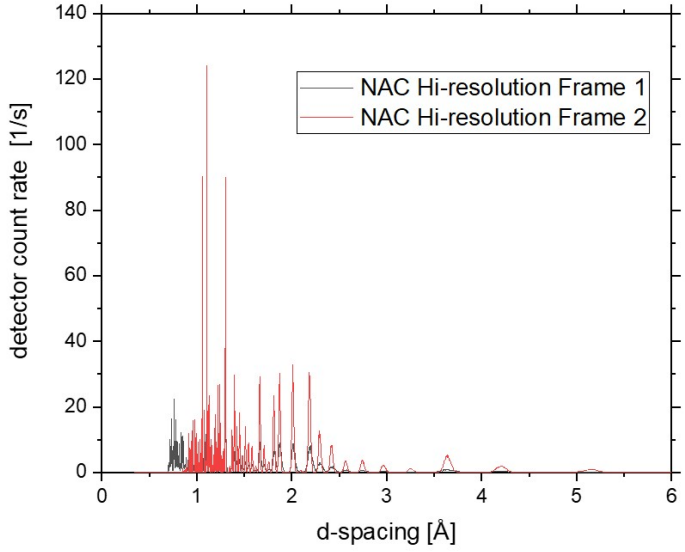

Figure V.7: *1D diffraction pattern of the NAC sample, separated into the contribution from the 1st (black) and 2nd sub-frame (red) for the high resolution setting.*

V.2.4 Data evaluation

Figure V.8 shows that the peak shape is close to a Gaussian function. Therefore, usual data evaluation routines can be used. However, this does not exploit the full potential of a TOF-diffractometer: Because of the large bandwidth used, each diffraction line stretches over a certain range in θ (see Fig. V.9) and thus over a range of different resolutions. Therefore, summing up all events belonging to one reflection for a 1D diffraction pattern I(d) (see Fig. V.7) is not the ideal way to evaluate the data. Instead a 2D-diffraction pattern allows using only those parts of the pattern where lines are resolved or, even better, use directly the information of the 2D pattern for the data evaluation ([JHS+17]). This software has already been used to display Figure V.9. Evaluation of the simulated spectra is on the way.

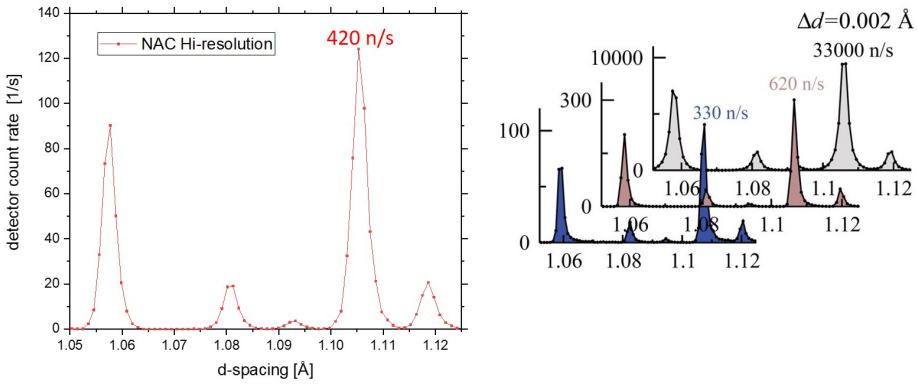

Figure V.8: Shapes and intensities of the intense lines between 1.05 and 1.12 Å of the NAC diffraction pattern obtained for the HBS diffractometer (left, red) in comparison with simulations on other sources: WISH at ISIS (blue), POWGEN at SNS (brown) and DREAM at ESS (grey). Figure on the right side taken from reference [SVL+16]

V.2.5 Polarization

Most measurements will not use polarized neutrons. Polarization could be realized as an add-on by exchanging a part of the straight guide by a polarizing V-cavity with a guide changing mechanism. As an analyzer, a solution seems useful that can be used at different instruments and is therefore a decision for the whole facility.

V.2.6 Requirements

Sample environment. This instrument is designed for a broad range of applications from high resolution measurements to low resolution kinetic measurements. Accordingly, all usual kinds of sample environment have to be available: high magnetic fields, pressure cells, a very large temperature range from helium temperature to at least 1000°C, supply of different kinds of gases etc.

Shielding. The highest particle energy in the system is 70 MeV, which is more than one order of magnitude lower than on spallation sources and also lower than at reactor sources. Additionally, guide cross-sections are smaller so that less radiation is getting out of the TMR shielding and the

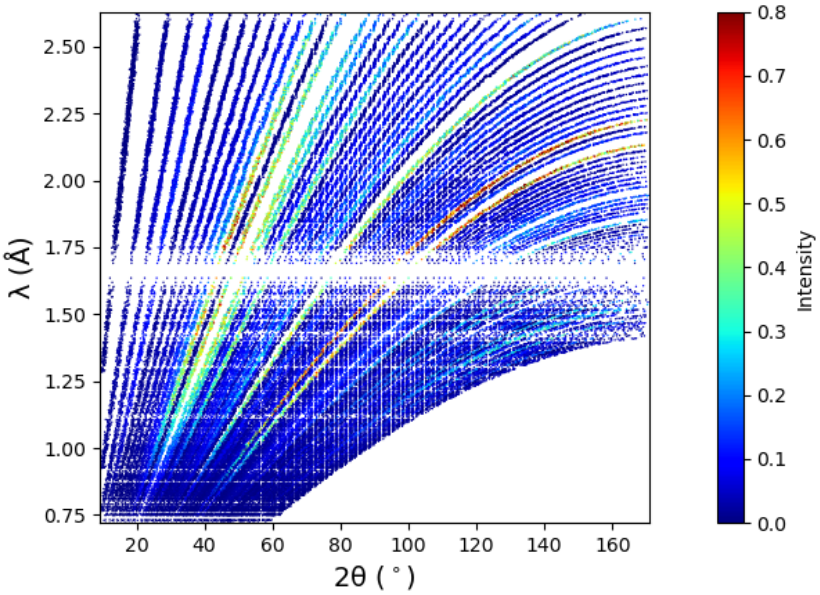

Figure V.9: 2D representation $I(\theta, \lambda)$ of the NAC diffraction pattern from simulation of the high resolution set-up of the Thermal Powder Diffractometer.

bunker. Therefore a shielding as used at reactor sources like FRM-II will be sufficient. This instrument has no requirements for especially low radiation background.

Floor space. 6 of the 7 choppers have to be close to the neutron source and close to each other, i.e. from 2 to 4 m from the moderator (see Figs. V.2 and V.3). So they must all be in the bunker. The detector around the sample has a size of 1.6 x 1.6 m². Around that there is space needed for hardware of the instrument control (electronics, pumps, computers ...). An area for sample preparation and space for users is also necessary. Altogether, 25 m² seems appropriate. Between bunker wall and detector area, there will only be few components: a chopper (40 m from the source), maybe a guide exchanger for polarization (between 20 and 40 m from the source) and a guide exchanger for divergence control (the last 4.5 m before the sample).

Labs and Workshops. A chemical lab containing chemicals for wet chemistry, fume hood, glove box, ball milling, ... will be most important. The common workshops will be sufficient, as there are no special components in the instrument.

Cranes. During operation, a crane will be needed to exchange sample environment. For maintenance and reparations, transport of shielding blocks, choppers and guide sections maybe. A weight of 1 or 2 tons seems sufficient. For the construction, the heaviest piece is probably the detector, which weighs about 2 tons. A crane to lift the detector is only needed, if access to the instrument on the ground floor is not possible.

Hardware and Software. As usual for a time of flight instrument, the data will be recorded in event mode, which requires about 10 Byte per detected neutron. The virtual experiments of the NAC sample yielded detector count rates of 2.6 Mio, 83000 and 9300 n/s. As the high-intensity mode will probably not be the preferred choice, we can estimate an average of about 100'000 n/s. Assuming

200 days of operation per year and 20 hours of measurement per day gives 72 GByte per day or 14.4 TByte per year that needs to be stored.

As stated above, the data evaluation has to make use of the wavelength dependent resolution, (cf. Fig. V.9) to exploit the full potential of a TOF-diffractometer. This new kind of software is already under development for the TOF diffractometers POWTEX and will probably be available before this instrument is in operation ([JHS+17]). Common instrument control software will be used.

V.2.7 Cost estimation

The detector is by far the most expensive component of this instrument. The very large solid angle coverage of the Powtex instrument is chosen for the texture applications. This diffractometer with structure determination of powder samples as the main application, can also be equipped with only 1/4 instead of 3/4 of the cylinder (between 45 and 135 det scattering angle) covered by a detector, which gives more space for sample environment and reduces area and price by 40%. Additionally, it is assumed that finally 6 choppers will be sufficient as discussed above. This gives 4800 k€ for the detector, 2100 k€ for the choppers and 9650 k€ in total (see Table X.1)

V.3 Single Crystal Diffraction: MacroMolecular Diffractometer (MMD)

Tobias E. Schrader, Zhanwen Ma, Klaus Lieutenant, Jörg Voigt

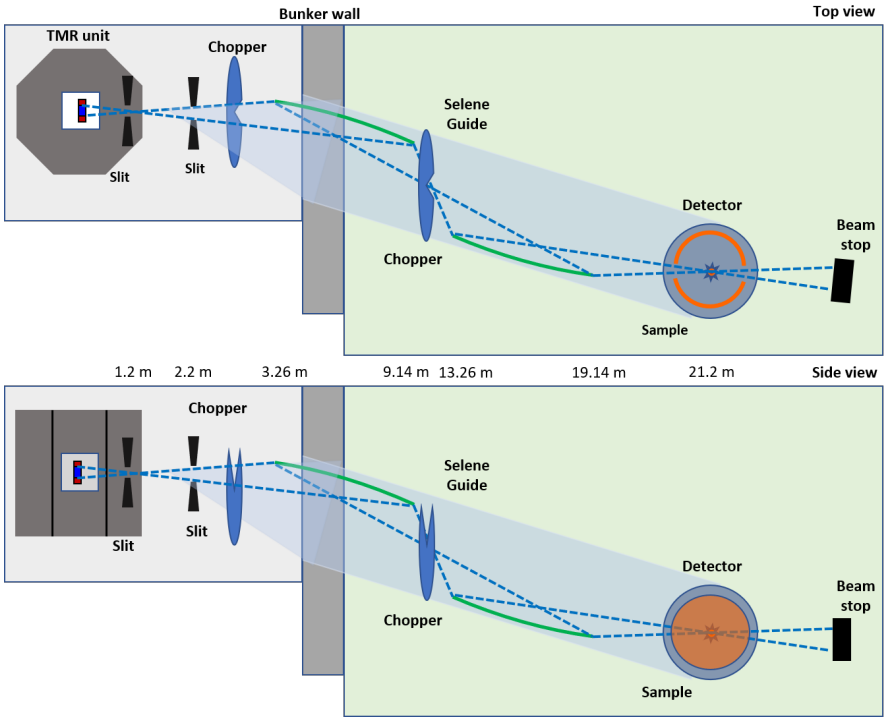

Figure V.10: *The Selene version of the instrument with a spherical detector.*

V.3.1 Introduction and Description of the Science Case

In all forms of life on earth, enzymes are crucial to promote all chemical reactions needed to support their metabolism. These enzymes reduce the activation energy of chemical reactions so that they can take place close to room temperature. They also manage to synthesize their products in a stereo-selective way. Some enzymes need co-factors which control their effectiveness. This provides an easy way to control certain metabolism pathways. These co-factors usually bind on the outside surface of the enzymes. Ligands bind in the active centre and are then processed by the respective enzyme.

Enzymes consist of proteins and co-factors. Typically the protein part of an enzyme adopts a certain structure which is crucial for its function. A vast number of drugs influence the human body or bacteria by competing with the binding of the natural ligand to the active centre. Thereby, drugs block the enzyme. It is crucial to know about the charge distribution and hydrogen bonding opportunities of the active centre of the enzyme, since then drugs can be designed to mirror these charges. This is why it is important to know about protonation states of amino acid residues close to the active site.

Structures of proteins and other biomolecules are solved by X-ray scattering at synchrotron sources. Necessary information about protonation is, however, only available by neutron scattering. The

challenge is to grow crystals of these biomolecules large enough for neutron single crystal diffraction. Often these crystals involve unit cell sizes beyond 90 Å.

There are also scientific questions related to the location of hydrogen atoms in crystals of smaller molecules which then often have smaller unit cell sizes of less than 40 Å. Or one wants to observe phase transitions in these crystals. The incommensurate magnetic structures and the diffuse scattering can be measured better on the Polarized Diffuse Neutron Scattering instrument (see section V.4).

V.3.2 Design considerations

It is very instructive to look at the formula which calculates the intensity of one Bragg peak [Jau97]:

$$I_{bragg} = \frac{\phi(\lambda)\lambda^4}{2(\sin\theta)^2}\frac{V_S}{V^2}\|F_H\|^2 A t_{meas.} \tag{V.7}$$

where λ is the wavelength of the neutrons contributing to this Bragg peak. The symbol in the beginning $\phi(\lambda)$ denotes the time averaged differential flux at the sample, V_S the sample Volume, V the unit cell volume, $\|F_H\|$ the structure factor amplitude, A the transmission factor and $t_{meas.}$ the counting time. The notation follows largely the one of W. Jauch [Jau97].

It is the primary aim of the instrument under discussion here to measure the intensity of thousands of these Bragg peaks as accurately as possible. It can therefore be regarded as the target signal. The noise sources blurring the signal and defying an accurate determination of their intensity are:

1. incoherent scattering of the sample crystal itself. For the protein crystals, this is predominantly due to the residual hydrogen atom content of the crystal.

2. incoherent and some coherent scattering of the sample environment, i. e. a glass capillary around the crystal or a pressure cell

3. air scattering of the primary beam

4. Scattered neutrons from neighbouring instruments and γ-radiation from absorbed neutrons, in case the detector has some sensitivity also for γ-radiation.

For the instrument designer, the incoherent scattering of the residual hydrogen atoms in the crystal is an unavoidable source of background and often it is the predominant one. All other noise or background sources can be reduced by using proper shielding, reducing the mass of material in the primary beam or other suitable measures. To calculate this incoherent background, one can come up with the following formula:

$$B_{inc} = \phi(\lambda)\Delta\lambda\frac{V_S}{V}\frac{N_{inc}\sigma_{inc}}{4\pi}N_{inc}\sigma_{inc}\Delta\Omega A t_{meas.} \tag{V.8}$$

Besides the symbols explained after equation V.7 the number of residual hydrogen atoms N_{inc} in the unit cell and their incoherent scattering cross section σ_{inc} can be found in this equation. This means that a good exchange of the mother liquor around the crystal with a deuterated one is really helping to reduce the background. $\Delta\lambda$ and $\Delta\Omega$ are the wavelength interval and the angular dimension on the detector contributing to the Bragg reflection.

At first glance, the flux cancels out when one calculates the signal to noise value. But in fact, a deeper analysis taking into account the needed beam time for a certain precision of the data set sees the beam time inversely proportional to the incoming flux and proportional to the volume of the unit cell [Jau97].

An increase in time of flight resolution (and thereby an increase in resolution in reciprocal space) will lead to a reduced background since for example the neutrons, which are undergoing inelastic scattering will be spread out more in time.

From the above mentioned formulas, one can set some priorities for the design of the instrument:

1. Incoming neutron flux
2. Resolution in reciprocal space
3. Round beam with a radial symmetry of the detector around the incoming neutron beam

The last item ensures that Friedel-pairs and symmetry related Bragg peaks can be measured with a very high precision so that they can be used for the scaling of the data set, for the r-factor determination and for an empirical absorption correction.

We consider here two instruments, one at the 96 Hz TMR station with Selene type neutron optics of 20 m length, and another one at the 24 Hz TMR station with a conventional neutron guide of 80 m length, both using a cold moderator.

The 80 m long instrument would imply the use of a conventional ballistic neutron guide with a collimation in the vicinity of the sample and the detector to shape the beam spot and the divergence. While this might lead to worse background conditions and requires a significant beamline shielding, it would add the flexibility to use a pulse shaping chopper, if one aims at improving the wavelength resolution to resolve unit cells with lattice parameters reaching up to 180 Å. The investigation of this concept has just begun and will be published elsewhere.

Time and space permitting we focus here on the description of the 20 m instrument at the 96 Hz TMR unit with Selene type neutron optics. Selene focusing optics allows defining both the beamspot size and the divergence range already close to the source.

Using a length of about 20 m gives 2 Å bandwidth - typical range 2 - 4 Å - and sufficient resolution at the 96 Hz source. Virtual experiments of a myoglobin crystal on this diffractometer show an excellent performance of the instrument.

Instrument parameters	
Target	TS-96
Moderator	Liquid para-hydrogen
Moderator-to-sample distance	21.2 m
Sample-to-detector distance	0.3 m
Wavelength band	1.9 Å, 2.0 Å $< \lambda < 3.9$ Å
Wavelength resolution	$0.012 < \delta\lambda/\lambda < 0.023$
Total resolution	$0.012 < \delta d/d < 0.107$
Detector range	$5^\circ < 2\theta < 175^\circ$
Flux	4.1×10^6 n cm^{-2} s^{-1} for 0.38° divergence
	1.8×10^7 n cm^{-2} s^{-1} for 0.80° divergence

Table V.5: *Instrument parameters for the Single Crystal Diffractometer (MMD)*

V.3.3 Layout

The instrument uses neutrons emitted from the liquid para Hydrogen moderator of the 96 Hz target station. The instrument length is defined by the required wavelength resolution to separate different

Bragg peaks for large unit cells. For a moderator-to-detector distance $L_{\mathrm{Det}} = 21.53$ m the neutron pulse length of 250 μs yields a wavelength resolution $\delta\lambda = \frac{h}{m_n}\frac{\tau_{\mathrm{Mod}}}{L_{\mathrm{Det}}} = 0.047$ Å. At the same time, the bandwidth $\Delta\lambda = \frac{h}{m_n}\frac{1}{f_{\mathrm{src}}L_{\mathrm{Det}}} = 1.9$ Åallows the usage of the most intense part of the moderator spectrum 2 Å $< \lambda <$ 3.9 Å. In this range, the brightness varies only a bit, so all wavelength of the band will be recorded with comparable statistics. Accordingly, the relative wavelength resolutions varies between $\delta\lambda/\lambda_{\mathrm{max}} = 1.2\%$ and $\delta\lambda/\lambda_{\mathrm{min}} = 2.3\%$ for this specific band. Since the resolution requirements are already fulfilled, when the full pulse is accepted, the chopper system consists of bandwidth and frame overlap choppers only. An optional chopper to cut the tail of the moderator pulse can also be used to shorten the effective pulse, if a narrower wavelength resolution is requested.

With this instrument we want to determine integrated intensities of small single crystal specimen with a volume ≤ 1 mm^3. At the same time, the sample shall be illuminated by a reasonably collimated beam $\delta\theta \leq 0.4^\circ$ to distinguish different Bragg reflections from crystal with typical unit cell sizes of 12 nm $\times$ 12 nm $\times$ 12 nm. The concept of a Selene guide, that has been recently proposed for several instruments [SPF$^+$11, SFP12, KBFS18, AAJ$^+$20], is ideally suited, to image a small and collimated beam. The original Selene concept images rays from one focal point by two elliptic mirrors across an intermediate focus onto the sample focus. Here the reflections at the second elliptic mirror correct the coma aberration introduced by the first elliptic mirror. While the virtual source size can be tuned within a certain range to control the image size and hence the illuminated volume, the fraction of the ellipse that is covered with a neutron mirror defines the width of the divergence distribution. This width and thus the divergence at the sample can be controlled by a second slit before the first Selene guide.

It has been shown [SG16a] that the required mechanical stability can be achieved by state of the art technology for a distance < 30 m between the virtual source and the sample focus. The instrument proposed here combines the Selene concept both for the horizontal and vertical direction to tailor the phase space illuminating the sample far upstream from it. The direct line of sight is broken twice for this design and it doesn't require additional collimation close to the sample position. The small beamspot minimizes also the illumination of sample environment, where scattering would be difficult to distinguish from scattering at the sample. Hence, the entire design aims to optimize the signal-to-noise ratio at the detector.

V.3.4 Detector

The most important part of this instrument is the detector. The best detector for this method is the perfect sphere. But since this is not easy to produce, tiling of the sphere with individual flat detector modules is a common practice. Since the beamtimes will be typically on the order of weeks, the requirements on the temporal stability of all parameters of the detector are very high. The requirements on such a detector can be listed as follows:

1. Homogeneity of detectivity across the complete surface area, or at least its stability over time
2. High solid angle coverage and good temporal stability of the frame holding the individual detector modules
3. Good dynamic range: Count rate capabilities for intense Bragg peaks but also single neutron detection capabilities for weak reflections.
4. Good spatial resolution to match with the low divergence of the primary neutron beam.
5. A reasonable trade off between the size of each detector module and the parallax error it causes to the neutrons hitting it towards the edges of each module.

The spatial resolution of the detector should be chosen such that at least 10 data points (voxels) contribute to the determination of the Bragg peak. This would enable profile fitting techniques which have proven to be very successful when reducing data from monochromatic instruments. Based on the experience at BIODIFF a voxel size of 250 μm will match the primary collimation at a sample-to-detector distance of $L_{\mathrm{SD}} \approx 30$ cm. This small sample-to-detector distance enables also an efficient solid angle coverage. The dynamic range of detector images at BIODIFF is 16 bit per pixel, so the dynamic range requirements on the detector are fairly modest. It is more the dead time after the detection of a neutron which may lead to systematic errors.

Existing time-of-flight diffractometers employ the Anger cameras [CSH+10] at the instrument MANDI at the SNS in Oak Ridge, Tennessee (USA) or wavelength shifting fibre detectors at iBIX at J-PARC, Japan. In the past banana shaped ^{3}He gas detectors have been successfully used at the Protein Crystallography Station (PCS) at the Los Alamos Neutron Science Center (LANSCE) [SL04]. Here a larger sample-to-detector distance of 70 cm was chosen to make up for the lower spatial resolution of the ^{3}He-detector [Sch10a]. For the future NMX instrument at the ESS, GEM detectors are in development which provide sufficient temporal and spatial resolution [MNAO20]. Wavelength shifting fibre detectors are actively developed and improved [MSSR21]. At BIODIFF a scintillator camera based detector has been developed and successfully used for data collection. A new development of scintillator based detectors employing new generation of image intensifiers and single photon counting cameras with time stamp capabilities will be tested soon on BIODIFF for their suitability for the diffraction technique [LHS+21].

By far the most important feature of a neutron detector for a macromolecular diffractometer is the homogeneity and the temporal stability of its detectivity over weeks. Only then one can scale the data set recorded in up to 30 crystal orientations with the help of Friedel pairs or symmetry related Bragg peaks.

V.3.5 Performance

In Fig. V.11, we show the position, angle and phase space distributions at the sample position. It is obvious, that the optic illuminates only a narrow beam spot with a very well defined angular distribution with squared intensity distributions in space and angle. More than 98% of the transported neutrons arrive on the small sample within the requested collimation. We have investigated the effect of gravity and find that, for this compact design and the considered wavelength range, it has only a weak effect. We find that the transport deteriorates, when a larger beam spot should be illuminated. The divergence distribution becomes skewed and flux within the beam spot gets significantly reduced, if we increase the entrance aperture beyond 2 mm $\times$ 2 mm. This does not affect the performance for the science case addressed by the instrument.

In Fig. V.12 we present a Laue diffraction pattern obtained by monitoring the angular distribution diffracted by a myoglobin sample in an virtual experiment. Each Bragg reflection results in a peak, whose area is defined by the angular collimation of the beam coming from the Selene mirrors. In the figure, we ignore the neutron weight from the simulations to check possible overlap of reflections. The color of the different peaks indicates the wavelength for which the Bragg condition was fulfilled. We see quite a few reflections overlapping in their angle position, in particular in the zoomed fraction of the picture in the right panel of Fig. V.12. But it is obvious that the wavelength resolution by the time of flight $\delta\lambda \approx 0.047$ Å allows the separation of them.

V.3.6 Sample environment

For its application in protein crystallography this instrument needs mostly a nitrogen gas stream at 100 K temperature to keep the sample crystal frozen at this temperature throughout the whole mea-

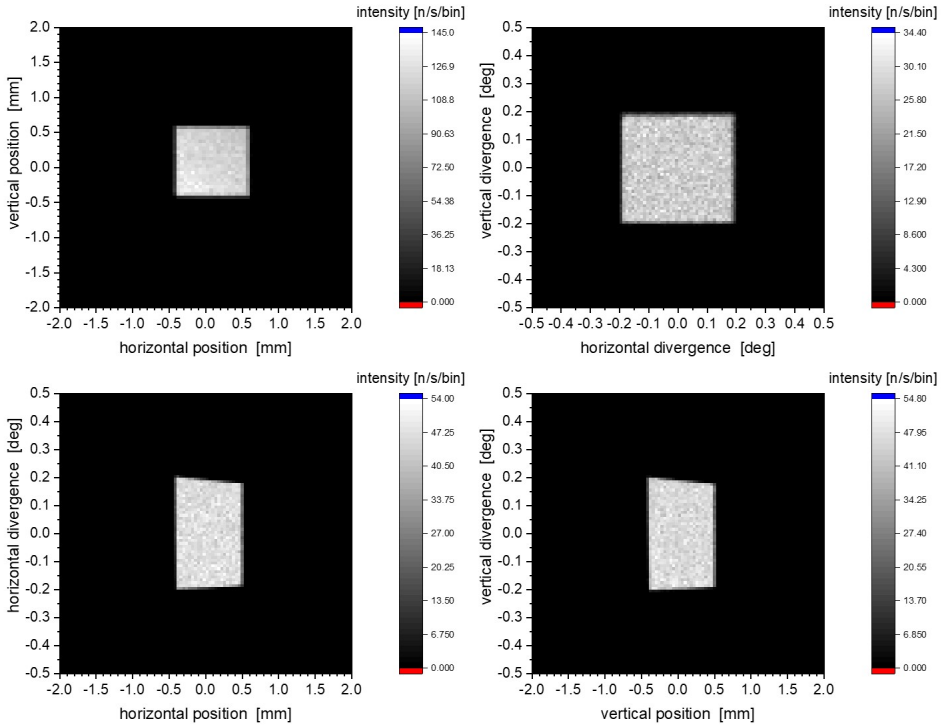

Figure V.11: *Spatial (top left) and divergence (top, right) distribution as well phase space distribution in horizontal (bottom, left) and vertical (bottom, right) direction at the sample position*

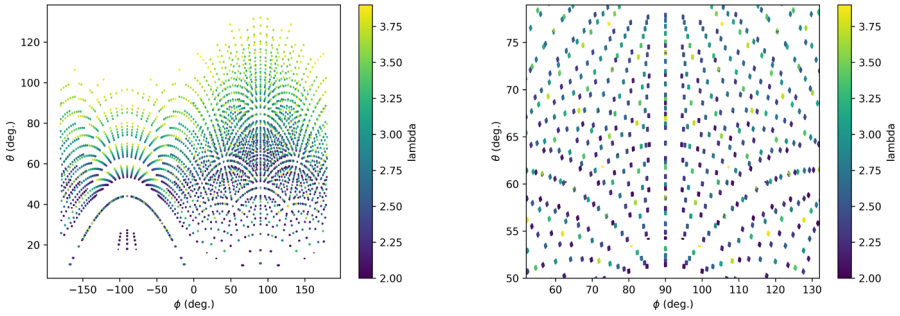

Figure V.12: *Simulated angular distribution of neutrons diffracted from a hypothetical myoglobin sample (minimum d-spacing in data: 1.4 Å) ignoring simulated neutron weights to indicate all potential overlap of reflections. The color scale corresponds to the wavelength for which the Laue condition is fulfilled. Left) Full solid angle, right) zoomed angular range from 20 to 79 deg in polar angle and from 52 to 132 deg in azimuthal angle.*

surement time. This has been demonstrated to work on BIODIFF, for example. Measurements at 100 K allow to compare the neutron structure to the X-ray structure measured at the same temperature. In about half of the proposals on BIODIFF room temperature measurements are requested. Here, just a goniometer head accepting sample capillaries of lengths of up to 12 cm is required.

Besides the applications in protein crystallography, the mm-sized beam spot of the Selene optic fits also other applications, where the sample volume is limited. Among them we mention the application of pressure and large magnetic fields. The latter can profit immediately from the beam properties and the large free area around the sample position. The former would prefer bands at shorter wavelength to give access to smaller lattice spacings.

V.3.7 Shielding

Due to the limited average source flux and the definition of the neutron beam within the target shielding, the instrument requires only light shielding outside the bunker. Choppers will be placed inside the bunker and hence do not need separate shielding. The second mirror, which is positioned outside the bunker, reflects nearly all neutrons impinging. Hence, it does not produce a large amount of gamma radiation by absorption of non-reflected neutrons.

While the sample flux within the beam spot is high, the total beam intensity is small compared to the existing instruments, that transport large and divergent beams to the sample area. The sample area still must be fenced off, but shielding around the detector is used to suppress the instrumental background and not for radiation protection.

V.3.8 Requirements

A floor load < 5 t/m^2 will be sufficient for the instrument in general. Locally the load might exceed this value and require additional enforcement. The hall crane will cover all operations during construction and operation.

Since typical experiments on this instrument will run for a week or more, an instrumental hutch or office space is needed, where users can work on the data reduction and initial data analysis. Many of the corrections, such es extinction correction, absorption correction or Lorentz correction have to be adapted to the illumination by a continuous wavelength spectrum [ACH$^+$99]. On the other hand, the Laue condition provides precise information about the neutron trajectory arriving at any pixel (or voxel) of the detector. So exploring the higher dimensionality of the time-of-flight data should allow a higher statistical significance of the extracted information. This requires the development of a tailored software solution, which is already ongoing at several spallation based facilities and has to be started also in the JCNS well before the instrument becomes operational.

V.4 Polarised Diffuse Neutron Scattering (PDNS)

Werner Schweika, Klaus Lieutenant, Zhanwen Ma

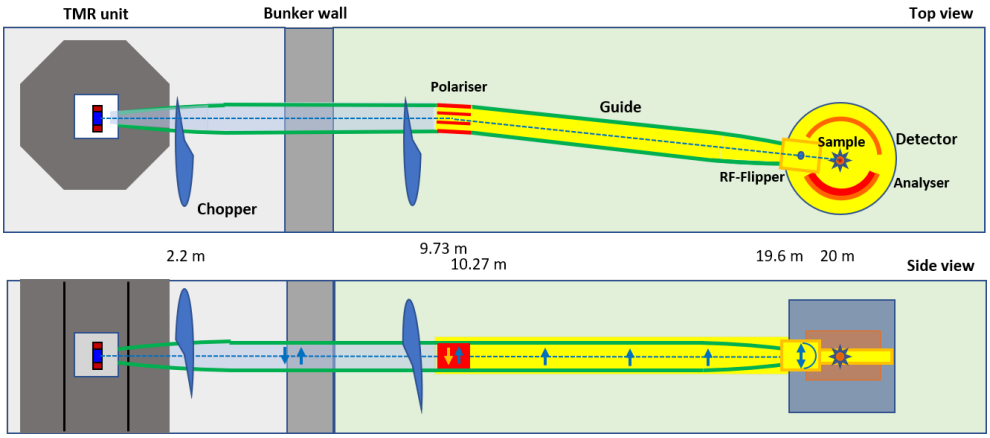

Figure V.13: *Layout of the Polarised Diffuse Neutron Scattering instrument (PDNS).*

V.4.1 Science case and motivation

Research in magnetic structure and dynamics is a strong domain of neutron scattering. The most challenging topics can be found in the field of highly frustrated magnetism with the emergence of strong but often hidden correlations in the apparent disorder of spin liquid systems. Among these, the low spin systems and quantum entanglements are most interesting as well as experimentally demanding and represent particular challenges for appropriate instrumentation. These properties can be revealed in most detail by studies of the diffuse magnetic scattering from single crystals. In particular, polarised neutrons and polarisation analysis are required for utilising the vector properties of the neutron probe, for a clean separation of magnetic from nuclear scattering and for revealing scattering contributions which remain hidden otherwise, i.e. chiral spin correlations appearing in skyrmionic matter and in many systems with broken spatial symmetry along exchange paths. Measuring single crystal Bragg peaks and applying polarised neutron beams with polarisation analysis is further of particular advantage for solving complex antiferromagnetic structures.

The ability to separate nuclear scattering background from magnetic scattering provides extremely clean diffraction patterns by using the XYZ separation technique for powder samples [SC93] and single crystals [Sch10b], and as exemplified for powder diffraction from MnNCN [KHaWSD09] and for separating a weak magnetic diffuse signal from single molecule magnets $Mo_{72}Fe_{30}$ [FKR$^+$06]. In view of the more complex structural patterns of spin spiral structures, neutron polarization analysis of diffraction from single crystals clearly may shed new light on it, revealing the vector chiralities, i.e the turning of helices and cycloids that remains hidden to unpolarized neutrons [Sch10b].

Furthermore, neutron polarisation analysis separates coherent scattering from spin-incoherent scattering, which is typically a disturbing large background in materials that contain hydrogen. In addition, the separated incoherent background may serve for a precise intrinsic calibration. The separation of spin-incoherent scattering background is of high value for material research containing hydrogen, see for example studies of the polymer glass PMMA [GAA$^+$06].

V.4.2 General design considerations and layout

The design of the instrument for polarised diffuse scattering is optimised for the above prime science case. Applying neutron time-of-flight Laue diffraction with the pulsed polychromatic beam gives a very large access to the reciprocal space of interest. It is typical that the Q-resolution can be relaxed for increase of neutron flux. Hence the parameters of the HBS with a 250 μs pulse at 96 Hz appear to be favourable for this instrument case. As many samples, especially single crystals, come in small quantities, optional focusing to small samples will certainly be desirable. The most useful Q-range can be covered with 2 Å bandwidth within the wavelength spectrum from 2 to 6 Å from a cold moderator at the 96 Hz target station. Two choppers are needed, one at 9 m selects the wavelength band, the other close to the target at approximately 2 m prohibits time-of-flight frame overlap. An **inelastic option** for this instrument is highly desirable and requires a third chopper. Therefore using a monochromating Fermi-chopper, the instrument can be converted to a spectrometer. This option will be rather complementary to the cold chopper spectrometer using a wide angle ^{3}He-polarisation analyser. The PDNS instrument is more optimised and efficient for small crystals, with high degree of polarisation at medium energy resolution, but with less solid angle coverage and without a vacuum tank for background suppression as typical for spectrometers. In order to enable the requests for diffuse and Bragg diffraction, the analyser and detector have a homogeneous response and are optimised for 2D resolution and high count rate capability.

V.4.3 Polarised neutrons

Including polarised neutrons and moreover polarisation analysis impose severe boundary conditions for the instrument design. The incoming beam is most efficiently polarised in a guide piece at half distance from moderator to sample using a polarising reflection by FeSi supermirrors with m=4. The polarisation is kept by guide fields from the polariser to the sample. The horizontal kink in the guide avoids fast neutron background or the need for a T0 chopper. The horizontal beam and sample sizes are limited to less than 5 mm width as accepted by the polarization analyser. The sample height can be larger, here chosen up to 20 mm, by using an elliptic guide geometry.

For XYZ-polarisation analysis, we propose a Si-wafer solid state device as developed for the ESS instrument MAGIC. This concept provides a high degree of polarisation $P = 0.99$ with m=3.2 supermirrors for the wavelength band of interest [2 Å, 6 Å] and is sketched in Fig. V.14. This setup assures a high figure of merit $P^2T > 0.3$ compared to the ideal case $P^2T = 0.5$ with transmission of one

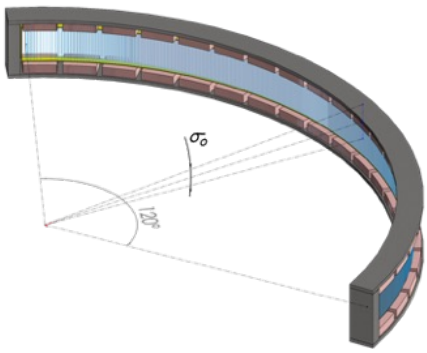

Figure V.14: Wide angle polarisation analyser based on Si-wafers coated with FeSi polarising supermirrors in a saturating permanent magnetic field enclosure of 0.1 T.

spin state.

Alternatively, V-shaped cavities as used for POLANO have a comparable performance. Geometrical constraints for polarisation limit the sample size to 5 mm width. Both concepts are challenging and rather costly when aiming for a large solid angle coverage with polarisation analysis. The setup in Fig. V.14 covers up to 120 degree in the horizontal scattering plane and 6 degree vertically, combined with a 2D position sensitive detector. A second detector on the opposite side of the sample provides a larger vertical solid angle without polarisation analysis. The method implies magnetic guide fields and adiabatic field rotators. Radio-frequency flippers are applied to reverse the polarisation of the incoming polychromatic neutron beam.

Instrument parameters	
Target station	TS-96
Moderator	Liquid para-hydrogen
Moderator-to-sample distance	20 m
Sample-to-detector distance	1 m
Wavelength band	$\sim$ 2 Å, typical 2 - 4 Å
Wavelength resolution	$0.012 \leq \frac{\Delta\lambda}{\lambda} \leq 0.024$
Detector range	120° in $2^\circ \leq 2\theta \leq 160^\circ$ (2.1 sr)
Flux at sample	$5.2 \cdot 10^7$ n/s in 5 mm (h) $\times$ 20 mm (v)

Table V.6: *Instrument parameters for the polarized diffuse neutron spectrometer*

V.4.4 Performance

The neutron beam at the sample position has a divergence of about ±0.5° horizontal and ±1.0° vertical respectively (see Fig. V.15). The expected polarised flux is approximately $5 \cdot 10^7$ n/s cm^2 for the most interesting wavelength band of 2 to 4 Å. The polarisation by the FeSi-coated supermirror assembly in the central part of the guide yields a very high polarisation quality near 99 %. Compared to the DNS instrument at MLZ, or similarly the D7 at ILL, the flux is higher by approximately a factor 5 with better resolution properties, with respect to wavelength but particularly with respect to divergence. One may note that as it is favourable, the HBS instrument is designed for smaller samples. Furthermore, the choice of the new MAGIC type analyser concept is better performing with high efficiency for 2

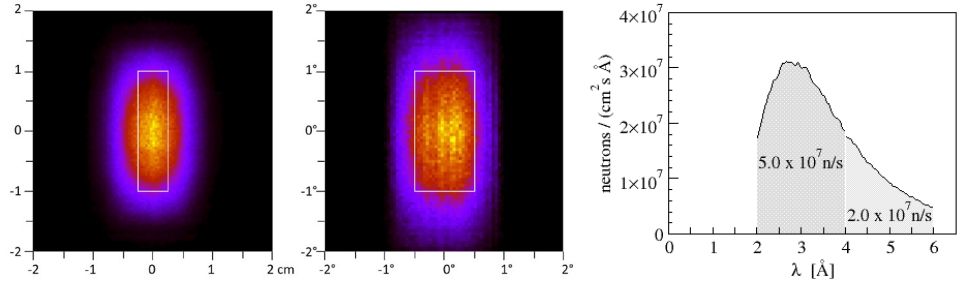

Figure V.15: *Spatial (left) and divergence distribution (middle) at the sample position. The rectangles indicate the sample size of 5 mm x 20 mm (middle) and divergence range of 1° x 1.5° (right). The divergence is only shown for the neutrons inside the sample area. Polarised flux (right) versus wavelength on a 5 mm $\times$ 20 mm sample.*

Å short wavelength, which will allow covering a larger reciprocal space volume. There are further advantages. The analyser setup is continuously covering the solid angle. The detector is 2D position sensitive with high resolution which immediately gives access to the variation in scattering out-of plane. The count rate capabilities of the B-10 multi-wire chamber detector are very high, which give better opportunities to measure diffuse and Bragg intensities simultaneously. The concept of time-of-flight Laue diffraction offers a particular advantage compared to monochromatic instruments. Certainly, this instrument, we may call it "Little MAGIC" will be clearly superior to its reactor based instruments DNS and D7. Compared to the MAGIC instrument at ESS at 5 MW, - since it has a similar layout -, its performance is about 20 times lower in terms of integrated polarised incoming flux.

Considering the most suitable sample environment for the science case, it is most important to cover low and lowest temperatures. Furthermore, pressure cells will be important.

Shielding requirements will be minor. The incident flux is transported in guides of Boron glass. Absorbing essentially all neutrons by a "bad sample" into gamma radiation, one may expect a radiation level of $1\mu\mathrm{Sv/h}$ at 4m from the sample position. Assuming there is sufficient space, shielding will be built primarily as a barrier to access the sample under study when the beam is on.

V.5 Diffuse Elastic Neutron Scattering (DENS)

Werner Schweika, Klaus Lieutenant

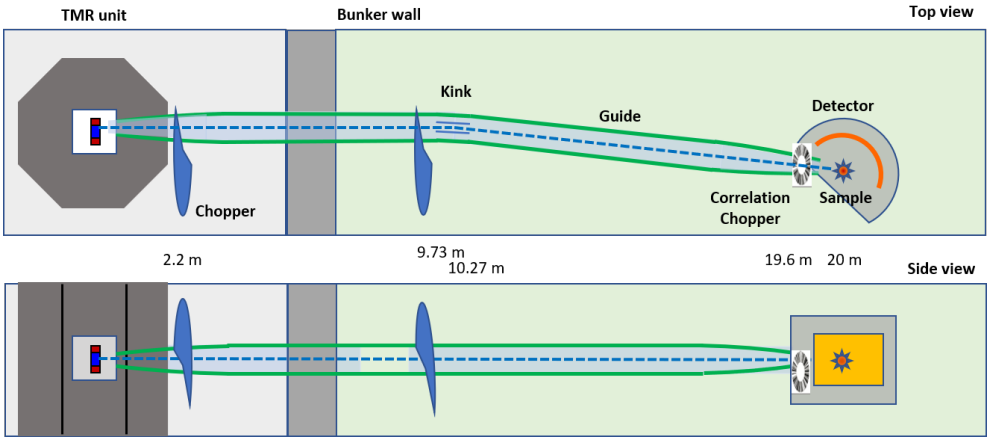

Figure V.16: *Layout of the Diffuse Elastic Neutron Scattering instrument (DENS).*

V.5.1 Science case and motivation

Material research is steadily driving towards more complex and designed structures, with challenging interplay of structural, electronic and magnetic properties. Often, a challenge for understanding is the disorder or short-range order in materials. This requires comprehensive studies involving the full three-dimensional structural properties from single crystal diffraction. The diffuse signals from short range order are very weak compared to Bragg intensities from the average structure. In order to reveal the complex material properties including the short-range order, the exploration of the reciprocal space and careful suppression of undesirable background is often indispensable.

V.5.2 General design considerations

The method of time-of-flight Laue diffraction is ideal to cover a large section of the 3D reciprocal space in a single setting of the experiment. In order to remove inelastic background, which is typically in the same order or higher than the diffuse elastic signal, a most efficient discrimination is possible with a high speed pseudo-statistical chopper. It offers a high duty cycle of about 50% and elastic data are obtained by cross-correlation analysis of the data. This method has been successfully developed and applied at the instrument CORELLI at SNS (https://neutrons.ornl.gov/corelli). The proposed instrument here is conceptually very similar. There are differences due to the source properties with a longer pulse at the HBS that lowers the possible incoming energy resolution of the neutrons. This resolution relaxation is acceptable and well matched to the final energy resolution for 1.2 m sample-to-detector distance and the time resolution of the correlation chopper, which results in a comparably high, intense flux. The compact size allows for an efficient coverage of detection angle. For better background suppression the instrument is housed into a vacuum vessel. Avoiding direct line of sight by a kink in the middle of the guide will further avoid background due to the fast neutrons of the prompt pulse. The 2D position sensitive detector will be either assembled by ^{3}He tubes or ^{10}B-multiwire elements of the Jalousie type covering a large solid angle, $\pm 30^{\circ}$ vertically and horizontally, from 10° to 160°. Designing the transport for a minimum wavelength of 2 Å matches

the Q-range, where magnetic and atomic pair correlations are typically still easy to separate, it is an appropriate choice with respect to the available time resolution of the source, and it makes efficient use of the cold moderator peak flux.

V.5.3 Layout

Instrument parameters	
Target station	TS-96
Moderator	Liquid para-hydrogen
Moderator-to-sample distance	20 m
Sample-to-detector distance	1.2 m
Wavelength range	2 Å - 6 Å
Wavelength band	1.9 Å
Wavelength resolution	$\leq 0.025 \leq \frac{\Delta\lambda}{\lambda} \leq 0.027$
Correlation chopper	350 Hz, $d = 70$ cm, duty cycle 0.5
Incident energy	2.2 meV - 20 meV
Elastic energy resolution	0.1 meV - 1.4 meV, $\leq$ 7%
Q-range	≤ 6.3 Å^{-1}
Q-resolution	0.07 - 0.14 Å^{-1}
Divergence	$\sim 1^\circ \times 2^\circ$ (h×v)
Beam size	$8\,\mathrm{mm} \times 12\,\mathrm{mm}$ (h×v)
Flux at sample	$5 \cdot 10^7$ n/cm^2/s for 2 Å< $\lambda <$ 3.9 Å
Detector coverage	$10^\circ \leq 2\theta \leq 160^\circ$, vertical $\pm 30^\circ$ (5.2 sr)

Table V.7: Instrument parameters for the diffuse elastic neutron spectrometer

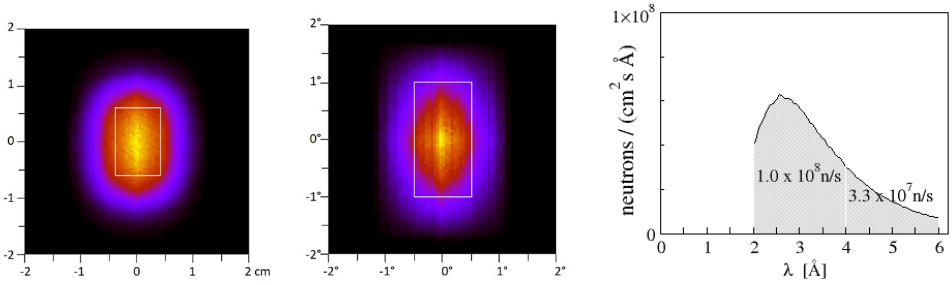

Figure V.17: Spatial (left) and divergence distribution (middle) at the sample position. The rectangles indicate the sample size of 8 mm x 12 mm (left) and a divergence range of 1° x 2° (middle). The flux integrated over the sample area of 8 mm x 12 mm is shown to the right, and 50% less when using the correlation chopper for elastic scattering.

V.5.4 Performance

The neutron beam at the sample has a divergence of about $\pm 0.5^\circ$ horizontal and $\pm 1^\circ$ vertical. The expected flux is approximately 1.0×10^8 n/scm^2 in diffraction mode. Applying the correlation chopper with its high duty cycle of 50% reduces the chopped pulse accordingly. The high speed of the chopper disks, and the well matched initial and final time resolution, yields a favourable energy resolution of few percent on the elastic line at very high intensity. The distance sample-to-detector is 1.2 m which allows an efficient coverage of solid angle for detection. The detector will be 2D position sensitive and will be either assembled by ^{3}He tubes or ^{10}B-multiwire elements of the Jalousie type covering a large solid angle, horizontally from 10° to 160° and $\pm 30^\circ$ vertically. The instrument may compare best to the highly performing CORELLI instrument at SNS with respect to many properties and similar neutron flux. One may note that because of the restriction to wavelengths larger 2 Å the proposed instrument will cover not the same large Q-range and the real space resolution will be more limited. However, for most interesting cases, and in particular for measuring magnetic short range order and spin correlations the performance will be comparable.

V.6 Engineering Diffraction (EngDi)

Jochen Fenske, Igor Krasnov

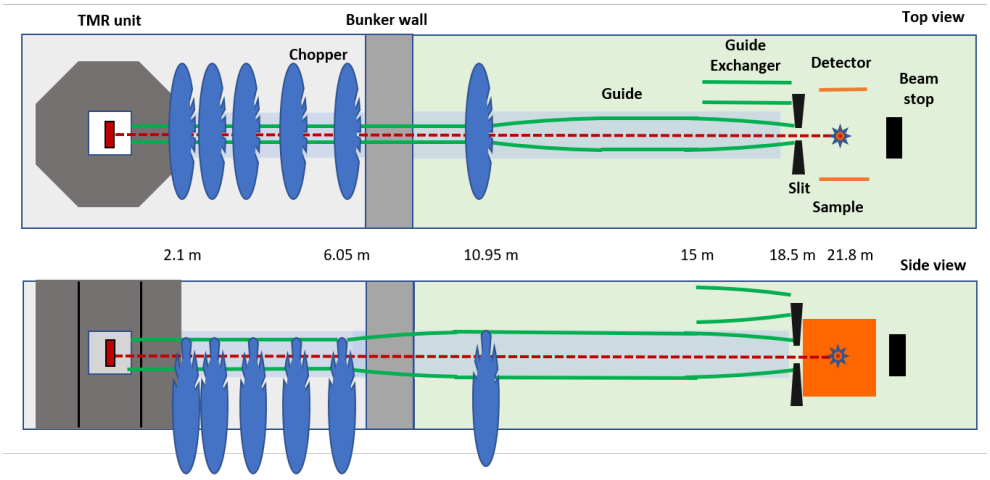

Figure V.18: *Layout of the Engineering Diffractometer (EngDi).*

V.6.1 Science Case

An engineering diffraction Instrument is usually designed to allow for the analysis of stresses, phases and textures of materials. The range of materials that are investigated on engineering diffractometers is broad. It includes for example lightweight materials like magnesium or aluminium used in the transport sector, high temperature materials like TiAl used in turbo chargers, batteries or smart materials, e.g. shape memory alloys. Often it is of interest to investigate the behaviour of materials during or after they have been in operation or processed by different methods, e.g. when they are welded, forged, grinded, charged or otherwise treated and exposed to different environments. An engineering diffractometer is therefore not only interesting for the science communities who want to understand fundamental processes in materials but also for the industry to improve their fabrication processes.

V.6.2 Design Considerations

The design of the here presented engineering diffractometer is mainly driven by the investigation of residual stresses. The investigation of slight shifts of diffraction peaks caused by stresses or strains in materials requires a high instrumental resolution (or alternatively, a precise knowledge of the resolution function for de-convolution, which would lead to higher intensities and a simpler instrument). Today's engineering diffractometers at the most powerful neutron sources like the ESS aim for instrumental resolution down to $\Delta d/d = 0.1\%$ but also at high to medium flux neutron sources, instruments reach resolutions of $\leq 0.3\%$ like at STRESS-SPEC at the MLZ or ENGIN-X at ISIS. On the upper side instrumental resolutions about 1% are sufficient to allow for high flux measurements with reduced resolution. While the instrumental resolution is one important factor, also the available wavelength band is important. To define the exact gauge volume in a sample, also during rotation of the sample, a scattering geometry that allows for a scattering angle near $2\theta = 90^\circ$ is favorable. To reach this for diffraction peaks like 220 and 311 of important materials like Aluminum,

Copper, stainless steel or Nickel based alloys a broad wavelength band is necessary. Here we aim for $\lambda_{min} \sim 0.8$ Å and $\lambda_{max} \sim 2.78$ Å. To collect a high scattering intensity also the detector should have a significant size. A larger detector area will also be beneficial to cover a broader d-range, which is not only useful for texture measurements. To cover two strain components at once two detectors at $2\theta = \pm 90^\circ$ are important to reduce the measurement time. Therefore, two $1 \times 1\,\mathrm{m}^2$ detectors are foreseen for the Engineering Diffractometer proposed for the HBS. For an engineering diffractometer, the available space at the sample position is an important factor. The space shall be sufficient to install different, often bulky, sample environments, which ranges from conventional stress-rigs, dilatometers to user designed sample environments. Another driver for the instrument design is to have a compact instrument at a high current accelerator driven neutron source. A short instrument length will require less space and save costs for shielding material around the long transport guide. A disadvantage of the compact design is that often more choppers are required to reach the required instrument resolution.

V.6.3 Layout

The distance from source to detector defines the time of flight length of 21.8 m. The instrument is sitting on a target station with a frequency of 96 Hz with a pulse separation of 10.4 ms. The thermal PE moderator provides a neutron pulse length of about 250 µs. The general instrument layout is shown in Fig. V.18. The design consists of in total 6 choppers, a transport neutron guide with changeable elements for focusing onto the sample, and two detectors placed at $2\theta = \pm 90^\circ$ in 1.8 m distance from the sample. The components are described in more detail in the following discussion.

Choppers. The neutron flight path of 21.8 m is not sufficient to provide the needed wavelength resolution of the instrument; therefore, a chopper cascade has been introduced into the instrument design. The first chopper is placed behind the shielding of the TMR unit at 2.1 m. In such a distance the chopper provides a wavelength band of about $\Delta\lambda = 0.471$ Å. To make use of the full natural bandwidth of the instrument, that is for the 21.8 m long diffractometer $\Delta\lambda = 1.887$ Å, the disk has 4 openings. It allows to extract 4 sub frames with $\Delta\lambda = 0.471$ Å. Together with the second disc, that also has 4 openings, the Wavelength Frame Multiplication method is used to provide the necessary wavelength band and the wavelength resolution. The second disc is operated in such a way that it is opening when the first disc closes. This so-called optical blind mode provides a wavelength independent wavelength resolution. Both choppers are sitting on linear tables that allow changing the distance between the two discs from 0.05 m to 0.2 m. Thus, providing together with the instrument length a tunable wavelength resolution between $\Delta\lambda/\lambda = 0.25\%$ and 1.02%. It should be noted that for the closest distance of 0.05 m between the discs the position of the first disc changes from 2.1 m to 2.175 m, thus reducing the wavelength band of each frame to $\Delta\lambda = 0.455$ Å. The other 4 choppers prevent cross talks between the 4 sub frames generated by the first two WFM discs as well as overlaps between consecutive source pulses. The time-distance diagram of such a set-up is shown in Fig. V.19.

Neutron Transport System. The neutron guides start in 0.4 m distance from the source. The first guide elements consist of straight segments with a cross section of 18.84 mm x 40 mm (W x H) and a m= 2 coating. The elements are interrupted to leave space for the choppers. Where possible, the guide and chopper housing should share a common vacuum. From 6.05 m to 10.85 m, the neutron guide is horizontally straight and follows an elliptical shape vertically, with focal points at the source and the sample. The cross section expands here from 18.84 mm x 40 mm to 18.84 mm x 43.34 mm. From 10.95 m to 15 m the guide follows vertically and horizontally an elliptical shape with a cross section of 16.39 mm x 37.71 mm at 15 m. The last guide section in front of the sample from 15 m to 18.5 m sits on a guide exchanger, which allows choosing between two options. The first one is a neutron guide that focuses only vertically on the sample; this option is used for the high-resolution mode. The vertically elliptical shaped guide focus the neutron beam on the sample. The top and

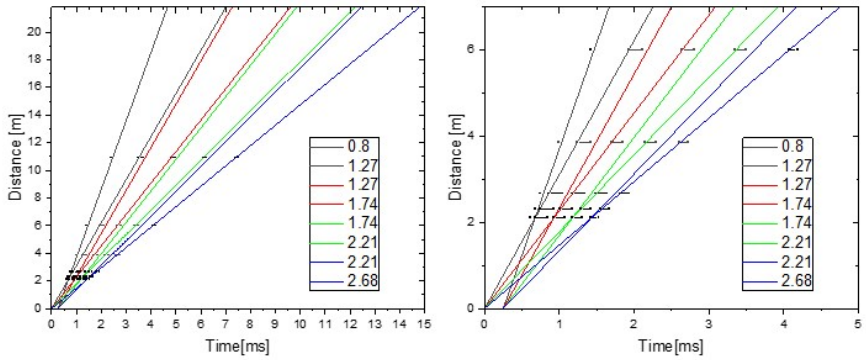

Figure V.19: *Time Distance Diagram of the WFM set-up. On the left for the whole instrument length showing the 4 generated sub frames. On the right a closer look on the first 7 m of the instrument.*

bottom parts are coated with m$= 3$ while the sidewalls of the guide are absorbing thus providing a low divergence horizontally. The second option is a double focusing guide, which focus the neutron beam in both, horizontal and vertical direction onto the sample. Here, the supermirror coating is m$= 3$ for all walls of the neutron guide.

Sample Exposure System. At the sample position different sample stages can be placed like a Hexapod or a Robotic system which allow moving the sample environment and the sample in the necessary positions, for example for stress scanning experiments or to rotate the sample for texture measurements. The robot system can also be used to exchange samples automatically in case of larger sample series.

Detector System. For the detector system two detectors with an active area of 1×1 m^2 are foreseen to be placed in 1.8 m distance to the sample leaving enough space for sample environment and radial collimators. With slits in front of the sample, the radial collimators will define the gauge volume in the samples. The two detectors should have a resolution of 2 mm horizontally and at least 5 mm vertically. The technology can be based either on ^{3}He tubes or on $^{10}B_4C$ converters. The two detectors will cover a range of $2\theta = 74.5° - 105.5°$. Taking the given wavelength band of $\Delta\lambda$ (0.8 - 2.68) Å into account, a d-range from d $= 0.5 - 2.2$ Å can be covered.

V.6.4 Performance

The performance of the above described instrument design has been simulated with the neutron ray tracing program McStas. Two extreme modes have been considered: The high-resolution mode (no horizontal focusing onto the sample, WFM Chopper distance 0.05 m) and the high flux mode (horizontal and vertical focusing onto the sample, WFM Chopper distance 0.2 m).

Wavelength Band and Resolution. In Fig. V.20 the time-of-flight against the wavelength is visualised for the high-resolution and high flux mode showing clearly the 4 sub frames extracted by the WFM method. No cross talks between the sub frames are visible as well as no other unwanted wavelength.

Divergence Distribution. The divergence distribution for the two modes for a sample of 5×10 mm^2 in size is shown in Fig. V.21 and Fig. V.22. In both modes the divergence is almost homogeneous distributed. In the high-resolution mode the HWHM of the horizontal divergence is about 0.12% and

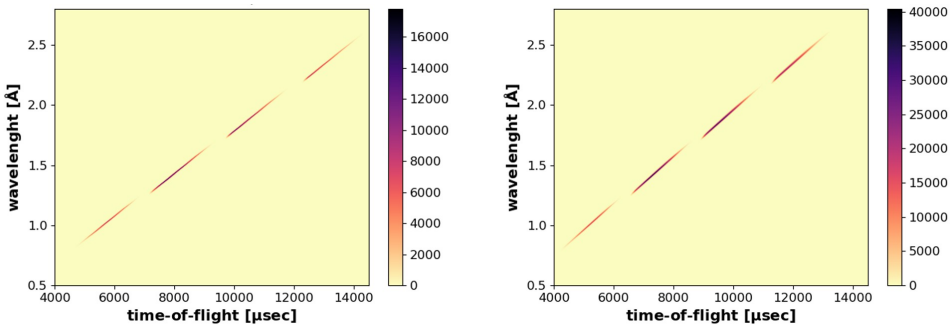

Figure V.20: Time-of-Flight vs. wavelength for the high-resolution mode (left side) and high flux mode (right side).

vertically about 0.36%. Considering the other parameters thus leading to an instrument resolution of $\Delta d/d = 0.36\%$ horizontally and $\Delta d/d = 0.7\%$ vertically. In the high flux mode the horizontal divergence increases to 0.33% while the vertical divergence stays almost constant. Considering the relaxed wavelength resolution in this mode the instrument resolution is lowered to $\Delta d/d = 1.05\%$.

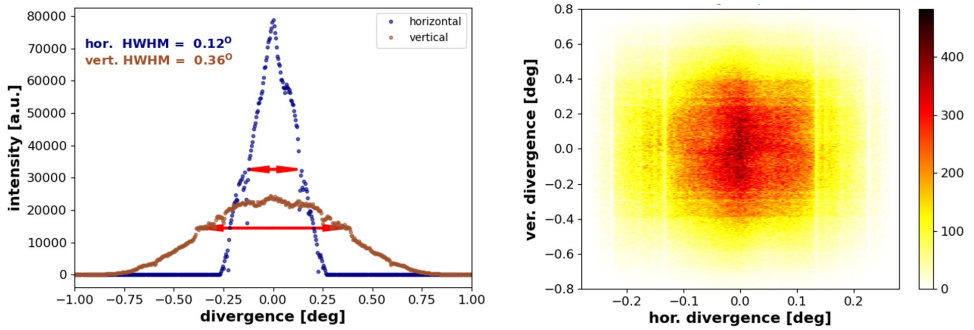

Figure V.21: Divergence distribution for the high-resolution mode.

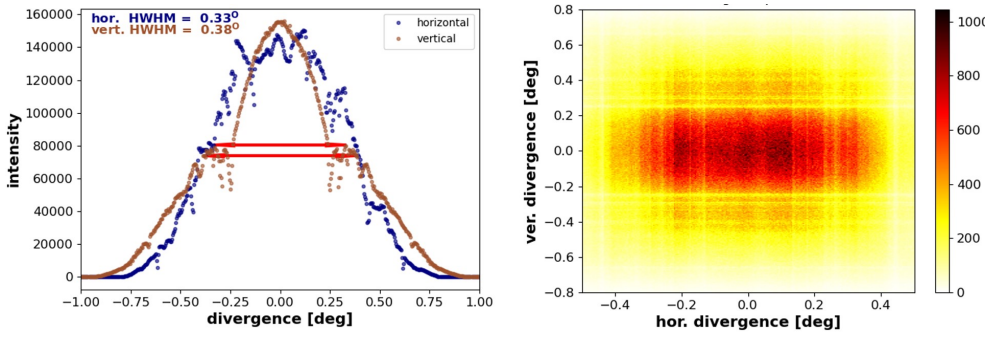

Figure V.22: Divergence distribution for the high flux mode.

Spatial Distribution. In Fig. V.23 and Fig. V.24 the spatial distribution of the neutron at the sample is visualized. Considering a typical sample size or area of interest of 5×10 mm it can be seen that this area is almost homogeneous illuminated by the neutrons.

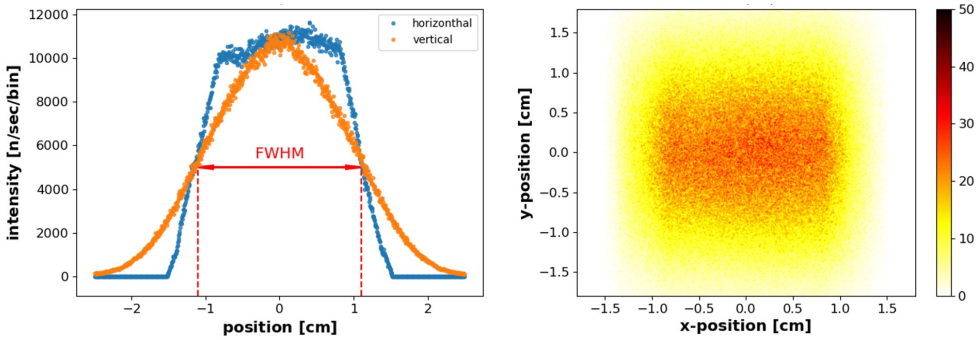

Figure V.23: Spatial distribution of the neutrons at the sample position for the high-resolution mode.

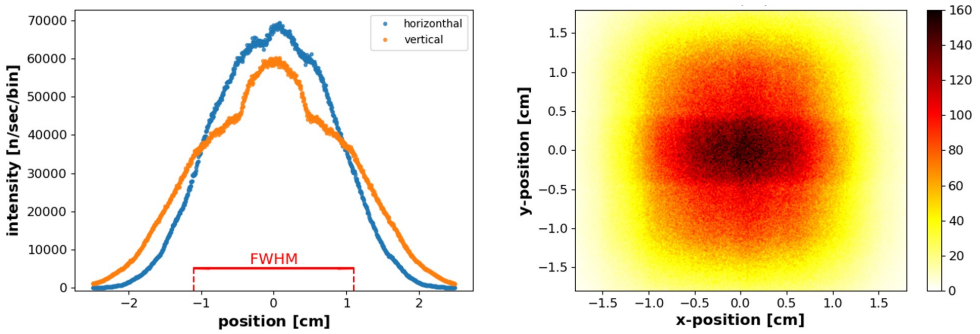

Figure V.24: Spatial distribution of the neutrons at the sample position for the high flux mode.

Flux. The simulated time averaged flux is about 2.3×10^5 n/s/cm^2 in the high-resolution mode and in the high flux mode about 1.5×10^6 n/s/cm^2.

Alternatively, the instrument could be placed on the 24 Hz target station. It would profit from the higher peak brightness of this target station, the longer pulse, which has an extended brightness plateau from which the pulse can be cut, and reduced losses in the wavelength frame multiplication system, as only two frames must be stitched together. To check this option, a first simulation, based on the design of the thermal powder diffractometer, was performed (see section V.2) . The moderator - sample distance of 79.2 m was taken from the TPD, and the sample - detector distance of 1.8 m from the other option for the engineering diffractometer. The guide of the TPD was shrinked to 50% of the cross-section of the TPD and used in its high-resolution option to reach a sufficient low divergence for the high resolution option of this diffractometer. The chopper system was taken from the thermal powder diffractometer and used in the medium resolution setup (pulses of about 100 and 200 µs). The result was an average flux of about 4.4×10^5 n/s/cm^2 for the high resolution option of the engineering diffractometer. For the high intensity option, where the resolution is relaxed by a factor of 3, the pulse lengths as well as the horizontal and the vertical divergence can all be increased by

a factor of 3 so that a gain in flux of one order of magnitude can be expected.

A comparison with a similar engineering diffractometer at a pulsed source like ENGIN-X at ISIS, however, shows that the flux in the high-resolution option of an engineering diffractometer at HBS is about a factor of 3 lower. In high-intensity mode, on the other hand, the same flux should be reached, because an intensity gain by relaxing the time resolution is not feasible on a short pulse spallation source like ISIS. Furthermore, a performance comparison must also consider parameters like used wavelength band, detector coverage, etc. With only 0.69 sr detector coverage, ENGIN-X can easily be outperformed by a factor of 3.

Instrument parameters	
Target station	TS-96 Hz
Moderator	Water
Moderator-to-detector distance	21.8 m
Sample-to-detector distance	1.8 m
Wavelength band	1.88 Å, typical 0.8 - 2.68 Å
Wavelength resolution	0.25 % $< \delta\lambda/\lambda <$ 1.02 %
d-spacing range	0.50 Å $< d <$ 2.21Å
Resolution	0.33 % $< \delta d/d <$ 1.08 %
Detector range	$74.5° < 2\theta < 105.5°$, 0.57 - 2.52 sr
Flux	2.3×10^5 n/s/cm^2 (high resolution mode)
	1.5×10^6 n/s/cm^2 (high flux mode)
Target station	TS-24 Hz
Moderator	Water
Moderator-to-detector distance	81.0 m
Sample-to-detector distance	1.8 m
Wavelength band	2.03 Å, typical 0.7 - 2.73 Å
Wavelength resolution	0.36 % $< \Delta\lambda/\lambda <$ 0.70 %
d-spacing range	0.44 Å $< d <$ 2.26Å
Resolution	0.41 % $< \delta d/d <$ 0.78%
Detector range	$74.5° < 2\theta < 105.5°$, 0.57 - 2.52 sr
Flux	4.4×10^5 n/s/cm^2 (high resolution mode)

Table V.8: *Instrument parameters for the engineering diffractometer*

The current design of an engineering diffractometer for the HBS shows that these kinds of measurements are feasible on a high current accelerator driven neutron source and that the expected performance is close to a well-established "workhorse" instrument like ENGIN-X.

Instruments for the Study of Large Scale Structures

The diffractometers presented before determine the content of the crystallographic unit cells and and/or probe correlations on the length scale of a few nm. In terms of wavelength and resolution they probe a coherence volume that is typically smaller than 100 nm × 100 nm × 100 nm. In particular in soft matter and in biological samples, the building blocks are of comparable size or larger. Also artificially layered structures and nanoparticles feature often structure sizes larger than 10 nm which are correlated over many building blocks So the instrumentation to resolve the spatial correlations require the use of long neutron wavelength and highly collimated neutron beams to increase the coherence volume up to the µm range. These requirements are perfectly suited for the HBS source thanks to the directed emission characteristic of the cold moderators. Furthermore the instruments can profit from compact instrument designs providing matched wavelength resolution and wide neutron bandwidth.

The corresponding Small Angle Neutron Scattering (SANS) instruments and reflectometers belong to the most productive diffractometers also because the scattering cross sections are very high allowing a high throughput of samples and user groups. As a consequence, these instruments are also the most requested ones at existing facilities and therefore the provision of sufficient beam time is crucial for the user communities from polymer research and life science.

The present HBS layout contains therefore 2 SANS instruments, one optimized for high throughput and one with an option for grazing incidence small angle scattering. One reflectometer is optimized for buried interfaces and the vacuum-solid interface with a horizontal scattering geometry. The second instruments reflects neutrons vertically from a flat surface to allow also studies of liquid-liquid or liquid-solid interfaces. All instruments are designed to provide polarization analysis to explore the unique sensitivity to magnetism and to provide an additional degree of freedom for contrast variation in crowded systems.

V.7 Small Angle Neutron Scattering (SANS)

Sebastian Jaksch, Henrich Frielinghaus

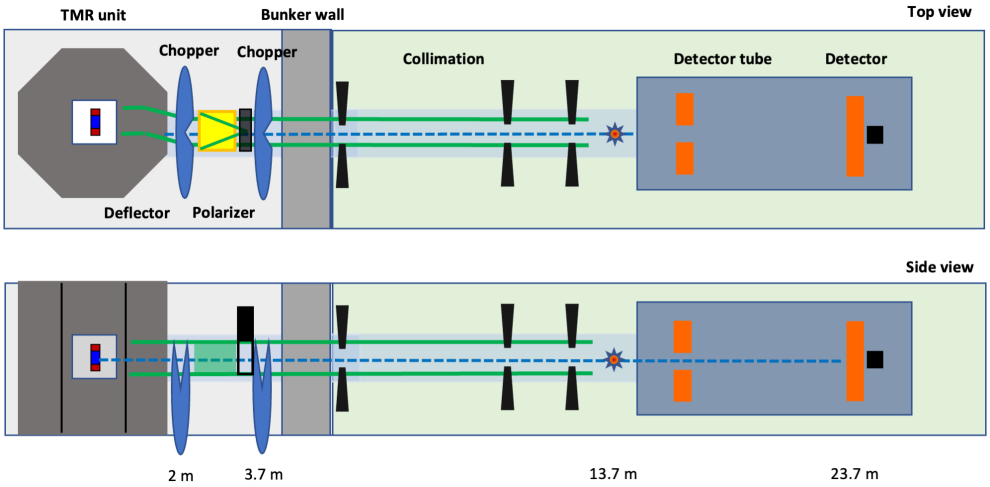

Figure V.25: *Scheme of the high throughput SANS. The total length is determined by the 10 m collimation and 10 m detector distance.*

V.7.1 Introduction for High-Throughput SANS

A high throughput SANS instrument is indispensable for any neutron facility. The proposed instrument is optimized for ease of use and standardized fast data collection and reduction and hence the number of different instrument configurations is limited. One can take the BioSaxs at the EMBL / DESY in Hamburg [RKR+07] as example where this aim is achieved. For this, we need robots to perform the sample changes, artificial intelligence to optimize the acquisition times, and automated data parsing with artificial intelligence to produce even first results on what the real space structure may be. However, the sample space shall be kept rather large at 2 x 2 m^2 in order to allow standardized sample environment with standardized alignment and standardized media connections in order to reach out for a broader use with little waste of time for user changes. Here, the general idea of the SKADI sample environment at the ESS [JMRO+14, JCD+21] serves as a prototype with even larger space. The instruments at the HBS, however, are kept smaller because the high brightness does not necessarily demand for very large samples (and environments).

V.7.2 Science Case

The science case for this high throughput SANS instrument ranges from polymers, colloids and complex fluids (i.e. the classical soft matter) over membranes, proteins and protein complexes (i.e. the bio-related topics) and skyrmions, flux lines and spintronics (the magnetic topics) to steels, rocks and composites (the various materials). However, there are topics such as food science, lithium batteries, magnetic colloids and energy materials in general that touch various abovementioned fields simultaneously. Their complexity usually demands for many complementary methods in order to tackle the multiple length scales and compositional complex chemistry properly.

V.7.3 Layout

The classical SANS Q-range from 0.002 to 1.8 Å^{-1} (the latter often emerges from SANS at pulsed sources) shall be achieved for the proposed instrument at a single shot. This ensures that the data of all detector distances are taken at the same time and makes the data more consistent. Furthermore, kinetics would be observable in a consistent way. From the high brightness of the source we would only need neutron guides of $2 \times 2\,\mathrm{cm}^2$ cross section. This still fits to the standard sample size of $1 \times 1\,\mathrm{cm}^2$ area in terms of optimal resolution. The latter size is recommended for collecting good statistics in a short time, but also smaller samples would be allowed if expensive materials are employed. The given dimensions naturally lead to a $10 + 10$ m instrument (collimation and detector tube). In this way, the smallest Q-values can be collected reasonably with good statistics. As for SKADI the theme holds: "Do not wait for too long for the good statistics of underrepresented wavelengths" (the intensities of longer wavelengths in the spectrum of a cold source drop very quickly with λ^{-4} to λ^{-5}). Then, this longer instrument can easily accommodate a transmission polarizer that can be exchanged with a simple neutron guide (for polarization off). As we experienced with a single V-polarizer on KWS-1 the polarization in the range of 95% is often not high enough, and a double-V or X-polarizer would be preferred to safely reach 99%+ polarization. This polarizer would have a length in the range of 1.4 m.

This is to say that the layout of the instrument is rather simple (as displayed in Fig. V.25). The deflector starts at 48 cm from the cold source of 3 cm diameter and provides an off-set of 4 cm from the direct line of sight. The underlying cross section of all neutron guides is $2 \times 2\,\mathrm{cm}^2$ and an m-value of 1.0. All guides are evacuated. Then, there are two choppers (pulse shaping chopper at 2.05 m and frame overlap chopper at 3.68 m) with sufficient space for a polarizer changer (no polarizer, 1.4 m and 0.76 m X-shaped polarizers for 3-10 Å and 7-20 Å neutrons with an m-value of 3.6). After that, the 10 m long collimation starts. There should be collimation apertures at 10, 4, and 2 m from the sample with rectangular blades. The sample area would leave room for approximately $2 \times 2\,\mathrm{m}^2$. That shall provide enough space for rheological or stress tools, magnets, and a polarization analysis with ^{3}He. The detector tube would host two $1\,\mathrm{m}^2$ detectors. One can be moved from 1 m to 4 m distance from the sample. It has a squared hole of $20 \times 20\,\mathrm{cm}^2$ in the center. The second detector would be fixed at 10 m distance. The whole detector tube is evacuated and is shielded with absorbers from the inside.

Instrument parameters	
Target station	24 Hz
Moderator	Liquid parahydrogen, 3 cm diameter
Moderator-to-sample distance	13.7 m
Sample-to-detector distances	1 to 4 and 10 m
Wavelength band	6.8 Å, e.g. 3 - 9.8 Å
Q-range	10^{-3} Å^{-1} < Q < 1.8 Å^{-1}
Flux	3.4 to 4.1 $\times$ 10^7 n cm^{-2} s^{-1}

Table V.9: *Instrument parameters for the high resolution SANS instrument*

V.7.4 TOF-Scheme and Resolution

The resulting time-of-flight scheme from the instrument layout is depicted in Fig. V.26. As one can see, the bandwidth is 6.8 Å. The frame overlap is inhibited well for 2nd and 3rd order neutrons. The resulting resolution is discussed with respect to Fig. V.27. The pure wavelength resolution is extremely good as a result of a long instrument. This would be highly important for a GISANS use, but could also be interesting at larger Q. The complete Q-resolution is discussed on the right panel. While for the 10 m detector the contribution of the collimation dominates, a shorter detector distance can well make use of the very good resolution. A typical resolution of 2 to 5% is obtained. This would be highly interesting for liquid crystalline samples, such as quasi crystals, colloidal crystals or ordered diblock copolymers, and ordered magnetic particles and flux lines.

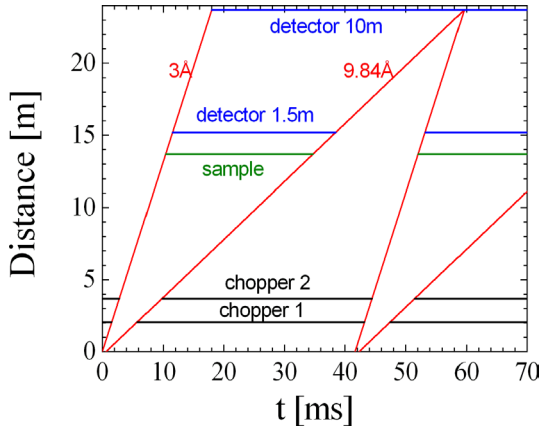

Figure V.26: *Time-of-flight scheme of the high throughput SANS with a usable bandwidth of 6.8 Å. The choppers, the sample, and the 2 detectors are indicated.*

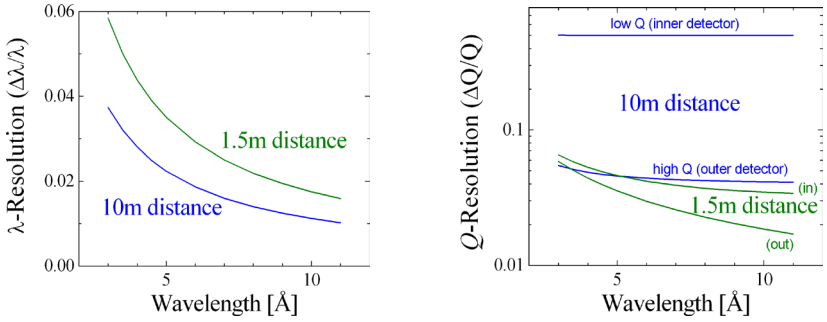

Figure V.27: *(left) The neat wavelength resolution of the* $10 + 10$ *m SANS instrument. (right) The actual* Q*-resolution of the instrument with 10 m collimation and the two detectors at 1.5 and 10 m distance.*

V.7.5 Polarization Analysis

The polarization analysis would be achieved best by ^{3}He analyzers that are continuously pumped (SEOP). At JCNS at MLZ, there exists a long history of ^{3}He polarizers (see Fig. V.28). In the figure

the sample position is depicted with the neutron flight path from the right to the left. One can see the sample aperture, the 3 T magnet, the ^{3}He polarization (non-pumped currently) and the detector tube.

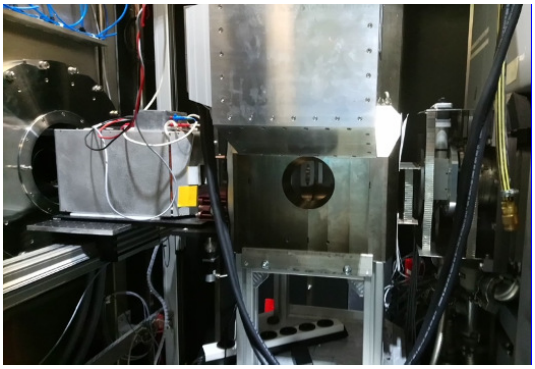

Figure V.28: *The polarization analysis set-up (left) with a 3 T magnet (center) at the sample position of KWS-1, one SANS instrument at JCNS/MLZ in Garching.*

V.7.6 Performance

The instrument has been simulated in terms of a working deflector, the polarization, the choppers and the collimation/detector setting. A simulated sample provides reasonable scattering images. The most important figure of these simulations is the resulting intensity of 3.4 to 4.1×10^7 n/cm^2/s for a 2 m collimation. As anywhere else in the world, the maximum flux with a 2 m collimation (this limit is due to the $m = 1$ coverage of the guides) is usually given as the benchmark intensity. This flux is somewhat lower than that of the ILL SANS instruments D11 [LLG07], D22 [MGZ$^+$21] and D33 [DGH$^+$16] or the MLZ instruments KWS-1 [FFD$^+$15], KWS-2 [RPFA12] and SANS-1 [MHW$^+$16]. One has to keep in mind, that the HBS instrument refers to a 2×2 cm^2 entrance aperture, while the reactor based instruments usually refer to a 5×5 cm^2 aperture. Typical for time-of-flight SANS instruments the resolution is 2 to 5 times better compared to reactor based instruments. Another aspect is the time-of-flight use of the instrument at a pulsed source. On the one hand, this provides interesting single-shot broad-band information. On the other hand, more information needs to be collected in this single shot. This strength of time-of-flight SANS experiments is beneficial for most applications.

V.7.7 Additional Options

One additional option that deviates from a simple instrument may be a dynamic Q-adaption: The entrance aperture could be varied quickly within a single pulse (large openings for short wavelengths and small openings for long wavelengths), and focusing lenses close to the sample would focus the long wavelengths while the short wavelengths would stay normally focused. For this option, the 10 m detector must also have a higher resolution (of 2-3 mm) in the center. This option is still at a very experimental stage and needs further discussion.

A second option that needs to be considered from an early stage on is a simultaneous SAXS option in the perpendicular direction to the neutron beam. The molybdenum based SAXS instruments [BFS$^+$16] (or indium metal jet) provide good options to take the same classical glass cuvettes for both probes. Just the needed space for source and detector is larger in the perpendicular direction to the neutron beam (compared to the initial 2 m). Since the HBS is a low background source, the experience must

be much better compared to the N-REX [GKP+22] experience, where X-ray reflectometry was not possible with an operating reactor. The neutron reflectivities become quickly very low at larger angles, much quicker than in most SAXS patterns. So an emphasis of SAXS on typically slightly higher Q, say 0.01 to 0.6 Å^{-1} actually complements the usual application of SANS. Proteins and lipid bilayers usually display here additional fringes that are largely suppressed by SANS measurements. So here, the advantages of SAXS really add an additional value. Other experience with a SAXS option has been gathered on the instrument D22 [MGZ+21].

All in all, the current concept provides a very good bread and butter SANS instrument with manifold applications.

V.7.8 Instrument construction

To construct the instrument, investments of about 6.6 Mio EUR are estimated which are mainly due to the costs of the large detector areas and the necessary shielding (for details see Table X.1).

V.8 Grazing-Incidence Small Angle Neutron Scattering (GISANS)

Sebastian Jaksch, Henrich Frielinghaus

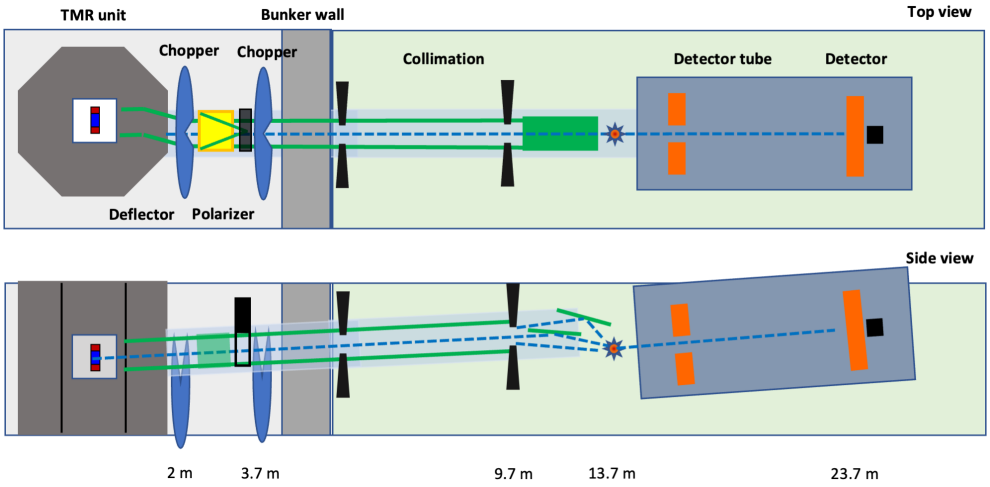

Figure V.29: *Scheme of the GISANS instrument.*

V.8.1 Introduction for GISANS

The GISANS instrument at the HBS [JLBF23] needs to be optimized for highest possible flux because often the slit geometry is used (i.e. smaller apertures than for SANS) and the scattering volume is small. So, usually, a large sample is beneficial for the experiment. Enhancement effects, such as the evanescent wave or a possible resonator, may turn the intensity balance to the better. However, the acquisition times stay usually still longer than for classical SANS. In this sense, the neutron extraction and guidance shall be optimized for flux, i.e. brightness. A second point for a GISANS instrument is the measurement of the reflectivity curve at the beginning of each experiment. This verifies that the sample-substrate structure is correct, and possibly already the structure of the sample can be observed. Only then, the instrument is switched to the GISANS mode to observe the details of the lateral structure.

V.8.2 Science Case

The science case of the GISANS instrument ranges from lipid bilayers (be it supported from a substrate or at the air-liquid interface), membranes from fuel cells or reverse osmosis, lithium batteries, thin skyrmion layers, and spray deposition of varnishes or cellulose fibrils (for sensors). One emphasis is the air-liquid interface, where many surface-active substances shall be studied close or above the critical micelle concentration (which usually means low concentrations, i.e. low scattering intensities). Another important aspect of neutrons is the solid-liquid interface because only neutrons penetrate centimeters of solid substrate. Here, many important chemical processes shall be investigated such as electrochemical processes (batteries) and catalysis for instance. As implicitly indicated, the chemical process as such is in the focus which demands for short acquisition times to resolve its kinetics. Another aspect of kinetics is the spray deposition of various materials where the drying and vapor exposure are the key.

V.8.3 Resolution

For highest intensities, it shall be allowed to take samples of the size 2 to 5 cm width and 15 cm length. Important corner points of the GISANS instrument are: (a) the measurement of reflectivity with $Q_{z,\max} = 0.2\,\text{Å}^{-1}$, (b) a high scattering depth resolution for near surface structures and (c) a relatively usual SANS resolution, may it be $Q_y = 0.002$ to $1.8\,\text{Å}^{-1}$. It turns out that the scattering depth resolution is tightly connected to the wavelength resolution, because the slit geometry suppresses divergence effects strongly. This argues for a long instrument that for simplicity is chosen to be $10 + 10$ m (collimation and detector distance). The Q_y resolution is obtained naturally. The $Q_{z,\max}$ demands a large divergence in the vertical direction, if we want to cover many incident angles simultaneously. Using mirrors, several distinct beams can be directed to the sample. For further intensity enhancement in the GISANS mode, resonators may be embedded in the substrate. As the instrument is long, the implementation of polarizers is simple. The polarization initially is in the vertical direction and may be adiabatically turned by 90° amid the collimation.

V.8.4 Scattering Depth

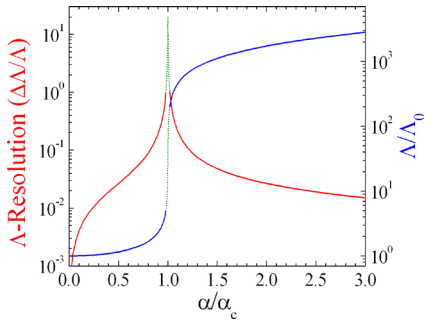

Figure V.30: *Resolution scheme of the evanescent wave to study the structure in the normal direction. The scattering depth Λ (blue curve) switches between evanescent wave and damped wave. The derivative (red curve) determines the resolution of the depth-resolved GISANS measurement. The green dotted line indicate the forbidden range.*

The scattering depth Λ as a function of the incidence angle is depicted in Fig. V.30 (blue curve, scale on right side). Below the critical angle, the evanescent wave determines the irradiated depth. The range of the accessible scattering depths varies between 200 ($= \Lambda_0$) and 2000 Å. The smallest incident angles are not reasonable because the footprint becomes very small and the GISANS scattering intensity vanishes. The scattering depth Λ_0 can be shifted additionally, by changing the overall scattering length density of the sample. Above the critical angle, the scattering depth is dominated by absorption, and strong small angle and incoherent scattering. The depicted curve corresponds to such a strong scatterer, and for weaker cases the plateau can lie orders of magnitudes higher. The derivative of this curve determines the depth resolution of a GISANS experiment (red curve, scale on left side). It is shifted by the wavelength resolution, and it lies rather low for this long GISANS instrument. The typical depth resolution for small incident angles lies in the 2% range. The maximum depth resolution shall be below 100%. So a gap for the resolved depths opens up. In the considered example, a single order of magnitude is inaccessible. But it can also be several orders. So a very good wavelength resolution is surely highly recommended for depths of up to a few 1000 Å. The range of the high scattering depths remains an issue to the scattering strength of the sample which cannot always be chosen purposely by a certain deuteration (isotope) scheme. However, the future

will show how the method of depth resolution can be applied to GISANS experiments even at larger angles.

V.8.5 Layout

The layout of the instrument is based on the demand of Q_z for air-liquid interfaces (Fig. V.29). On the one hand, the vertical divergence must be relatively large, and we want to use the down-directed neutrons for the smallest incident angle without mirrors. After careful considerations, we chose distinct incidence angles of $0.4°$, $1°$ and $2.5°$ (that reach up to $Q_z = 0.2\,\text{Å}^{-1}$ with wavelengths from 3 to 9.8 Å). For the lowest incidence angle of $0.4°$, the whole instrument may be pivoted upwards by $0.65°$ and the upper and lower mirrors of the guides shall have an m-value of 3.85. The reflectivity measurements shall be conducted with a collimation distance of 4 m. Two mirrors reflect the rays with incidence angle of $1°$ and $2.5°$. The detector tube is connected to an arm virtually anchored at the sample position and can be tilted between $0°$ and $5°$ in the vertical direction. As for the SANS instrument, two 1 m^2 detectors will be placed at 1 to 4 m (movable) and at 10 m (fixed). The collimation may vary between the distinct values of 10 m and 4 m (and maybe also 2 m). The beam extraction from the source of 3 cm diameter is performed by a deflector that shifts the beam by 4 cm. A cross section of $2 \times 2\,\text{cm}^2$ is used for the whole guide system. The choppers are placed at 2.05 m and 3.68 m with enough space for the polarizer. The whole extraction concept corresponds to the high-throughput SANS which ensures an optimal divergence transport to the sample. The sample space is approximately 2×2 m. The instrument can also be operated as a classical SANS instrument if the number of proposals is low for GISANS applications.

The reflected beams to a high-resolution detector at 4 m distance with an active area of $75 \times 75\,\text{cm}^2$ are depicted in Fig. V.31, left side. One can see the reflected beams of the upper hemisphere, and the bypassing beams in the lower hemisphere. The distinct beams correspond to incidence angles of $0.4°$, $1°$ and $2.5°$ (and $4°$ for up to $Q_z = 0.3\,\text{Å}^{-1}$). The corresponding mirrors must be coated with m-values of 4, 4, 7 and 9. The last value documents that the highest possible angle remains to be achieved in the future due to this high m. Additionally, this option of a fourth mirror reduces the sample space by approx. 60 cm along the neutron flight path. So, the three-beam option seems to be more reasonable. An important feature of the three beams is the adapted resolution that relaxes with higher angles. This would also be done in a reactor based experiment. Currently, the simulations base on planar mirrors and so the collected intensities are relatively weak for the $2.5°$. Focusing mirrors would also increase the collected intensities for the three beams and so adapt them to the relaxed resolution.

Instrument parameters	
Target station	TS-24
Moderator	Liquid para-hydrogen, 3 cm diameter
Moderator-to-sample distance	13.7 m
Sample-to-detector distances	1 to 4 and 10 m
Wavelength band	6.8 Å, e.g. 3 - 9.8 Å
Q-range	0.001 Å^{-1} < Q_y < 1.8 Å^{-1}
	0.01 Å^{-1} < Q_z < 0.2 Å^{-1}
Flux	3.4 to 4.1 × 10^7 n cm^{-2} s^{-1}

Table V.10: *Instrument parameters for GISANS instrument*

V.8.6 Performance

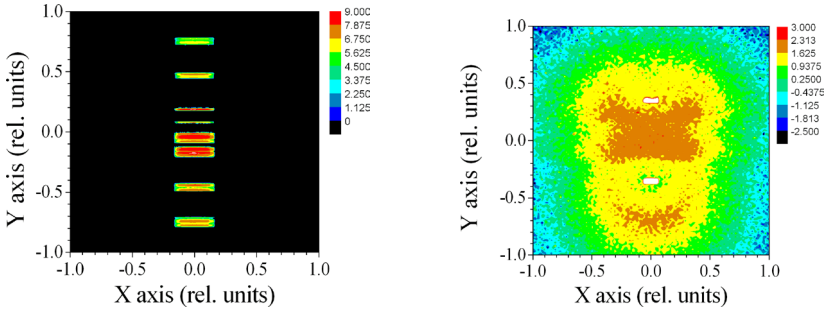

Figure V.31: (left) The reflected and bypassing beams from the mirrors at incidence angles of $0.4°$, $1°$, $2.5°$ (and $4°$) in reflectometry mode. The upper hemisphere depicts the reflected beams, and the lower hemisphere the bypassing beams. The displayed range reflects a detector size of 75×75 cm^2, which is not the detector size of the proposed instrument. (right) A simulated GISANS image on the 10 m detector of a microemulsion for relatively high incident angles. Color scale of all intensities is logarithmic. The displayed range reflects a detector size of 1×1 m^2, which is the proposed detector size.

A GISANS image for the 10 m detector is simulated for a microemulsion and relatively high incident angles (Fig. V.31 right). The simulated expected intensities of this instrument refer to the standard collimation of 2 m in the SANS mode. 3.4 to 4.1×10^7 n/cm^2/s are to be expected. For the reflectometry mode with 3 beams (with focusing mirrors) and a 2 cm wide and 15 cm long sample this corresponds to approx. 4×10^5 n/s, 3×10^6 n/s and 1×10^6 n/s in the three beams (due to increasing divergence and footprint). With a reflectivity in the range of 10^{-6}, still good statistics shall be collected within tens of minutes of exposure times. So, already the reflectometry mode is capable of following kinetics reasonably well. Good GISANS images will be collected within an hour if the scattering power of the sample is comparable to microemulsions. This information is also important for the observable time scales of kinetics.

All in all, this GISANS instrument will play in the international upper league of reflectometers and (GI)SANS instruments.

V.8.7 Instrument construction

To construct the instrument, investments of about 6.6 Mio EUR are estimated which are mainly due to the costs of the large detector areas and the necessary shielding (for details see Table X.1).

V.9 Horizontal Multi-beam Reflectometer (HorRef)

Artur Glavic

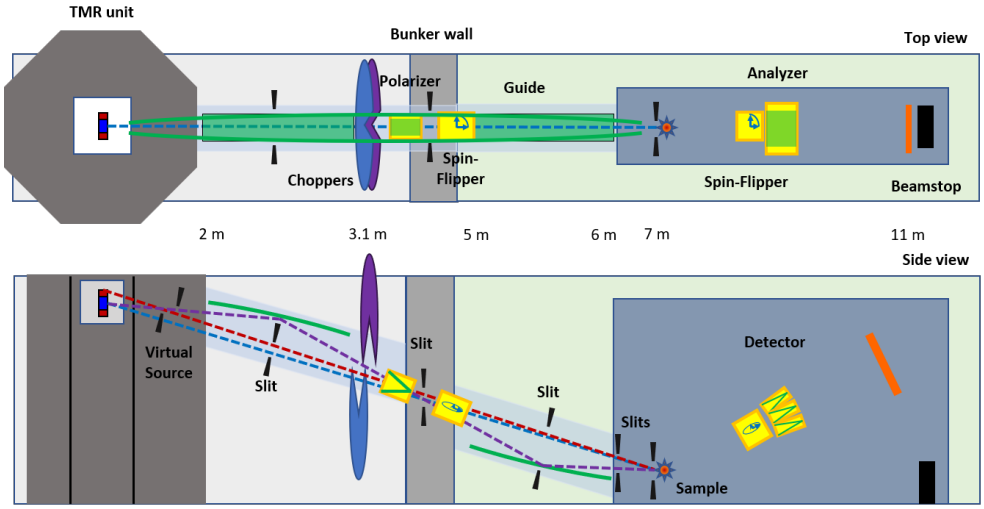

Figure V.32: *Layout of the Horizontal Reflectometer (HorRef)*

V.9.1 Overview of the Horizontal Reflectometer (HorRef)

The Horizontal Multi-beam Reflectometer (HorRef) is a short instrument for reflectometry for the full range of surface science from soft-matter biology to quantum materials and magnetism. It is optimized for the 96 Hz target station, but could be scaled to 24 Hz by increasing the moderator-to-sample distance, which would increase the instrument cost and precision requirements.

The instrument can be operated in various modes selected with a set of slits and masks that allow high intensity specular reflectivity from small samples using focusing reflectometry, multi-beam fast kinetic measurements from free liquids or high resolution off-specular or GISANS scattering.

A general layout of the instrument is shown in Figure V.32. The beamline axis is slightly tilted down to hit a horizontal sample (liquid) at a shallow angle. Distances from the moderator are labeled below the drawing for components of interest. The instrument layout presented here is optimized for a 96 Hz beam with $\Delta t \approx 250 \mu s$ pulse length. Together with the 11 m source-to-detector distance, this leads to a relative wavelength resolution ($\delta\lambda/\lambda$=5.6% @ 1.6 Å wavelength and $\delta\lambda/\lambda$=1.8% @ 5.0 Å) well suited for reflectometry experiments. With a brightness of 10^{12} n/cm²/s/sr/Å kinetic studies could be conducted in seconds. Focusing reflectometry from samples of 1 cm² with polarization analysis down to 10^{-6} or even 10^{-7} in reflectivity should also be feasible.

V.9.2 Expected Performance

All subsequent simulations were carried out with an older estimation of the source characteristics and will need to be carried out with updated moderator flux and proper, position dependent spectrum in the future.

Figure V.33 shows the fast 4-beam mode intensity (see section 9.2.2 and Fig.V.35). With this, it

Instrument parameters	
Target station	TS-96
Moderator	Liquid para-hydrogen and water
Moderator-to-focal point distance	1 m
Focusing section length	6 m
Sample-to-detector distance	4 m
Incidence angle (free liquid)	0.5° - 1.4° and 2.1° - 2.2°
Wavelength range	1.6 - 8.8 Å
Wavelength bandwidth	3.6 Å / 7.2 Å
Wavelength resolution	5.6 % - 1.0 %
Flux for multi-beam mode	$10^7 s^{-1} cm^{-2}$ (estimated for updated moderator flux)
Q-range free liquid	0.01 $Å^{-1}$ - 0.3 $Å^{-1}$

Table V.11: *Instrument parameters for a reflectometer with a Selene derived optics.*

is feasible to measure a large q-range from 0.015 $Å^{-1}$ to 0.2 $Å^{-1}$ in 1-10 s, allowing fast kinetic measurements. For features at lower q-vector, even single pulse measurements may be feasible.

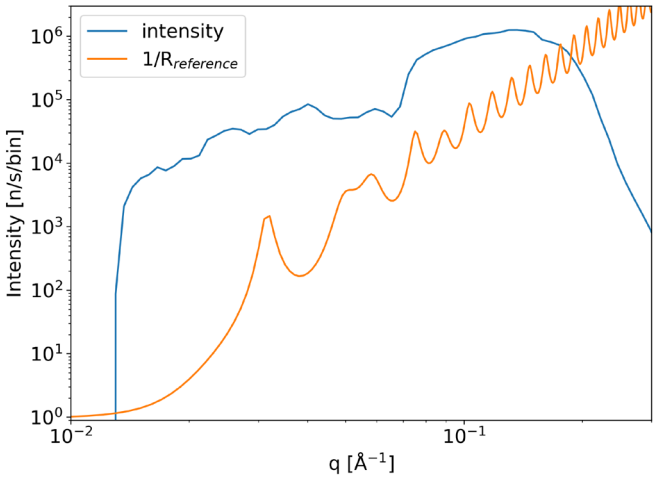

Figure V.33: *Simulated intensity for a 2x5 cm² footprint using the 4-beam mask mode. 5% q-bins are used and the inverse of a simulated sample reflectivity is shown for comparison.*

Figure V.34 shows the simulated intensity in the focusing mode using just the Selene guide with wavelength band starting at 4.5 Å. With polarization and good statistics, a typical measurement of a q-range up to 0.15 $Å^{-1}$ could easily be conducted in less than 1 h counting with 3 sample angles.

V.9.2.1 Target and moderator

A part of the beam is extracted from a thermal moderator (upper beam 2, see Fig. V.35), while most of it uses a cold moderator with approximately 20 mm diameter. (Rectangular shape would

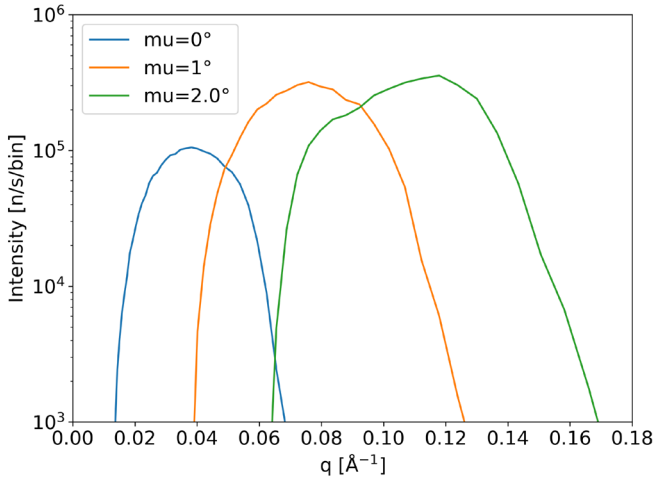

Figure V.34: *Simulated intensity using the Selene guide focusing on a 1x1 cm² footprint. 5% q-bins are used to model a moderate resolution. The tilt of the sample with respect to the horizontal plane is denoted as mu.*

be optimal.) The Virtual Source at 1 m from the moderator requires movable absorber blades to be precisely positioned with respect to the Selene optics. If this area is inaccessible for active components like motors, it could be connected with a mechanical system and integrated into the target design.

V.9.2.2 Beam transport

The beam transport concept is complex as illustrated in Figure V.35. There is a conceptual separation between the horizontal and vertical plane.

Horizontally, a large elliptical guide is employed that starts at 0.5 m and ends at 6.5 m from the source, 0.5 m from the sample. If the horizontal size of the moderator is larger, this start could be moved downstream. The symmetric arrangement with around 3 cm opening leads to most efficient illumination of a 2 cm area on the sample, which is placed horizontally. Guide reflection angles are generally modest between 0.5° and 1.2° with coating optimized for the shortest wavelength of 1.6 Å, but to a maximum that is still affordable (e.g. m=5). For most of the guide m=3-4 will be sufficient. The elliptical shape will be approximated with flat mirrors to allow the highest degree of flatness to avoid cross-talk between the horizontal and vertical planes.

In the vertical plane, two beams can be extracted. Beam 2 uses a direct view from the source to the sample to ensure highest brilliance transfer even for short wavelengths. It hits the sample under 2.1° to 2.2° incident angle and has a spectrum that shifts from cold to thermal with increasing angle. Beam 1 is defined with a Virtual Source (VS) at 1 m from the source and then projected onto the sample with two elliptical reflectors (Selene guide) that correct aberration effects. The Selene guide is optimized for longer wavelength. The beam hits the sample at smaller angles between 0.5° and 1.4°.

The whole guide system is placed in a common vacuum build up from different chambers connected with bellows. As the guide is always open at one or two sides and high placement precision is required, the guide cannot be used as vacuum vessel. There are two bandwidth selection choppers

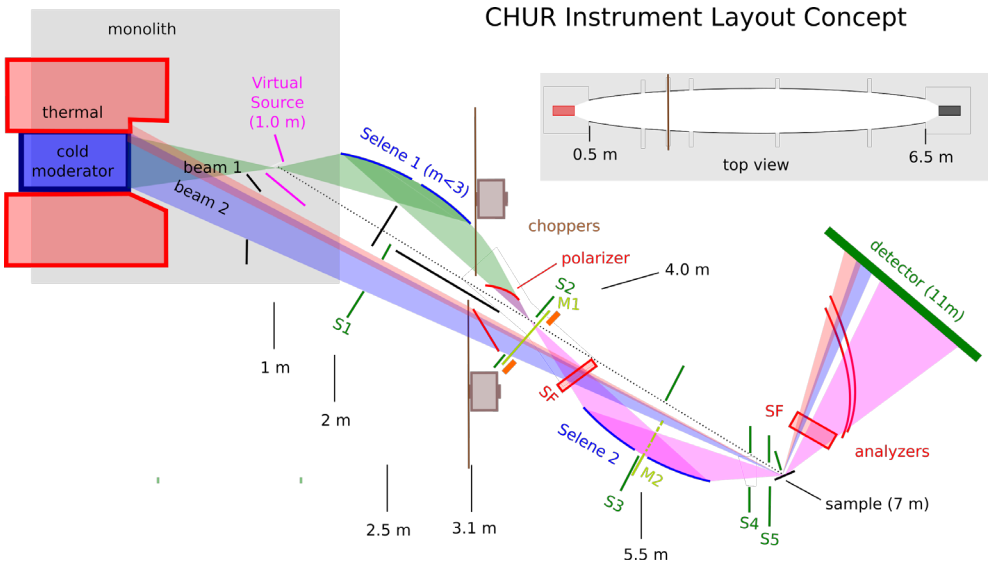

Figure V.35: *Sketch of the HorRef instrument: neutron guide and end-station layout*

at 3.1 m from the source that cut either Beam 1 or Beam 2 and thus allow selection of different bands. The operation is 96 Hz or slower for pulse-skipping mode to extend the bandwidth. Figure V.36 shows the time-distance diagram for a chopper phase set to the shortest wavelength of 1.6 Å. The bandwidth at 11 m distance is 3.6 Å. The first frame overlap is expected at 18 Å and, depending on the expected source intensity, can be filtered with a frame overlap mirror. Both choppers at 3.1 m can be standard disc choppers. The guide width to be covered is around 4 cm. As both choppers are essentially at the same location (top+bottom), maintenance access from the side may be needed that will block a large angular spread from the source. Due to the low proton energy it is expected that no significant background is expected from fast neutron contributions. Some heavy collimation around the guide will act as fast neutron shielding and albedo transport should be minimal as the neutron guide is open on either top or bottom. If simulations still show increased background levels due to fast neutron contribution, a T0 chopper with a few cm of copper could be installed in the middle focus position between the two Selene guides.

The horizontal placement of the sample position allows measurements on free liquid surfaces. Various slits and/or masks can be inserted to choose one of several optimized operation modes:

- **High intensity and low background focusing mode.** For experiments on small solid samples, the Selene optics are used, while the absorbers S1, S2 and S3 can be used to fully block beam 2 and the virtual source is set to the size of the sample. A wavelength band from 5.0 Å to 8.64 Å is chosen to avoid any Bragg scattering from windows, sample environment or substrate crystal. In this configuration, all neutrons entering the neutron guide will be reflected on the sample. All reflections in the neutron guide happen at m<1.71 in the vertical and m<2.35, where a reflectivity of >95% can be expected. Thus the total brilliance transfer is above 80%. The detector resolution is used to determine the reflection angle. Polarization and its analysis can be performed using logarithmic spiral shaped transmission polarizers (double-coated, two mirrors)[SG17] that lead to 99% polarization efficiency.

- **Multi-beam for fast kinetic measurements.** In this mode large samples like free liquid surfaces are placed at the sample location. A fixed footprint of 50 mm is set with the virtual

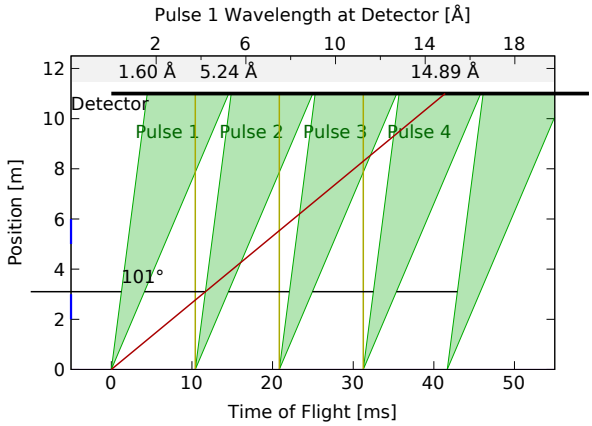

Figure V.36: *ToF-distance diagram for shortest wavelength band*

source. Masks at M1 and M2 as well as a proper setting of S1 allow beam 2 and three sub-beams of beam 1 to arrive at the sample. Beam 2 uses a short wavelength of 2.4-6.0 Å while beam 1 is set to 4.0-7.6 Å. Each of the beams has an angular resolution of 5%. With these four beams, a continues coverage of 0.015 $Å^{-1}$ up to 0.2 $Å^{-1}$ can be reached for fast kinetic measurements within seconds. The background in these experiments is dominated at high q-values by incoherent scattering from the liquid. While adding the lower angles increases the covered q-range, the additional background compared to just the highest angle measurement is small as the incident intensity scales with the square of the angle (fixed relative resolution and projected footprint).

- **Collimated mode.** This is the traditional neutron reflectometry using two collimation slits to define the resolution. It can be employed for beam 2 using S1 and S5. Due to the high flatness of the elliptical guide segments no significant blurring of the resolution by the horizontal reflections is expected. This mode is used for off-specular scattering experiments and allows almost 100% brilliance transfer for longer wavelengths due to the direct view of the source (see beam 2 in Fig. V.37). For extremely clean experiments or GISANS, the second half of the guide can be lifted out of the beam (staying aligned using kinematic mounts). Using S1 as resolution slit, the collimation for GISANS is 4.5 m and thus well matched to the sample-to-detector distance of 4 m. Long wavelengths of >5 Å will be optimal for GISANS, where relative bandwidth is less important than wavelength resolution and intensity. As there is no reflection, the brilliance transfer in this mode is always 100%. Depending on the location of S1, different parts of the moderator can be viewed to deliver a cold, hybrid or thermal spectrum to the sample.

V.9.2.3 Sample Exposure Systems

The sample requires a standard positioning stack. S5 in front of the sample has to be movable/removable to allow closest placement to the sample as possible and access for large magnets or cryostats. Moderate magnetic fields, temperatures down to 4 K and optimized sample equipment for liquid-air and solid-liquid experiments will be required. No particularly challenging controls will be needed.

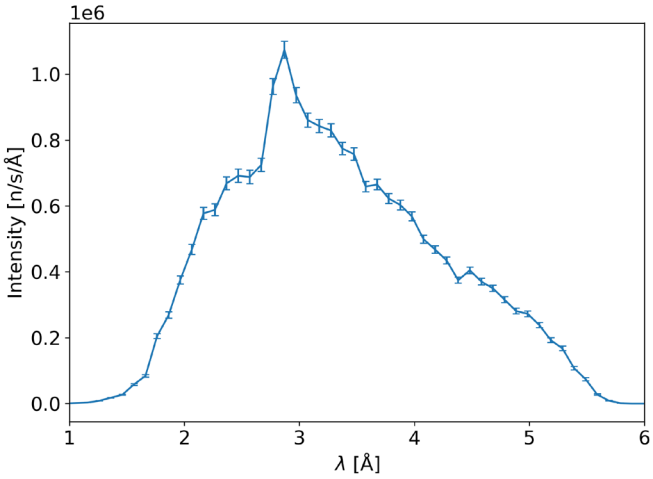

Figure V.37: *Intensity on a 2x2 cm² sample with collimated mode under 1.9° incident angle with* $\frac{\Delta\theta}{\theta} = 10\%$.

V.9.2.4 Detectors

The detector arm has to be lifted against gravity. Detector-to-sample distance will be around 4 m. A resolution of at least 1 mm in reflection direction and 5 mm in horizontal direction is required. Time resolution has to match the source pulse length. Different detector technologies might be suitable for the instrument. Existing developments from ESS as the SONDE SANS detector [SRK+18] or multi-blade reflectivity detector[MMA+18] would be suitable. Count rates will be very high in reference measurements for focusing reflectometry or in the direct beam for collimated mode. An important aspect is background from cross-talk of high intensity hitting the detector ($<10^{-4}$). A single crystal entrance window or very thin aluminum foil will thus be needed. The detector should cover an area of around 200x500 mm² to allow off-specular experiments. A minimum of 100x200 mm² is required. Between sample and detector a flight tube filled with Ar or He will increase transmission and shield from background.

V.9.2.5 Experimental cave

If no unexpected sources of background are found in the instrument hall, no experimental cave will be required. Depending on the source characteristics, there may be some shielding walls needed, but those will probably be compact (<10 cm steel).

V.9.2.6 Instrument control and monitoring

The Selene optics will require custom adjustment and sensing options that allow in-situ alignment within the vacuum vessel. Due to the use of a single bandwith chopper, none or simple beam monitoring will be required. The optical path will be aligned with the help of a laser fiber system that is shined down the beamline from the backside of the virtual source. A CCD camera at the sample or middle focus location can be used to visualise the optical beam on a screen or the neutron beam on a scintilator plate.

V.9.2.7 Software

The data will be recorded in event mode in dependence of the detector pixels. Extraction of the reflection angle, wavelength and corresponding wave vector transfer will be done according to proven algorithms already being used at other facilities. This data reduction together with appropriate normalization using reference measurements will result in specular reflectivity datasets or 2D/3D off-specular or GISANS maps. These can be analyzed with existing software tools like RefNX[NP19], Refl1D[KKM+12], GenX[GB22] or BornAgain[PVHB+20].

All standard instrument actions (change of angle, wavelength band, polarisation, instrument configuration and collimation) have to be automatized and controllable through scripting. As many experiments can be run over night, a remote way of viewing the status and remote control for instrument scientists is required.

V.9.2.8 Floor space and requirements

Figure V.38 shows a sketch of the required area for the instrument. On one side of the neutron transport, free access is required to be able to maintain the active components of the beamline as well as the guide adjustment mechanism. The experimental area needs to be sufficiently large for low temperature and high field sample environments and has to be fenced off. Additional space is needed for the instrument operator (control hutch) as well as for control racks that can be placed at various locations in close proximity of the beamline.

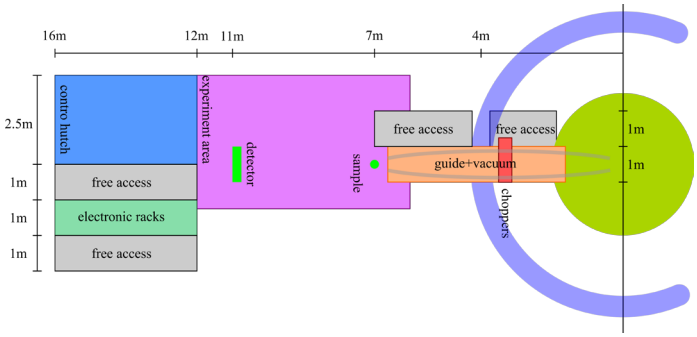

Figure V.38: HorRef floor plan with estimated areas

The instrument floor load will be modest with <5 t/m² with local loads (<50 cm) potentially reaching 20 t/m². For changes of instrument configuration and sample environment the hall crane will be used. A 1 t crane will be sufficient for most operations.

For solid-liquid and liquid-air experiments, a close chemical/biological preparation laboratory as well as a small preparation area with fume hood at the instrument will be required.

Other required infrastructure include power and cooling water for high field magnets, motion cabinets and detectors, helium recovery (if non closed-cycle systems are used), detector gas, 2-3 vacuum pumps, IT-network infrastructure.

The instrument will require a standard control hutch with a separate control and analysis computer as well as sufficient desk space to accommodate 4 users and one instrument scientist. Standard desktop computer will be sufficient.

V.9.3 Health and safety

Considering the limited average source flux, it is expected that no guide shielding outside the bunker will be required. The experimental area will have to be fenced off when the beam is open, with PSS access controlled doors, and there may be a need for a suitable beam-stop behind the detector. If low-activation materials are used close to the beam, all components outside the bunker should be accessible shortly after closing the shutter. For in-bunker components, an access for radiation workers should also be possible directly after opening the shielding.

V.9.4 Instrument construction

All technologies used in the concept have been successfully employed at other neutron facilities. Due to the compactness of the optical and active components within the bunker area, a significant design effort is required to adopt these existing technologies to the available space. With the precision used for the neutron guides of the PSI AMOR [SG16b, SFP12] and ESS Estia [GSS16, AAJ^{+}20] instruments, the Selene guide will be able to deliver focus sizes smaller then 0.2 mm. As only two 1 m pieces of such precision reflectors will be needed, a higher shape accuracy should be reached to further decrease these values.

For best performance, all vacuum vessels should be connected with bellows, reducing the number of required windows to a minium. The beam transport will be separated into four parts: the Selene 1 area within the bunker wall, the chopper area before the bunker wall, a small in-bunker section, and the Selene 2 area until an exit window before the sample. These areas can be pre-assembled and tested.

The highest technical risks are the possibility of cross-talk between horizontal and vertical optical plane as well as the lifting of the detector arm of 4 m length. To mitigate the former, all vertical reflectors should be made of high flatness substrates with sufficient thickness. Experiments should be conducted on SANS beamlines to verify the maximum beam-broadening that can occur from one reflection. For the latter risk, close collaboration with experts from other facilities with similar instruments (ILL, SINQ, ISIS) is encouraged.

From an operations point of view, the failure of the virtual source slit or one of the choppers could not be fixed quickly as they are within the shielding bunker. Any such failures would still allow a limited operation of the instrument by either using only collimated mode (VS or chopper for beam 1) or employing S1 and S3 to collimate the beam from the Selene guide for experiments that can't use the focusing mode.

V.10 Vertical Reflectometer for Off-specular Scattering (OffRef)

Ulrich Rücker, Stefan Mattauch

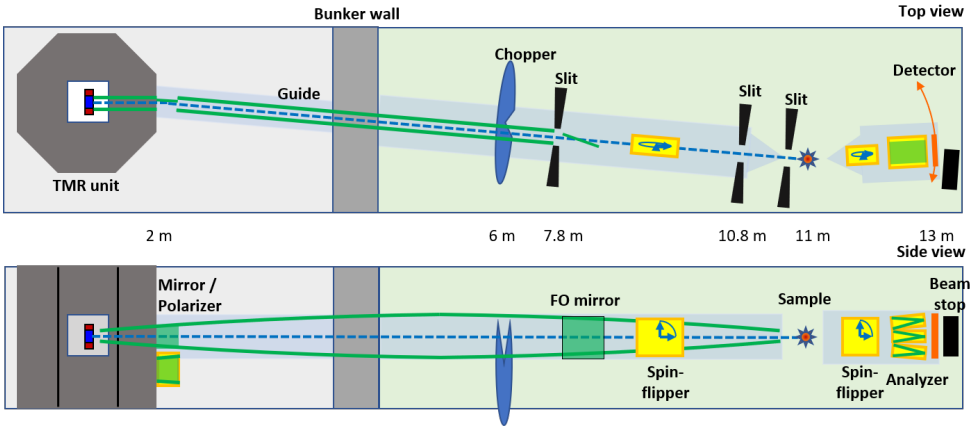

Figure V.39: *Schematic layout of the Vertical Reflectometer*

V.10.1 Overview to the Vertical Reflectometer (OffRef)

The Vertical Reflectometer for Off-specular Scattering is placed at the 24 Hz target station for high intensity combined with moderate wavelength resolution. Together with a collimation of the incident beam, the instrument allows to measure the specular reflectivity together with the off-specular scattering simultaneously on the position sensitive detector. A total length of 13 m yields sufficient bandwidth and resolution (s. Table V.12) to measure the complete reflectivity pattern of a sample in at most three angular settings. Like the horizontal reflectometer (s. section V.9), an elliptic guide is used to deliver high flux to the sample position, but now in vertical direction. In horizontal direction the divergence is defined by a variable collimation slit system to define the divergence and size of the incoming beam.

As the instrument is designed for off-specular measurements, great care is taken to reduce the background as much as possible: a mirror is used to get out of the direct line of sight, data acquisition will not take place during the proton pulse, neutrons above $\lambda = 25$ Å are filtered by a frame-overlap mirror, and the beam is transported mostly in vacuum and will be reduced to the sample size.

The vertical arrangement offers the advantage that the beam impinging on the sample is always at the same place even for higher angles of incidence, which allows easy installation of heavy sample environment at the sample position, e.g. an electromagnet. Larger scattering angles can be reached by moving the detector in the horizontal plane while the weight of the detector assembly is constantly held by the support structure. The setup is also optimal for in-situ experiments that can be mounted in a fixed geometry. The large wavelength band allows the investigation of a decent Q range without the need of adapting the geometry, so that the reflection pattern can be recorded in real time as a function of the state of the sample. This option can be interesting e.g. for observing the growth of layers during deposition, the reaction of samples with gases at elevated temperatures, or the influence of applied voltages inducing ferroelectric or electrochemical effects.

This instrument geometry is suitable for the investigation of layered structures of solid matter or of soft matter at a solid-liquid interface. In both cases, lateral structures with characteristic length

scales of a few μm typically emerge from the preparation conditions, in the case of multilayers often as correlated roughness. The off-specular scattering from these lateral correlations appears around and below the specular reflection. A standardized measurement of the off-specular scattering allows to precisely correct the specular reflectivity signal from the off-specular contribution at the same place. Additionally, modelling of the off-specular scattering allows understanding the nature of the lateral structures in the sample. The optional use of polarized neutrons and polarization analysis gives access to the magnetic moments in layered structures and allows suppressing the incoherently scattered neutron background in experiments with samples in contact with hydrogenated liquids.

V.10.2 Layout

A reflectometer needs a very anisotropic beam: it is highly collimated in the scattering plane (here horizontally) and focused on the sample position in the other direction (here vertically). The instrument starts with a liquid parahydrogen moderator of 2 cm diameter. This moderator offers the highest brightness of neutrons in the range 3 - 5 Å. The drop in the spectrum towards longer wavelengths is compensated by the higher reflectivity at smaller Q values. The small size can nicely be imaged by an elliptical guide onto the sample.

The neutron guide starts close to the cold source and includes a detachable guide nose between the second collimation slit and the sample position to provide highest intensity to small samples, while allowing more bulky sample environment with the nose removed. In the vertical direction, the guide has an elliptical shape with 20 mm opening in the beginning and a maximal height of 184 mm. At the end of the detachable nose, i.e. in front of the sample position, the guide opening is 12 mm high. The coating of the elliptical guide is a supermirror with m-values up to 4 at both ends.

In horizontal direction, the guide is straight, 11 mm wide, and built from uncoated glass, as m=0.3 is sufficient to transport all divergence that can be accepted by the collimation. The first 1.8 m guide are straight inside the extraction plug, then a 0.7 m long m=4.5 mirror at an angle of 0.9° reflects the wavelengths above λ = 2 Å. The angle is chosen so that the optional polarizer at this place (see section V.10.4) properly suppresses spin down neutrons for wavelengths up to λ = 12 Å. Another uncoated straight guide section of 3.3 m length is followed by a collimation of two 2-segment slits at a distance of 3 m. The last slit at the end of the detachable nose is only used for background reduction by limiting the over-illumination of small samples. It does not contribute to the collimation.

The sample stack allows the alignment of the sample (ideally including the sample environment) in all 6 degrees of freedom. To be able to carry heavy magnets, it needs to have a maximum load of at least 800 kg.

The detector arm can be rotated in the scattering plane from -5° to 40°. A 2D position sensitive detector at 2 m distance from the sample records the specular reflectivity and the off-specular scattering simultaneously. In horizontal direction, a spatial resolution of 2 mm and a detector size of 400 mm are required to properly resolve the specular and the off-specular signals, in vertical direction the detector needs to be 800 mm high with a resolution better than 5 mm to cover the entire vertical divergence.

V.10.3 ToF scheme and resolution

Figure V.40 shows the Time-of-Flight scheme of the instrument. A bandwidth chopper with an opening of 130° turning synchronously to the source with 24 Hz at a distance of 6 m from the moderator defines the wavelength band. The blue lines in fig. V.40 show the shortest wavelength of 2 Å, the green lines the longest wavelength of 12 Å. At the detector position at 13 m from the moderator, the neutrons of the longest wavelength arrive before the next proton pulse, so that the measurement of all useful neutrons can be performed without any background of prompt fast neutrons.

Frame overlap would appear for wavelengths above 29 Å, which would be a severe problem for the operation of a reflectometer, as the reflectivity for the longer wavelengths in the frame overlap band is much higher than for the regular neutron wavelengths. To prevent from this source of high-intensity parasitic background signal, a polished Si wafer is integrated as a frame overlap mirror just after the first collimation slit to reflect all neutrons with wavelengths above 25 Å out of the beam path.

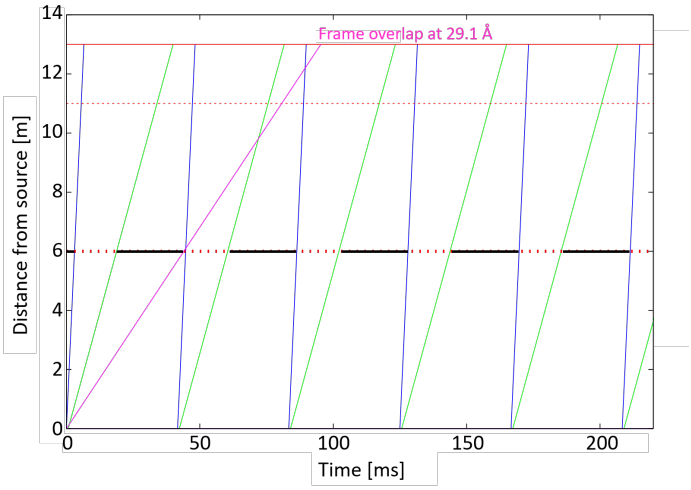

Figure V.40: *Time-of-flight scheme of the reflectometer for off-specular scattering.*

Figure V.41 shows the relative wavelength resolution of the instrument. The wavelength resolution in the entire band is better than 10%, which is well suitable for the investigation of thin layers. For the investigation of multilayer structures, sometimes a resolution better than 3% is requested, which is available above 6 Å wavelength, i.e. in 2/3 of the wavelength band used. Still then the first part of the band can be used to investigate the thinner constituents of the structure with lower resolution.

The main contribution of the resolution of the reflectometer is due to the angular resolution of the incoming beam. The 3 m long collimation with 4-segment slits offers optimal tuning of the incoming beam divergence to the properties of the sample under investigation.

V.10.4 Optional polarization analysis

The instrument allows to provide polarized neutrons and polarization analysis as an option without the necessity of larger changes in the setup. The polarizer is installed in a motorized exchanger with the deflection mirror just after the shielding of the target station. A m = 4.5 Fe/Si supermirror polarizer is suitable for the polarization of the entire wavelength band between 2 Å and 12 Å with the angle of incidence set to 0.9°. This angle is above the critical angle for spin down neutrons at 12 Å wavelength. Using this device, the instrument can switch from operation with the full intensity of non-polarized neutrons to polarized neutrons within one minute.

Two material-free RF spin flippers allow to choose the polarization of the incoming beam as well as the analyzed polarization without affecting the angular resolution.

A fan-type assembly of transmission polarizer cavities provides polarization analysis covering the entire area of the PSD without changing the direction of the neutron in the scattering plane, so that the

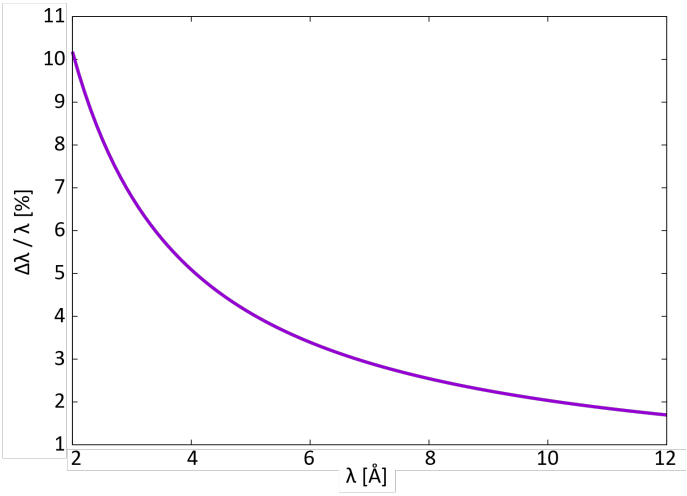

Figure V.41: Relative wavelength resolution as a function of the wavelength at the detector position

angular resolution for specular reflectivity and off-specular scattering is not harmed. This analyzer can be removed by a motorized stage to allow measurements with unpolarized neutrons without intensity compromises.

V.10.5 Performance

The main instrument parameters are listed in Table V.12. The intensity at the sample for the 3 different inclination angles is shown in Fig. V.42. The reflectivity curve obtained from a virtual experiment of a model sample (200 Å thick polystyrene film on a Si wafer, 1 cm^2 surface area) using the VITESS simulation program [ZLNF14] is shown in Fig. V.43. It can clearly be seen that the resolution at high Q in each of the three measurements is compromised by the relaxed wavelength resolution for neutrons below $\lambda = 2$ Å (Fig. V.41).

Instrument parameters	
Target station	TS-24
Moderator	Liquid parahydrogen, 2 cm diameter
Moderator-to-sample distance	11 m
Sample-to-detector distance	2 m
Wavelength band	2 - 12 Å
Resolution	10.1 - 1.7 %
Q range	0.001 - 1 $Å^{-1}$
Flux	4.8×10^7 n cm^{-2} s^{-1} for 1.1° divergence

Table V.12: Instrument parameters for the Vertical Reflectometer

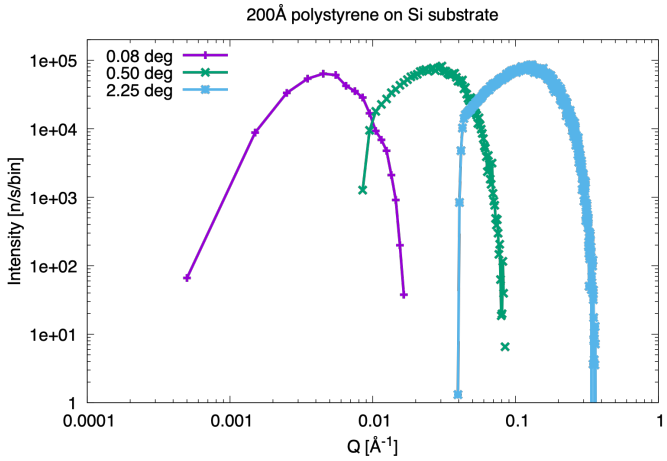

Figure V.42: *Intensity impinging on a sample of 1 cm^2 surface area at different angles of incidence. The binning size in Q is 10^{-3} Å^{-1}.*

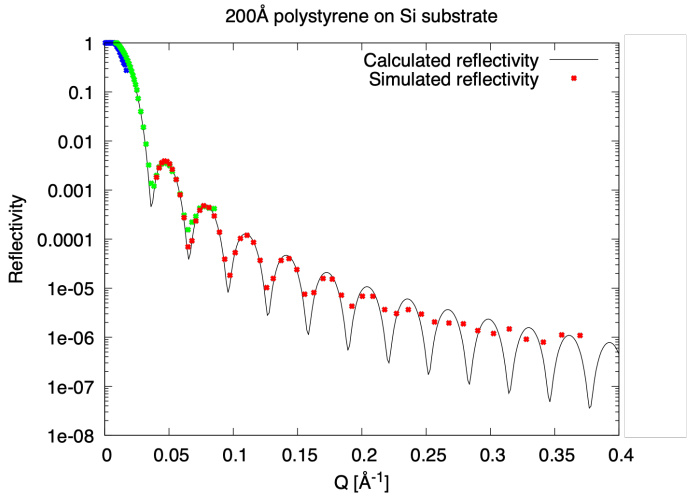

Figure V.43: *Simulated reflectivity measurement of a 200 Å thick polystyrene film on a Si wafer of 1 cm^2 size. Three measurements at different angles of incidence have been simulated: 0.08° (blue), 0.5° (green), and 2.25° (red).*
The 'calculated reflectivity' does not take the convolution with resolution into account.

V.10.6 Sample environment

The Vertical Reflectometer can easily be equipped with all standard sample environment that can be placed on the sample position, but some specific sample environment is especially useful for such an instrument.

A compact cryostat with an optical window perpendicular to the sample surface allows measurements at low temperatures with still an easy access for a laser beam for convenient alignment.

An electromagnet with horizontal poles offers to measure magnetization of layered structures as a function of the applied magnetic field with polarized neutrons and polarization analysis. The combination of the compact cryostat with the electromagnet is suitable for almost all investigations of magnetic layered structures.

For the investigation of biological membranes at the solid-liquid interface, a cell based on a thick Si block is valuable, where the membrane can be illuminated from the substrate side through the Si block. This geometry minimizes the intensity loss due to incoherent scattering in the liquid environment. In such a cell, the liquid phase can be exchanged without the need of re-adjustment, so that the influences of changing pH or salt concentrations, etc. can efficiently be investigated.

VI.

INSTRUMENTATION FOR NEUTRON SPECTROSCOPY

Inelastic neutron scattering provides unique information about dynamic properties of condensed matter. Computer modelling of the inelastic neutron scattering cross sections allows one to obtain parameters of model Hamiltonians, such as inter-atomic forces or exchange constants, which enable the prediction of the macroscopic response of a material and thus lead to a microscopic understanding of the relation between structure and function. Neutron spectroscopy gives direct access in absolute units to self-, pair-, and spin-correlation functions, which are the fundamental quantities derived by modern ab-initio theories. Thus, the simplicity of the neutron cross sections and the fact that they can be measured on an absolute scale allows benchmarking of ab-initio theories and computer modelling with huge impact in many different scientific fields. In this important aspect, neutrons are unrivalled, as no other method can provide such a stringent test of microscopic theories. It is true that particular problems can nowadays be addressed with modern synchrotron radiation techniques: steep phonon branches can be determined with high resolution ($\approx$ 1 meV) inelastic x-ray spectroscopy; element specific partial phonon density of states can be measured for certain elements by nuclear resonance scattering; slow dynamics in colloids can be followed by coherent x-ray correlation spectroscopy; and high energy magnon dispersions by resonant inelastic x-ray scattering (RIXS). All these x-ray techniques are largely complementary to inelastic neutron scattering, but none of them gives the same direct and universal access to absolute scattering functions as does neutron spectroscopy. To give an example: due to the restricted resolution, RIXS can only be used to determine relatively high energy magnetic excitations. But due to the resonance process involved, with its unknown transition matrix elements, RIXS cannot provide a model-free access to the eigenvectors, which neutrons naturally do. For these quite general arguments, neutron spectroscopy will remain essential and unrivalled for many decades to come.

The study of spin excitations in topological materials are recent highlights of cold neutron spectroscopy, e.g. resolving the magnetic interactions in materials hosting Skyrmions. Many emergent magnetic phenomena in novel materials rely on frustration, resulting in small diffuse signals. The spectrometers at the HBS are perfectly suited to explore the magnetic correlations here, because neutrons are highly sensitive to the atomic magnetic moments and the instruments feature a coherence length matching the correlation range in the materials for different kinds of applications.

New functional materials, e.g hybrid perowskites or metal or organic frameworks, promise new applications but have often technological issues, which can both be related to the hydrogen and its motions. Here the HBS provides instruments to probe local and/or spatially correlated motions on the timescale from ps to μs, which are relevant to understands their function or failure.

Biological samples are a special class of functional materials. The spectrometer suite of HBS can address local and collective dynamics in a wide time window to understand e.g., the transport and diffusion across membranes or the protein-protein interactions.

In this volume we present designs for two direct geometry spectrometers in the cold and thermal energy range. We discuss inverted geometry instruments for the study of coherent excitations in single crystals. A near backscattering instrument provides access to the energy resolution range below 10 μeV. A suite of resonant and high resolution spin echo spectrometers allows studies on time scales from ps up to several 100 ns.

VI.1 Cold Chopper Spectrometer (CCS)

Nicolo Violini

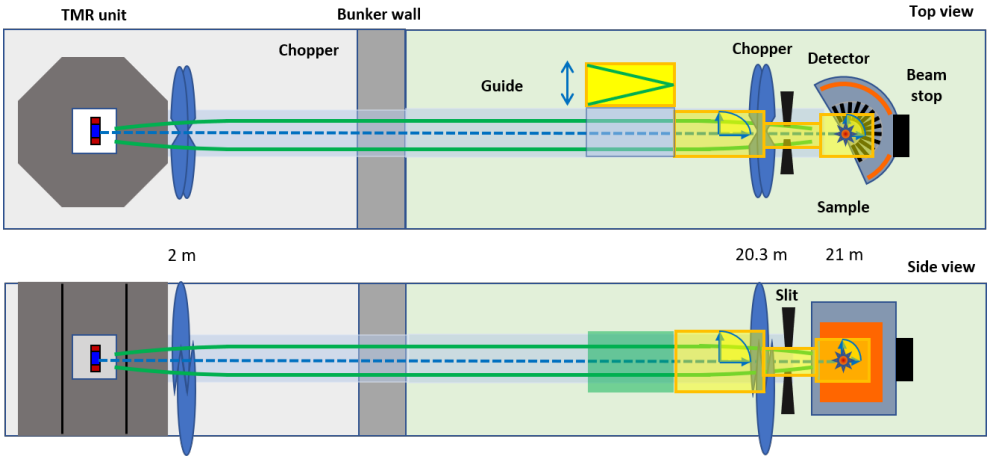

Figure VI.1: *Schematic top and side view of the cold chopper spectrometer CCS.*

Cold chopper spectroscopy is a key method to study different time and lengths scales in one instrument. This requires a wide range of initial neutron energies to be combined with flexible resolution settings. Successful instruments are operated both at continuous and pulsed neutron sources. Instruments at pulsed sources profit from the high peak flux, while reactor based instruments use repetition rates that are matched to the requested dynamical range of an individual experiment. They are typically in the range of 100 Hz, i.e a time frame of about 10 ms is requested to record the inelastically scattered neutrons of interest. So the 96 Hz target station provides just the right time frame and hence the detectors record 'useful' events for 100% of the time. The required flexibility on the resolution can be realized by a system of fast spinning choppers, which control the wavelength selection and illumination time in a wide range. Hence the instrument features a rather compact layout with sample-to-detector distance of 3 m and moderator-to-sample distance of 21 m. The instrument is designed for spectroscopy in a wide range of science fields from soft-matter and biology to quantum materials and magnetism.

The instrument can operate in various energy resolution modes spanning from the highest elastic energy resolution of 1% to a more relaxed resolution of 5%. Measurements can use an incident neutron energy range between 1 and 30 meV (1.6 - 9.0 Å).

The simulated performance enables the option to implement polarisation analysis. Also here, the intensities are promising for a very competitive instrument. An overview of the instrument layout is shown in Figure VI.1.

VI.1.1 Science case

For the scientific challenges of the future, many different research fields will benefit from a cold direct geometry chopper spectrometer operating at a neutron source such as the HBS. The areas of potential applications range from biological and soft matter materials to materials science questions or novel magnetic quantum materials. Common to these diverse fields is the fact that they all require an instrument capable to probe time scales from pico- to nano-seconds on a length scale

Instrument parameters	
Target station	TS-96
Moderator	Liquid parahydrogen
Moderator-to-sample distance	21 m
Sample-to-detector distance	3 m
Initial energy range	1 meV$< E <$ 30 meV
Final energy range	0.8 meV $< E <$ 100 meV
Energy resolution range	0.02 meV$< \Delta\hbar\omega <$1 meV
Detector range	$3^\circ < 2\theta < 150^\circ$
	$-3^\circ < 2\theta < -30^\circ$
Flux @ $\lambda = 5$ Å, $\delta\hbar\omega = 100\mu$eV	3.4×10^5 n cm^{-2}s^{-1}

Table VI.1: *Instrument parameters for the cold chopper spectrometer*

from Ångström to nanometers. Moreover, the instrument will help investigate not only model systems, but also materials that are more realistic and hence technological more relevant, which often implies higher complexity of the investigated systems in terms of composition when moving away from isolated substances to composites or crowed solutions. For a detailed understanding, the dynamic landscape needs to be probed over a large scale, i.e. it is mandatory to access different time domains experimentally.

In the area of biological applications, the instrument will have a high impact in investigations of protein dynamics that can occur on a wide range of time scales. Sample sizes are typically small and the signal of interest might be well concealed in the scattering originating from other parts of the sample, especially if partial deuteration proves difficult. With the concurrent characterization of such samples in many time domains at an instrument with excellent signal-to-noise ratio and a large Q-range, the dynamics of different bound water populations can be probed in unprecedented detail and thus new insights in the interconnection of motion and dynamics in biological systems are to be expected. The high energy resolution option of the instrument allows to also explore the slow dynamics region (down to the μeV range) to gain sufficient overlap with instruments dedicated to measure slow dynamics such as back-scattering or neutron spin echo spectrometers.

In the area of soft condensed matter, the instrument can contribute to reveal dynamic features in polymers, lipid membranes, or molecular liquids, which are prevailing in a number of technological important fields, e.g. pharmaceutical applications, gas and oil industry, manufacturing involving polymers and plastics or food industry.

In the area of functional materials and materials science, the instrument can reveal features that will help understand atomic mobility on a microscopic level as a prerequisite for materials development. The examples are numerous and cover a wide range of different areas such as ultra high strength concrete, ion mobility in ionic liquid electrolytes, proton diffusivity in ceramic perovskites, gas adsorption in porous materials for CO2 sequestration, or diffusion dynamics in metal alloy melts, for instance in porous metal-organic framework systems (MOFs).

Finally, in the area of magnetism, the instrument can help to understand magnetic materials on a microscopic scale with a huge impact on technological applications as well as on fundamental science. In particular for the low energy spin excitations, neutron spectroscopy is the unique tool to study dynamics of the electronic spins in novel and technologically relevant materials. Examples are charge and spin ordering in multiferroics, or the symmetry changes observed in the spin dynamics in high temperature superconductors. To further understand these phenomena and to benchmark theory with experimental results, neutron spectroscopy is the ideal tool to probe excitation modes on

various length and energy scales. Further areas of applications include molecular magnets, which can be used in such diverse fields as e.g. spintronics for ultra high density magnetic recording or biological applications.

The successful experiment in any of these fields depends on high intensity, a clean resolution function, excellent signal-to-noise ratio, and a large as possible dynamic range.

The proposed instrument will have the necessary capabilities to be able to bring significant progress in both, fundamental science and technological application, especially in the above listed areas of interest:

- the chopper system of the instrument enables to focus on the time domain of interest by choosing the appropriate energy resolution,
- the guide system is optimized for maximum flux for cold neutrons,
- most experiments are expected to utilize the standard guide configuration with an extended beam spot size of 10 x 10 mm^2 at the sample position.

VI.1.2 Layout

In this section we describe in more details the instrument layout.

VI.1.2.1 Target station and moderator(s)

The liquid para H_2 moderator provides a high brightness in a wide wavelength range allowing experiments with initial neutron energy between 20 meV and 0.5 meV (2.0 - 12.8 Å). As mentioned above, the 96 Hz provides a well adapted time frame to operate the instrument in a monochromatic mode similar to a reactor instrument, which allows a comparably straight forward and simple way to analyse the data.

VI.1.2.2 Beam extraction and transport

The neutron guide features an elliptic profile with a focal point 20 cm behind the moderator and the other one at the sample position. The maximum width (and height) is 6 cm. Entrance and exit size is 2×2 cm^2. The profile of the tapered guide is coated with m=3 supermirrors.

VI.1.2.3 Choppers

The instrument is equipped with 4 chopper discs grouped in two assemblies. Each assembly consists of two counter rotating discs mounted up-under. The first assembly is placed at 2 m from the moderator (pulse shaping), the second at 20.3 m from the moderator (monochromating). All four discs have 700 mm diameter and a maximum speed of 288 Hz. At this frequency, the instrument provides its highest resolution of 1% elastic energy resolution. The energy resolution resolution can be traded for flux by variation of the repetition rate of the chopper assembly in steps of 96 Hz.

VI.1.2.4 Polarization equipment

The instrument will be equipped with various components to enable x-y-z polarisation analysis. The incident neutron polarisation is provided by a high performance multi-V polarising cavity. Its function is to polarise the neutron spin along the z direction. Depending on the experiment, once neutrons

Choppers	Position	opening size [deg]	speed [Hz]
Pulse Shaping	2 m	20	288
Monochromating	20.3 m	4	288

Table VI.2: Choppers parameters for the cold chopper spectrometer

are polarised along z direction, their polarisation needs to be either kept or rotated while travelling to the sample position. Therefore the polarisation equipment includes a spin holding system and a system to implement adiabatic rotation. In order to perform the analysis of spin after scattering, the instrument will be equipped with a ^{3}He based analyser, whose design will be based on the magic PASTIS set-up, that has been developed at JCNS [VBB10]. In order to perform the polarised experiments, it is required to select only materials with low magnetic permeability in the area where polarisation equipment is installed and in general within 1 m from the sample position.

VI.1.2.5 Radial oscillating collimator

The background from parasitic scattering at the sample environment is a relevant contribution to the background noise in neutron spectroscopy and it can represent a limitation to investigate weak signals. Therefore we envisage to implement a radial oscillating collimator, which is a quite standard solution to reduce this source of background and achieve a better signal-to-noise-ratio. The size of the collimating blades should cover approximately the range from 50 cm to 70 cm from the sample position in radial direction. While the motion doesn't require a significant development, a careful attention should be put into selecting the proper drives to meet the non-magnetic requirements.

VI.1.2.6 Detector

For this instrument we envisage the option to procure a ^{3}He detector, given that the required pressure is not as high as for thermal neutron spectrometers and therefore the required cost does not seem a limiting factor. 3He PSD tubes can cope with the detection rate generated by this instrument and are rather insensitive to Gamma radiation to enable a very good signal-to-noise ratio. They represent state-of-the-art technology for these applications and therefore the implementation of the DAQ-system is straightforward. The tubes will be placed at approximately 3 m distance from the sample and will be 2 m high to cover scattering angles from -15 deg to 25 deg in vertical direction. The tubes will be arranged in a way to cover the angles from -30 deg to +150 deg on the horizontal plane. The forward direction within -3 deg and +3 deg will not be covered with detectors, in order to install a get-lost tube and a beam stop.

VI.1.3 Sample environment

Being a multi-purpose instrument, users may request the use of many types of standard sample environment equipment to control and vary the sample state, such as temperature, pressure, humidity, electric and magnetic fields. We envisage the ability to adapt to sample environment provided by the users, as well.

VI.1.4 Shielding

The most relevant contribution to the shielding of this instrument comes from gammas generated at the neutron guide. At the moment we don't have enough information to estimate the amount

of gammas and therefore the shielding power required to meet safety requirements. However, we can envisage a relatively simple shielding composition mostly based on concrete. However, facility requirements need to be carefully considered. From the viewpoint of scientific performance, the instrument requires a good shielding design in the secondary spectrometer. The vacuum chamber hosting detectors should feature neutron absorbing vanes to avoid cross talk between opposite or nearly opposite tubes, it should include a neutron absorbing inner structure to avoid back-scattering from the vacuum chamber itself, and it should include a properly designed beam-stop, which fulfils both a safety function and a noise reduction function.

VI.1.5 Requirements

The instrument will feature a big vacuum tank to host the detectors, which could easily take a volume in between 70 and 80 m^3 and require a floor space of 50 m^2 to enable installation and maintenance work. In addition to this, the users will need some space for sample preparation and the dedicated technical groups will need space for sample environment hand-over and maintenance of gas and other types of supply (potentially adding up to 20 m^2). The instrument control room needs space as well (nearly 10 m^2). However, we may envisage a facility design effort to design the space for all neighbour instruments.

The demand of electricity for this instrument is mostly dominated by the 4 choppers and the vacuum pumps for the big vacuum tank.

Existing software solutions for the data acquisition and reduction could be used on this instrument, cause it operates a single-E_i mode. This does not exclude, that some development effort could be initiated to deliver a new software to improve the data analysis for specific applications.

VI.2 Hybrid spectrometer Crystof

Jörg Voigt

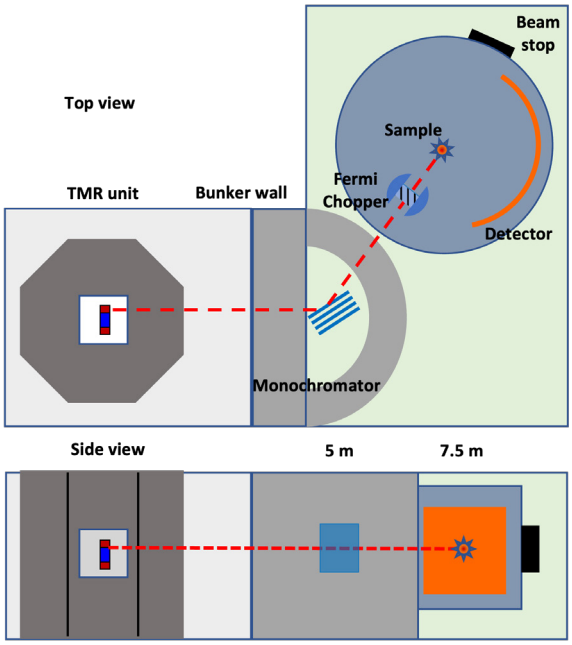

Figure VI.2: *Schematic top and side view of the hybrid spectrometer CRYSTOF.*

Instrument parameters	
Target	TS-epi (96 Hz)
Moderator	Water
Moderator-to-sample distance	7.5 m
Sample-to-detector distance	2 m
Initial energy range	10 meV$< E <$ 130 meV (0.8 - 3 Å)
Energy transfer range	-5 meV$< \hbar\omega <$ 100 meV
$\delta E/E$	$> 1.5\%$, depending on Bragg angle and monochromator crystal
Detector range	$5^\circ < 2\theta < 155^\circ$
Flux @ $\lambda = 1.47$ Å, $\delta E = 1.1$ meV	$2{\times}10^5$neutrons cm^{-2}s^{-1}

Table VI.3: *Instrument parameters for the thermal crystal-chopper spectrometer*

VI.2.1 Introduction

The hybrid spectrometer CRYSTOF is conceived to enable deep inelastic scattering in condensed matter research. The neutron energy range from 10 to 100 meV covers a wide range of coherent and localized excitations in condensed matter. The instrument addresses specifically the lattice dynamics in functional materials and the low energy range of vibrational spectroscopy. Here it profits on

one hand from the mapping capabilities of the position sensitive detector and on the other hand from the large solid angle coverage analyzing a large fraction of the neutrons scattered by localized excitations such as molecular vibrations or crystalline field excitations in rare earth materials. Also the mapping of high energy spin excitations, e.g. in high temperature superconductors or materials, where some states are topologically protected, can be accomplished by this instrument.

VI.2.2 Instrument concept

Thermal and epithermal spectrometers at spallation sources rely on the μs neutron pulses provided for the energy range at short pulse spallation sources. During the design of T-REX [AAJ+20]it became clear, that realizing a high initial resolution with pulse shaping choppers becomes difficult and inefficient for neutrons with a wavelength well below 1 Å. Even the high frequency target station at the HBS features a pulse length, that is too long to provide a sufficient wavelength resolution within a reasonable total instrument length.

The lighter shielding of the HBS as compared to spallation sources enables also direct geometry spectrometers, which employ a large crystal monochromator at a comparable short distance from the source. The primary wavelength resolution is controlled completely by the monochromator properties in a very similar way as for the new PANTHER spectrometer at the ILL [FRMM22]. Compared to this instrument, CRYSTOF benefits from the the pulsed nature of the source, which creates much less fast neutron background, which can further be discriminated in a straightforward way. The resolution can then also be tailored by the choice of the monochromator crystal.

The secondary spectrometer of the CRYSTOF instrument is optimized for scattering with large neutron energy loss. A sample-to-detector distance of $L_{\mathrm{SD}} = 2$ m is therefore sufficient to match the resolution of primary and secondary spectrometer in the range of large energy transfer. It should be noted that this choice results in a fairly relaxed elastic energy resolution, but low energy excitations are not in the focus of this instrument. If required, this dynamic range can be accessed by a measurement at the long wavelength limit of the instrument $\lambda_{\mathrm{max}} \approx 3.5$ Å.

The secondary energy resolution is also determined by the illumination time of the sample. It is controlled by a chopper close to the sample in a distance $L_{\mathrm{CS}} = 0.5$ m. The optimization for large neutron energy loss also allows a comparably relaxed time resolution to yield a high sample flux. The required pulse length of approx. 20 µs can be realized by a Fermi chopper with a relaxed collimation. The frequency of the Fermi chopper is determined by two additional conditions: (i) It must be a multiple of the target station frequency of 96 Hz: $f_{\mathrm{Chop}} = m \times f_{\mathrm{Src}}$. (ii) As the source frequency results in a secondary bandwidth that ranges beyond $\lambda' = 20$ Å, we extend the concept of Repetition rate multiplication to the case of hybrid instruments giving the condition:

$$\frac{h}{m_n} \left(m \times L_{\mathrm{Chop}} \times f_{\mathrm{Src}}\right)^{-1} = 2d \sin\theta (1 - n^{-1}). \tag{VI.1}$$

So one matches the repetition wavelength of the chopper (or a multiple of it) on the left of the above expression to the wavelength difference between the harmonic and the fundamental of the monochromator or also between different harmonics on the right, see the left panel of Fig. VI.3. In this acceptance diagram, green areas indicate the emission from the moderator. The horizontal red areas show the acceptance of the monochromator, which is of course time-independent. The Fermi chopper transmits neutrons from the moderator in the blue acceptance regions, where the slope depends on the distance between the chopper and the moderator surface. Choosing appropriate values for m and n a variety of different initial energies E and resolution conditions can be realized. Furthermore, the measurement at the longest wavelength will provide also a reasonable resolution for lower neutron energy loss despite the relaxed time-of-flight resolution.

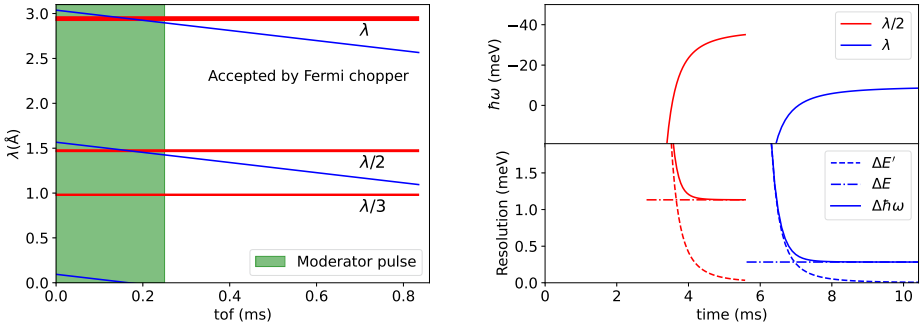

Figure VI.3: *Left: Acceptance diagram for the hybrid chopper spectrometer: Red areas indicate the Bragg reflected wavelength from a PG crystal with mosaic spread of 0.4°, while the acceptance regions of the Fermi chopper with a repetition rate of 384 Hz are shown in blue. The green area is the emission time from the thermal moderator of the 96 Hz target station. Right: Energy transfer range (top), primary, secondary and total energy resolution (bottom) as a function of the arrival time at the detector within one period of the 96 Hz target station.*

VI.2.3 Layout

CRYSTOF employs a large area monochromator with direct view onto the thermal moderator of the 96 Hz target station. Assuming that the instrument is placed at a position, where the target station is close to the bunker wall and installing a virtual source slit inside the target shielding the center of the monochromator can be at 5 m distance from the moderator surface. The 60 mm diameter of the thermal moderator in combination with typical crystal sizes of monochromator arrays yields the initial collimation impinging on an individual crystal of the mononchromator array to values $< 0.5°$ which can fully be accepted by PG crystals. Large monochromators up to a size of 300 mm $\times$ 200 mm can image a large solid angle from the moderator onto the sample. The monochromators used on the instrument should feature intense Bragg peaks with strong higher harmonics. High grade PG is an obvious choice, as one may use any combination of $\lambda, \lambda/2, \lambda/3$. For high resolution applications and for small samples bent Si (220) will be employed.

The monochromatic beam is chopped by a Fermi chopper to resolve the secondary time of flight with sufficient resolution. As this instrument focuses on large energy loss scattering, we prefer monochromatic focusing over time focusing. While the latter would provide best resolution for a specific and adjustable energy transfer, the former provides a flat resolution curve in the neutron energy loss range. The required pulse length can be prepared with a collimation that matches the collimation of the beam after being diffracted from the monochromator.

The sample stage is placed 50 cm downstream the Fermi chopper, similar to the present situation at PANTHER. This provides sufficient space for sample environments, while the short distance assures that the incoming pulse does not broaden significantly in time. The sample stage provides additional degress of freedom to orient and rotate a single crystal for mapping of excitation landscape in the thermal energy regime.

Optimizing the instrument for large neutron energy loss results also in relaxed resolution conditions on the secondary time of flight spectrometer. Therefore a sample to detector distance $L_{\mathrm{SD}} = 2$ m resolves the secondary time-of-flight sufficiently. It should be noted, that the usage of the higher harmonic and and fundamental wavelength of the monochromator still provides a large dynamic

range, which is measured with good energy resolution. The detector covers an angular range from 5 to 155 degrees in the horizontal plane, in a way that neutrons are detected, which have been deflected in different directions at the monochromator and at the sample. This non-dispersive arrangement provides the best Q-resolution at the detector. As for large neutron energy loss the final neutron wavelength of interest is $\lambda > 1.5$ Å, ^{3}He detector tubes of 1 inch diameter at a modest pressure from 6 to 8 bar yield a reasonable detection efficiency. With a detector height of 2 m, the detector has an area of 10.5 m^2 which puts it in the intermediate size and price range.

VI.2.4 Performance

We have modelled the instrument employing a PG monochromator. As an example setting, we choose to spin the Fermi chopper with a straight slit package at a frequency $f_{\mathrm{Fermi}} = 192$ Hz, and set the Bragg angle to 26°, which selects the (002),the (004) and the (006) reflection at a wavelength of 2.94, 1.47 and 0.98Å, respectively. According to equation VI.1, the Fermi chopper transmits then only λ and $\lambda/2$. If we use instead a chopper frequency of 576 Hz, which is available with state-of-the-art chopper technology, also neutrons reflected by (006) can pass through the Fermi chopper (not shown).

The first pulse at $\lambda/2$ covers the dynamic range up to 40 meV neutron energy loss as shown in the right panel in Fig. VI.3 in red. For an energy loss $>$ 10 meV, the resolution is dominated by the contribution from the monochromator, yielding an overall resolution $\Delta\hbar\omega \approx 1.1$ meV. Hence it can be tailored by an appropriate choice of the Bragg angle and the monochromator crystal. The second pulse, shown in blue, covers the dynamic range from the elastic line up to 9 meV neutron energy loss with a narrow resolution below 300 μeV for large neutron energy loss. So extracting 2 monochromatic pulses from one machine pulse with a high flux monochromator crystal such as PG provides already a very good energy resolution in a wide dynamic range. The combination of other monochromator angles and repetitions rates of the monochromator gives a wide range of adapted resolution conditions across the entire dynamic range, that is typically covered by thermal neutron spectroscopy, i.e. $-100\mathrm{meV} < \hbar\omega < -5\mathrm{meV}$. Further investigations using ideal bent monochromator crystals are ongoing and will allow to push the energy resolution even further.

For the aforementioned conditions, the simulations yield a monochromatic sample flux of 2×10^5 neutrons cm^{-2}s^{-1} from the (004) reflection of the PG at a wavelength $\lambda = 1.47$ Å, which is comparable to the simulations results for the TOPAS spectrometer under construction at the FRM II [VBB10]. Due to the wider absolute wavelength resolution of the (002) reflection at $\lambda = 2.94$ Åprovides a pulse with an intensity of 10^5 neutrons cm^{-2}s^{-1} , adding additionally higher resolution for lower energy transfers. However, it should be noted, that the collimation is about 2.5 times wider in the case of CRYSTOF, which we consider acceptable for the envisioned applications of the instrument.

VI.2.5 Requirements

Beside the common requirements for sample environment, sample preparation and an instrument control hutch with sufficient work places, the instrument needs a special position with no neighboring instrument to one side to swing the spectrometer vessel around the monochromator. The take-off angle of the monochromator varies between 30° and 70°, resulting in a space requirement of 6 m × 7.5 m. The monochromator and Fermi-chopper will be housed in a monochromator shielding similar to existing instruments.

VI.3 Crystal AnalyzerSpectrometers for Reciprocal Space Mapping (CAS)

Jörg Voigt, Karin Schmalzl, Robert Bewley

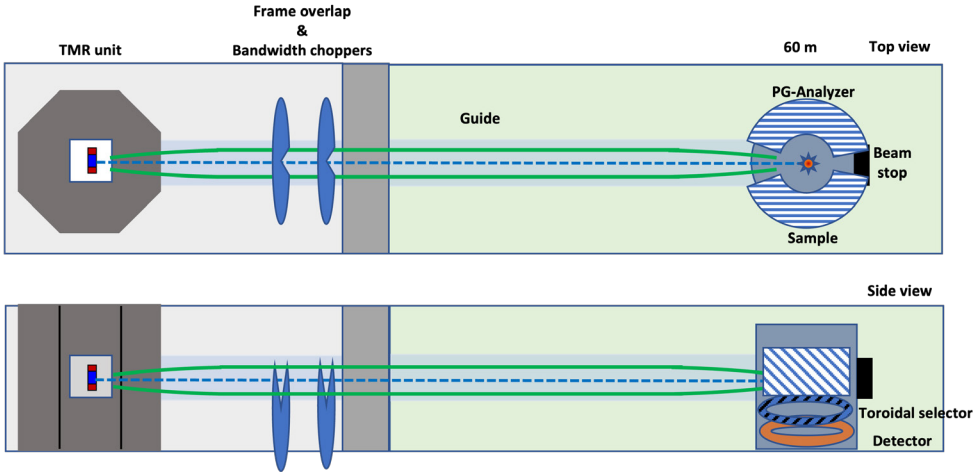

Figure VI.4: *Instrument sketch for an inverted geometry spectrometer using the MUSHROOM concept [Bew21]*

VI.3.1 Science case

The study of coherent excitations in condensed matter and in particular of excitations of the spin system is a major strength of neutron scattering, as it often presents the ultimate test for advanced theoretical models due to the completely understood cross sections for the interaction of slow neutrons with matter. Investigations of single crystal are indispensable to explore the dispersion of structural and magnetic excitations. As these have typically a size in the order of 1 cm^3 or less, which is in particular true for novel materials, many experiments are flux limited. The traditional tool for these investigations is the three axis spectrometer, where the flux on the sample is optimized employing focusing Bragg optics with the related prize one has to pay in terms of energy and momentum resolution. Chopper spectrometers have entered this field only in the last decades thanks to the progress in focusing supermirror optics and the advent of high power spallation sources.

For the HBS we propose the development of inverted geometry spectrometers as an additional tool to combine the strength of multiplexing TAS with the 'free' primary energy selection at pulsed sources by measuring the time-of-flight (ToF)

VI.3.2 Instrument concept

The key feature of a spectrometer is not mainly the flux that it delivers onto the sample, but the number of recorded neutrons in the detector after interaction with the sample.

To maximize the former, inverted geometry spectrometers at HBS can access a wide divergence range of $\pm 2^\circ$ in vertical and horizontal direction and image a beamspot of 10×10 mm^2 onto the sample position, thanks to a short distance between moderator surface and the neutron guide entrance $L_{\mathrm{guide}} < 0.5$ m and the high brightness of the liquid para-H_2 moderator.

Instrument parameters	
Target station	TS-96
Moderator	Liquid parahydrogen
Moderator-to-sample distance	60 m
Detector-to-analyser distance	1 m
Initial wavelength range	$1.8 < \lambda < 6.0$ Å, $\Delta\lambda = 0.66$ Å
Scattered wavelength	$4.1 < \lambda' < 4.8$ Å
Analyser range horizontal	$10^\circ < 2\theta < 150^\circ$
Analyser range vertical	$10^\circ < \phi < 0^\circ$
Energy resolution range	60 μeV $< \delta\hbar\omega <$ 400 μeV
Flux ($1.8 < \lambda < 2.5$ Å, $\delta\hbar\omega = 400$ μeV at $\hbar\omega = 20$ meV)	2×10^8 n cm^{-2}s^{-1}

Table VI.4: Instrument parameters for the inverted geometry spectrometers.

This small beamspot enables making use of the prismatic focusing effect to increase the number of neutrons, whose energy can be analysed by secondary Bragg optics: Neutrons scattered by the sample are imaged by analyser crystals with a wide mosaic spread onto different positions of the detector. The position encodes in this case the neutron energy with a precision defined by the collimation between sample and analyzer crystal and the position resolution of the detector. The accepted wavelength range of the analyser and hence the number of recorded scattered neutrons is increased by a wide mosaic spread, e.g. $\Theta \approx 2^\circ$ for PG .

Recently, two instruments have been proposed, that make use of this concept by two different realisations: **BIFROST** [AAJ+20] at the ESS collects the neutrons scattered in the horizontal plane. It increases the analyzed k' range by stacking a row of analyzer crystals in radial direction with decreasing Bragg angles, making use of the good transmission of pyrolitic graphite. **MUSHROOM** [Bew21] proposed for ISIS multiplexes the covered solid angle both in the horizontal and in the vertical direction. Both concepts are suitable for the HBS. Thanks to the lower shielding requirements one could envision to switch between the different secondary spectrometers depending on the experiment under study, as it is realised e.g. at synchrotron beamlines.

The high repetition rate of the HBS 96 Hz target station distinguishes the mode of operation from the low frequency spallation sources. The envisioned instrument length of 60 m yields a bandwidth $\Delta\lambda \approx 0.7$ Å. For a typical $k' \approx 1.3$ Å^{-1} one will therefore probe a narrow spectral range with a high intensity of approx. 10^8 neutrons cm^{-2}s^{-1}, depending where the initial band is chosen. Similar to todays TAS experiments one can extend the measured dynamic range by scanning the initial band by changing the phase of the band selection chopper. It enables also to prevent the illumination with the higher harmonic of the analyzer crystal in order to reduce the contamination of the recorded spectra.

Without additional pulse shaping, the instrument length is sufficient to realise energy resolution comparable to exisiting cold TAS spectrometers, ranging from 400 μeV at 20 meV energy transfer down to 60 μeV at the elastic line. Optionally we can include a pulse shaping chopper to provide an even narrower energy resolution, but also to get rid of the slightly asymmetric resolution function due to the moderator pulse shape.

VI.3.3 Layout

The concept of prismatic focusing requires the illumination of a small beam spot with a wide divergence. Therefore the instrument features a neutron guide, that can extract a wide divergence from

a 20 mm $\times$ 20 mm surface of the para-Hydrogen moderator. This moderator provides a very high brightness in the wavelength range 1.8 Å$< \lambda <$ 6 Å, covering the full dynamic range of cold TAS instruments. Placing the neutron guide at a distance of 50 cm from the moderator surface, one can feed a wide divergence range of 4°$\times$ 4°. A ballistic guide transports this divergence range with a brilliance transfer from 60% to 80% depending on the neutron wavelength. The chosen instrument length provides a wavelength resolution $\delta\lambda = 0.016$ Å. While the contribution from the neutron pulse is still dominating the overall energy resolution, it still matches the rather narrow energy resolution of typical cold TAS instruments. Therefore the chopper system of the instrument consists of a band width chopper and a cross talk chopper, with the option for an pulse shaping chopper, if it turns out, that the initial neutron energy resolution shall be improved.

The instrument will be equipped with a typical TAS sample stage, which can carry heavy and bulky sample environments and provides the degrees of freedom to align the sample and to explore the full $S(\vec{Q},\omega)$ space. As cold neutron spectroscopy is a unique tool to probe spin dynamics, both, very low temperatures and very high magnetic fields will be requested by the users. The case of strong magnetic fields can be ideally covered by the BIFROST type analyzer. The narrow sample spot required for the prismatic focusing will be also beneficial for suppressing the background, as it illuminates only a small volume around the actual sample position, reducing the scattering contribution from the sample environment.

As instruments at HBS will be optimized for signal-to-noise, the suppression of the higher orders of the analyzer is a critical issue for these types of instruments. Different means are already proposed to address this issue on Bifrost and Mushroom, which are also applicable for an instrument at the HBS.

On top of this, the narrow bandwidth allows to avoid the higher harmonics in the primary band for many cases. For both of the different analyzer concepts, the position sensitive detector is a critical component for the instrument. The area, that needs to be covered, is below 5 m^2, as compared to direct geometry chopper spectrometers with detector areas > 15 m^2. Therefore the instruments will be equipped with ^{3}He detector tubes with modest pressure providing a very good detection effenciency for the comparably low final neutron energy and a position resolution matching the energy resolution requirements.

VI.3.4 Performance

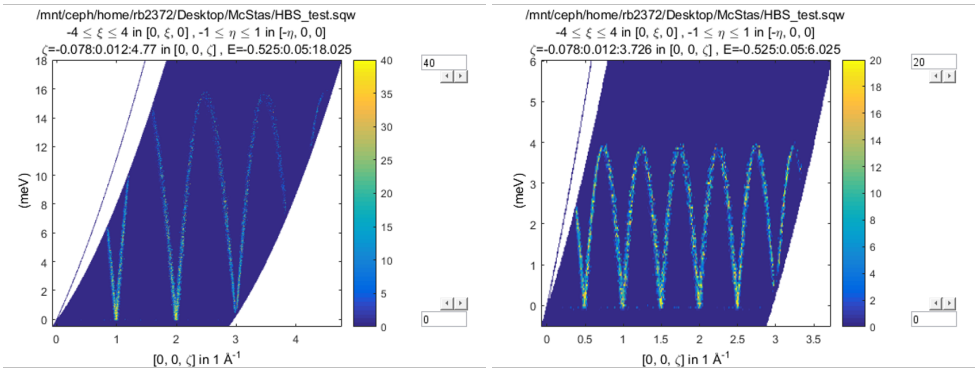

Figure VI.5: *Simulated $S(\vec{Q},\omega)$ for a 1D dispersion with zone boundary energy of 16 meV (left) and 4 meV (right). Data has been simulated with McStas, output as a Nexus event file and then processed with Mantid and HORACE.*

To address the momentum and energy transfer resolution we have setup a virtual experiment in McStas with a sample featuring a 1-dimensional dispersion using a MUSHROOM-type secondary spectrometer. In Fig. VI.5 we present the results for a dispersion for an acoustic excitation with zone boundary energy of 16 meV (left) and 4 meV (right) to confirm that the wide divergence allows a fast mapping of dispersive excitations with reasonable resolution. For the narrow dispersion, we need to combine data from 3 different bands, while for the wide dispersion, 5 different chopper settings are required providing in both cases sufficient overlap for the combination of the different data sets.

As mentioned above, the requirements on the primary spectrometer are similar for the different analyzer concepts. So we investigated the beam extraction and the beam transport only once. A ballistic guide has been modelled in Vitess to extract a phase space of $4^\circ \times 4^\circ$ collimation and 10 mm $\times$ 10 mm area. The straight section of the ballistic guide requires a supermirror coating with $m = 2$, while the elliptic end sections are coated with supermirrors up to $m = 4$. This design provides a sample flux of 2×10^8 neutrons cm^{-2}s^{-1} with a energy resolution $\delta\hbar\omega = 400\mu$eV at $\hbar\omega = 20$ meV for the band $1.8\text{Å} < \lambda < 2.5\text{Å}$

VI.4 Backscattering Spectrometer (BSS)

Jörg Voigt, Reiner Zorn

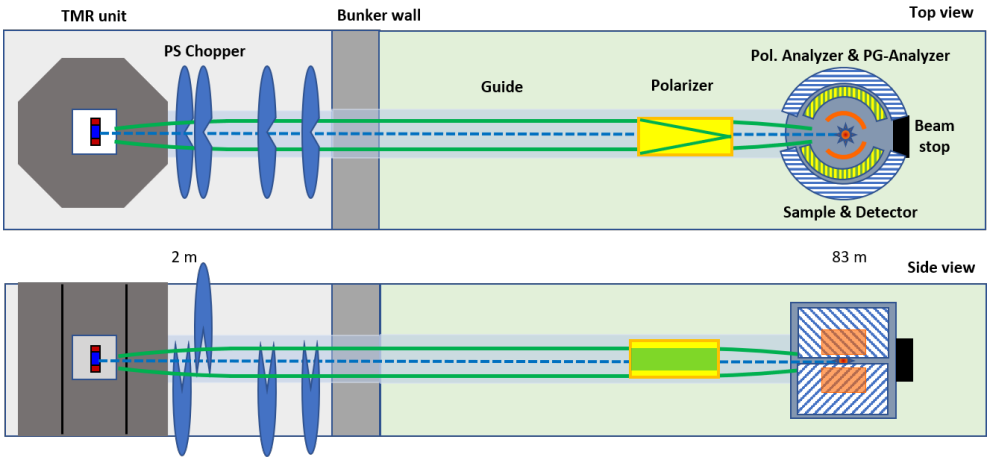

Figure VI.6: *Instrument sketch for an inverted geometry near backscattering ToF spectrometer.*

VI.4.1 Introduction

To study relaxation phenomena on small samples we propose an inverted geometry near backscattering spectrometer. It will be optimized for investigations in a dynamic range beyond $\pm$ 100 μeV energy transfer to explore local motions on the ns timescale.

Instrument parameters	
Target station	TS-24 (alternatively TS-96)
Moderator	Solid methane
Moderator-to-sample distance	83 m
Detector-to-analyser distance	2 m
Initial wavelength range	$\Delta\lambda = 1.8$ Å, $\lambda > 4$ Å
Scattered wavelength	6.61 Å
Analyser range horizontal	$10^\circ < 2\theta < 170^\circ$
Analyser range vertical	$-22^\circ < \phi < 22^\circ$
Energy resolution range	5 μeV $< \delta\hbar\omega <$ 20 μeV
Flux @ $5.7 < \lambda < 7.62$ Å, $\delta E = 3$ μeV	7×10^6 n cm^{-2}s^{-1}

Table VI.5: *Instrument parameters for the backscattering spectrometer*

VI.4.2 Science case

The proposed backscattering spectrometer will mainly serve for the investigation of slow relaxation/diffusion processes ($>$ 20 ps) which cannot be covered by neutron time-of-flight spectroscopy

without sacrificing too much of intensity. The main field of application will be quasielastic neutron scattering from Soft Matter (polymers, biological systems, glassforming liquids) and slow diffusion in materials as battery and fuel cell electrolytes and solid state ionics. As a minor but still important field of application we envisage inelastic neutron scattering from quantum-mechanical tunnelling systems.

With an ultimate energy resolution of $5\,\mu$eV, the instrument probes shorter times than a 'true' backscattering spectrometer, which reaches $\delta\hbar\omega < 1\mu$eV. On the other hand, the inverted geometry gives access to a larger energy transfer range ($\pm 100\,\mu$eV) than a 'true' backscattering spectrometer where energy transfer is realised by the Doppler effect and limited by the maximum monochromator speed that can be reached. Therefore, the instrument allows a seamless connection to the time range of a time-of-flight spectrometer. Its data may thus also serve as a 'bridge' between time-of-flight spectroscopy and higher-resolution techniques as neutron spin-echo and 'true' backscattering.

An important innovation of this instrument is the possibility of polarisation analysis. This makes the separation of coherent and incoherent scattering possible. First and foremost, it allows measuring pair and self correlation on the *same* sample, e.g., collective and self diffusion. At the moment such studies are performed by isotopic (mostly H/D) substitution which is not undisputed because of known chemical differences between H and D. But also in cases where only one of the scattering functions is desired the separation by polarisation analysis is advantageous. It will be possible to measure coherent scattering in (mostly H-containing) samples, which produce a large incoherent background and, vice versa, incoherent scattering in samples where the incoherent scattering cross-section is low.

Another advantage of the instrument is the small focus which enables the use of small samples. This is especially important in fields, where the amount of sample is a critical limitation, e.g., in biology. The reduction of Q resolution necessarily connected is not important in the fields of application where one deals with amorphous structures.

VI.4.3 Layout

A backscattering spectrometer provides extremely high resolution by defining the energy resolution of the initial neutrons to the level of $10^{-3}(dE/E)$ and by analyzing the final energy ideally to the same degree. Therefore it is crucial to maximize the acceptance both of the neutron transport system as well as the acceptance of the analyzer: As the neutron guide can be placed already at a distance of 0.5 m from the moderator surface, it can extract a large phase space volume of $5^\circ \times 5^\circ$ and 10 mm $\times$ 10 mm. Since only neutrons with a wavelength $\lambda > 4$ Å shall be transported an efficient ballistic transport that prevents the line of sight can be realized using super mirrors with comparably low coating and therefor reasonable cost.

The angular acceptance of the analyzer is optimized by two analyzer banks above the below the scattering plane covering a range from 10° to 170° horizontally and -22° to 22 ° vertically, respectively. Thanks to the prismatic focusing effect, the PG analyzer with a mosaic spread $\delta\phi = 2^\circ$ increases the acceptance of each analyzer crystal, but still provides a resolution $\delta E' \approx 3\mu$eV by imaging a small divergent beam of less than 10 mm$\times$ 10 mm onto the position sensitive detector.

About the choice of the target station, the user group that was present at the spectrometer workshop was undecided. One party opted for an instrument with a wide bandwidth $\Delta\lambda \approx 2$ Å placing the instrument at the 24 Hz target station. The other party was in favour of operating the instrument at the 96 Hz target station, which concentrates the intensity in a bandwidth $\Delta\lambda \approx 0.5$ Å. Simulation showed, that both options provide a very similar sample flux, and, as the energy resolution is defined by the pulse shaping chopper assembly, also the same resolution.

In case of the 96 Hz target station, distributing the bandwidth symmetrically around the elastic line of the analyzer, the instrument would cover a dynamic range of -0.12 meV$< \hbar\omega < 0.12$ meV.

This can be extended by a shift of the band towards higher or lower energy covering either an asymmetric dynamic range or stitching different bands together. In case of the 24 Hz target station, one has to integrate longer to reach the same statistics in the range of low energy transfer, as the sample flux is distributed over a wider band, while also larger energy transfers are covered in the same run. For this TDR we have chosen a position at the 24 Hz target station, to have less variation across the initial spectrum, as the pulse of the 24 Hz target station has a brightness plateau.

To match the 3μeV resolution of the final neutron energy provided by the analyzer, the neutron pulse must cut to a pulse length $\tau \approx 60\mu$s. This pulse is realized by a pair of counter rotating fast spinning choppers at the closest distance from the moderator $L_P = 2$ m. At a sample distance of $L_M = 83$ m the band passing through choppers covers most of the time frame of the target station $1/f_{\mathrm{src}}$, leaving a small gap to distinct subsequent frames. Thus the detector records neutrons scattered from the sample basically continuously. The chopper system is complemented by two more choppers spinning at the source frequency to cleanly separate different bands and avoid cross talk to former pulses.

An upper and a lower detector bank consist of individual ^{3}He detector tubes with 10 mm diameter providing a similar spatial resolution along the tube. These tubes provide excellent detection efficiency for the analyzer wavelength, low sensitivity for Γ radiation and provide the expected count rate capabilities.

The use of 1-dimensional polarization analysis in QENS allows the separation of local and coherent dynamics and therefore a more unambiguous analysis of the scattered signal. But only recently first experiments have been performed at cold chopper spectrometers. This instrument will allow polarization analysis in a energy resolution range well below 10 μeV.

At the end of the ballistic section, where the beam has a narrow collimation, an optional V-cavity can be inserted to polarize the incoming beam with a very high efficiency, as it can be optimized for the narrow wavelength range. We will explore alternative solutions for a wide angle narrow band analyzer: Within the JCNS we have developed wide angle polarized ^{3}He analyzers, which could be employed close to the sample. Alternatively, one can also employ supermirror devices for the wavelength range accepted by the analyzer. Recently radial transmission benders have been developed and used with a large acceptance and without affecting the trajectory of the analyzed spin state. Therefore such a device has no effect on the energy analysis. We consider also a solution with a reflecting radial bender in front of the detector. It could serve additionally as a filter suppressing the $\lambda/2$ contribution passing through the analyzer and originating from the warm sample itself, which could improve the signal-to-noise ratio at the detector significantly.

VI.4.4 Performance

We have estimated the performance of the instrument by means of simulations of the primary spectrometer and analytical considerations to estimate the achievable energy resolution of the instrument.

The prismatic focusing decouples the energy resolution from the width of the mosaic spread. Choosing an analyzer Bragg angle $\theta = 80°$, the analyzer resolution can reach $\delta E' = 3\mu$eV [Bew19]. The pulse shaping chopper assembly consisting of two counter rotating chopper discs spinning at up to 288 Hz can provide a pulse length down to 60 μs, providing an initial energy resolution $\delta E \approx 3\mu$eV accross the band $5.7\text{Å} < \lambda < 7.62$ Å. So the instrument can provide a total energy transfer resolution $\delta\hbar\omega \approx 5\mu$eV, including contributions from analyzer and the detector. Under these conditions the simulated sample flux yields 7×10^6 neutrons cm^{-2}s^{-1}, similar to the existing backscattering instruments at ISIS, albeit with a 3 times better energy resolution.

VI.4.5 Requirements

The instrument requires a total lenght of approximately 90 m, placing the instrument in the guide hall for the long instruments. The spectrometer will be housed in a vacuum vessel with a diameter of 5 m and height of 2.5 m. PE shielding around the spectrometer increases the foot print to a diameter of 5.5 m. To evacuate the spectrometer vessel, a large vacuum pump will be installed close to the instrument. If the instrument opts for a ^{3}He filter cell polarization analysis, the facility supplies either a central filling station or a local small scale filling station based on the experience in JCNS. Besides these special requirements, users will need access to biological and chemical laboratories. An instrument control hutch with a workspace for four persons will be installed close to the spectrometer.

VI.5 Neutron Spin Echo (NSE) Spectrometers

Stefano Pasini, Christian Franz

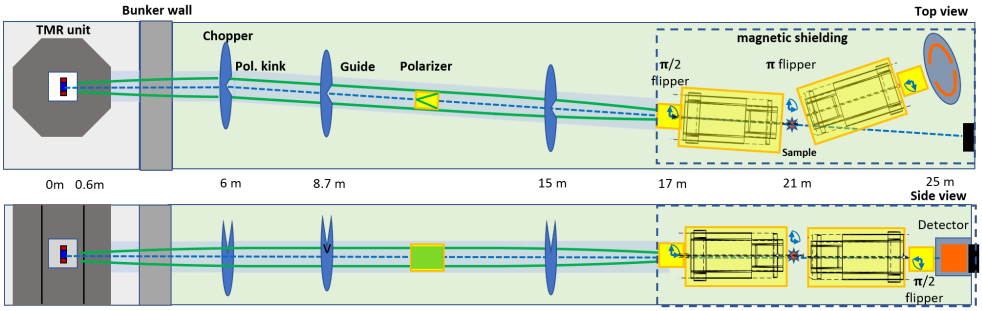

Figure VI.7: *Possible layout of the high resolution NSE at the HBS. The chosen option of a tapered neutron guide helps to allocate the optics elements. The suggestion for the magnetic coils fulfils the criteria of an optimized magnetic field with low inhomogeneity and an intrinsic homogeneity of ca. 300 ppm.*

Instrument parameters	
Target station	TS-24
Moderator	Liquid parahydrogen (or other moderator optimized for long wavelengths)
Moderator-to-sample distance	21 m
Sample-to-detector distance	4 m
Wavelength range	3.4 Å $< \lambda <$ 16 Å (standard: 3.4 - 10.0 Å)
average Flux (up to)	2.8×10^6 cm^{-2} s^{-1}

Table VI.6: *Instrument parameters for an NSE spectrometer based on the design of the ESSENSE spectrometer proposed at the ESS.*

VI.5.1 Overview and motivation

Among all neutron scattering spectrometers, Neutron Spin-Echo is the one with the highest resolution. The effective energy and the dynamical range reached by NSE extend over 6 decades down to neV, thus contributing to close the gap with other spectrometric techniques. In the frame of multi-methodic sample characterization NSE locates itself very strategically thanks to its complementarity to other techniques like NMR, electron microscopy and x-ray scattering. Moreover, NSE gives direct access to the time-Fourier transform of the scattering function and therefore it is easily comparable to results from numerical simulations. In combination with MD simulations or methods of machine learning, NSE can be used to test molecular theories and boost in general the synergy between computer simulation and experimental confirmation.

Neutron spin echo instruments are well suited for pulses sources, which has been already demonstrated with the NSE at SNS. In this respect, JCNS has a large experience in designing, constructing and

operating NSE spectrometers; we mention here the NSE's of new generation at MLZ (J-NSE Phoenix and RESEDA) and at NIST (in refurbishment) as well the SNS-NSE.

Due to the broad spectrum of applications (from soft-matter to magnetism, from protein dynamics to hydrogen diffusion in energy materials) dedicated types of NSE have been developed and are in operation worldwide: the generic IN11 type (i.e. IN15 at ILL, J-NSE at MLZ or the SNS-NSE), the Wide Angle NSE spectrometer - in the form first demonstrated by the SPAN (HZB), then expanded for the new WASP at ILL - and the resonance spin-echo that replaces each large magnetic coil with two resonant flippers, like the RESEDA at MLZ. In its MIEZE configuration the resonance spin-echo is particular suitable for magnetic scattering, while standard NSE instruments are very well suited for soft matter and life sciences. Past experiences have shown that dedicated instruments are to be preferred to "many-purposes" solutions and that these can provide more efficiently a systematic access to experiments pertaining also very different grand-challenges areas. With the aim of addressing as large as possible science areas both in soft matter and magnetism and of supplying support to the increasing demand of experiments at NSE machines we propose here two different types of high-resolution neutron spin echos spectrometers as an indispensable constituent of the instrumentation suite of a new source like the HBS: these are a standard and a resonance NSE.

VI.5.2 Scientific case

Following the trends in condensed matter, the research in neutron scattering points towards the investigation of complex matter and mesoscopic time and length scales. These experiments rely on the appropriate enhancement of the energy resolution, which is typically far beyond 1μeV, or correlation times much larger than 1 ns. Thus, high resolution spectroscopy is required in these cases. This can be addressed by the NSE techniques, on condition that a sufficiently high flux at long wavelengths is provided by the source. The NSE and especially those of new generation (at ILL, MLZ and NIST) [FFH$^+$15, PHK$^+$19] made accessible the investigation of large scale domain dynamics relevant for Life Sciences, Biomedical Research and Health as well as Soft Matter. In the life and soft matter sciences, the major scientific drivers for NSE research can be identified in the following areas.

- Polymer dynamics: New topologies as well as mixtures of molecules with different topologies, but also polymers under inclusion promise to show new effects and provide new insights in the field of polymer dynamics. The ever increasing complexity of such systems often leads to the demand for ever longer Fourier times. Being able to achieve such time ranges is fundamental to clarify the topology-driven dynamics of ring polymers and to claim that these are different from the dynamics of polymers with chain ends [KMA$^+$20]. High-resolution incoherent NSE can also be used to detect small changes in the segmental dynamics in nanocomposites [MOF$^+$20].
- Dynamics of biological molecules and systems: Dynamic changes in denaturation or dynamic signatures of intrinsically unfolded proteins, but also fluctuations of biomembranes and their vesicle models in the presence of incorporated bio- or drug-molecules, provide information that improves the understanding of processes in cell membranes and is relevant for drug design. Here, the high resolution improves the performance of NSE over the greater part of the Fourier times with respect to standard NSE types (with no optimised magnetic fields) as it allows any given time to be measured at a lower wavelength than before, i.e., with much higher intensity. Comprehensive approaches to NSE spectroscopy with other techniques (such as NMR, DLS, but also molecular dynamics simulations) has proven successful in investigating the bending stiffness of lipid membranes with interesting implications for medicine pertaining for example the effects of cholesterol [CDM$^+$20] or the functionality of fusion peptides in HIV-1 viruses [HZ19].

- Complex fluids: Systems such as microemulsions, i.e. mixtures of water and oil and a surfactant, or macromolecules such as proteins, polymers, microgel particles or other colloidal nanoparticles in solution are present in many biological and technical-engineering systems with important functions. CO_2 is often regarded as a green (non-toxic) solvent, its applicability can be increased by the use of microemulsions containing an aqueous component that is sensitive to water-soluble substances. Experiments with microemulsions with supercritical CO_2 as the "oil" component [KSS+12] showed that the membrane becomes increasingly stiff with increasing pressure.

- Glasses: Polymers and low molecular weight glasses are an issue since the early days of NSE research [CAR+03]. Most of this research has been done using coherent scattering to study the density autocorrelation function. Since the relaxation times increase sharply at the glass transition, NSE is an essential technique here. The challenge here would be to go beyond conventional Q-scaling methods for characteristic times in the Q region below the structure factor peak [BAA+09], because both the coherent and incoherent scattering intensities are low in these cases. Glass transition, gelation, and aggregation are closely related, and only the broad coverage of the Q and energy space of NSE techniques can help distinguish such dynamics [GEFS20].

- Topological spin textures: In the quest for new materials for applications in quantum and information technology, topological spin textures, such as skyrmion lattices in chiral magnets are an emerging field. These structures are of mesoscopic scale and exibit nanosecond dynamics. As a external magnetic field is often used to stabilize the structure, MIEZE is the ideal technique for the investigation of the dynamical properties.

- Superconductors: Up to date unsolved is the mystery of unconventional superconductivity in copper oxide-, rare earth- and iron-based materials, where a coupling via magnetic in contrast to nuclear excitations is the putative driving mechanism. Ultra-high resolution studies are needed to benchmark models beyond standard BCS theory of phonon coupling. Moreover, the flux pinning and flux lattice melting are still fairly unexplored microscopically awaiting high resolution spectroscopic studies.

- Second order phase transitions: Low energetic fluctuations drive the critical phenomena at second order phase transitions. The exact knowledge of the critical exponents is crucial to check the validity of present models. NSE is the only method available that can directly access the underlying fluctuations.

- Ionic liquids and ion conduction: Among the "new solvents" ionic liquids have a very high temperature stability and high conductivity and they are gaining importance in many different contexts, like for example in energy materials. These materials are often characterized by a nanometer/nanosecond dynamics and in many systems the interest lies in the long-range translational diffusion coefficient of the center-of-mass of the whole cation. NSE can play an important role in this case for the NSE signal is very sensitive to the dynamics of the side-chains [FBZ+17].

- Li batteries: Fundamental research on lithium ion dynamics in solids is important to develop functional materials for, e.g. sensors or energy storage systems, but also in catalytic processes e.g. to increase efficiency in chemical processing. For the investigation of polymer-based batteries, NSE offers the advantage to look directly at the polymer dynamics. For example, the dynamics of Li+ transport in mixtures of polyethylene oxide (PEO) and lithium bis(trifluoromethanesulfonyl)imide (LiTFSI) have been investigated by means of a combination of neutron spin echo experiments with dielectric measurements and MD simulations [DLD+13]. Such investigations yield decisive experimental evidence of the role played by the polymer

cages around each Li ion for their transport as well as for their life time and characteristic length.

VI.5.3 Layout of the high-resolution Neutron Spin Echo (NSE) spectrometer

NSE instruments consist of a primary and of a secondary spectrometer: the former is responsible for the transport and the polarization of the beam while the latter, the core of the instruments, coincides with the Lamor-precession-area of the spin. Recently two NSE of new generation (the J-NSE Phoenix and the NIST-NSE, the latter still under refurbishment) have been endowed with a set of superconducting coils that represent the actual state of the art in terms of optimization of such precession magnets.

For the NSE machine a moderator window of 3 cm diameter at the 24 Hz source with a pulse length of 667μs is the best among the available options. This will allow a wavelength band of circa $\Delta\lambda = 4.7$ Å, for a moderator-detector distance (D_{MD}) of 35 m or $\Delta\lambda = 6.6$ Åfor $D_{MD} = 25$ m. Any larger band, e.g. $\Delta\lambda = 8$ Å, for $D_{MD} = 20.5$ m, can be used but the practical gain will not grow proportionally. We choose here a total length of $D_{MD} = 25$ m, which is comparable with those of other existing NSE spectrometers. This length is enough to allocate up to three disk choppers running at the source frequency and positioned at, e.g., 6 m, 8.7 m and 15 m.

The layout of the primary spectrometer (figure VI.7) can be quite simple and it consists of a straight neutron guide starting at a distance of 0.5-0.6 m from the cold moderator. A kink of 3.2° with a polarizing FeSi multilayer mirror can be adopted to move the sample out of the direct line of sight and to achieve a polarization of ca. 99 % of the beam up to 8-10 Å. A second polarizer (cavity) provides the desired polarization for longer wavelengths. The sample is located at 21 m from the moderator and ca. 4 m from the end of the neutron guide and it has a standard dimension of 3 cm x 3 cm.

For longer wavelengths, a transmission polarizer shall be inserted in the neutron guide between choppers or close to the end of the neutron guide. After the installation of a new set of superconducting main precession coils in the J-NSE Phoenix at MLZ, a factor 2.5 improvement in the intrinsic homogeneity of the field-integral, i.e., in the resolution, was achieved with respect to non-optimized coils. This was made possible by a new and unique optimization of the field shape, with enhanced intrinsic homogeneity, fringe-field compensation, and high stability. A similar concept was realized for the NSE of NIST. Based on these results, we propose here for the secondary spectrometer a set of two superconducting solenoids similar to those mentioned above. A set of two $\pi/2$ and one π flippers and a multilayer analyzer, followed by a ^{3}He detector with a sensitive area of 30 cm diameter, complete the layout of the secondary spectrometer for the proposed high-resolution NSE. The second arm shall be rotated around the sample position in order to reach scattering angles up to ca. 85-90 degrees (depending on the maximum available space).

VI.5.4 Performance of high-resolution NSE spectrometer

For a polarized beam the transmission of an ideal instrument is $T = 0.5$. The figure of merit (FOM) for the performance of the beam transport

$$Q = P\sqrt{T} \tag{VI.2}$$

is used, the optimum value is $Q = 1/\sqrt{2}$. Here, P is the polarization and T is defined and simulated as the flux onto the sample for a layout of the primary spectrometer as described above with respect to a straight guide of the same length with coating $m = 2$, which is tested to transport 99.9 % of the flux from the moderator to the sample. The simulated FOM is shown in figure VI.8.

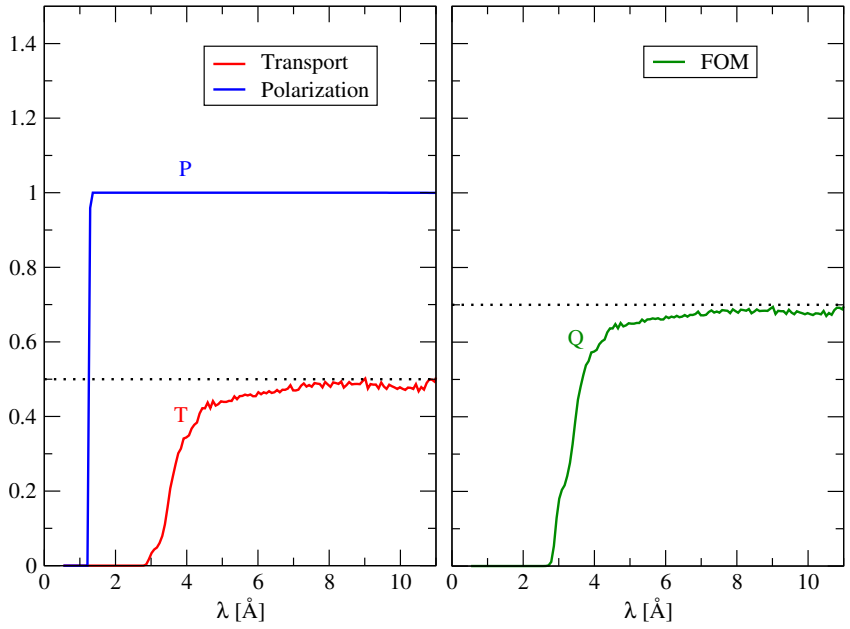

Figure VI.8: *Simulated performance of the high-resolution NSE-instrument.*

The proposed NSE spectrometers at the HBS have the potential to reach a maximum field integral $J_{\max} \geq 1.5\,\mathrm{Tm}$ and Fourier times up to hundreds of nanoseconds, depending on the usable maximum wavelength of the cold neutrons (as the longest Fourier times are reached at long wavelengths). The optimization of the moderator as well of the transport system aims at a neutron flux at the sample as compared to J-NSE and RESEDA at MLZ. Further gains due to the wavelength frame width of

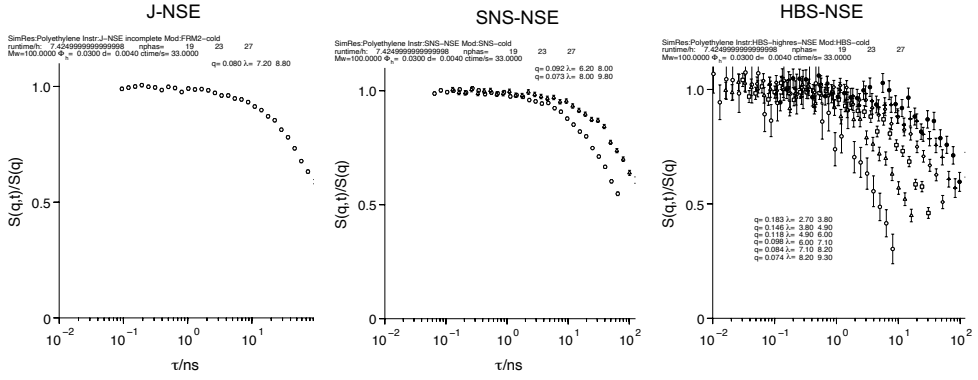

Figure VI.9: *Simulated intermediate scattering function for the spectrometer J-NSE, SNS-NSE and the proposed NSE for the HBS, with the layout of transport as described above and a flux of* $2.8 \cdot 10^6$ *n/(cm*^{2}*s) at 6 Å. The transport and the flux of the J-NSE and SNS-NSE spectrometer reflect the original ones. The simulated curves are for a polyethylene polymer. The counting time per point is the same (33 s) for the three cases.*

6 to 7 Å will be of the order of **g = 5** (e.g. for a frame extending from 6 to 12 Å) in comparison to a reactor instrument with a 15% velocity selector. The fringe-field compensation and the low cross-talk of the magnetic coils will allow large scattering angles and Q-values, generally difficult to achieve with copper-based precession coils.

Based on the presented FOM, figure VI.9 shows a simulated performance of the proposed high-resolution standard NSE for HBS compared to that of the existing J-NSE and SNS-NSE for a standard sample: polyethylene polymer.

VI.5.5 Special requirements

A magnetically quiet environment, an environment with no magnetic external disturbances is essential for a stable and reliable operation of all NSE spectrometers. The advantage of superconducting coils, fully compensated and with very low fringe-fields is that a μ-metal magnetic shielding around the secondary spectrometer is possible. This already proved to be effective and beneficial at the SNS-NSE spectrometer. In the other case of magnetically sensitive neighbour instruments, its benefit will also be to shield the magnetic field of the NSE.

VI.5.6 Layout of the High-resolution Neutron Resonance Spin Echo (NRSE) spectrometer

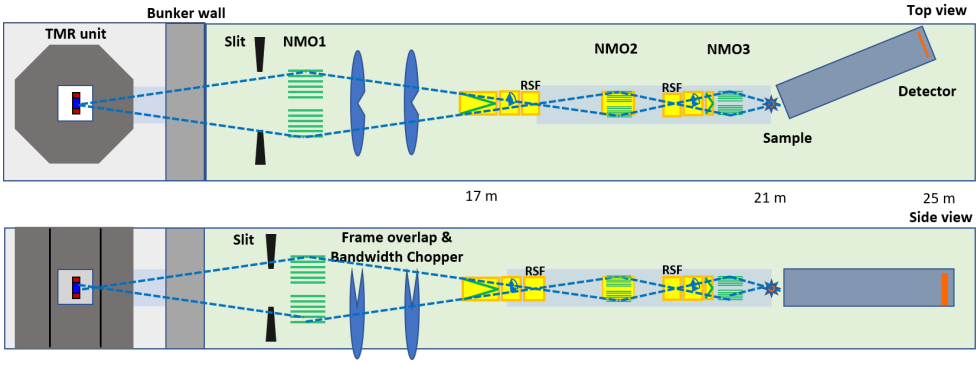

Figure VI.10: *Schematic layout for a MIEZE instrument at the HBS. The instrument makes use of nested mirror optics (NMO) to achieve a perfect image of the moderator at the sample position. The resonant spin flipper are positioned at the focal points.*

The requirements of a resonant spin echo instrument as regards wavelength band and wavelength resolution are identical to standard NSE. Therefore the 24Hz source with 667μs pulse length and a moderator detector distance of 25 m is the best choice. This allows the extraction of a 6.6 Å wavelength band around the peak flux, e.g. 3.4-10 Å. The good wavelength resolution between 1% (10 Å) and 3.6% (3.6 Å) relaxes the required positioning accuracy of the detector in MIEZE mode and allows using several detector foils (CASCADE detector) even at high resolution settings. This enhances the detector efficiency compared to reactor instruments.

In comparison to conventional NSE spectrometers, the large solenoids on the primary spectrometer arm are replaced by a set of two radio-frequency (RF) flippers, comprising a static longitudinal (i.e. in beam direction) field and a transverse oscillating field. One $\pi/2$ flipper in front and one after the set act as boundaries for the precession area. The analyser is moved in front of the sample area, removing all spin manipulation devices from the secondary spectrometer arm. This transforms MIEZE essentially into a spin-echo TOF method, and justifies the need for a fast neutron detector. The detector itself sits in a SANS-type detector tube to remove unwanted scattering from air.

At a pulsed source, the field of the $\pi/2$ flippers as well as the magnitude of the oscillating field need to be ramped up during the neutron pulse, whereas the static field and the oscillating field frequency remain unchanged. The feasibility has already been proven in real-life experiments. Additionally, the detector readout needs to be capable of hundreds of thousands of time bins per pulse, multiplied with anticipated 256x256 pixels of spacial resolution. An advanced version of the commercially available CASCADE detector seems to be a viable solution.

As MIEZE focusses very often on single crystals, which are typically 10 mm in diameter, and on small scattering angles, a moderator of similar size might be employed to increase the brightness of the source. In order to achieve a 1:1 optical image of the source at the sample position, we envision the usage of nested mirror optics (NMOs) instead of elliptic neutron guides. The first mirror assembly will focus the beam on the first RF flipper, the second assembly on the second flipper, and finally the third assembly on the sample. This allows not only very good brilliance transfer, but also minimizes the beam diameter at the position of the RF flippers. This leads to smaller coils and in turn higher frequencies, boosting the resolution of the spectrometer. A single four-blade aperture shadowing the outer mirrors is enough to adjust the beam divergence in the case of SANS applications. An alternative approach may be provided by Selene optics, minimizing flight path differences between the resonant coils. However, the technical implementation seems more challenging.

VI.5.7 Performance of the High-resolution NRSE spectrometer

The performance of the instrument is mainly determined by the achievable neutron flux at the sample position and the maximum achievable resolution, i.e. spin echo time.

The instrument benefits from the focus on small samples. Modern mirror optics allow a brilliance transfer close to one from the moderator to the sample. Additional gains in the order of 5 are possible by the use of wide band of neutron wavelength in one pulse in comparison to the narrower 12% band at reactor based instruments.

Smaller coils in the focal point of the mirror optics allow higher frequencies up to potentially 8 MHz, leading to a field integral of 0.55 Tm for a coil distance of 2 m. Fig VI.11 shows the dependence of the resolution from neutron wavelength and difference frequency of the resonating coils. Best resolution is achieved for the highest wavelength, whose intensity depends on the moderator. MIEZE is essentially a time-of-flight technique, and therefore prone to flight path differences, possibly destroying the oscillating signal. Again, the focus on relatively small sized single crystal samples helps to mitigate the effect.

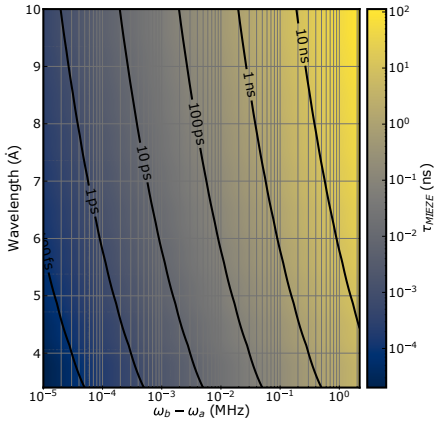

Figure VI.11: Resolution as a function of neutron wavelength and difference frequency between resonating coils.

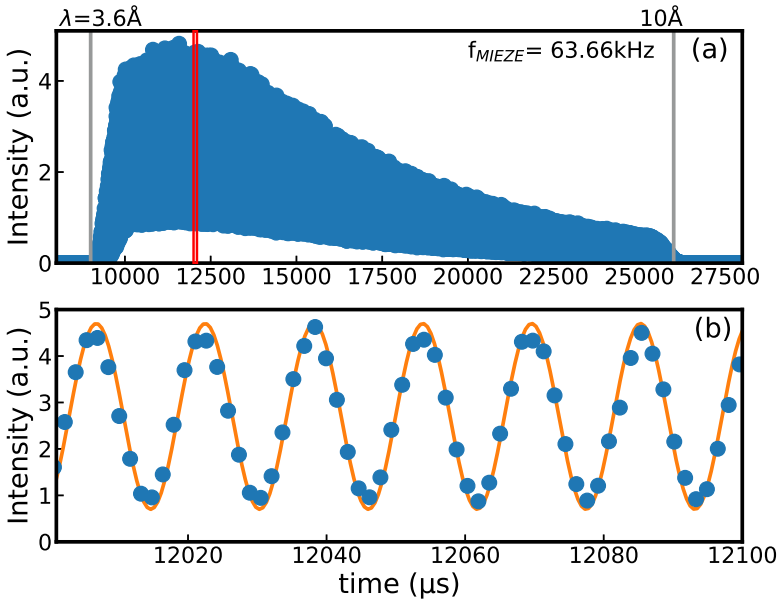

Figure VI.12: *McStas simulation of the proposed instrument at a beam intensity oscillation frequency of 63.66 kHz. (a) Full spectrum from 3.6 Å to 10Å extracted from the 24 kHz cold moderator. (b) Detailed view on the red rectangle in (a). The beam oscillations are visible now, with an orange line as guide to the eye.*

Fig. VI.12 shows a simulation of a HBS neutron pulse on the fast time resolved detector for the desired wavelength band between 3.6 Å and 10 Å. Panel (b) shows a zoom on the area marked by a red rectangle in (a), clearly revealing the MIEZE intensity oscillations with a period of 15.7μs. The wavelength range corresponds to spin echo times spanning from 75 ps to 1.67 ns over the pulse.

VII.

INSTRUMENTATION FOR IMAGING AND ANALYTICS

The neutron radiography is a powerful non-destructive method for the investigation of objects from various fields of r esearch. The high penetration power allows investigations of bulky sample, e.g. from the fields of geology or engineering, or of complex devices for in-operando studies. In combination with the weak interaction, neutrons are a truly non-destructive probe, allowing investigations of precious and unique specimen from archaeology and cultural heritage. The technique is in particular sensitive to the spatial distribution of light elements and especially hydrogen. With the advent of the hydrogen economy, neutron imaging will become a critical method in engineering and energy research. Performing tomography it will provide 3d images of the interior of complex devices, which cannot achieved by any other means. Instruments at the HBS will excel here in particular by the ease of access both to the facility but also to the sample, which enable ancillary measurements simultaneously to the radiography measurements. The different mechanism of interaction of the neutrons with matter compared to x-rays makes neutron radiography a complimentary technique to the classical X-ray radiography. For the HBS, we envision a suite of imaging instruments that cover the neutron energy range from fast neutrons coming unmoderated from the target to look tenth of centimetres below the sample surface, down to cold neutrons to vary the imaging contrast by different means providing the highest spatial resolution. For the definitions of the energy ranges used, we refer to the table in the appendix.

VII.1 Cold Neutron Imaging (C-NI)

Markus Strobl, Norberto Schmidt

Cold neutrons appear best suited for a large range of neutron imaging applications. They provide high contrast and suitable penetration for many investigations where other means and in particular imaging methods fail. Cold neutron imaging is the technique of choice in a plethora of scientific cases profiting from its high sensitivity to e .g. hydrogenous materials in representative sample volumes of relevant materials, which allows cold neutron imaging to make an impact in the search of improved materials and processes as well as in the understanding of complex materials, structures and their interplay. Numerous studies, for example in engineering, energy research, hydrogen economy, nuclear safety and construction materials, natural materials with regards to geology, but also environment, biology and agriculture, cultural and natural heritage underline the outstanding relevance of cold neutron imaging. These scientific studies are complemented by a large number of industrial applications from the automotive, the aerospace and medical sector, to name but a few. In addition, many advanced neutron imaging techniques targeting magnetic, microscopic and crystalline

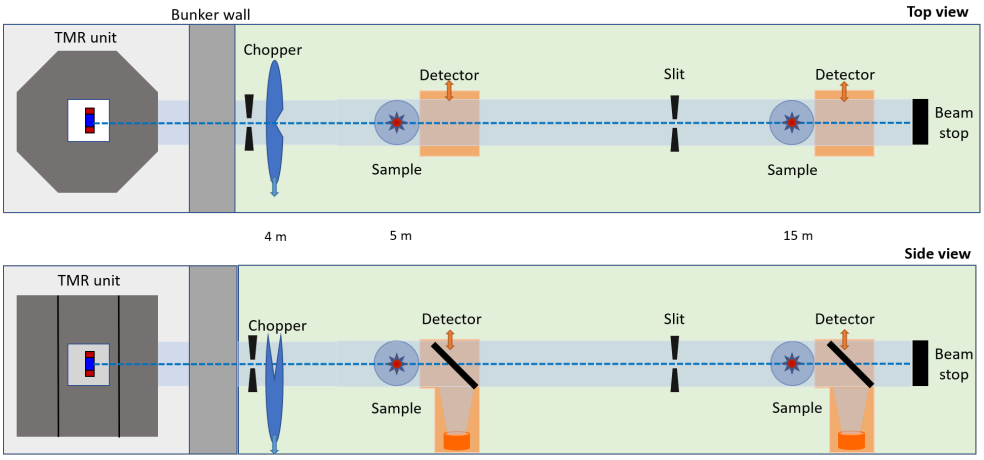

Figure VII.1: *Proposed layout for the cold neutron imaging (C-NI) instrument at the HBS.*

structural features of condensed matter and specific applied materials are enabled by cold neutron interactions and corresponding imaging instrumentation. The introduction of complementary in-situ techniques, in particular concurrent x-ray imaging have enabled further studies and enriched the critical information content especially in porous media applications like in engineering, geology, soil science but also such investigating extraterrestrial specimen.

VII.1.1 Cold neutron instrument description

A cold neutron imaging instrument at HBS will be competitive and able to make significant contributions in all these fields of cold neutron imaging research through state-of-the-art instrumentation. To that end, a dedicated cold neutron imaging instrument has been designed to profit from a 96 Hz target station and a cold moderator. Two particular imaging positions along the beamline at about 5 m and 15 m from the moderator will enable efficient trading of flux, field of view and resolution. The 5 m position provides limited collimation corresponding to an L/D of 200 (D = 2.4 cm moderator size viewed at L = 5 m) but particularly high neutron flux (3×10^6 n/(cm^2 sec)) for fast studies on a field of view of up to 200 x 200 mm. The second position at around 15 m (variable 10-18 m) allows for larger samples, but through the larger L/D of 625 also for high spatial resolution. The flux at this position is estimated to be about 3×10^5 n/(cm^2 sec) and is thus highly competitive for studies at highest resolution or large sample size, including time resolved investigations (see Table VII.1).

In addition, the intrinsic time structure of the source offers wavelength resolutions of $\tau/ToF(\lambda) = \delta\lambda/\lambda$ of around 5% (4 Å) and 1.7% (4 Å) at the chosen sample positions, respectively. Depending on the required resolution, the position will be chosen for the different methods: highly efficient wavelength resolved neutron imaging for quantitative dark-field imaging (SANS mapping) and Bragg edge imaging as well as polarization contrast imaging . The wavelength resolution at position 2 is sufficient for Bragg edge studies targeting crystalline phase and phase transition mapping studies as well as assessment of texture variations, as it is highly relevant not only for additive manufacturing research. Polarized neutron imaging as well as dark-field contrast are well suited at the given flux values to study ferromagnetic phases and domain structures as well as in the case of dark-field contrast microstructures in various materials including such in soft matter and food.

The relaxed wavelength resolution and high flux at position 1 provide the instrument with outstanding

Instrument parameters	
Target station	TS-96
Moderator	Liquid para-hydrogen
Moderator to sample distance	5 m
Collimation ratio L/D	200
Wavelength range / bandwidth	$1 - 15$ Å/8.2 Å
Beamsize up to	20 cm
Potential wavelength resolution	5% (4 Å)
Spatial detector resolution up to	10 μm
Detector integration time	ms to s
Flux (up to)	3×10^6 n/(cm^2 s)
Moderator to sample distance	15 m
Collimation ratio L/D	625
Wavelength range / bandwidth	$1 - 15$ Å/2.7 Å
Beamsize up to	55 cm
Potential wavelength resolution	1.7% (4 Å)
Spatial detector resolution up to	10 μm
Detector integration time	ms to s
Flux (up to)	3×10^5 n/(cm^2 s)

Table VII.1: *Instrument parameters for the cold neutron imaging beamline*

efficiency and performance for low wavelength resolution based studies, where the instrument can be expected to even outperform other state of the art instruments, e.g. in dark-field contrast imaging. In particular the novel method of high duty cycle neutron imaging targeting inelastic/quasi-elastic cross section mapping can be applied efficiently. It is aimed at enabling the study of hydrogen dynamics, chemical binding states and temperature distributions in complex and bulk components, devices and processes such as in batteries or additive manufacturing..

In order to enable wavelength resolved neutron imaging at position 2, a frame overlap chopper has to be installed between position 1 and 2, which requires extra beam size limitations for such applications. This however correlates with typical fields of view for such investigations and could be shown in simulations to not impact the performance. For large field of views chopper and beam limiters can be removed and adapted accordingly.

The geometry of the beamline allows effective instrumentation and neutron transport without the need for a neutron guide, which improves the expected beam homogeneity for imaging applications even at high resolutions and on large fields of view. Background considerations for such direct view geometry have to be considered and optional filters have to be available at an upstream position.

VII.2 Diffractive Neutron Imaging (D-NI)

Markus Strobl, Norberto Schmidt

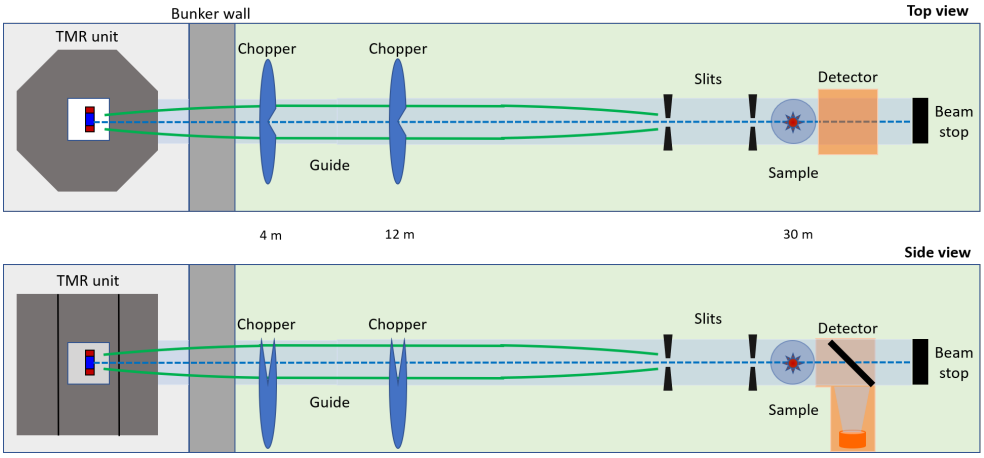

Figure VII.2: *Proposed layout for the diffractive neutron imaging (D-NI) instrument at the HBS.*

VII.2.1 Diffractive neutron imaging instrument description

Instrument parameters	
Target station	TS-96
Moderator	Liquid para-hydrogen
Moderator to sample distance	30 m
Wavelength range / bandwidth	1-15 Å, 1.35 Å
Collimation ratio L/D	300
Beamsize up to	10 cm
Potential wavelength resolution	0.8% (4 Å)
Spatial detector resolution up to	100 μm
Detector integration time	600 ms
Flux (up to)	2×10^6 n/(cm^2 s)

Table VII.2: *Instrument parameters for the diffractive neutron imaging beamline*

Neutron imaging instruments at pulsed sources provide access to mapping crystallographic features of sample materials in particular with regards to engineering materials, additive manufacturing research and industrial components, but also applications in e.g. energy research and cultural heritage have been reported. Diffractive neutron imaging is generally based on mapping Bragg edges in the transmission spectrum and analyzing their positions, heights etc. While some of this work is enabled at the cold neutron imaging instrument, in particular strain mapping requires sub percent wavelength resolution. Thus, for the given time structure of a HBS 96 Hz cold beamport, an instrument length beyond that enabled at the cold neutron imaging instrument is required. Therefore, the dedicated

diffractive neutron imaging instrument will feature a length of more than 30 m, to provide sufficient resolution, especially around 4 Å, where generally the most prominent Bragg edges are located. The extended instrument length limits the bandwidth for ToF imaging to below 1.5 Å, which is particularly well suited for high wavelength resolution imaging measurements.

On the other hand, the significant instrument length at the given moderator size implies the need for a neutron guide to transport a significant flux and divergence to a pinhole position about 5-10 m upstream of the sample detector position. A guide optimized to transport a sufficient divergence and imaging the moderator source to the pinhole has to accommodate at least two bandwidth choppers. Particular attention has to be paid to achieve a large and homogeneous field of view on the detector of at least 100 x 100 mm. A pinhole exchanger and filters will enable variable spatial resolution capabilities. The chopper system has to efficiently limit the bandwidth and enable a flexible choice of wavelengths. The option of continuous phasing or pulse suppression can be considered for measurements requiring a wider wavelength range. In addition, complementary diffraction detectors, potentially based on the novel TPX-Cam technology have to be considered. Specific characteristics and performance parameters are presented in Table VII.2.

VII.3 Thermal Neutron Imaging (T-NI)

Nikolay Kardjilov, Norberto Schmidt

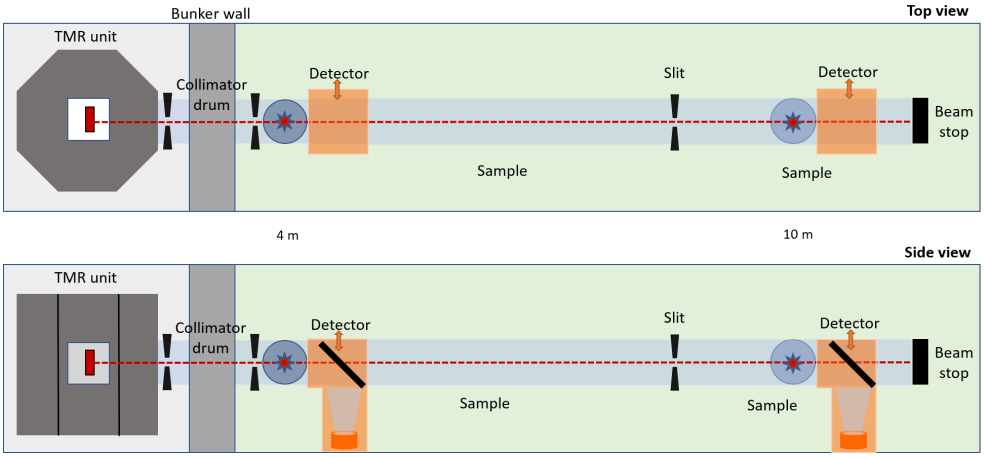

Figure VII.3: *Proposed layout for the thermal neutron imaging (T-NI) instrument at the HBS.*

The imaging with thermal neutrons allows a high transmission through metals and heavy elements contrary to X-rays and cold neutrons and provides sufficient contrast for light elements like hydrogen, lithium and boron. In addition to this, thermal neutrons distinguish between isotopes due to their different attenuation coefficients which can be used for various dynamic studies where changes in the isotope distributions can be mapped. The design and the construction of the thermal neutron imaging instrument at HBS requires the optimization of a great number of parameters concerning the beam geometry, the shielding design, adapted detectors and many others.

Our vision for the facility is to design a setup performing an image quality competitive to the best neutron radiography facilities worldwide and allowing the development of non-conventional image techniques like wavelength-selective radiography, phase-contrast imaging, refraction tomography, imaging with polarized neutrons and real-time radioscopy. In this way, the existing options in neutron radiography for advanced neutron imaging will be extended. To realize such a multipurpose facility, the setup design should give the flexibility to easily change the beam geometry by positioning various static and dynamic neutron components in the beam changing its energy and spatial distribution in an appropriate way. Considering that, we decided to arrange the facility similar to a classical optical bench where the whole distance between the source (the collimator in our case) and the detector is accessible for various neutron optical components providing the desired beam modulation.

VII.3.1 Beam characteristics

The design of the thermal neutron imaging instrument at HBS considers the use of a H_2O moderator in combination with a 96 Hz pulsed beam with pulse width of 250 μs. This determines a highly intensive beam ($\approx 10^9$ n/cm^{2}s) at the entrance of the instrument with a broad thermal neutron spectrum between 0.4 Å and 2.9 Å. Such spectral beam characteristics are very suitable for a non-conventional imaging due to the following reasons:

- The Bragg edges for many crystalline materials are in this energy range which allows ra-

diography contrast variations by applying of wavelength-selective imaging techniques using time-of-flight analysis.

- The wavelength interval and the beam intensity are optimal for various neutron optic components like slits, pinholes and solid-state polarizers, which can be successfully used for different beam modulations. In this way appropriate beams for wavelength-selective imaging, phase-contrast radiography and neutron polarizing imaging experiments can be prepared.
- The high penetration power of thermal neutrons in combination with large beam size is a good precondition for investigation of large samples which is important for different industrial applications.
- The high neutron flux in the order of magnitude of 10^7 n/cm^{2}s at the sample position is suitable for the conduction of real-time imaging experiments.

The beam advantages mentioned above will allow the performance of unique experiments and will make the facility without analog worldwide.

VII.3.2 Geometrical characteristics

The proposed length of the instrument varies between 4 and 10 m, which, in combination with a corresponding diaphragm of diameter D (typical values range from 1 to 3 cm), will define the level of the beam collimation, the so-called L/D ratio. Simulations show that at L/D of 500 (diaphragm of D = 2 cm) the expected flux at the sample position is $\approx 3.5 \times 10^5$ n/cm^{2}s. Smaller diaphragm can be used to improve the collimation ratio, e.g. D = 1 cm (L/D = 1000); the corresponding flux will be 1×10^5 n/cm^{2}s, which is still reasonable for radiography investigations.

An additional measuring position at 4 m distance from the diaphragm can be used for investigations requiring higher neutron flux where 10^7 n/cm^{2}s will be available at L/D of 100. The flight distance between the diaphragm and the sample position determines the beam size at the detector position. At a distance of 10 m the simulations show a beam cross-section at the sample position of 35 cm in diameter, while at the high flux measuring position at 4 m the beam size is reduced to 15 cm, see Table VII.3. These beam sizes are sufficient for most of the experiments considering that for standard tomography applications the investigated sample should be completely in the beam by a rotation of 180 degrees.

Instrument parameters	
Target station	TS-96
Moderator	Water
Moderator to sample distance	4 m
Collimation ratio L/D	100
Beamsize up to	15 cm
Flux (up to)	10^7 n/(cm^2 s)
Moderator to sample distance	10 m
Collimation ratio L/D	250
Beamsize up to	35 cm
Flux (up to)	1.5×10^6 n/(cm^2 s)

Table VII.3: *Instrument parameters for the thermal imaging beamline*

VII.3.3 Foreseen experimental methods for a beamline use

- *Conventional neutron radiography and tomography:* These are the main experimental techniques that will be used for a non-destructive investigation of different samples from the science and the industry. In this respect, the facility will be optimized to fulfil the requirements of these techniques for a better beam collimation and a high neutron flux at the sample position. Since the better collimation reduces the beam intensity and vice versa, the facility is planned to have three modes of exploitation:

  - *High-intensity mode:* With a poor collimation characteristic (L/D of 100) and a high neutron flux at the sample position of $\approx 10^7$ n/cm^{2}s.
  - *Optimal mode:* With a good L/D ratio of 250 and a reasonable neutron flux of $\approx 1.5 \times 10^6$ n/cm^{2}s.
  - *High-resolution mode:* With a high L/D ratio of 500 and a moderate neutron flux of $\approx 3.5 \times 10^5$ n/cm^{2}s.

  The appropriate mode will be chosen depending on the sample and the corresponding detection system. The expected experimental time for a radiography projection at the optimal mode is ~ 5 s which sets the time for a complete tomography experiment to ~ 1 h.

- *Wavelength-selective radiography and tomography:* The method will allow radiography and tomography investigations at different thermal neutron wavelengths. At these wavelengths, the neutron attenuation for many metals changes drastically – so-called Bragg edges. This can be used successfully for appropriate image contrast variations in radiography and tomography investigations. In addition, the radiography and tomography experiments with monochromatic beam don't suffer from spectral effects like beam hardening, which allows a better quantification of the data. A double-crystal monochromator, which allows the selection of a single wavelength between 0.4 Å and 2.9 Å with a resolution of $\Delta\lambda/\lambda \approx 1$ %, will be used. The appropriate parameters can be chosen in respect to the required experimental conditions and the investigated sample.

- *Phase-contrast imaging:* By this experimental method a neutron beam with a high spatial (transverse) coherence is used for a visualization of phase shifts produced by the investigated sample. To provide appropriate conditions for a phase contrast imaging a small pinhole in a combination with a large distance between the pinhole and the sample is necessary. A measure for the achieved spatial coherence is the so-called coherence length $l_c = L\lambda/D$, where L is the distance between the sample and the pinhole, D is the diameter of the pinhole and λ is the neutron wavelength. In our case for a neutron beam spectrum with a maximum at 2 Å and setup parameters D = 0.5 mm and L = 10 m, the obtained coherence length is 4.5 μm.

- *Imaging with polarized neutrons:* Different kind of polarizers (solid-state benders or ^{3}He spin filter cells) can be used for a neutron beam polarization. The analysis of the transmitted beam through the sample can be performed by the same devices setting them in an analyzing mode. In this way magnetic properties of the sample and magnetic fields around it can be visualized by standard position-sensitive detectors.

- *Real-time radioscopy:* The high neutron flux at the 4 m position of $\approx 10^7$ n/cm^{2}s allows a real-time imaging of fast repetitive processes. For this purpose, a sCMOS camera with a fast-time gated image intensifier can be used as a detection system.

VII.3.4 Conclusion

The thermal neutron imaging facility planned at HBS will be competitive to the best existing facilities concerning the beam collimation and the neutron flux, which are important for conventional applications – neutron radiography and tomography. The facility will be worldwide without analog concerning its flexibility and capability for advanced thermal neutron imaging.

VII.4 Epithermal and High Energy Neutron Imaging

Norberto Schmidt, Eric Mauerhofer

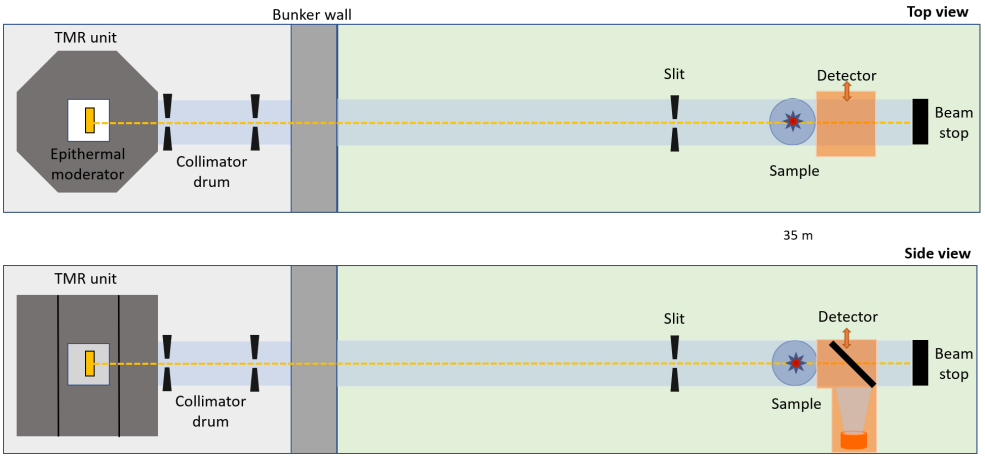

Figure VII.4: *Proposed layout for the epithermal neutron imaging station at the HBS.*

Neutron imaging with epithermal and high energy neutrons has gained importance in recent years. Its interest lies in the fact that it will allow the study of denser and larger objects considering the penetrating power of the more energetic neutrons. Conventionally, the integrated flux extracted from a moderator region allowing the extraction of an intense epithermal beam is used, to explore the inner structure of large and bulky specimen In addition, if neutron pulse structure can be exploited and the method is combined with the time-of-flight technique, it is possible to discriminate the atomic composition of samples considering the various resonances of interest in the range of 1 eV to 1 keV. The required time-of-flight resolution can be achieved by a special temporal pulse patterning of the proton pulse, as the time distribution of neutrons far above the thermal equilibrium energy closely follows the structure of the proton pulse. The main scientific application cases for an epithermal and high energy neutron imaging instrument range from the characterization of archaeological objects

Instrument parameters	
Target station	TS-epi (96 Hz)
Moderator	Epithermal
Pulse width by accelerator pulse patterning	between 1 and 10 μs
Moderator to sample distance	35 m
Viewed source size	6 cm
Energy range	1 eV to 1 keV
Collimation ratio L/D	590
Beamsize up to	50 cm
Potential energy resolution	5% (1 keV)
Spatial / temporal resolution up to	500 μm / ms to s
Flux (up to)	2×10^5 n/(cm^2 s)

Table VII.4: *Instrument parameters for the epithermal neutron imaging station.*

122 TDR Instrumentation | HBS

with a variety of isotopic contents to the study of large and dense objects such as large batteries or aeronautical components.

VII.4.1 Instrument description

A moderator to optimize the epithermal spectrum is under design, which would allow the beam geometry to be configured according to the user's requirements. Due to the high velocity of epithermal neutrons, short proton pulses will be necessary for time-of-flight studies. Therefore, the accelerator could be operated exceptionally to have pulses ranging from 1 to 10 microseconds at third target station (TS-epi, 96 Hz).

The epithermal neutron imaging instrument will have one position at 35 m from the source, and will be ideal for combining the time-of-flight method with the transmission of the resonances. It will have a collimator drum which will allow the beam collimation to be varied in order to obtain different beam sizes depending on the size of the sample to be studied. In particular, if a neutron micro-pulse of 4 μs is considered, the energy resolution for the 1 keV neutrons will be of the order of 5% at the sample position. Table VII.4 reports the main expected values for the epithermal neutron imaging station, while figure VII.4 shows the proposed layout.

VII.4.2 High energy instrument description

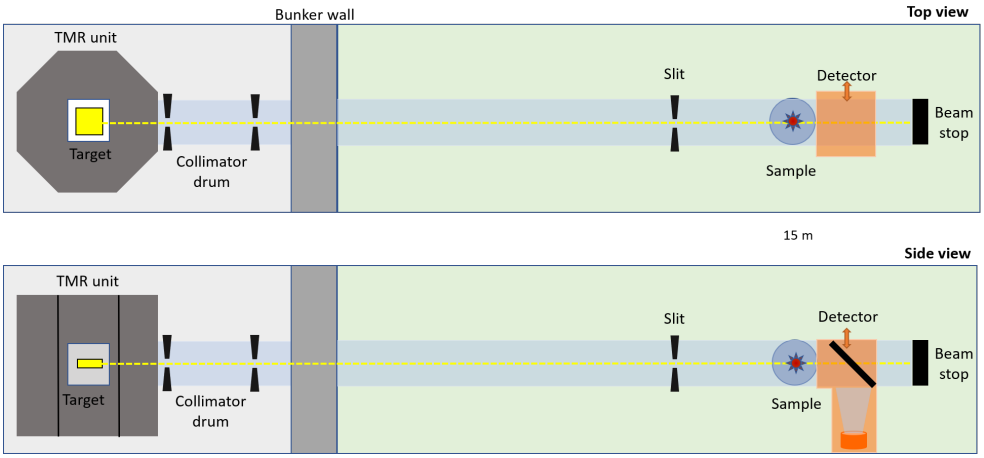

Figure VII.5: Proposed layout for the high energy neutron imaging station at the HBS.

Instrument parameters	
Target station	TS-epi (96 Hz)
Moderator	None (Ta target)
Pulse width	167 μs
Moderator to sample distance	10 m
Viewed source size	6 cm
Energy range	1 keV to 10 MeV
Collimation ratio L/D	170
Beamsize up to	20 cm
Spatial resolution up to	500 μm
Flux (up to)	8×10^7 n/(cm^2 s)

Table VII.5: Instrument parameters for the high energy neutron imaging station.

Considering that the HBS target will generate fast neutrons of about 1 to 10 MeV, it would be possible to generate neutron images with a beam directly observing the fast source at the target station.

The high energy neutron imaging instrument will have a single position at 10 m from the source, in order to maximize the neutron flux into the sample. A collimator drum will allow the desired collimation to be set. Due to the small size of the neutron target, the source will function as a point source, thus obviating the need for a pinhole. Furthermore, considering the high brightness of the source, fluxes of the order of 8×10^7 n/(cm^2 s) are expected at the sample. Table VII.5 reports the main expected values for the high energy neutron imaging instrument, while figure VII.5 shows the proposed layout.

VII.5 Prompt Gamma Neutron Activation Analysis (PGNAA)

Eric Mauerhofer

Prompt Gamma Neutron Activation Analysis (PGNAA) is a nondestructive analytical method for determination of elemental composition of samples or items of diverse origins. It is commonly based on the detection of isotope specific prompt gamma rays induced by the capture of cold or thermal neutrons by atomic nuclei ((n,γ)-reaction). PGNAA allows a panoramic analysis, since all elements, excepted helium, emit prompt gamma rays. It is particularly useful for the accurate detection of light elements, for which not many nondestructive analytical techniques are available. PGNAA is an unique method to determine hydrogen in any kind of samples with a detection limit at ppm level or below and, at the same time, to provide the elemental content of the investigated sample. It is highly sensitive for certain elements such as boron, cadmium, mercury and rare earth elements which can be detected at the ppb level. Furthermore, PGNAA may be used for in-situ investigation of chemical processes like catalytic reactions. Large objects may be investigated to some extent by PGNAA using cold or thermal neutron beams. However, fast neutrons are of a better choice for the bulk analysis of large and thick items, in particular due to their high penetration depth. In this case, prompt gamma rays generated from the inelastic scattering of fast neutrons with atomic nuclei ((n,n´γ)-reaction) are measured. This method is a particular type of PGNAA and is called, here, Prompt Gamma Analysis based on Inelastic Neutron Scattering (PGAINS). Applications of PGNAA cover a wide range of disciplines such as nuclear physics, material science, geochemistry, mineralogy, petrology, chemistry, environmental science, agriculture, food analysis, biology, medicine, forensic, archaeology, cultural heritage, cosmochemistry and other areas including specific industrial issues.

VII.5.1 ToF-PGNAA

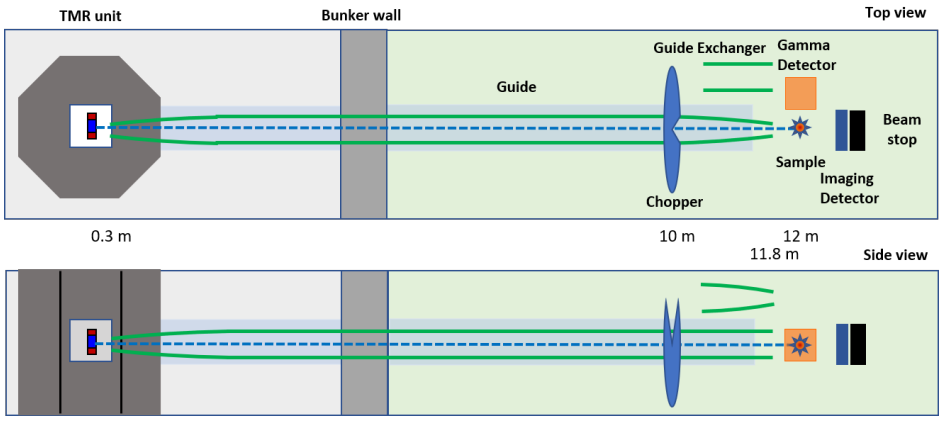

Figure VII.6: *Schematic top and side view of the ToF-PGNAA instrument with neutron transmission imaging.*

PGNAA is routinely applied at continuous neutron sources i.e. research reactors using either a thermal or cold neutron beam without any neutron time-of-flight (ToF) information. However, selecting neutrons in the cold, thermal or resonance energy range provides an elemental selectivity for accurate quantification by eliminating interference or by increasing the signal-to-background ratio. Furthermore, neutrons with different energies have different sample penetration depths and therefore interrogate different sample volumes, providing information on the sample homogeneity or sample depth resolved information. The time structure of HBS offers the possibility to perform Time-of-Flight

PGNAA (ToF-PGNAA) of small-to-medium sized samples within the neutron energy range 1 meV to 80 eV, providing great flexibility according to the sample type and information required. Neutron energy-dependent gamma-ray spectra are measured with a well-shielded high purity germanium detector (HPGe-detector) using the time-of-flight method. The HPGe-detector counts are recorded as a function of the gamma energy (y-axis) and the neutron time-of-flight i.e. the neutron energy (x-axis) to produce a two dimensional matrix for data analysis. A vertical cut along the y-axis at a chosen neutron energy provides the prompt gamma-ray spectra recorded for this neutron energy. A horizontal cut along the x-axis at a chosen gamma-ray energy delivers neutron capture spectra showing the variations in neutron capture cross sections i.e. isotopic sensitivity as a function of the neutron energy. Isotopic contrast and selectivity is obtained by screening over the detector events in neutron and gamma-ray energy.

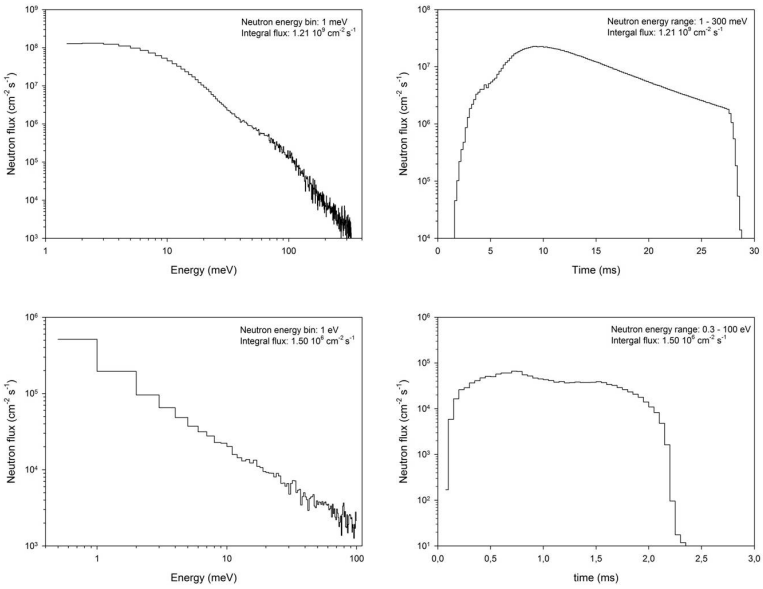

Figure VII.7: *Neutron flux spectrum and time distribution at sample position for cold and thermal neutrons energy range 1 to 300 meV (upper diagrams) and for epithermal neutrons energy range 0.3 to 100 eV (lower diagrams).*

The ToF-PGNAA instrument is placed at the 24 Hz target station and uses a cold (bi-spectral) moderator (liquid para-hydrogen, 10 cm length and 1.2 cm radius) providing a cold, thermal and epithermal neutron flux at the sample position. Neutrons are extracted 30 cm from the source. Cold and thermal neutrons are guided towards sample using a neutron guide m=3 with a cross section of 3 x 3 cm^2 and a length of 11.5 m. The sample is placed 20 cm from the end of the neutron guide. The distance of 12 m between sample and neutron source allows the time-resolved acquisition of prompt gamma-ray spectra at various neutron energies ranging between 1 meV and 80 eV (0.032 - 9 Å). They arrive at the sample 0.1 - 28.4 ms after the proton pulse, (if the whole energy range is used). To measure delayed gamma-rays from activation products, there is only 11 to 12 ms left before the start of the next neutron pulse, because the period of the source is 41.67 ms and the pulse 0.67 ms FWHM plus tail. If a longer time for delayed gamma-ray spectra is wanted, the long wavelength are cut, e.g. at 1 Å, which reduces the TOF range at the detector to 0 - 3.2 ms and thus extends the time range for delayed gamma-rays to about 27 ms. This is realized by a bandwidth chopper positioned 2 m upstream the sample. A beam size changer allows samples of various size to be investigated.

Instrument parameters	
Target station	TS-24
Moderator	Liquid para-hydrogen
Moderator-to-sample distance	12 m
Sample-to-detector distance	0.3 to 0.5 m
Beam size	3×3 cm^2
Neutron energy range	1 meV to 80 eV
Average thermal-equivalent flux	6.8×10^8 cm^{-2}s^{-1}
Peak flux at sample position1)	1.2×10^5 cm^{-2}s^{-1} (40 - 80 eV)
	6.2×10^5 cm^{-2}s^{-1} (1 - 40 eV)
	5.4×10^6 cm^{-2}s^{-1} (0.1 - 1 eV)
	3.0×10^8 cm^{-2}s^{-1} (10 - 100 meV)
	5.3×10^8 cm^{-2}s^{-1} (3 - 10 meV)
	3.8×10^8 cm^{-2}s^{-1} (1 - 3 meV)

(I) Determined with the simulation tool VITESS using neutron guide equipped with a m=3 supermirror and a cross section of 3 x 3 cm^2

Table VII.6: *Parameters of the instrument ToF-PGNAA*

Furthermore, the broad neutron energy range and the medium beam size also allows gaining additional information for sample composition determination by using a suitable neutron transmission imaging detector for spatial and time resolution. The schematic view of the instrument is shown in Fig.VII.6. The neutron flux spectrum and the time distribution at the sample position determined with the simulation tool VITESS are shown in Fig.VII.7. The parameter of the instrument are given in Table VII.6. The instrument delivers an average thermal-equivalent neutron flux of 6.8×10^8 cm^{-2}s^{-1} at sample position, which is comparable the flux achieved for PGNAA instruments at research reactors ($6.5 \cdot 10^9$ cm^{-2}s^{-1} at NIST, $2 \cdot 10^9$cm^{-2}s^{-1} at FRM II and $9.6 \cdot 10^7$ cm^{-2}s^{-1} at BRR).

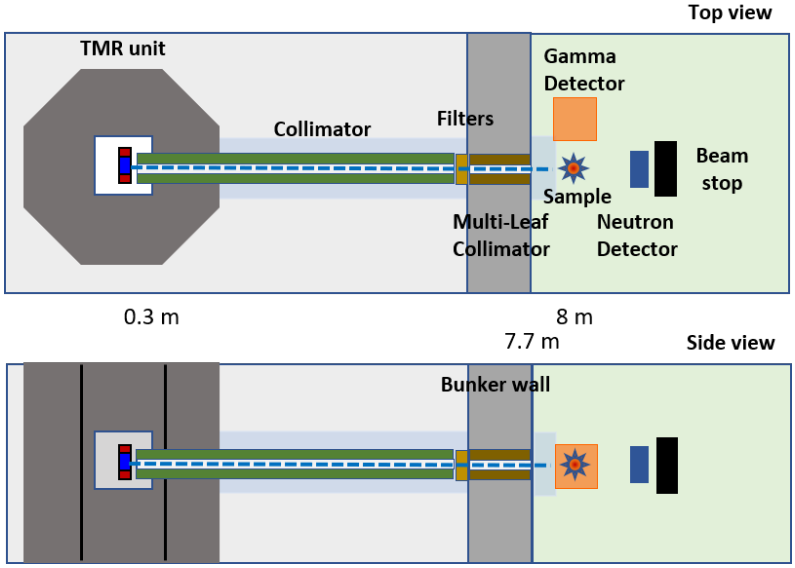

Figure VII.8: Schematic top and side view of the PGAINS instrument with fast neutrons.

Prompt Gamma Analysis based on Inelastic Neutron Scattering (PGAINS) is dedicated in particular to the determination of the elemental composition of large and thick items with fast neutrons though small and thin samples can also be investigated for example for nuclear data measurements. The instrument is placed at the third target station (96 Hz) optimized for epithermal and fast neutrons. Fast neutrons are extracted tangentially at the height of the tantalum target and collimated over a length of 7.4 m with a beam size of 6 cm diameter. The sample is located 8 m from the neutron source. The neutron beam size can be reduced and shaped with a multi-leaf collimator inserted into the bunker wall. In order to filter out the epithermal neutrons from the fast neutron beam and to attenuate gamma radiation coming from the tantalum target, a boron carbide plate with a thickness of 1 cm and lead plate with a thickness of 5 cm are placed upstream beam side of the multi-leaf-collimator. Gamma radiation is measured with a well-shielded high purity germanium detector (HPGe-detector) which is placed together with the sample in an irradiation room.

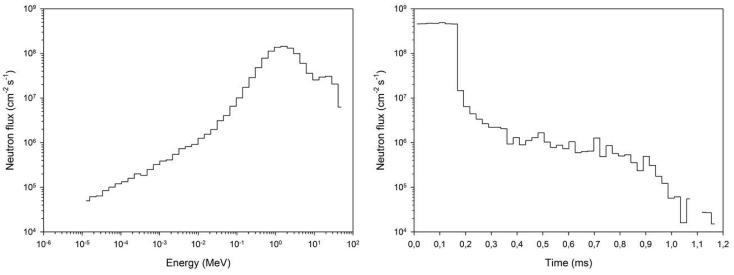

Figure VII.9: Neutron flux spectrum (peak flux) and time distribution at sample position for the PGAINS instrument

Instrument parameters	
Target station	TS-epi (96 Hz)
Moderator	None (Ta target)
Source-to-sample distance	8 m
Sample-to-detector distance	0.6 to 1 m
Beam size	6×6 cm^2
Neutron energy range	0.6 eV to 50 MeV
Peak Flux	1.0×10^9 cm^{-2}s^{-1} (10 keV - 50 MeV)
	5.5×10^6 cm^{-2}s^{-1} (0.5 - 10 keV)
Time-average flux	1.6×10^7 cm^{-2}s^{-1} (10 keV - 50 MeV)
	8.9×10^4 cm^{-2}s^{-1} (0.5 - 10 keV)

Table VII.7: *Instrument parameters for Prompt Gamma Analysis based of Inelastic Neutron Scattering (PGAINS) with fast neutrons*

The prompt gamma rays induced by fast neutron inelastic scattering are detected during the fast neutron pulses (167 μs). Additional information of the sample composition can be obtained from the prompt gamma rays generated by capture of epithermal neutrons and the delayed gamma rays of activation products which are measured during the 1 ms from the end of the pulse and during the 9 ms before the next pulse, respectively. The average fast and epithermal neutron flux in the sample is evaluated from transmission measurements with a suitable neutron detector. The schematic view of the instrument is shown in Fig.VII.8.

The neutron flux spectrum and time distribution at the sample position determined with the Monte Carlo particle transport simulation code PHITS are shown in Fig.VII.9. The parameter of the instrument are given in Table VII.7. With a fast neutron flux of 1.6×10^7 cm^{-2}s^{-1} and a fast-to-epithermal neutron flux ratio of 185 at sample position the instrument can be considered as competitive for the analysis of large samples.

VII.6 Neutron Depth Profiling (NDP) and Versatile Test Reflectometer

Egor Vezhlev

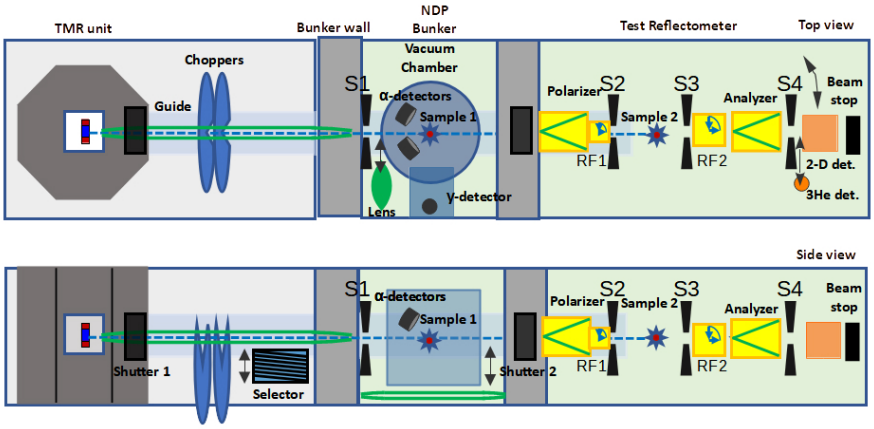

Figure VII.10: *Schematic top and side views of the NDP/Test Reflectometer beamline*

VII.6.1 Introduction and science case

The Neutron Depth Profiling (NDP) technique allows studying near-surface distributions of several light isotopes with relatively high neutron absorption cross-section (^{3}He, ^{6}Li, ^{10}B, ^{14}N and others) in solid materials. Absorption of a neutron results in a nuclear decay with emission of a mono-energetic charged particle (alpha particle, proton or Triton) and a recoiling nucleus. Before escaping the sample surface, each particle loses a certain amount of energy depending on the stopping power of the host material. The detected energy spectrum depicts the in-depth distribution of a corresponding absorbing isotope. After unfolding the spectra by an appropriate algorithm one obtains the concentration versus depth profile in absolute units, which is difficult for light elements by any other commonly used analytic technique (i.e. by different ion beam analysis techniques). Recently, NDP has gained a lot of interest due to its sensitivity to the isotope ^{6}Li, because Li is a key element of currently widely spread lithium-ion batteries. NDP provides insight on new developments in the field, i.e. rechargeable lithium-ion batteries with solid electrolytes. Because of its sensitivity to ^{22}Na isotope, NDP could also be applied to studies of the most promising competitor of commercial lithium-ion batteries – all-solid-state sodium-ion batteries. As NDP can be considered to be non-destructive, batteries can be explored *in situ* and *operando* for many cycles of battery charging and discharging, which is of high demand in the battery community.

VII.6.2 Instrument Description

The NDP instrument is foreseen to be built at the 24 Hz target station with a liquid para-hydrogen cold neutron moderator. The NDP technique is based on neutron absorption, thus the instrument will require a white neutron beam, preferably in the cold neutron regime, where the absorption cross-section is generally proportional to the neutron wavelength $\sigma_a \sim \lambda$. As an absorption method, NDP is also insensitive to the neutron beam divergence, so that neutron beam focusing can be effectively applied in the instrument design. The beam transport system will be equipped with a 6.5 meters 2-D fully elliptic guide. A basic set of choppers will be placed inside the TMR bunker to allow

monochromatisation and frame overlap cancellation if required by an experiment (e.g. time-resolved experiments). To maximise the flux at the sample an additional neutron focusing lens (supermirror-multichannel or capillary) can be optionally offered for experiments. Such a lens could be of a particular interest for performing sample surface scanning.

The NDP vacuum chamber, i.e. sample area, will be made out of stainless steel with thin aluminium windows for beam entrance and exit. Additional shielding blocks will be installed inside to additionally cover the charged particle detectors from unwanted background coming along the neutron beam. Altogether the NDP chamber will be located in a separated, well-shielded bunker to minimise possible background coming from nearby beamlines. Following the current state-of-the-art, the NDP chamber will be equipped with a multidetector system for collection of charged particles signal. We plan to have up to 4 detectors and thus have a gain factor of up to 4 times in signal. Additionally the chamber will be equipped with HPGe detector for detection of prompt-gamma rays coming from a sample. On the one hand, such a feature will help to reveal a gamma background spectrum coming from the sample and, on the other hand, can serve as a standalone PGAA facility if needed. The performance of the NDP spectrometer in neutron flux and signal-to-noise ratio is projected to be competitive with the world-leading NDP facilities (NIST, TUM, JCNS).

Instrument parameters	
Target	TS-24
Moderator	Liquid para-hydrogen
Moderator-to-sample distance	8 m
Beam size	1.2× 1.2 cm^2 (focused)
Beam parameters	white beam
Peak cold neutron flux	6.8 × 10^9 $cm^{-2}s^{-1}$ (focused)
	1.7 × 10^9 $cm^{-2}s^{-1}$ (non-focused)
Time-average thermal equivalent flux	2.1 × 10^8 $cm^{-2}s^{-1}$ (focused)
	5.3 × 10^7 $cm^{-2}s^{-1}$ (non-focused)

Table VII.8: *Instrument parameters of the Neutron Depth Profiling (NDP) spectrometer*

VII.6.3 Polarized Test Reflectometer

The rather compact dimensions of the NDP instrument shielding bunker allows to extend the beamline further and introduce downstream a test reflectometer facility. As at any neutron source, such a test beamline should serve the needs of supporting groups, like those working on neutron optics, detectors or neutron polarization and analysis. It can also accommodate any other valuable instrument design related experiment. Being, at the same time, a fully equipped polarised reflectometer, such an instrument can be used for standard neutron reflectometry and diffraction measurements.

VII.6.3.1 Instrument Description

Neutron reflectometry requires a flat beam divergence perpendicular to the scattering plane, thus the NDP beamline should be equipped with an additional exchangeable guide downstream the beamline to shift the (vertical) focal spot towards the sample position of the reflectometer and simultaneously suppress unwanted horizontal beam focusing. For that purpose exchangeable guide section would be introduced on demand through NDP bunker up to the slit S2. The first pair of collimating slits S1 will be installed already before the NDP chamber to provide sufficient collimation base. The additional slits S3 and S4 will be installed after the sample position and before the 2-dimensional detector, respectively,

in order to suppress the background for specular reflectometry measurements. In addition to the 2-dimensional detector, a He-3 single detector will be installed after the S4 slit pair for high signal-to-noise ratio measurements. The polarization of the neutron beam will be realised with a two stage reflecting polarizing supermirror, and analysis with a multi-channel polarising supermirror analyser situated immediately before the detector. RF-flippers after the polarizer and before the analyzer respectively will be utilised to perform full polarization analysis (also for off-specular reflection). The entire detector arm will be placed in a tight vacuum container. This measure significantly reduces the background contribution from scattering in open air.

Instrument parameters	
Target	TS-24
Moderator	Liquid para-hydrogen
Moderator-to-sample distance	10 m
Sample-to-detector distance	2 - 4 m
Beam size at the sample	2×1 cm^2 (vert. focused)
Wavelength range	2 - 10 Å
Wavelength Resolution	2 - 10 %
Detector movement range	$-10^\circ < 2\theta < 90^\circ$
Polarization and analysis	Supermirrors (spec. and off-spec.)
Peak cold neutron flux	1.5×10^7 cm^{-2}s^{-1} (1.2° hor. collimation)

Table VII.9: *Instrument parameters of the versatile test reflectometer*

The reflectometer will be operable in either time-of-flight mode or in more conventional constant wavelength mode. For the second option a multi-blade velocity selector will be installed within the TMR shielding bunker to allow working at wavelength resolution of 10%. We expect an integral non-collimated (with fully open instrument slits) neutron flux approximately around $4 \cdot 10^7$ cm^{-2} s^{-1} at such a facility that gives rather promising estimates for performing fast and effective test

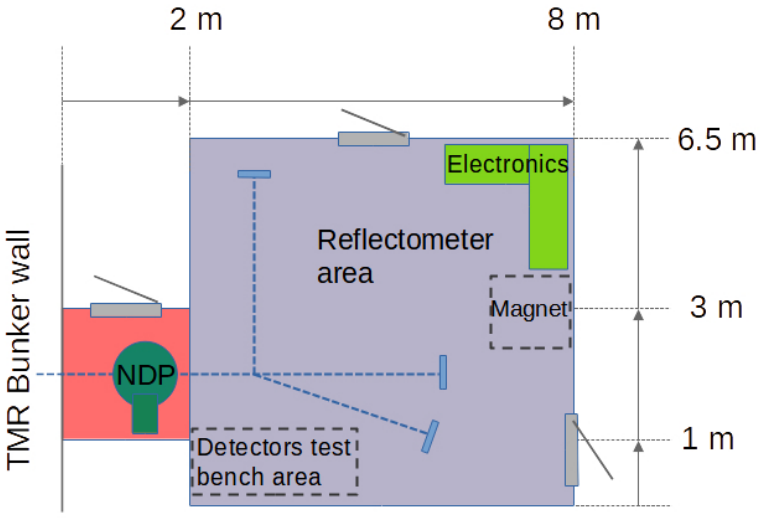

Figure VII.11: *Estimated area plan of the NDP beamline*

reflectometry measurements.

VII.6.4 Floor plan of the NDP beamline

In figure VII.11, one can see a preliminary floor occupation plan of the NDP beamline. The sketch depicts the area outside the TMR assembly bunker. The first part, shown in red, is a shielded bunker of the NDP. Due to the high sensitivity of the charged particle detector system, this room should be designed in a way to provide high electrical noise cancellation. The following blue area is foreseen for the accommodation of the test reflectometer and its components. This room should possibly be shielded from gamma and neutron background originating from the neighbouring beamlines. For performing reflectometry measurements the area should have a polished floor (Tanzboden). The reflectometer area should be equipped with a compact crane to be able to move freely heavy sample environment equipment (like e.g. a magnet) or bulky samples (e.g. a detector assembly).

Other generally required infrastructure like cooling water, pressurised air, vacuum pumps, IT-infrastructure etc. must also be foreseen accordingly.

VIII.

INSTRUMENT SUITE AT TARGET STATIONS

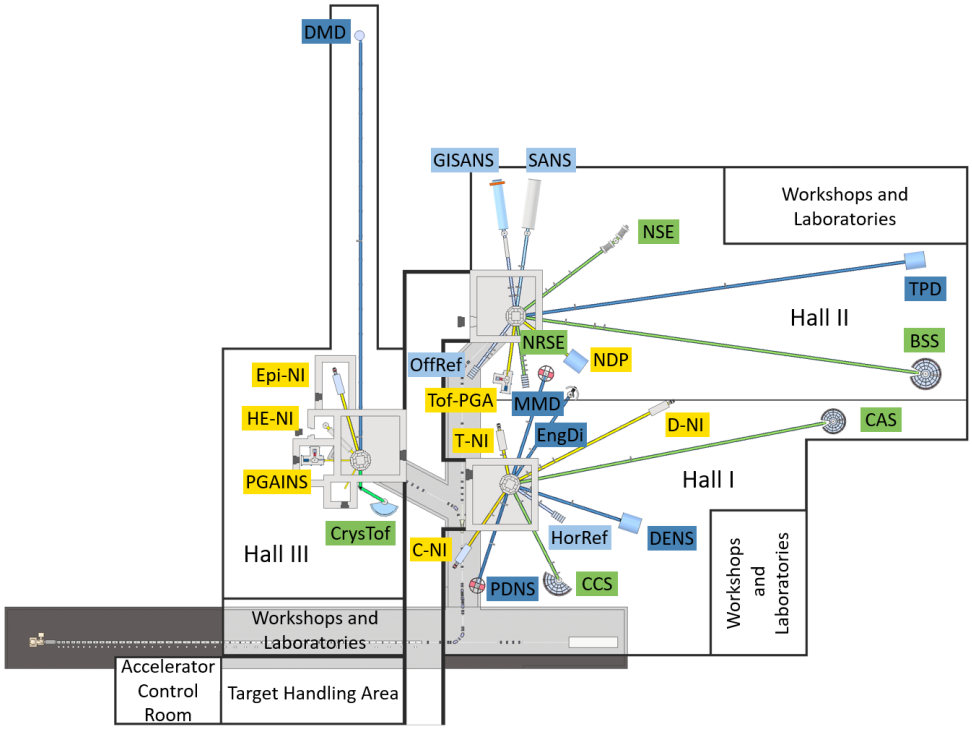

Figure VIII.1: *Layout of instruments at the HBS experimental halls. The different instruments are labelled according to Tab. VIII.1. The colors of the neutron guide and labels indicate the instrument class as introduced in Tab. VIII.1. Additional buildings for the accelerator, the proton beam dump and the beam transfer are also indicated.*

In Table VIII.1 we summarise the key figures of all instruments that have been introduced in the preceding section. In Fig. VIII.1 these instruments have been distributed around the different target stations in the three experimental halls. The guide halls are aligned in a way that one of them can host the long instruments from the 24 and 96 Hz target stations.

The shorter hall hosts most of the instruments served by the 96 Hz target station. The characteristic

	Instrument	τ_{pulse} [μs]	L_{tot} [m]	Det. Cov. [sr]	λ_{min} [Å]	λ_{max} [Å]	$\frac{\delta\lambda_{\text{pulse}}}{\lambda_{\text{min}}}$ [%]	$\frac{\delta\lambda_{\text{pulse}}}{\lambda_{\text{max}}}$ [%]	ϕ_{average} 10^6 [n/cm^{2}s]	Remarks
SANS	High-Throughput SANS	667	23.7	0.01	3.0	9.8	3.7	1.1	0.41	Low angle
			14.7	0.81	3.0	9.8	8.8	2.0	41	Wide angle
GISANS	SANS with GISANS option	667	23.7	0.01	3.0	9.8	3.7	1.1	0.41	Low angle
			14.7	0.81	3.0	9.8	5.9	1.8	41	Wide angle
OffRef	Offspecular Reflectometer	667	13.0	0.08	2.0	12.0	10.1	1.7	48	
TPD	Therm. Powder Diffr.	30	80.0	5.71	0.6	2.7	0.2	0.1	0.55	High Res., 2 frames
		667	80.0	5.71	0.6	2.7	5.5	1.2	160	High Int., 2 frames
NSE	NSE Spectr.	667	25.0	0.04	6.0	16.0	1.8	0.7	2.8	Very cold neutrons
NRSE	NRSE Spectr.	667	25.0	0.04	6.0	16.0	1.8	0.7	2.8	Very cold neutrons
BSS	Backscattering Spectr.	60	85.0	3.66	5.6	7.6	0.06	0.04	7	
Tof-PGA	TOF-PGNAA	667	12.4		0.03	9.0			130	
NDP	Neutron Depth Profil.	667	8.2		0.0	20.0			210	White beam
HorRef	Hor. Reflectometer	252	11.0	0.01	5.0	8.6	1.8	1.1	7	Small sample
		252	11.0	0.01	1.6	8.8	5.7	1.0	10	Multi beam
EngDi	Engineering Diffr.	35	21.8	2.52	0.8	2.7	0.8	0.2	0.23	4 frames
DENS	Diffuse Elast. Neutron Scat.	252	21.2	5.24	2.0	3.9	2.4	1.2	50	
PDNS	Pol. Diffuse Neutron Scat.	252	21.0	2.09	2.0	4.0	2.4	1.2	52	
MMD	Single Crystal Diffr.	252	21.5	9.39	2.0	3.9	2.3	1.2	18	for 0.8 deg FWHM div.
CCS	Cold Chopper Spectr.	252	24.0	2.07	1.6	10.0	2.6	0.4	0.34	
CAS	Crystal Analyzer Spectr.	252	60	0.85	1.8	6	0.9	0.3	200	for 1.8 Å$< \lambda <$ 2.5 Å
C-NI	Cold Neutron Imaging	252	15.0		1.0	15.0	6.6	0.4	0.3	High Res.
		252	5.0		1.0	15.0	20	1.3	3	High Int.
T-NI	Thermal Neutron Imaging	252	10.0		0.5	4.5	20	2.2	0.35	High Res.
		252	4.0		0.5	4.5	50	5.5	10	High Int.
D-NI	Diffractive Neutron Imaging	252	30.0		1.0	15.0	3.3	0.2	2	
DMD	Disord. Mat. Diffr.	167	85.0	6.42	0.10	0.58	7.8	1.3		
PGAINS	PGAINS	167	8.6		0.00	0.37			16	
Epi-NI	Epitherm. Neutron Imaging	2	35.0		0.01	0.29	2.5	0.1	0.2	
HE-NI	Hi-Energy Neutron Imaging	167	10.0		0.00	0.01			80	
CrysTof	CRYSTOF	252	9.5	2.34	0.83	2.86	12.6	3.7	0.2	

Table VIII.1: *Key figures for the instrument suite presented. Flux and resolution values are quoted for typical configurations of the instruments. The colors indicate different instrument classes also used in Fig. VIII.1: Light blue: Large scale structure instruments, Dark blue: Diffractometers, Green: Spectrometers, Yellow: Imaging and analytics instruments.*

of this target station is distinct from other pulsed sources, as the source repetition rate is higher compared to other pulsed sources. The instruments here use intense, narrow bands and rely typically on the TOF-resolution provided by the neutron source. Also the imaging instruments, which use slow neutrons, extract neutrons from this target station.

The 24 Hz target station hosts many of the workhorse instruments of the facility. The SANS instruments and Spin Echo instrument can digest the full pulse at this target station to realize high intensity by relaxing the wavelength resolution. Instruments that use pulse shaping, profit from the broad pulse, which reduces the intensity variations across the used band.

The instruments around the second 96 Hz target station have special requirements in terms of beam size, spectral range and/or pulse shape. While the thermal moderators of the two other target stations have been optimized to feed the cryogenic moderators, the target-moderator-reflector assembly on this target station provides optimal conditions to extract fast, resonance and (epi)-thermal neutrons.

Instruments making use of these high energies provide their own instrument bunker for radiological reasons. For this target station we envision also special proton pulse patterns to allow time-of-flight methods for high energy neutrons.

IX.

INSTRUMENT SUPPORT AND NEUTRON TECHNOLOGIES

IX.1 Instrument control and automation system

IX.1.1 Requirements and functionality

Conceptionally, each neutron instrument can be grouped into sections such as beam definition, sample area, beam analysis and neutron detection as shown in Figure IX.1. Beam definition may include choppers, selectors, or monochromators for energy definition, devices for beam polarization or variable collimations. The sample area contains mechanical devices for sample exposure such as sample tables, goniometers and sample-changers, as well as devices for the definition of the sample environment, e.g. pressure, temperature or magnetic field. In the beam analysis section, specific energy ranges or polarization states may be filtered out of the scattered beam. In the detection section, scattered and filtered neutrons are recorded by a wide range of detector systems.

Figure IX.1: Schematic generic structure of a neutron instrument

A major task in neutron instrument control is the movement of a large variety of mechanical axes to realize ideal configurations for the individual experiments performed at the instruments. In the future we expect, that artificial intelligence will be employed to optimize the experimental setup based on the already acquired data.

In addition, a wide range of sensors, programmable power supplies and controllers for physical parameters such as temperature or pressure must be controlled and monitored. Since event rates and event sizes in neutron detection systems are relatively low compared to nuclear or high energy physics, neutron instruments do not have a dedicated data acquisition system. Data acquisition is also part of the control system: typically detector device servers residing on the resource tier do continuous detector readout during measurement and store the acquired data into data files.

In the HBS neutron instruments, detectors as well as choppers have to be synchronized with the pulses of the source via a connection to the timing system. In order to allow later dynamic re-binning and measurement during mechanical movements, neutron data will not be stored in the form of histograms but as event-mode data, which means that each detected neutron is recorded

with a timestamp. Therefore all other process data, e.g. mechanical positions, or sample environment parameters have to be time-stamped, too, and the corresponding devices must have an interface to the HBS timing system.

In comparison to the HBS machine, the HBS instruments are much more dynamic. They will experience continuous setup changes, especially in the sample environment. There will be a steady change of measurement scenarios, for which dynamic measurement sequences have to be programmed and executed. As a consequence, a more or less static Human Machine Interface (HMI) as required by the HBS machine control system is not appropriate for the instrument control system. Instead, the neutron instruments will be controlled by a dedicated instrument measurement program. The measurement program will have a client server structure. The server part runs on the middle tier of the control system and the client part on the presentation tier. Using the client, it is possible to define, start and stop dynamic measurement sequences, which will be executed by the server. A GUI tool and a scripting language tool are necessary for the definition of measurement sequences.

All instruments are equipped with a beam shutter that shuts off the beam for instrument access. The required personal safety subsystem in each instrument control system is responsible for the implementation of an interlock between the beamshutter and instrument access.

IX.1.2 Architecture and implementation

The Jülich Centre for Neutron Science (JCNS) of the ForschungsZentrum Jülich (FZJ) has been developing neutron instruments for decades and operates 12 instruments at its main outstation at the MLZ in Garching. All these instruments share the same architecture and technologies for the instrument control systems. In order to minimize implementation by relying on existing developments and the support of trained personnel, all HBS instrument control systems shall be implemented with the same architecture and the same technologies.

The instrument control systems will all be based on TANGO which has been developed by the European Synchrotron Radiation Facility in Grenoble. TANGO is an open-source software toolkit for the development of control systems according to a three-tier architecture, see Fig. IX.2. Relational Databases such MySQL will be used to store and access from the supervisory control and data acquisition system (process archives, alarm/logging archives, configuration databases) at the middle tier. TANGO systems are consistently object-oriented and employ CORBA and zeromq for communication with device servers. All instrument computers running TANGO device servers, middle tier components or clients in the presentation tier will use a Linux operating system. At the resource tier, industrial PCs will be installed.

The Networked Instrument COntrol System (NICOS), at MLZ Garching in collaboration with the Paul Scherrer Institute and the European Spallation Source, will used to control the HBS instruments and keep track of all machine and instrument parameters with the required timing resolution to allow

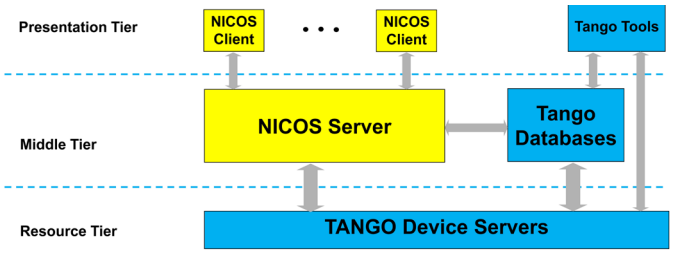

Figure IX.2: Software structure of the HBS instrument control systems

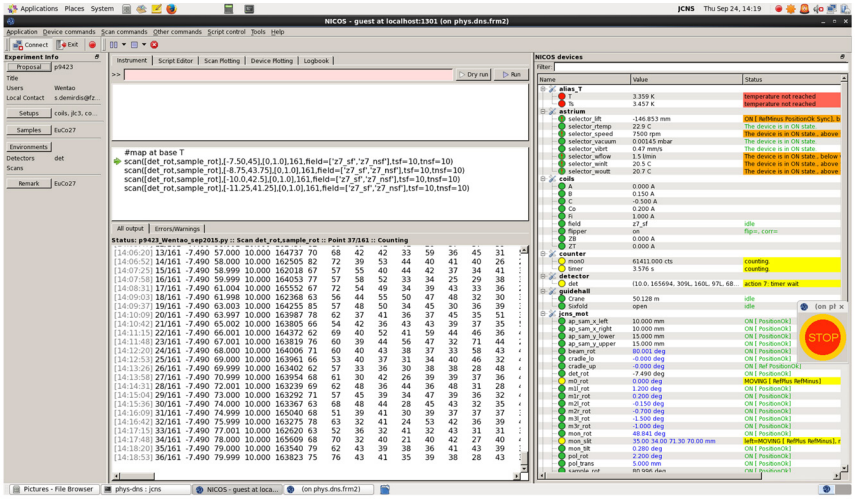

Figure IX.3: NICOS client GUI for the time-of-flight instrument DNS at MLZ.

event-mode based data analysis. NICOS offers scripting in Python and in a simpler command language, as well as a configurable graphical user interface. Functionalities comprise an electronic logbook, history plots and detector data plots. NICOS follows a multiple-client/single-server model, where the server acts as the execution environment for scripts and any device access. It also refines the TANGO device model. As an example, Figure IX.3 shows the NICOS client GUI for the time-of-flight instrument DNS at MLZ. Figure IX.2 shows the overall software structure of the HBS instrument control systems.

Besides detector electronics, the front-end equipment mainly consists of electromechanical devices such as motors, switches, encoders, pumps, valves and different kinds of sensors. Similar to the HBS machine control system, all these devices will be controlled by Siemens S7-1500 PLCs with ET200SP and ET200MP peripheral systems. For interconnection, the fieldbus systems PROFINET, PROFIBUS, AS-i and IO-Link will be used. As a typical example, Figure IX.4 shows the physical architecture of the instrument control system of the small angel scattering instrument KWS3 at MLZ, which is still using the S7-300 PLC, the predecessor of the S7-1500.

IX.1.3 Support for instrument control and automation

Each instrument at the HBS will define a specific set of automated motions and supervisioned parameters. The instrument control and automation experts will support the instrument teams during the design. They will provide a list of devices for common automation tasks and verify the specifications for custom solutions. Cables and connectors will also be standardized as much as possible to assure maintainability and reach a high level of availability. The group will also provide solutions for the instrument specific SCADA and human-machine interfaces. The group will be involved and perform the commissioning of the motion control systems including the PLC. At an pulsed neutron source, neutron choppers are critical components, which will be employed at most instruments.

To provide support for installation, commissioning and maintenance, sufficient engineering and technical staff will be available. 2 Labs with a total lab space of 500 m^2 will be required, providing a protected area, where choppers can be taken into operation.

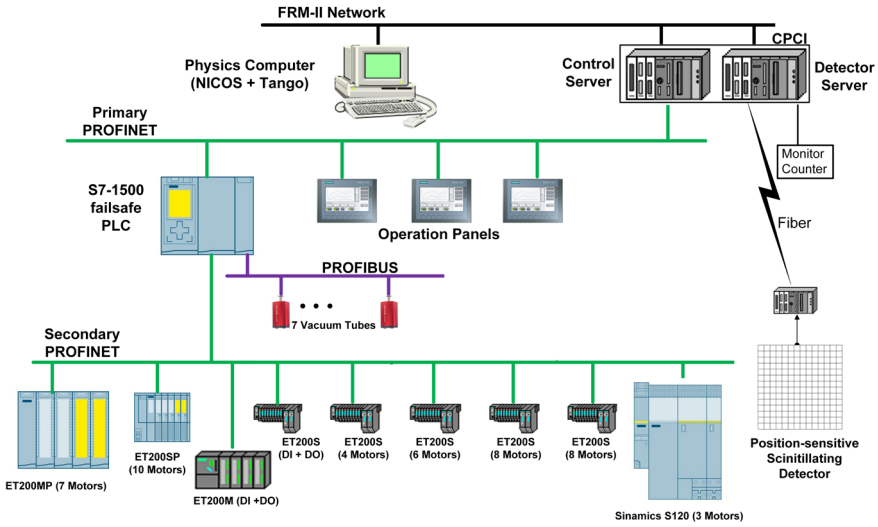

Figure IX.4: Present physical architecture of the instrument control system of KWS3

IX.2 Neutron detection and Data Acquisition

The instrument concepts presented in this TDR rely on state-of-the-art detector technology that are available on the market. The HBS will provide the capabilities to commission, maintain and operate the variety of different detector technologies. Detectors are responsible for registering the neutrons at instruments and thus play a crucial role in conducting scattering investigations. The number of registered neutrons, their positions and the time of their detection are essential observables in measurements.

Neutrons are detected indirectly by measuring reaction products that result from their nuclear interaction with the detector material. At low neutron energies of several meV to a few eV, a neutron capture reaction in a suitable atomic nucleus is used, in which the nucleus then decays into charged particles. Thereby it is important that the daughter products of the decay can generate a sufficiently measurable ionisation with a clear signal signature to distinguish from interfering radiation. The three isotopes ^{3}He, ^{10}B and ^{6}Li meet these requirements and show a high cross section for the neutron capture reaction, which is why they are mainly used as converters for the detection of low energy neutrons.

IX.2.1 Detector Technologies

With regard to the resulting performance of the detectors, the requirements for detectors for the instruments at the HBS do not differ significantly from the requirements of time-of-flight instruments at reactor or spallation sources. They are achievable with today's commercially available technologies or with the expected performance of currently ongoing detector developments. However, the number of electronic readout channels will drastically increase and it must be considered that detector electronics will play a key role for detector systems. Some of the detector technologies are briefly presented below.

Detectors based on ^{3}He gas as converter are a well established and very often applied technology for neutron detection at scattering instruments. The gas is used in proportional counter tubes, posi-

tion sensitive detector tubes or multiwire proportional chambers which are commercially available in various designs. Due to the low atomic number of ^{3}He, such detectors show a low Gamma-sensitivity of 10^{-7}, which avoids the detection of spurious radiation. The detection efficiency of these detectors depends on the ^{3}He gas pressure and can reach up to 70–80% at 1 Å neutron wavelength for 1 inch diameter tube-based designs. Large area detector systems can be built with a stack of ^{3}He-filled position sensitive tubes, and high global count rates can be achieved through the individual count rate capability of about 40 kHz per tube with acceptable dead time. The lateral spatial resolution and the time resolution are determined by the diameter of the tubes, while typically about 1% of the tube length can be achieved for the longitudinal spatial resolution. A higher spatial resolution can be achieved by using ^{3}He-filled multi-wire chambers, which also allow the realization of specially adapted geometries. However, a disadvantage of using ^{3}He for neutron detection is the price of the gas, which has increased drastically in recent years due to intensive use in the field of homeland security and the resulting lack of availability. Alternatives should therefore also be considered, especially for large-area detectors that require a large amount of ^{3}He gas.

Another method for detecting neutrons is based on the use of ^{10}B converter layers. Developments of such detectors have been intensively promoted in recent years as an alternative to large-area ^{3}He detector systems and for detectors with high spatial resolution and count rate capacity. ^{10}B has a high neutron absorption cross section, but the self-absorption of the reaction products in boron only allows the use of thin layers. A ^{10}B layer suitable for neutron detection has a thickness of approx. 1 - 1.5 µm and allows a detection efficiency of approx. 3% at 1.0 Å. For the realization of efficient ^{10}B detector systems, several layers placed one behind the other are therefore used, which are usually positioned inclined with an angle to the neutron irradiation direction, which significantly increases the effective path length of the neutrons in the converter material and thus the detection efficiency. Multi-wire chambers with conventional counting gases such as Ar/CO_2 are typically used to register the reaction products emerging from the converter foils. Only about atmospheric pressure is necessary, which avoids thick entrance windows and enables large-area detectors. Depending on the selected detector layout, detection efficiencies of $>$50% at 1 Å neutron wavelength and spatial resolutions down to the submillimeter range can be achieved. Also tube-based designs with ^{10}B converter layers are used in neutron detection. The tubes have typically a very small diameter of a couple of millimeters and have a converter layer on the inside of the tube. By stacking a large number of tube layers also by this method a high detection efficiency is achieved.

Neutron detectors based on solid-state scintillators enable thin neutron converters that can have a high detection efficiency due to the relatively high density of the scintillation material. For example, using ^{6}Li-based glass scintillators, a detection efficiency of about 75% for thermal neutrons can be achieved even with a thickness of 1 mm and they are also well suited for detectors with a high rate due to a fast decay time of the light emission. Ceramic scintillators based on a mixture of ^{6}LiF and ZnS are also often used for neutron detection. These scintillators have a very high luminous efficiency, but due to the self-absorption of the emitted light, their thickness is limited to 450–500 µm, which limits the detection efficiency of a single layer to around 40% at 1 Å. However, the disadvantage of scintillation detectors is their gamma sensitivity, which is higher than with other technologies. Vacuum photomultipliers are normally used to detect the scintillation light. An alternative, especially when operating in magnetic fields, is offered by silicon-based photomultipliers, but their properties deteriorate with longer exposure to neutrons. Position-sensitive neutron detectors can be realized using ^{6}Li-Glass scintillators with the Anger method or using ^{6}LiF/ZnS scintillators with the capture and transmission of the emitted light via an arrangement of wavelength-shifting fibers to photomultipliers. With such methods, local resolutions in the sub-millimetre range with high time resolution can be achieved, which due to the small thickness of the scintillators have almost no parallax effects. Extremely high spatial resolutions in the range below 100 µm are achieved by reading out the scintillator light using mirrors with CCD cameras or CMOS sensors. If the spatial resolution to be achieved is in the range of the pixel size of photomultipliers, direct pixel-based readout of the light is possible, which enables very high count rates.

At the HBS, also fast and epithermal neutrons will be used mainly for analytics and radiography applications. While the former detect basically the gamma radiation emitted by activation products, the later require neutron detectors with a position resolution on the cm scale. Typically, measurements are performed using the integrated spectrum emitted from the regions close to the target. Due to the decreasing interaction cross sections with increasing neutron energy, fast neutron detectors based on neutron induced reactions also have low detection efficiencies. The most common method for detecting fast neutrons is based on elastic scattering in hydrogen-containing material. Here, some of the neutron's kinetic energy is transferred to the hydrogen nucleus, resulting in a recoil proton whose energy is deposited in the detector material. Organic liquid or solid scintillators are often used as detection material for neutron energies up to 9 MeV. They can achieve a high time resolution in the ns-range and an somewhat rather high detection efficiency (e.g. 10% for 2.5 MeV neutrons with 2 cm thick scintillator). In order to build position sensitive fast neutron detectors, an arrangement of plastic scintillating fibres or polypropylen/ZnS-mixtures with wavelength-shifting fibers light transmission can be used, e.g. at Radiography station NECTAR at the MLZ.

IX.2.2 Support for detectors

The early establishment of a detector group at HBS will contribute to an optimization of the detector systems used on the instruments and help to avoid costly errors. The first task is to make recommendations for the selection of suitable detector technologies and associated readout electronics, which requires a sound overview of the current state of the art and current developments. The detector group should therefore include personnel with expert-level knowledge of detector physics, the specific methods of nuclear pulse processing, and readout electronics. In the instrument design phase, this will require 2-3 experienced detector physicists, 2 electrical engineers with expertise in FPGA technologies, and 2-3 technicians with knowledge of CAD/CAE systems. In order to draw objective comparisons between different detector technologies, test measurements with available prototypes on existing instruments have to be performed by this group. In addition, the interfaces of the respective detector electronics are to be evaluated with respect to maintainability as well as uniform instrument control and data storage. The progress of the project phases at HBS will lead to an increase of work in the detector group, which has to be compensated by additional personnel. However, an estimate of the staff needed can only be made after specific technology decisions.

To accommodate various activities within the detector group, special laboratories and workshops are necessary. These include a source laboratory with a neutron source for testing detectors, a clean room for inspecting, repairing and, if necessary, assembling the very sensitive detectors, a laboratory with a ^{3}He recovery facility for recovering the very expensive ^{3}He gas, an electronics laboratory with ESD workstations and electronics laboratory equipment, and a workshop area with a crane for assembling and temporarily storing detector components. It is estimated that approx. 300 m^{2} will be required for this.

IX.3 Data management and Software for Instruments

To offer a substantial benefit in the field of data management and scientific computing the HBS will bundle its activities here in a structure similar to the JCNS Neutron SimLab. This structure shall be aligned with the fields of action of the Helmholtz Digitization Strategy. Its role will be that of coordinating science-, method- and technology-oriented digitization projects and the management of the corresponding IT infrastructure for the HBS. The organisation at HBS will contain the following dedicated groups: Instrument control, Cloud infrastructure, Data management, AI Methods and Scientific software.

Figure IX.5 presents a typical research workflow starting from an idea or a scientific question and

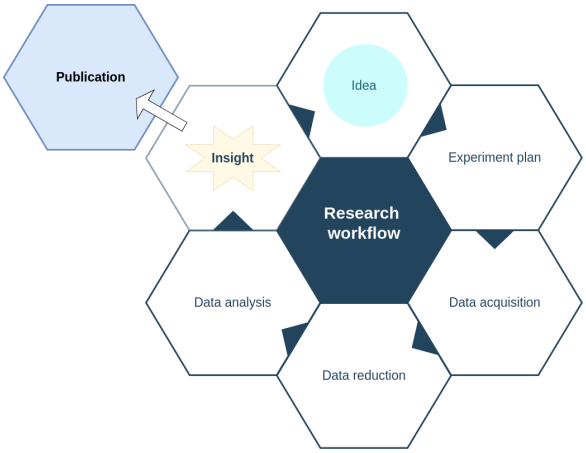

Figure IX.5: *Research workflow at HBS: From idea to publication.*

finishing with an insight which usually leads to a new scientific question or to a publication or both. The aim is to support facility users and scientists at each step of this workflow.

Experiment preparation. Once a potential user comes with an idea of an experiment or with a particular scientific question, HBS will provide an infrastructure to choose the most suitable instrument and to plan a neutron experiment. At this step, access to HBS *cloud infrastructure* should be provided, where a virtual neutron experiment could be performed remotely. This requires development of digital twins of all available HBS instruments as well as the enrolment of a cloud infrastructure. HBS will strongly rely on the expertise and collaboration of MLZ, ESS and other large-scale neutron facilities, as well as on existing software solutions to establish this environment. A flexible digital twinning platform is one of the essential requirements both for an efficient offer of remote access as well as for the long-term training of future neutron scientists. This will allow performing virtual and complex experiments by exploiting the active connection to the control system of such instruments and thereby optimizing experiment preparation and improving the quality of peer-review proposals.

Data acquisition. Once a proposal has been approved and the experiment has been planned and scheduled, the next step, data acquisition, starts. At this step, contributions of the following groups play an important role:

- *Instrument control group.* Development and maintenance of the data acquisition software. Here solutions developed at MLZ, for example, NICOS, will be utilised. Data is typically taken in event-mode, meaning continuous acquisition of timestamped neutron events as well as motor positions, I/Os and sample environment data during measurement, allowing for later rebinning and analysis. For synchronisation of the event data stream with the metadata, adjustments and further developments will be required.

- *Cloud infrastructure group.* Management and maintenance of the fast access cloud storage for collected neutron data. All measured data will be copied to the central storage systems at PGI-JCNS-TA and also to cold storage systems, e.g. tape storage for long term archival. Measured data stored on the fast storage systems at the beamlines will be wiped once there is not enough capacity for the next ten days of beamtime, but is still available on the central storage systems. At HBS we expect data flow of about 1 PB per year of raw event data. The volume of the processed data will be similar. The storage must be fast enough to enable reading and writing of such amount of data within a reasonable time. Fast internal network

is crucial. Data may be removed from the central storage systems, but can be restored from the cold storage systems for further analysis for at least 10 years. The hierarchical storage architecture allows to scale over the lifetime of the facility.

- *AI Methods group.* Development of AI-assisted data acquisition techniques similar to *data-driven discovery* group at MLZ. As experience of MLZ and other neutron and synchrotron facilities shows, AI-assisted DAQ can save the beam time noticeably and increase scientific output from each experiment.

- *Data management group.* All collected data, including metadata, will be included into the facility data catalogue.

Data reduction. The aim of this step is to apply corrections to the measured data, i.e. absorption, detector efficiency, flipping ratio, multiple scattering, background, etc., as well as to filter and generate histograms of the event data. This is required to be able to proceed with a data analysis. Considering the rather high data flux, this step will be performed on facility servers (*cloud infrastructure*) and automated whenever possible (*AI methods group, Scientific software group*). The storage requirements for the processed data are comparable to the raw data, as experienced by operating pulsed neutron sources. All the performed steps will be logged and saved to the data catalogues to ensure the reproducibility of the data reduction.

Data analysis. To lower the accessibility barrier, the data analysis should be enabled on the facility servers maintained by the *cloud infrastructure group* using the software developed and maintained by the *scientific software group*. It will provide tools for state-of-the-art modeling combined with simulations of the digital twins of the instruments to include resolution effects. Whenever possible, the data analysis will be automated using developments of the *AI methods group*. The performed steps, as well as the software used will be logged and saved to the data catalogues to ensure the reproducibility of the data analysis.

Scalability of the access of the growing user community to digital twins and data analysis services (DAaaS) will be guaranteed by the use of Kubernetes, an open-source system for automating deployment, scaling and management of containerized applications. Thus, a comprehensive and scalable support will be offered for the workflow lifecycles for the experiments at HBS with fast access to raw data, data reduction and analysis.

Evaluating predictions from virtual experiments with observations from physical experiments will allow to adjust and thereby optimize the experiment procedures as well as increase the efficiency of experiment time usage. Specific applications can be found in material research and in topics like bio-based sustainable materials, energy conversion materials and advanced engineering materials. An exchange with the European Open Science Cloud (EOSC) and with similar platforms based on other infrastructure, like e.g. photons, will enhance the exploitation of the complementarity of different characterization methods.

Data management. Based on the experience in data mangagement at MLZ the instruments at the High Brilliance neutron Source (HBS) implement a hierarchical storage architecture. Each instrument is operated in its own network decoupled from the campus-wide so called JuNet. Neither instruments can interfere with each other nor networking issues in any other instrument network or in the JuNet affect instrument control and data acquisition. Each beamline is equipped with a fast storage system, based on the estimated flux and count rate on the detector and capacity for at least ten days of beamtime.

The data management at HBS will be performed according to the F.A.I.R. (findable, accessible, interoperable, reproducible) principles and maintained by the dedicated group. It includes the development of the high-performance data formats, metadata structures, management of the data catalogues and electronic laboratory books, data curation, development and management of the data access and

DOI policies and, finally, data archiving. For the hot-access-datasets (datasets under investigation and analysis) the fast cloud storage maintained by the HBS *cloud infrastructure group* will be used. However, for the data archiving federated solutions in cooperation to other ErUM facilities and/or libraries would be preferable.

IX.4 User service and support facilities

Following the established organization of the user service at national and international neutron facilities the user service will be organized by a central User Office service unit. The User Office will be in charge of the organisation of all things related to the scientific usage of the research infrastructure. This huge portfolio not only asks for highly motivated and broadly experienced staff but also for a dedicated software platform to handle the administrative and organisational means. HBS will use here the established software platform Ghost of MLZ, which contains everything needed to manage the user service. The most common tasks in this context include:

- Proposals: submission, checks (safety, technical)
- Review: review panels handling, scientific review, results to users
- Experiments: scheduling (by instrument scientists), handling resources (sample environment), invitations to users
- User visit: information, access preparations, additional services (visa invitations, hotel booking etc), sample tracking, assistance on short notice
- Follow up: travel reimbursement (if applicable), requesting experimental reports, following up publications

Due to the fact that the User Office collects all relevant data of the scientific operation, it will also produce any kind of statistics necessary in the operation and management of the facility. Furthermore, the User Office takes care of information of users on access, proposal deadlines, scientific, instrument and facility news via dedicated web pages, circular emails, social media or other publications. The User Office will also present the scientific possibilities at suitable scientific conferences, web platforms, social media and publications in order to attract new users and maintain the existing user community. HBS will largely profit form the long experience of JCNS in running the User Office at MLZ.

The radiation protection group will ensure that experiments are performed in a safe and sustainable manner. It will validate and verify the shielding equipment and support and advise the teams during the instrument construction. During the operation of the facility, the group advises the users in terms of radio protection and controls the treatment of activated equipment and samples. Finally, it organizes the storage and disposal of activated samples and the communication with the supervising authorities. As the HBS will be realized in different stages, also this group can start with a small staff number and grow according to the number of experiment days and users.

X.
INFRASTRUCTURE AND BUILDINGS

The conventional facilities and infrastructure will be presented in a dedicated volume of the Technical design report. Here we summarize briefly the requirements and features related directly to the instrument construction and operation.

X.1 Buildings and construction

In order to have a concrete basis for the planning, it was assumed that the facility is built on the campus of the Forschungszentrum Jülich (FZJ). It could also be realized in the vicinity of the Forschungszentrum with access to and support from the central facilities available on the campus, while any green field solution would increase the price and also the construction time.

The main parameters influencing the design of the buildings are space requirements, deformation requirements, radiation protection, required volumes, logistics and costs. The scientific and symbolic value of the facility called for a work of architectural and functional excellence to satisfy the FZJ and local community in Jülich and the science community collaborating with HBS. Many of the buildings are technical utility buildings of an industrial nature, which poses specific limits and further challenges on the architectural design. Sustainability is of special importance for FZJ and this includes meeting energy-related objectives, creating a good working environment for employees and users (guests) during operation, accessibility, an outdoor environment, sustainable transportation and using environmentally sound material. The facility shall be constructed in compliance with the general national (German) laws and regulations including Environmental permit and Licensing by the German Radiation Safety Authority under the terms of the German Radioprotection Law and Ordinance: Gesetz zum Schutz vor der schädlichen Wirkung ionisierender Strahlung (Strahlenschutzgesetz - StrlSchG).

The main installations comprising the HBS are the accelerator, the targets and the instruments (see Fig. VIII.1). Each of these components requires its specific building structure including support structures, offices and infrastructures. The accelerator and the target station are discussed in detail in the corresponding volumes of this TDR and their requirements are stated here only briefly for the sake of completeness. Concerning an energy saving and CO_2 neutral construction and operation these aspects are outlined in the TDR Infrastructure and Sustainability separately.

Accelerator. The accelerator hall has a floor area demand of approximately 120 m in length and 10 m in width and is located in the basement for radiation safety reasons. It is composed by the linac tunnel (~1400 m^2), corresponding amplifier galleries, beam dump, multiplexer and beam transport tunnels (~1240 m^2), and operating rooms. The multiplexer and the High Energy Beam Transport (HEBT) will be installed in the two floor basement structure underneath the target and the experimental hall areas to allow the proton beam to impinge the target from the bottom. The operation of

the accelerator requires a connection load of around 12 MW and a corresponding coolant capacity. The different compartments will be equipped with a crane with a load bearing capacity of 5 t.

Target. The target zones are located inside the experimental halls. Each target zone has an inner size of 12 $\times$ 12 m^2 with a soil bearing capacity of 5 t/m^2; it will be equipped with a crane. The target zones are surrounded by 1.4 m thick concrete walls resulting in a floor area demand of about 220 m^2 . The operation of each target station requires a closed cooling circuit with 120 kW cooling capacity. The ground will be equipped with a collection tray to catch possible coolant leakage. For maintenance access and transport of used targets, all three target zones will be connected (at the ground floor) to a corridor leading to the central target storage and handling area (see Fig. VIII.1).

The target zones contain first instrument components, including pulse shaping choppers, which can be placed directly at the target station wall in a minimum distance of 2 m from the moderator surface. In particular for long instruments additional beam conditioning takes place inside the target zone, e.g. frame overlap choppers can be placed here. During the operation of a target station, access into the target zone is prevented. Each extraction channel is equipped with a Gamma beam shutter, that absorbs Gamma rays emitted by the activation products from the target area, so that the zone can be accessed for maintenance on the installed components, when the target station does not receive the proton beam.

Most of the instruments will also include the neutron beam shutter inside the target zone, which enables access to the experimental zones, but also to equipment that is installed downstream the target zone. The shielding of the zone is sufficient to operate components inside the target zone without individual shielding.

Experimental halls. HBS will consist of three experimental halls to host the three targets and the instruments allocated. The three experimental halls cover an approximate area of 3100 m^2, 5700 m^2 and 2000 m^2, respectively. Extensions in order to provide sufficient space for very long instruments are attached. All necessary office space, laboratories and workshops will be placed within or close to the experimental halls. The following functional areas and units will be implemented.

- **Laboratories.** Within the experimental halls space for sample preparation laboratories, workshops and instrument control rooms of about 1700 m^2 in total are embedded. They are distributed in such a way to keep transport distances to the instruments reasonably short. The laboratories will cover the main areas for sample preparation as i) chemical (with powder cabins and glove box), ii) biological (with fume hood), and iii) activated samples handling (radiation protection). Each instruments hall shall contain at least one of each laboratory mentioned above.

- **Workshops.** There will be at least 4 types of workshops: i) mechanical, ii) electrical, iii) detector, iv) sample environment. The instruments hall 1 and 2 shall contain all workshops mentioned above, while instruments hall 3 shall contain 1 mechanical workshop. Workplaces are also installed at each instrument. Furthermore additional space for preparation of the sample environment is available around the individual instruments.

- **Technical infrastructure.** All instruments can be reached with appropriate assembly hall cranes and a lifting range. They have a capacity sufficient to move the heavy components during instrument installation and during operation of the instruments. During operation they are used to lift heavy equipment and also shielding elements. The total height from the floor to the highest part of the instruments / shielding bunker shall be up to 6 m. Above this height, a space of at least 3 m shall be considered to move the components above the instruments. Therefore, the total height of the halls shall be at least 11 to 12 m depending on the final choice of cranes. The halls shall be equipped with an overhead crane with capacity for 10 t. The floor load of 5 t/m^2 in the experimental hall covers the demands from the instruments. If necessary, local enforcement has to be foreseen.

- **Accessibilty** The halls will have one loading bay with a door which fits a truck and shall have at least one access point for transporting components between levels.
- **Utility supply** The halls shall have equipment to provide a general distribution of common utilities for each instrument: power, cooling water, vacuum pumps, network, etc. The power consumption of the instruments varies depending on the instrument configuration. On average an instrument will require about 50 kW power, with peak power that can reach up to 100 kW, e.g. when the pumps for large vacuum recipients start up. Cooling water requirements Further considerations refer to a room for high power vacuum pumps to be considered due to possible noise limits in common working areas.
- **Electromagnetic compatibility.** The instruments put stringent requirements on the electromagnetic compatibility (EMC). Sensors, detectors and drives could be heavily affected by vagabonding currents or by grounding loops acting as antennas for radio frequencies as has been experienced at various facilities. EMC issues can limit the performance of the instruments substantially, e.g. electronic noise acting as background or broadening the signals. Therefore a zone concept will be implemented based on the experience from the guide halls in Garching and the lessons learned there. It provides individual grounding for each instrument zone and takes care that the supply of other media such as pressured air, water or vacuum lines enter the zone properly isolated.
- **IT service.** For data storage, analysis and archiving fast cloud storage performed on the facility servers and maintained by the HBS cloud infrastructure group will be implemented. All available HBS instruments will be available as digital twins. The HBS instrument control systems will be implemented with the architecture and technologies based on TANGO and NICOS as at MLZ. Appropriate server systems and high speed network connections will have to installed. All instrument computers running TANGO device servers, middle tier components or clients in the presentation tier will use a Linux operating system.
- **Environment.** For many experiments and devices a reasonably stable temperature and humidity control will be needed. The humidity and the temperature shall be kept constant at standard levels of room temperature. This does not require active air conditioning of the experimental hall, but will be considered in the construction and building of the halls.
- **Radiation safety.** The halls shall be a restricted access area with radiation control following the regulations mentioned previously. The halls shall have emergency exits according to German regulations. The access points and exits shall comply with radiation protection rules. The entrance area to the halls will contain the space for the dosimeters for staff and users, lab coats, lockers, the radiation control equipment, a recreation area with vending machine, water, etc.
- **User offices.** The offices for users could be an open space office to host up to 50 users when the facility is in full operation. It should focus on comfort, and have proximity to amenities such as toilets, kitchen, vending machines, resting and socializing area. In addition an external meeting area will be considered.

The technical and construction details on the experimental halls and supplementing infrastructure are outlined in the TDR Infrastructure and Sustainability volume.

X.2 Costing and timeline

Within this TDR, we present concepts and performance of neutron scattering instruments for operation at the HBS. An overview of the estimated investments for the instruments discussed is given in Table X.1 based on prizes by 2021.

	Instrument	Guide [k€]	Optics [k€]	Choppers [k€]	Detector [k€]	Sample [k€]	Shielding [k€]	Total [k€]
SANS	High Throughput SANS	100	200	400	5000	400	500	6600
GISANS	SANS with GISANS option	100	200	400	5000	400	500	6600
OffRef	Offspecular Reflectometer	400	400	250	1500	400	200	3150
TPD	Therm. Powder Diffr.	1300	200	2100	4800	100	800	9300
NSE	NSE Spectr.	300	2000	1200	600	150	100	4350
NRSE	NRSE Spectr.	300	1200	1200	650	150	100	3600
BSS	Backscattering Spectr.	1200	400	1100	4000	300	800	7800
T-PGA	ToF-PGNAA	220			230	50		500
NDP	Neutron Depth Profil.	270	300	350	250	700	500	2370
HorRef	Hor. Reflectometer	1500	1600	300	600	200	200	4400
EngDi	Engineering Diffr.	1000	400	1800	2500	1300	1000	8000
DENS	Diffuse Elast. Neutron Scat.	400		1000	4000	200	200	5800
PDNS	Pol. Diffuse Neutron Scat.	500	3000	500	2000	100	200	6300
MMD	Single Crystal Diffr.	1500	100	600	4500	200	200	7100
CCS	Cold Chopper Spectr.	500	600	1800	5000	1000	800	9700
CAS	Indirect Geom. Spectr.	1100	500	400	5000	500	800	8300
C-NI	Cold Neutron Imaging		300	350	200	150	700	1700
T-NI	Thermal Neutron Imaging		300		200	150	700	1350
D-NI	Diffractive Neutron Imaging	500	300	700	200	150	700	2550
DMD	Disord. Mat. Diffr.	1400	150	400	2600	150	700	5400
PGAINS	PGAINS		200		120	50	1000	1370
Epi-NI	Epitherm. Neutron Imaging		300		200	150	700	1350
HE-NI	Hi-Energy Neutron Imaging		300		200	150	700	1350
CrysToF	CRYSTOF		450	200	4000	1000	700	6350
	Total							115290

Table X.1: *Costing estimates for the instruments presented based on 2021 prizes.*

The construction of the instruments will run in parallel with the accelerator and target station construction, but the installation schedule will be governed by the progress of the installation of the accelerator and the target. The operation of the facility will be started, once the first sections of the accelerator including the proton source, the first cavities to reach an energy of 30 MeV, the proton beam dump and one HEBT section are ready. Innovative concepts, that profit in particular from the source concept and are heavily demanded by the user community and therefor promise a successful early science program, will be realized first. It should be noted, that in this stage the system can and will also be used to implement and test different operations modes, to gain experiences and improve also the design for the following target stations.

With the upgrade of the accelerator to the final energy and full power, it can serve more target stations. It should be noted, that the cost to add a target station in an existing building is comparable to the cost for an expensive instrument. Therefore subsequent target stations will be implemented to provide dedicated neutron sources for the instruments that will be proposed then. We envision here an instrument building process involving universities, e.g. via ErUM-Pro, or other partners from science and industry.

Finally the HBS will host three target stations with a capacity to run 25+ instruments operating for 5000 hours per year. The facility will be operating for a minimum of 30 years after the completion of the last stage. It must be emphasized, the target stations and experimental halls have capacity to host further 11 instruments, i.e. up to 36 instruments, and thus can be further expanded at a later stage.

XI.

AUTHOR LIST AND ACKNOWLEDGEMENTS

XI.1 Volume author list

M. Ganeva, G. Kemmerling, H. Kleines, E. Mauerhofer, U. Rücker, N. Schmidt, W. Schweika, P. Zakalek
Forschungszentrum Jülich GmbH, Jülich Centre for Neutron Science, JCNS-2/PGI-4, Jülich, Germany

A. Houben
Forschungszentrum Jülich GmbH, Jülich Centre for Neutron Science, JCNS-2/PGI-4, Jülich, Germany and RWTH Aachen, Institute of Inorganic Chemistry, Aachen, Germany

K. Schmalzl
Forschungszentrum Jülich GmbH, Jülich Centre for Neutron Science, JCNS-2/PGI-4, Jülich, Germany and Institute Laue-Langevin, Grenoble, France

C. Franz, H. Frielinghaus, S. Jaksch, S. Mattauch, S. Pasini, T. Schrader, E. Vezhlev
Forschungszentrum Jülich GmbH, Jülich Centre for Neutron Science and Heinz Maier-Leibnitz Zentrum MLZ, JCNS-4, Garching, Germany

N. Violini, R. Zorn
Forschungszentrum Jülich GmbH, Jülich Centre for Neutron Science, JCNS-1/IBI-8, Jülich, Germany

M. Feygenson
Forschungszentrum Jülich GmbH, Jülich Centre for Neutron Science, JCNS-1/IBI-8, Jülich, Germany and European Spallation Source, Lund, Sweden

N. Kardjilov
Helmholtz-Zentrum Berlin for Materials and Energy, Berlin, Germany

J. Fenske, I. Krasnov, Y. Meinerzhagen
Helmholtz-Zentrum Hereon, Geesthacht, Germany

R. Bewley
ISIS Neutron and Muon Facility, Rutherford Appleton Laboratory, Didcot, England

A. Glavic, Z. Ma, M. Strobl
Paul Scherrer Institut, Villigen, Switzerland

XI.2 Acknowledgments

This Technical Design Report has been compiled with the kind support of a large number of colleagues at the Jülich Centre for Neutron Science and other collaborating institutes and universities. The editors

would like to thank in particular:

J. Baggemann, Th. Brückel, J. Chen, T. Claudio Weber, T. Cronert (†), Q. Ding, P.-E. Doege, M. El Barbari, T. Gutberlet, J. Li, Z. Ma, E. Mauerhofer, N. Ophoven, I. Pechenitzky, T. Randriamalala, U. Rücker, N. Schmidt, A. Schwab, E. Vezhlev, P. Zakalek
Forschungszentrum Jülich GmbH, Jülich Centre for Neutron Science, Jülich, JCNS-HBS, Germany

F. Beule, P. Kämmerling, H. Kleines, K. Lieutenant, F. Suxdorf, J. Voigt
Forschungszentrum Jülich GmbH, Jülich Centre for Neutron Science, Jülich, JCNS-IT, Germany

B. Daegener, F. Gossen
Forschungszentrum Jülich GmbH, Jülich Centre for Neutron Science, Jülich, JCNS-2, Germany

N. Bernard, H. Feilbach, J. Lipperts, J. Peetz, S. Pistel, J. Schnitzler
Forschungszentrum Jülich GmbH, Jülich Centre for Neutron Science, Jülich, PGI/JCNS-TA, Germany

R. Achten, Y. Bessler, R. Hanslik, F. Löchte, M. Strothmann, J. Wolters
Forschungszentrum Jülich GmbH, Central Institute of Engineering, Electronics and Analytics, Jülich, ZEA-1, Germany

O. Felden, R. Gebel, A. Lehrach, M. Marzen, M. Rimmler, R. Similon
Forschungszentrum Jülich GmbH, Nuclear Physics Institute, Jülich, IKP-4, Germany

B. Neumaier
Forschungszentrum Jülich GmbH, Institute of Neurosciences and Medicine, Jülich, INM-5, Germany

O. Meusel, H. Podlech
Goethe University Frankfurt, Institute for Applied Physics, Frankfurt, Germany

W. Barth
GSI Helmholtzzentrum für Schwerionenforschung, Darmstadt, Germany / Helmholtz Institute Mainz, Mainz, Germany

J. Fenske, M. Müller, A. Schreyer
Helmholtz-Zentrum Geesthacht, Geesthacht, Germany

S. Böhm, J.-P. Dabruck, R. Nabbi
RWTH Aachen University, Nuclear Engineering and Technology Transfer, Aachen, Germany

S. Eisenhut, Ch. Haberstroh
Technische Universität Dresden, Bitzer-Chair of Refrigeration, Cryogenics and Compressor Technology, Dresden, Germany

C. Lange
Technische Universität Dresden, Institute of Power Engineering - Chair of Hydrogen and Nuclear Energy, Dresden, Germany

A.
APPENDICES

Spectral range	Energy intervall
Fast neutrons	70 MeV $< E <$ 500 keV
Resonance neutrons	500 keV $< E <$ 10 eV
Epithermal neutrons	10 eV $< E <$ 500 meV
Thermal neutrons	500 meV $< E <$ 10 meV
Cold neutrons	10 meV $< E <$ 0.5 meV
Very cold neutrons	0.5 meV $< E <$ 0.01 meV
Ultra cold neutrons	0.01 meV $> E$

Table A.1: *Classification of the neutron energy*

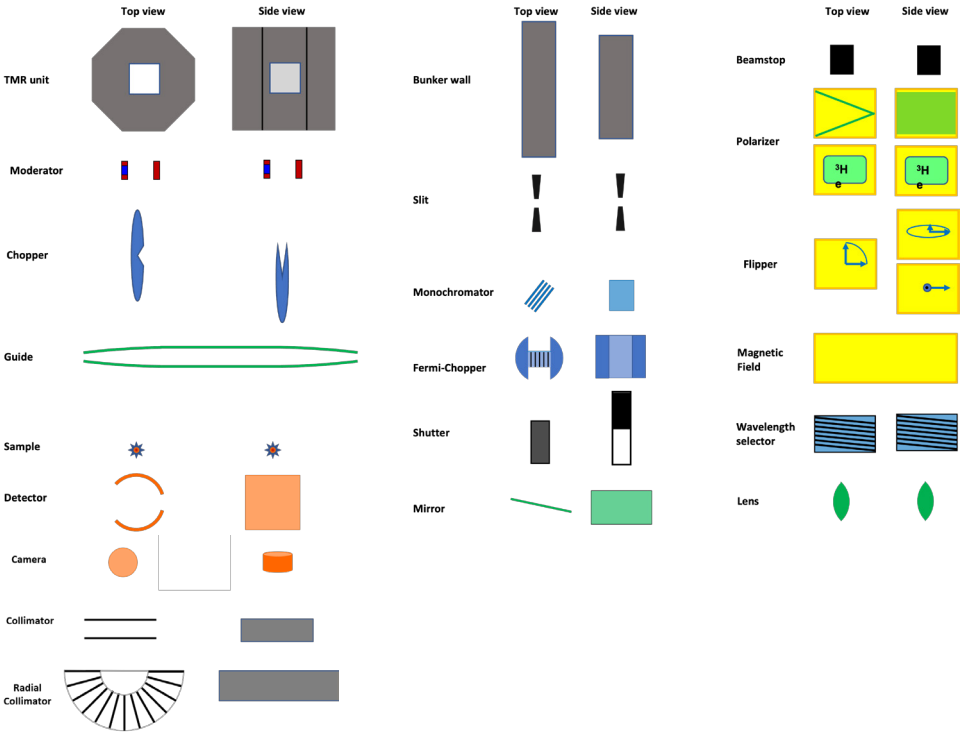

Figure A.1: *List of symbols used in the instrument sketches.*

Bibliography

[AAJ+20] K.H. Andersen, D.N Argyriou, A.J. Jackson, J. Houston, P.F. Henry, P.P. Deen, R. Toft-Petersen, P. Beran, M. Strobl, T. Arnold, H. Wacklin-Knecht, N. Tsapatsaris, E. Oksanen, R. Woracek, W. Schweika, D. Mannix, A. Hiess, S. Kennedy, O. Kirstein, S. Petersson Årsköld, J. Taylor, M.E. Hagen, G. Laszlo, K. Kanaki, F. Piscitelli, A. Khaplanov, I. Stefanescu, Th. Kittelmann, D. Pfeiffer, R. Hall-Wilton, C.I. Lopez, G. Aprigliano, L. Whitelegg, F.Y. Moreira, M. Olsson, H.N. Bordallo, D. Martín-Rodríguez, H. Schneider, M. Sharp, M. Hartl, G. Nagy, S. Ansell, S. Pullen, A. Vickery, A. Fedrigo, F. Mezei, M. Arai, R.K. Heenan, W. Halcrow, D. Turner, D. Raspino, A. Orszulik, J. Cooper, N. Webb, P. Galsworthy, J. Nightingale, S. Langridge, J. Elmer, H. Frielinghaus, R. Hanslik, A. Gussen, S. Jaksch, R. Engels, T. Kozielewski, S. Butterweck, M. Feygenson, P. Harbott, A. Poqué, A. Schwaab, K. Lieutenant, N. Violini, J. Voigt, T. Brückel, M. Koenen, H. Kämmerling, E. Babcock, Z. Salhi, A. Wischnewski, A. Heynen, S. Désert, J. Jestin, F. Porcher, X. Fabrèges, G. Fabrèges, B. Annighöfer, S. Klimko, Th. Dupont, Th. Robillard, A. Goukassov, S. Longeville, Ch. Alba-Simionesco, Ph. Bourges, J. Guyon Le Bouffy, P. Lavie, S. Rodrigues, E. Calzada, M. Lerche, B. Schillinger, Ph. Schmakat, M. Schulz, M. Seifert, W. Lohstroh, W. Petry, J. Neuhaus, L. Loaiza, A. Tartaglione, A. Glavic, S. Schütz, J. Stahn, E. Lehmann, M. Morgano, J. Schefer, U. Filges, Ch. Klauser, Ch. Niedermayer, J. Fenske, G. Nowak, M. Rouijaa, D.J. Siemers, R. Kiehn, M. Müller, H. Carlsen, L. Udby, K. Lefmann, J.O. Birk, S. Holm-Dahlin, M. Bertelsen, U. Bengaard Hansen, M.A. Olsen, M. Christensen, K. Iversen, N.B. Christensen, H.M. Rønnow, P.G. Freeman, B.C. Hauback, R. Kolevatov, I. Llamas-Jansa, A. Orecchini, F. Sacchetti, C. Petrillo, A. Paciaroni, P. Tozzi, M. Zanatta, P. Luna, I. Herranz, O.G. del Moral, M. Huerta, M. Magán, M. Mosconi, E. Abad, J. Aguilar, S. Stepanyan, G. Bakedano, R. Vivanco, I. Bustinduy, F. Sordo, J.L. Martínez, R.E. Lechner, F.J. Villacorta, J. Šaroun, P. Lukáš, M. Markó, M. Zanetti, S. Bellissima, L. del Rosso, F. Masi, C. Bovo, M. Chowdhury, A. De Bonis, L. Di Fresco, C. Scatigno, S.F. Parker, F. Fernandez-Alonso, D. Colognesi, R. Senesi, C. Andreani, G. Gorini, G. Scionti, and A. Schreyer. The instrument suite of the European Spallation Source. *Nuclear Instruments and Methods in Physics Research Section A: Accelerators, Spectrometers, Detectors and Associated Equipment*, 957:163402, 2020.

[ACH+99] S. Arzt, J.W. Campbell, M.M. Harding, Q. Hao, and J.R. Helliwell. LSCALE - The new normalization, scaling and absorption correction program in the Daresbury Laue software suite. *Journal of Applied Crystallography*, 32:554–562, 1999.

[BAA+09] M. Brodeck, F. Alvarez, A. Arbe, F. Juranyi, T. Unruh, O. Holderer, J. Colmenero, and D. Richter. Study of the dynamics of poly(ethylene oxide) by combining molecular dynamic simulations and neutron scattering experiments. *Journal of Chemical Physics*, 130:0– 0, 2009.

[BE20] T. Brückel and T. Gutberlet (Eds.). *Conceptional Design Report Jülich High Brilliance Neutron Source (J-HBS)*, volume 8. Forschungszentrum Jülich, 2020.

[BEB+23] T. Brückel, T. Gutberlet (Ser. Eds.), J. Baggemann, E. Mauerhofer, U. Rücker, and P. Zakalek (Vol. Eds.). *Technical Design Report HBS, Volume 2 - Target Stations and Moderators*. Forschungszentrum Jülich, 2023.

[Bew19] R. I. Bewley. FARO: A new type of neutron spectrometer with flux and resolution optimized. *Rev. Sci. Instrum.*, 90(7), 2019.

[Bew21] R.I. Bewley. The Mushroom neutron spectrometer. *Nuclear Instruments and Methods in Physics Research Section A: Accelerators, Spectrometers, Detectors and Associated Equipment*, 998:165077, 2021.

[BFS+16] L.K. Bruetzel, S. Fischer, A. Salditt, S.M. Sedlak, B. Nickel, and J. Lipfert. A mo-anode-based in-house source for small-angle x-ray scattering measurements of biological macromolecules. *Review of Scientific Instruments*, 87(2):025103, 2016.

[CAR+03] J. Colmenero, A. Arbe, D. Richter, B. Farago, and M. Monkenbusch. Dynamics of glass forming polymers by neutron spin echo. *Neutron Spin Echo Spectroscopy: Basics, Trends and Apllications*, 601:268–279, 2003.

[CDM+20] S. Chakraborty, M. Doktorova, T.R. Molugu, F.A. Heberle, H.L. Scott, B. Dzikovski, M. Nagao, L.R. Stingaciu, R.F. Standaert, F.N. Barrera, J. Katsaras, G. Khelashvili, M.F. Brown, and R. Ashkar. How cholesterol stiffens unsaturated lipid membranes. *PNAS*, 117:21896–21905, 2020.

[CGM+14] C.M. Casadei, A. Gumiero, C.L. Metcalfe, E.J. Murphy, J. Basran, M. Grazia Concilio, S.C.M. Teixeira, T.E. Schrader, A.J. Fielding, A. Ostermann, M.P. Blakeley, E.L. Raven, and P.C.E. Moody. Neutron cryo-crystallography captures the protonation state of ferryl heme in a peroxidase. *Science*, 345:193–197, 2014.

[CSH+10] L. Coates, A.D. Stoica, C. Hoffmann, J. Richards, and R. Cooper. The macromolecular neutron diffractometer (MaNDi) at the Spallation Neutron Source, Oak Ridge: enhanced optics design, high-resolution neutron detectors and simulated diffraction. *J. Appl. Cryst*, 43:570–577, 2010.

[DGH+16] C.D. Dewhurst, I. Grillo, D. Honecker, M. Bonnaud, M. Jacques, C. Amrouni, A. Perillo-Marcone, G. Manzin, and R. Cubitt. The small-angle neutron scattering instrument D33 at the Institut Laue–Langevin. *Journal of Applied Crystallography*, 49(1):1–14, 2016.

[DLD+13] C. Do, P. Lunkenheimer, D. Diddens, M. Götz, M. Weiß, A. Loidl, X.G. Sun, J. Allgaier, and M. Ohl. Li+ transport in poly(ethylene oxide) based electrolytes: Neutron scattering, dielectric spectroscopy, and molecular dynamics simulations. *Phys. Rev. Lett.*, 111:018301, 2013.

[FBZ+17] F. Ferdeghini, Q. Berrod, J.M. Zanotti, P. Judeinstein, V.G. Sakai, O. Czakkel, P. Fouquet, and D. Constantin. Nanostructuration of ionic liquids: impact on the cation mobility. a multi-scale study. *Nanoscale*, 9:1901, 2017.

[FFD+15] A.V. Feoktystov, H. Frielinghaus, Z. Di, S. Jaksch, V. Pipich, M.-S. Appavou, E. Babcock, R. Hanslik, R. Engels, G. Kemmerling, H. Kleines, A. Ioffe, D. Richter, and T. Brückel. KWS-1 high-resolution small-angle neutron scattering instrument at JCNS: current state. *Journal of Applied Crystallography*, 48(1):61–70, 2015.

[FFH+15] B. Farago, P. Falus, I. Hoffmann, M. Gradzielski, F. Thomas, and C. Gomez. The IN15 upgrade. *Scientific Review*, 26:15–17, 2015.

[FKR+06] Z.-D. Fu, P. Kögerler, U. Rücker, Y. Su, R. Mittal, and T. Brückel. An approach to the magnetic ground state of the molecular magnet Mo_72Fe_30. *Macromolecules*, 39:3947, 2006.

[FRMM22] B. Fåk, S. Rols, G. Manzin, and O. Meulien. Panther - the new thermal neutron time-of-flight spectrometer at the ILL. *EPJ Web Conf.*, 272:02001, 2022.

[GAA+06] A.-C. Genix, A. Arbe, F. Alvarez, J. Colmenero, W. Schweika, and D. Richter. Local Structure of Syndiotactic Poly(methyl methacrylate). A Combined Study by Neutron Diffraction with Polarization Analysis and Atomistic Molecular Dynamics Simulations. *Macromolecules*, 39:3947, 2006.

[GB22] A. Glavic and M. Björck. GenX 3: the latest generation of an established tool. *Journal of Applied Crystallography*, 55(4):1063–1071, 2022.

[GEFS20] J.S. Gardner, G. Ehlers, A. Faraone, and V. Sakai. High-resolution neutron spectroscopy using backscattering and neutron spin-echo spectrometers in soft and hard condensed matter. *Nature Reviews Physics*, 2:103, 2020.

[GJB+12] T. Goorley, M. James, T. Booth, F. Brown, J. Bull, L. Cox, J. Durkee, J. Elson, M. Fensin, R. Forster, J. Hendricks, H. Hughes, R. Johns, B. Kiedrowski, R. Martz, S. Mashnik, G. McKinney, D. Pelowitz, R. Prael, J. Sweezy, L. Waters, T. Wilcox, , and T. Zukaitis. Initial MCNP6 Release Overview. *Nuclear Technology*, 180:298–315, 2012.

[GKP+22] L. Guasco, Yu.N. Khaydukov, S. Pütter, L. Silvi, M.A. Paulin, T. Keller, and B. Keimer. Resonant neutron reflectometry for hydrogen detection. *Nature Communications*, 13(1):1486, 2022.

[GRM+20] T. Gutberlet, U. Rücker, E. Mauerhofer, P. Zakalek, T. Cronert, J. Voigt, J. Baggemann, J. Li, P. Doege, S. Böhm, M. Rimmler, O. Felden, R. Gebel, O. Meusel, H. Podlech, W. Barth, and T. Brückel. Sustainable neutrons for today and tomorrow — The Jülich High Brilliance neutron Source project. *Neutron News*, 32, issue 2-4:37–43, 2020.

[GSS16] A. Glavic, J. Stahn, and S. Schütz. Estia: design of the polarized, small sample reflectometer at ESS. *Swiss Neutron News*, 48:6–16, 2016.

[GV22] T. Gutberlet and J. Voigt. Instrumentation Workshop – Best Instruments for the Future Neutron Facility HBS. *Neutron News*, 33, issue 2-4:2–3 and 11–12, 2022.

[HAB+22] C. Hughes, M. Armstrong, R. Bucher, S. Kressierer, S. Chapman, and U. Gunsenheimer (Eds.). *Neutron Science in Europe*. League of advanced European Neutron Sources (LENS), 2022.

[HLH+16] S.L. Holm, K. Lefmann, P.F. Henry, M. Bertelsen, J. Schefer, and M. Christensen. HEIMDAL: A thermal neutron powder diffractometer with high and flexible resolution combined with SANS and neutron imaging – Designed for materials science studies at the European Spallation Source. *Nuclear Instruments and Methods in Physics Research Section A: Accelerators, Spectrometers, Detectors and Associated Equipment*, 828:229–241, 2016.

[HSBD12] A. Houben, W. Schweika, T. Brückel, and R. Dronskowski. New neutron-guide concepts and simulation results for the POWTEX instrument. *Nucl. Instrum. Methods Phys. Res. A*, 680:124–133, 2012.

[HZ19] W.T. Heller and P.A. Zolnierczuk. The helix to sheet transition of an HIV1 fusion peptide derivative changes the mechanical properties of lipid bilayer membrane. *BBA - Biomembranes*, 1861:565–572, 2019.

[Jau97] W. Jauch. Prospects of single-crystal diffraction at a long pulse spallation source. *Journal of Neutron Research*, 6:161–171, 1997.

[JCD+21] S. Jaksch, A. Chennevière, S. Désert, T. Kozielewski, H. Feilbach, P. Lavie, R. Hanslik, A. Gussen, S. Butterweck, R. Engels, H. Frielinghaus, S. Förster, and P. Müller-Buschbaum. Technical Specification of the Small-Angle Neutron Scattering Instrument SKADI at the European Spallation Source. *Applied Sciences*, 11(8), 2021.

[JHS+17] P. Jacobs, A. Houben, W. Schweika, A. L. Tchougréeff, and R. Dronskowski. Instrumental resolution as a function of scattering angle and wavelength as exemplified for the POWGEN instrument. *J. Appl. Cryst.*, 50:866–875, 2017.

[JLBF23] S. Jaksch, K. Lieutenant, E. Babcock, and H. Frielinghaus. The GISANS instrument at the HBS. *Nuclear Instruments and Methods in Physics Research Section A: Accelerators, Spectrometers, Detectors and Associated Equipment*, 1048:167919, 2023.

[JMRO+14] S. Jaksch, D. Martin-Rodriguez, A. Ostermann, J. Jestin, S. Duarte Pinto, W.G. Bouwman, J. Uher, R. Engels, and H. Frielinghaus. Concept for a time-of-flight Small Angle Neutron Scattering instrument at the European Spallation Source. *Nuclear Instruments and Methods in Physics Research Section A: Accelerators, Spectrometers, Detectors and Associated Equipment*, 762:22–30, 2014.

[KBFS18] C. Klauser, R. Bergmann, U. Filges, and J. Stahn. A Selene Guide for AMOR. In *22nd Meeting of the International Collaboration on Advanced Neutron Sources (ICANS XXII)*, volume 1021 of *Journal of Physics Conference Series*, 2018.

[KHaWSD09] M. Krott, A. Houben, P. Müller amd W. Schweika, and R. Dronskowski. Determination of the magnetic structure of manganese carbodiimide with diffraction experiments using polarized neutrons. *Phys. Rev. B*, 80:024117, 2009.

[KKM+12] B.J. Kirby, P.A. Kienzle, B.B. Maranville, N.F. Berk, J. Krycka, F. Heinrich, and C.F. Majkrzak. Phase-sensitive specular neutron reflectometry for imaging the nanometer scale composition depth profile of thin-film materials. *Current Opinion in Colloid and interface Science*, 17(1):44–53, 2012.

[KMA+20] M. Kruteva, M. Monkenbusch, J. Allgaier, O. Holderer, S. Pasini, and D. Richter. Self-similar dynamics of large polymer rings: A neutron spin echo study. *Phys. Rev. Lett.*, 125:238004, 2020.

[KSS+12] M. Klostermann, R. Strey, T. Sottmann, R. Schweins, P. Lindner, O. Holderer, M. Monkenbusch, and D. Richter. Structure and dynamics of balanced supercritical CO2 microemulsions. *Soft Matter*, 8:797–807, 2012.

[LHS+21] A.S. Losko, Y. Han, B. Schillinger, A. Tartaglione, M. Morgano, M. Strobl, J. Long, A.S. Tremsin, and M. Schulz. New perspectives for neutron imaging through advanced event-mode data acquisition. *Scientific Reports 2021 11:1*, 11:1–11, 2021.

[LLG07] K. Lieutenant, P. Lindner, and R. Gaehler. A new design for the standard pinhole small-angle neutron scattering instrument D11. *Journal of Applied Crystallography*, 40(6):1056–1063, 2007.

[LM06] K. Lieutenant and F. Mezei. MC Simulations of a Powder Diffractometer installed on a long pulse target station using Wavelength Frame Multiplication. *J. Neutron Res.*, 14:177–191, 2006.

[LN99] K. Lefmann and K. Nielsen. McStas, a general software package for neutron ray-tracing simulations. *Neutron News*, 10(3):20–23, 1999.

[MGZ+21] E. Metwalli, K. Götz, T. Zech, C. Bär, I. Schuldes, A. Martel, L. Porcar, and T. Unruh. Simultaneous SAXS/SANS Method at D22 of ILL: Instrument Upgrade. *Applied Sciences*, 11(13), 2021.

[MHH+14] G. Modzel, M. Henske, A. Houben, M. Klein, M. Köhli, P. Lennert, M. Meven, C.J. Schmidt, U. Schmidt, and W. Schweika. Absolute efficiency measurements with the 10B based jalousie detector. *Nuclear Instruments and Methods in Physics Research Section A: Accelerators, Spectrometers, Detectors and Associated Equipment*, 743:90–95, 2014.

[MHW+16] S. Mühlbauer, A. Heinemann, A. Wilhelm, L. Karge, A. Ostermann, I. Defendi, A. Schreyer, W. Petry, and R. Gilles. The new small-angle neutron scattering instrument SANS-1 at MLZ — characterization and first results. *Nuclear Instruments and Methods in Physics Research Section A: Accelerators, Spectrometers, Detectors and Associated Equipment*, 832:297–305, 2016.

[MLV+21] Z. Ma, K. Lieutenant, J. Voigt, T. Gutberlet, and T. Brückel. Performance of neutron guide systems for compact accelerator-driven neutron sources. *Nuclear Instruments and Methods in Physics Research Section A: Accelerators, Spectrometers, Detectors and Associated Equipment*, 1008:165479, 2021.

[MMA+18] G. Mauri, F. Messi, M. Anastasopoulos, T. Arnold, A. Glavic, C. Höglund, T. Ilves, I. Lopez Higuera, P. Pazmandi, D. Raspino, L. Robinson, S. Schmidt, P. Svensson, D. Varga, R. Hall-Wilton, and F. Piscitelli. Neutron reflectometry with the multi-blade 10 b-based detector. *Proceedings of the Royal Society A*, 474(2216):20180266, 2018.

[MNAO20] M. Markó, G. Nagy, G. Aprigliano, and E. Oksanen. Neutron macromolecular crystallography at the European Spallation Source. *Methods in Enzymology*, 634:125–151, 2020.

[MOF+20] D. Musino, J. Oberdisse, B. Farago, A. Alegria, and A.-C. Genix. Resolving segmental polymer dynamics in nanocomposites by incoherent neutron spin echo spectroscopy. *ACS Macro Lett.*, 9:910–916, 2020.

[MSSR21] G. Mauri, G.J. Sykora, E.M. Schooneveld, and N.J. Rhodes. Enhanced position resolution for ZnS:Ag/ 6 LiF wavelength shifting fibre thermal neutron detectors. *Eur. Phys. J. Plus*, 136:286, 2021.

[NP19] A. R. J. Nelson and S. W. Prescott. $<irefnxi>$: neutron and x-ray reflectometry analysis in python. *Journal of Applied Crystallography*, 52(1):193–200, 2019.

[PHK+19] S. Pasini, O. Holderer, T. Kozielewski, D. Richter, and M. Monkenbusch. J-NSE-Phoenix, a neutron spin-echo spectrometer with optimized superconducting precession coils at the MLZ in Garching. *Rev. Sci. Instrum.*, 90:043107, 2019.

[PVHB+20] G. Pospelov, W. Van Herck, J. Burle, J. M. Carmona Loaiza, C. Durniak, J. M. Fisher, M. Ganeva, D. Yurov, and J. Wuttke. Bornagain: software for simulating and fitting grazing-incidence small-angle scattering. *Journal of Applied Crystallography*, 53(1):262–276, 2020.

[RKR+07] M.W. Roessle, R. Klaering, U. Ristau, B. Robrahn, D. Jahn, T. Gehrmann, P. Konarev, A. Round, S. Fiedler, C. Hermes, and D. Svergun. Upgrade of the small-angle X-ray scattering beamline X33 at the European Molecular Biology Laboratory, Hamburg. *Journal of Applied Crystallography*, 40(s1):s190–s194, 2007.

[RPFA12] A. Radulescu, V. Pipich, H. Frielinghaus, and M.-S. Appavou. KWS-2, the high intensity / wide Q-range small-angle neutron diffractometer for soft-matter and biology at FRM II. *Journal of Physics: Conference Series*, 351(1):012026, 2012.

[SC93] O. Schärpf and H. Capellmann. The XYZ-Difference Method with Polarized Neutrons and the Separation of Coherent, Spin Incoherent, and Magnetic Scattering Cross Sections in a Multidetector. *Phys. Stat. Sol.*, 135:359–379, 1993.

[Sch10a] B.P. Schoenborn. A history of neutrons in biology: The development of neutron protein crystallography at BNL and LANL. *Acta Crystallographica Section D: Biological Crystallography*, 66:1262–1268, 2010.

[Sch10b] W. Schweika. XYZ-polarisation analysis of diffuse magnetic neutron scattering from single crystals. *J. Phys.: Conf. Ser.*, 211:012026, 2010.

[SFP12] J. Stahn, U. Filges, and T. Panzner. Focusing specular neutron reflectometry for small samples. *European Physical Journal - Applied Physics*, 58(1), APR 2012.

[SG16a] J. Stahn and A. Glavic. Focusing neutron reflectometry: Implementation and experience on the TOF-reflectometer Amor. *Nuclear Instruments and Methods in Physics Research Section A: Accelerators, Spectrometers, Detectors and Associated Equipment*, 821:44–54, 2016.

[SG16b] J. Stahn and A. Glavic. Focusing neutron reflectometry: Implementation and experience on the ToF-reflectometer Amor. *Nuclear Instruments and Methods in Physics Research Section A: Accelerators, Spectrometers, Detectors and Associated Equipment*, 821:44–54, 2016.

[SG17] J. Stahn and A. Glavic. Efficient polarization analysis for focusing neutron instruments. *Journal of Physics: Conference Series*, 862(1):012007, 2017.

[SL04] B.P. Schoenborn and P. Langan. Protein crystallography with spallation neutrons. *J. Synchrotron Rad*, 11:80–82, 2004.

[SPF+11] J. Stahn, T. Panzner, U. Filges, C. Marcelot, and P. Boeni. Study on a focusing, low-background neutron delivery system. *Nuclear Instruments and Methods in Physics Research Section A: Accelerators, Spectrometers, Detectors and Associated Equipment*, 634(1):S12–S16, 2011.

[SRK+18] J. Sebastian, E. Ralf, G. Kemmerling, U. Clemens, S. Désert, H. Perrey, C. Gheorghe, A. Fredriksen, P. Øya, H. Frielinghaus, K. Fissum, A. Jalgén, E. Rofors, K. Kanaki, R. Hall-Wilton, and R. Al Jebali. Recent developments SoNDe high-flux detector project. In *Proceedings of the International Conference on Neutron Optics (NOP2017)*. Journal of the Physical Society of Japan, 2018.

[SVL+16] W. Schweika, N. Violini, K. Lieutenant, C. Zendler, D. Nekrassov, A. Houben, P. Jacobs, and P.F. Henry. DREAM - a versatile powder diffractometer at the ESS. *J. Phys.: Conf. Ser.*, 746:012013, 2016.

[VBB10] J. Voigt, E. Babcock, and T. Brückel. Beam transport and polarization at TOPAS, the thermal time-of-flight spectrometer with polarization analysis. *Journal of Physics: Conference Series*, 211:012032, 2010.

[WZSM00] D. Wechsler, G. Zsigmond, F. Streffer, and F. Mezei. VITESS: Virtual instrumentation tool for pulsed and continuous sources. *Neutron News*, 11(4):25–28, 2000.

[ZLNF14] C. Zendler, K. Lieutenant, D. Nekrassov, and M. Fromme. Vitess 3 – Virtual Instrumentation Tool for the European Spallation Source. *J. Phys.: Conf. Ser.*, 528:012036, 2014.

[ZNL14] C. Zendler, D. Nekrassov, and K. Lieutenant. An improved elliptic guide concept for a homogeneous neutron beam without direct line of sight. *Nuclear Instruments and Methods in Physics Research Section A: Accelerators, Spectrometers, Detectors and Associated Equipment*, 746:39–46, 2014.

Schriften des Forschungszentrums Jülich
Reihe Allgemeines / General

Band / Volume 3
Advances in Nuclear and Radiochemistry
Extended Abstracts of Papers presented at the Sixth International Conference on Nuclear and Radiochemistry (NRC-6), 29 August to 3 September 2004, Aachen, Germany
edited by S. M. Qaim, H. H. Coenen (2004), XXXII, 794 pp
ISBN: 3-89336-362-9

Band / Volume 4
Wissenschaft im Zeichen der Zeit
Preisträger des Leibfried-Preises im Forschungszentrum Jülich 2000 – 2005
herausgegeben von R. Ball (2005), ca. 185 pp
ISBN: 3-89336-411-0

Band / Volume 5
Proceedings of the 1st International Conference on Natural and Biomimetic Mechanosensing
edited by: J. Casas, G. Krijnen, M. Malkoc-Thust, J. Mogdans, A. Offenhäusser, H. Peremans (2009), ca. 80 pp
ISBN: 978-3-89336-583-8

Band / Volume 6
Leo Brandt (1908-1971)
Ingenieur – Wissenschaftsförderer – Visionär
Wissenschaftliche Konferenz zum 100. Geburtstag des nordrhein-westfälischen Forschungspolitikers und Gründers des Forschungszentrums Jülich
herausgegeben von B. Mittermaier, B.-A. Rusinek (2009), I, 121 pp
ISBN: 978-3-89336-602-6

Band / Volume 7
Conceptual Design Report
NOVA ERA
(Neutrons Obtained Via Accelerator for Education and Research Activities)
A Jülich High Brilliance Neutron Source project
E. Mauerhofer, U. Rücker, T. Cronert, P. Zakalek, J. Baggemann, P.-E. Doege, J. Li, S. Böhm, H. Kleines, T. Gutberlet, and T. Brückel (2017), 68 pp
ISBN: 978-3-95806-280-1

Band / Volume 8
Conceptual Design Report
Jülich High Brilliance Neutron Source (HBS)
T. Brückel, T. Gutberlet (Eds.) (2020), 197 pp
ISBN: 978-3-95806-501-7

Schriften des Forschungszentrums Jülich
Reihe Allgemeines / General

Band / Volume 9-01
Technical Design Report HBS
Volume 1 – Accelerator
R. Gebel, A. Lehrach, H. Podlech (Vol. Eds.), T. Brückel, T. Gutberlet (Ser. Eds.)
(2023), 151 pp
ISBN: 978-3-95806-709-7

Band / Volume 9-02
Technical Design Report HBS
Volume 2 – Target Stations and Moderators
J. Baggemann, E. Mauerhofer, U. Rücker, P. Zakalek (Vol. Eds.),
T. Brückel, T. Gutberlet (Ser. Eds.) (2023), 118 pp
ISBN: 978-3-95806-710-3

Band / Volume 9-03
Technical Design Report HBS
Volume 3 – Instrumentation
K. Lieutenant, J. Voigt (Vol. Eds.), T. Brückel, T. Gutberlet (Ser. Eds.)
(2023), 163 pp
ISBN: 978-3-95806-711-0

Band / Volume 9-04
Technical Design Report HBS
Volume 4 – Infrastructure and Sustainability
T. Gutberlet (Vol. Eds.), T. Brückel, T. Gutberlet (Ser. Eds.)
(2023), 137 pp
ISBN: 978-3-95806-712-7

Band / Volume 9-Overview
Opportunities for Research with Neutrons at the Next Generation Facility HBS
Overview of the High Brilliance neutron Source (HBS) Technical Design Report
T. Brückel, T. Gutberlet (Eds.) (2023), 44 pp
ISBN: 978-3-95806-713-4

Allgemeines / General
Band / Volume 9-03
ISBN 978-3-95806-711-0

Mitglied der Helmholtz-Gemeinschaft

JÜLICH
Forschungszentrum